The effect of Western diet on the transcriptional memory of monocyte-derived cells

Dissertation

zur

Erlangung des Doktorgrades (Dr. rer. nat.)

der

Mathematisch-Naturwissenschaftlichen Fakultät

der

Rheinischen Friedrich-Wilhelms-Universität Bonn

vorgelegt von

Anna-Lena Hardt

aus

Köln-Porz, Deutschland

Bonn, Mai 2020

Angefertigt mit Genehmigung der Mathematisch-Naturwissenschaftlichen Fakultät der Rheinischen Friedrich-Wilhelms-Universität Bonn.

1. Gutachter: Prof. Dr. med. Joachim L. Schultze
2. Gutachter: PD. Dr. Marc Beyer

Tag der Promotion: 13.11.2020
Erscheinungsjahr: 2020

Table of content

Abbreviations

ANOVA	Analysis of Variance
APCs	Antigen presenting cells
ASC	Apoptosis-Associated Speck-Like Protein C
ATAC	Assay for Transposase Accessible Chromatin
ATF3	Cyclic AMP-dependent transcription factor
ATP	Adenosine triphosphate
BSA	Bovine serum albumin
cAMP	Cyclic adenosine monophosphate
CD	Cluster of differentiation
ChIP	Chromatin immunoprecipitation
ChIP-seq	Chromatin immunoprecipitation following deep sequencing
CTP	Carnitine Palmitoyltransferase
CSF	Colony Stimulating Factor
CVD	Cardio vascular disease
DAG	Diacylglycerol
DAMPs	Damage associated molecular patterns
DCs	Dendritic cells
DE	Differentially expressed
DNA	Deoxyribonucleic acid
dNTP	deoxyribonucleotide triphosphates

EDTA	Ethylene diamine tetra acetic acid
EGTA	ethylene glycol tetra acetic acid
ELISA	Enzyme-linked immunosorbent assay
ER	Endoplasmic reticulum
FACS	Fluorescence activated cell sorting
FAO	Fatty acid oxydation
FAS	Fatty acid synthesis
FC	Fold of change
FCS	Fetal calf serum
FDR	False discovery rate
FFA	Free fatty acid
FITC	Fluorescein isothiocyanat
FSC	Forward scatter
GATA3	GATA-binding protein 3
GFC	Group fold change
GM-CSF	Granulocyte-macrophage colony stimulating factor
GOEA	Gene ontology enrichment analysis
HDL	High density lipoprotein
H3K27Ac	Acetylation of lysine 27 on histone protein 3
H3K27me3	Trimethylation of lysine 27 on histone protein 3
H3K4me1	Monomethylation of lysine 27 on histone protein 3
H3K4me3	Trimethylation of lysine 4 on histone protein 3

HEPES	4-(2-hydroxyethyl)-1-piperazineethanesulfonic acid
HLA	Human leukocyte antigen
HM	Histone modification
IFN	Interferon
IFNy	Interferon gamma
iChIP	Indexing first ChIP
IFNR	Interferon receptor
Ig	Immunoglobulin
IL	Interleukin
IL-1β	Interleukin 1 beta
iNOS	Inducible nitric monoxide synthase
IP	Immunoprecipitation
IRF	Interferon response factor
IRS	Insulin receptor substrate
JNK	c-Jun N-terminal kinase
KEGG	Kyoto Encyclopedia of Genes and Genomes
LA	Linoleic acid
LDL	Low density lipoprotein
LPS	Lipopolysaccharide
LRR	Leucine rich repeats
LXR	Liver X receptor
MACS	Magnetic assorted cell sorting
MAL	MyD88-adaptor-like protein

MAP	Mitogen activated protein
MAPK	Mitogen activated protein kinase
M-CSF	Macrophage colony stimulating factor
MHC	Major Histocompatibility Complex
MUFA	Mono-unsaturated fatty acid
MyD88	Myeloid differentiation primary response protein 88
NaCl	Sodiumchloride
NEB	New England Biolabs
NEFA	Non-esterified fatty acid
NEXON	Nuclei Extraction by Sonication
NF-κB	Nuclear factor kappa-light-chain enhancer of activated T-cells
NGS	Next generation sequencing
NK-Cells	Natural Killer Cells
NLRs	Nucleotide-binding oligomerization receptors
NO	Nitric oxide
OA	Oleic acid
PA	Palmitic acid
PAMPs	Pathogen- associated molecular patterns
PBMC	Peripheral blood mononuclear cells
PBS	Phosphate buffered saline
PCR	Polymerase Chain Reaction
PE	Phycoerythrin

PGE2	Prostaglandin E2
PI	Propidium iodide
PKC	Protein Kinase C
PNK	Polynucleotide kinase
PPRs	Pathogen recognition receptors
PRRs	Pattern recognition receptors
PUFA	Poly-unsaturated fatty acid
qRT-PCR	Semi quantitative real time PCR
rh	Recombinant human
RIPA buffer	Radioimmunoprecipitation assay buffer
RNA	Ribonucleic acid
RNA-Pol II	RNA Polymerase 2
ROS	Reactive oxygen species
SA	Stearic acid
SDS	Sodium dodecylsulfate
Seq	Sequencing
SFA	Saturated fatty acid
siRNA	Small interfering RNA
SOCS	Suppressor of cytokine signaling
SSC	Side Scatter
TBE	Tris/Borate/EDTA
TCR	T cell receptor
T2DM	Type II Diabetes Mellitus

TE buffer	Tris-EDTA buffer
TF	Transcription factor
TGF	Transforming growth factor
Th1	T helper 1
Th17	T helper 17
TIR	Toll/IL-1 receptor
TLR	Toll like receptor
TNF-α	Tumor necrosis factor-α
TR	Transcriptional regulators
TRAM	TRIF-related adaptor molecule
Treg	Regulatory T cells
TRIF	TIR-domain-containing adaptor protein including IFN-β
VLE	Very Low Endotoxin

Summary

Monocytes and monocyte-derived cells are very plastic and versatile immune cells that react to different environmental signals. These signals include not only pathogen-associated molecular patterns (PAMPs) and damage-associated molecular patterns (DAMPs), but also dietary compounds, taken up into the blood stream. Circulating free fatty acids (FFAs) are associated with a multitude of chronic inflammatory diseases. It is well established that plasma FFA concentrations are significantly increased in close association with obesity, which in turn is associated with the accumulation of immune cells such as macrophages and dendritic cells. However, previous studies have shown that these immune cells react differently to saturated and unsaturated FFAs. For example, the saturated FFA palmitic acid (PA) has been shown to provoke a pro-inflammatory phenotype in cultured macrophages[1] while the mono unsaturated fatty acid (MUFA) oleic acid (OA) is rather described to triggers an anti-inflammatory phenotype[2]. In the current work, we combined the analysis of the direct effects of OA and PA on monocyte derived cells with the evaluation of provoked 'trained immunity' or 'tolerance'.

Therefore, we designed an experimental set-up in which freshly isolated human monocytes were first cultured in medium containing 100 µM OA or PA as well as in control medium for 24 hours, which was followed by a 72 hours wash-out phase. Finally, monocyte-derived cells were re-stimulated with 10 ng/ml of the bacterial endotoxin lipopolysaccharide (LPS). With this experimental set-up, we could show that exposure of monocyte-derived cells to the dietary fatty acids PA and OA lead to differential activation and differentiation of these cells and rendered the fate of the cells towards a more pro- or anti-inflammatory phenotype, respectively. A lasting influence on gene transcription was achieved in response to later simulation of bacterial infection (by LPS) which was determined by RNA-seq. analysis. The phenomenon of memory development after interaction with the tested FFAs is of high importance as gene expression levels diverge to quite some extend, depending on the priming stimulus the cells got. This phenomenon may on the one hand be explained by divergent differentiation of monocytes giving rise to different monocyte-derived cell functions. On the other hand, epigenetic modification of cellular chromatin is highly indicated by determined long-term effect of OA and PA in monocyte-derived cells.

Although gene expression data poke another expectation, in terms of TNF and IL-6 secretion data, we could show that either the UFA oleic acid as well as the SFA palmitic acid provoke trained immunity in human monocyte-derived cells, with OA inducing a stronger effect in sense of training than PA.

To understand the molecular mechanisms essential for the development of a training effect in monocyte-derived cells, a deeper view of epigenetic modifications initiated by fatty acid intermission, should be taken. The evaluation of such findings might enable us to better understand the effect of diet leading to immunological diseases.

1. Introduction

1.1 The innate immune system

Throughout life, each multicellular organism faces contact with microbial pathogens like bacteria, viruses and fungi or parasites. To ensure survival of the host organism invasion of pathogens and infections need to be eliminated immediately. Therefore, infectious microbes have to be recognized and appropriate defense programs need to be exhibited. There are two fundamental response mechanisms of the immune system which guard that. The first line of defense, called innate immune system, is evolutionary more ancient and recognizes two classes of molecules: pathogen-associated molecular patterns (PAMPs), associated with microbial pathogens, and damage-associated molecular patterns (DAMPs), which are associated with cell fragments released during damage or death of a cell[3]. These molecular patterns are specifically recognized by germ line encoded pattern recognition receptors (PRRs) mainly expressed by myeloid-derived cells, like monocytes, macrophages, neutrophils and dendritic cells (DCs), but are also expressed by lymphocytes, epithelial cells and fibroblasts[4]. The recognition of PAMPs and DAMPs by PRRs leads to the induction of inflammatory responses and innate host defenses which in turn activate the evolutionary attained adaptive immune system[5].

However, since the activation of adaptive immune responses is a delayed process the innate response is very essential. The first line of defense lies in the recognition and elimination of microbes by the myeloid cell linage as well as by the release of cytokines and chemokines, which attract further immune cells and activate the adaptive immune cell fraction. Cytokines like Tumor necrosis factor-α (TNF-α) and Interleukin-1β (IL-1β) have not only autocrine and paracrine effects, which lead to the local activation of macrophages, dendritic cells and neutrophils, they can also utilize endocrine effects when released in large amounts[6]. These effects may include the induction of acute-phase proteins in the liver, platelet activation, fever, fatigue and anorexia, signs of acute inflammation[6].

The PRRs responsible for the activation of the first response defense by antigen presenting cells (APCs) comprise several families of receptors including Toll-like receptors (TLRs), nucleotide-binding oligomerization receptors (NLRs), C-type lectin receptors (CLRs) and RIG-1 like receptors (RLRs)[7].

The TLRs make up the most studied family of PRRs till now. In humans ten TLR like PRRs have been identified and are distinguished by their ligand specificity, signal transduction and cellular localization[7]. TLRs that are located on the cell surface comprise TLR1, TLR2, TLR4, TLR5 and TLR6 and are largely involved in the detection of bacterial components. TLR3, TLR7, TLR8 and TLR9 belong to the endosomal TLRs which detect nucleic acids of bacterial or viral origin[7]. The interaction of the TLRs with the specific PAMPs ultimately induce the expression and signaling of the transcription factor (TF) nuclear factor κB (NF-κB) and mitogen-activated protein (MAP-) kinase pathway[8]. Activation of NF-κB is important for the induction of the transcription and secretion of pro-inflammatory cytokines and chemokines to elicit innate immune responses, as well as for the induction of co-stimulatory molecules on DCs for the subsequent development of adaptive immune responses.[9] The adaptive immune system comes into play when the innate immune cells, comprising monocytes, DCs, macrophages, neutrophils, mast cells and granulocytes, are not able to resolve the microbial threat. Then, a threshold dose of microbial antigen, presented by APCs, is generated which is directed to nearby lymphoid tissues. This initiates the adaptive immune response, which however becomes effective only after several days. The time is required for T- and B-cells to provide specific antigen recognition by clonal amplification of antigen specific receptors, to proliferate, and differentiate into armed effector cells. They clear the infection at the side needed and allocate a memory for rapid clearance of re-infection with the same microbial pathogen.[10]

1.2 Different monocyte subtypes

Monocytes are leukocytes that together with DCs and macrophages belong to the family of myeloid cells. They play an important role in immune defense, inflammation and homeostasis. Monocytes scan their local environment, clear dead cells and pathogens, initiate adaptive immune responses and they also provide a progenitor pool for inflammatory macrophages, DC-like cells and the replenishment of some tissue macrophages. After birth, monocytes derive from precursors, so called monoblasts in the bone marrow and circulate in the bloodstream where they typically persist for up to three days.[11,12] From the circulation, they are recruited to sides of tissue inflammation, where they differentiate into ‘inflammatory’ macrophage- and DC-like cells and support the tissue resident macrophages in the defense[13]. Mature monocytes make up 5-10 %

of peripheral blood lymphocytes and are morphologically heterogeneous[14]. In mice, they comprise at least two different subsets, namely classical (^{mice} Cx3CR1^{low}, CCR2^{+}, Ly6C^{high} // ^{human} CD14^{++}/CD16 $^{-}$) and non-classical (^{mice} Cx3CR1^{high}, CCR2^{neg}, Ly6C^{low} // ^{human} CD14^{low} CD16^{+}) monocytes[15]. In humans, the non-classical type, making up 10 % of monocytes, is thought to have patrolling function in the vessel walls and has endothelial cell-supporting function[16]. They are weak phagocytes that selectively remove virally infected or injured cells, preferentially take up oxidized low density lipoprotein (ox-LDL), but substantially they secrete inflammatory cytokines such as TNF-α, IL-1β and CCL3 after TLR-dependent activation[17,18]. The classical subtype is able to transmigrate through the endothelium and enter tissues due to stimulating signals[19]. These migratory monocytes express high levels of CD14 on the cell surface. They make up about 85 % of total monocytes and are functionally professional phagocytes that give rise to pro-inflammatory macrophages and foam cells that ingest native low density lipoprotein (LDL), create reactive oxygen species and secrete cytokines in response to lipopolysaccharide (LPS) during infection and inflammation[20,17].

In humans, a third monocyte subset was defined, the intermediate monocyte subset (CD14^{++}CD16^{+}), which is high in CD14 and intermediate in CD16 expression and contributes significantly to atherosclerosis as they show a rather spontaneous generation of reactive oxygen species and have the most pronounced proangiogenic capacity[21].

Till recently, it was thought that all monocytes that migrate from blood to tissue necessarily develop into mature macrophages. Meanwhile it is evident that monocytes can develop in several different ways. They either remain as monocytes in the emigrated tissue, gain antigen-presenting capacity, or develop into mature macrophages[22,23]. Emigration is a process that happens constitutively also in non-inflamed tissue. Upon inflammatory signal consumption monocyte migration increases significantly and monocytes gain pro-inflammatory properties due to which some may develop into pro- and later into anti-inflammatory macrophages[19,24,25].

1.3 Monocyte derived cells

The vertebrate immune system evolved to react to infection and injury caused by bacteria, fungi, viruses, and antigens by mounting protective immune responses that

improve survival. One major cellular compartment of the immune system is the mononuclear cell lineage which includes numerous cell subsets of the myeloid lineage comprising monocyte, macrophage, and dendritic cell populations that are phenotypically and functionally heterogenous[26]. These cell types were analyzed for decades to understand the roles they play in immune responses and metabolic functions. Literally, there has been tremendous progress in the understanding of the ontogeny of tissue macrophages, DCs, and monocytes during the last decade. Models of cellular ontogeny, activation, differentiation, and tissue-specific functions of myeloid cells have been revisited. Thereby, it could be demonstrated that most tissue macrophages are yolk-sac-derived, that monocytes and macrophages follow a multidimensional model of activation, and tissue signals have a significant impact on the functionality of these cells[27].

Macrophages are fundamental members of the innate immune system and among all immune cells have the greatest plasticity[28]. They drive many specialized functions not only in terms of host defense and inflammation, but also in homeostasis, developmental processes of the body, repair and they coordinate metabolic functions[29]. During embryonic organogenesis, macrophages derived from yolk sac and fetal liver precursors are distributed in the tissues and persist in adulthood as resident, self-maintaining populations, independently of circulating monocytes[30,31]. However, under pathological conditions, monocytes constitute a major source of effector cells, as they can transform into cells with inflammatory macrophage- or DC-like phenotypes after infiltrating the affected tissues[32].

DCs are antigen presenting cells, derived from hematopoietic stem cells in the bone marrow and are widely distributed as immature cells within all mammalian tissues, but particularly in those that interface with the external environment (like skin and mucosal surfaces) and in lymphoid organs. Immature DCs are recruited to sites of inflammation in peripheral tissues following pathogen invasion. Internalization of foreign antigens can subsequently trigger their maturation and migration from peripheral tissues to lymphoid organs where they present the antigens on their cell surface to naïve T-cells. Their antigen-presenting capacity plays a pivotal role at the interface of innate and adaptive immune responses.[33]

Based on DC ontogeny[34] three major DC subsets can be classified: Conventional DCs (cDCs), made up by cDC1s and cDC2s and plasmacytoid DCs (pDCs)[26,35–37]. DCs are

proposed to arise in a sequence of DC differentiation progresses from the common monocyte/macrophage DC progenitor (CMP) to a common DC progenitor (CDP) cell that can then differentiate only into cells of the DC lineage, including conventional DC lineages and pDCs[37,38]. pDCs are specialized to sense and respond to viral infection through several mechanisms by the rapid production of high quantities of type I and type III interferons and secretion of cytokines.[39,40] Conventional DC1s are specialized in cross-presentation of dead-cell-associated antigens and in T-helper type 1 (T_h1) and cytotoxic T lymphocyte priming and thus play a crucial role in fighting intracellular pathogens that have been engulfed[41], while cDC2s mainly present antigens to CD4 positive T-cells and elicit T_h2 and T_h17 responses upon exposure to extracellular pathogens[42,43]. The described DC subtypes are however further discriminated from monocyte-derived DCs (moDCs)[44,45].

Cells of the myeloid compartment are of great clinical relevance, as the evidence for their implications in the etiology and pathophysiology of diseases is ever growing. Inflammation for instance changes the composition of myeloid cell populations found in diseased tissue. As described earlier, monocytes are recruited to sides of inflammation, they infiltrate and acquire characteristics similar to the tissue-resident cells depending on the tissue environment as well as on the disease conditions. Another example is atherosclerosis, which is a pathophysiological condition in which myeloid cells play a crucial role in the etiology. In addition to the tissue-resident macrophages present in healthy and atherosclerotic aortic arches, plaques were found to contain monocytes, moDCs, and two atherosclerosis-specific populations of inflammatory macrophages, one of which was characterized as Trem2 positive[46].

So, human *in vitro* generated moDCs and macrophages (moM) are of clinical importance as they can be used to study induced immunity and the cell specific impact in environmentally induced diseases.

Murine granulocyte macrophage colony- stimulating factor (GM-CSF) or macrophage colony-stimulating factor (M-CSF) driven bone marrow-derived DC and macrophage cultures are frequently used to elucidate and assign molecular mechanisms of functions to subsets of mononuclear phagocytes. However, using high-dimensional techniques, scientists could recently elucidate transcriptional, phenotypic, and functional differences between human *in vivo* and *in vitro* generated mononuclear phagocytes showing that *in vitro* differentiated monocytes are transcriptionally unique

compared to *ex vivo* human peripheral blood cells[44]. Based on transcriptomic analysis, Sander J. *et. al.*, 2017 could though show that there is high correlation between *in vivo* inflammatory dendritic cells and *in vitro* cultured monocytes with GM-CSF and IL-4 and between *in vivo* inflammatory macrophages and both *in vitro* cultured monocytes with either GM-CSF or M-CSF. These findings reveal a close association of monocytes differentiated by M-CSF and GM-CSF, while IL-4 was shown to be the major driver for monocyte derived DC identity.

In more detail, the scientists found out that many genes associated with activated DCs (CCL22, MMP12, CD226, CCR7) were highly elevated in both inflammatory DCs and monocytes cultured with GM-CSF and IL-4, while typical macrophage genes (MARCO, CCL2, VSIG4) were most highly expressed in inflammatory macrophages and monocytes cultured with either M-CSF or GM-CSF[44]. Nevertheless, using gene ontology enrichment analysis (GOEA) they could also show a clear separation of cellular processes taking place in monocytes cultured with GM-CSF and such cultured with M-CSF, respectively. Enriched terms in MOs-GM-CSF were rather associated with immune response and regulation of protein metabolism, while most terms enriched in MOs-M-CSF were associated with metabolism and G-protein-coupled receptor signaling. A clear separation was also demonstrated in sense of identified master transcription factors. NFIL3, ATF4, and ETS2 seemed to be putative regulators of CD14+ monocytes, while TCF12, MEF2C, and ARID3A were shown to specifically regulate MOs-M-CSF, and ESR1, MTF1, and SREBF1 were shown to regulate MOs-GM-CSF identity. RELB, an important regulator of mouse DC differentiation[47], was thereby presented as central regulator of the transcriptional identity of MOs-GM-CSF-IL-4, which highlights the uniqueness of the transcriptional identity induced by GM-CSF and IL-4 together[44]. By the use of different durations of IL-4 stimulations they could however also demonstrate that monocytes integrate GM-CSF and IL-4 combinatorically and temporally, resulting in gradually changed transcriptional and functional identities of monocyte-derived cells[44].

The observations of Sander J. *et al*.,2017 support a dynamic differentiation model in which cell identity is not only a function of specific and combinatorial signal input but also of the duration of the input. Thus, the identification of specific monocyte-derived cell models was of pivotal importance to study inflammatory macrophage or DC subsets in disease states or under specific environmental conditions. However,

scientists should always be aware of the versatility of *in vivo* and *in vitro* cultured cells and therefore *ex vivo* results can just be taken as hypothesis and need to be confirmed *in vivo*.

1.3.1 Pattern recognition and induction of receptor signaling pathways

As previously described, the innate immune system uses germline-encoded PRRs for the initial detection of microbes by recognition of PAMPs and DAMPs. The TLR family of PRRs is thereby one of the best studied group of pattern recognition receptors. TLRs are localized at the cell surface or in intracellular compartments such as in endosomes, lysosomes, endo-lysosomes or the endoplasmic reticulum (ER) where they recognize PAMPs such as lipid, lipoprotein, protein, and nucleic acid[48,49]. TLRs are type I integral membrane receptors, with an N-terminal ligand recognition domain, a single transmembrane helix, and a C-terminal cytoplasmic signaling domain[50]. The ectodomain with leucine-rich repeats (LRRs) mediates PAMP recognition and the cytoplasmic Toll/IL-1 receptor (TIR) domain initiates downstream signaling[51].

After ligand binding, individual TLRs differentially recruit members of a set of TIR domain-containing adaptors such as myeloid differentiation primary-response protein 88 (MyD88) and MyD88-adaptor-like protein (MAL/TIRAP), or TIR domain-containing adaptor protein inducing IFN-β (TRIF) and TRIF-related adaptor molecule (TRAM)[51]. MyD88 is utilized by all TLRs except TLR3[52] and triggers activation of the transcription factor NF-κB and mitogen activated protein (MAP)-kinases for the induction of inflammatory cytokine gene expression, including TNF, IL1B and IL6. MAL, also termed TIRAP, is involved in bridging MyD88 to the receptor complex for TLR2, TLR4 as well as for endosomal TLR9 signaling in response to PAMP recognition.[53]

TRIF on the other hand, is recruited to TLR3 and TLR4 and provokes an alternative pathway which leads to the activation of the transcription factor IRF3, NF-κB and MAP kinases for the induction of type I interferons and pro-inflammatory cytokine gene expression such as IFNB1, CCL5 and CXCL10[53,54]. The gene product of IFNB1, IFN-β binds to the type 1 IFN receptor (IFNR), which, in turn, activates a JAK-STAT pathway inducing the expression of surface molecules required for the interaction with T-cells, such as CD40, CD80, and CD86[55,56]. Together, the activation of NF-κB and JAK-STAT also induces the expression of inducible nitric monoxide synthase (iNOS),

whose product, nitric oxide (NO) is an important mediator of inflammation serving the elimination of microbes, parasites and cancer cells[57,58].
While TLR3 directly interacts with TRIF, TLR4 requires the adapter protein TRAM for interaction. Hence, TRAM provides specificity for the MyD88-independent component of TLR4 signaling.

Collectively, depending on the adaptor usage, TLR signaling is largely divided into two pathways: the MyD88-dependent and TRIF-dependent pathways, counting for an inflammatory or regulatory-inflammatory state of the cell, respectively.

Several reports showed a possible mechanistic link between free fatty acids (FFAs) and innate immune toll-like receptors in metabolic disease[59]. Further, palmitic acid (PA), and other saturated fatty acids are known to stimulate pro-inflammatory responses in human myeloid-derived cells via activation of TLR4[60]. However, recently scientists provided evidence that TLR4 indirectly regulates long chain saturated fatty acid induced inflammation by altering macrophage lipid metabolism[61]. It also has been described that TLR4 mediates LPS-induced macrophage activation of IL-1β and IL-6 gene expression, chemotaxis, phagocytosis, and oxidative ability[62]. Moreover, previous studies showed that activation of TLR4 by LPS results in epigenetic re-programming which may result in increased responsiveness to other pathogenic factors but is known to result in tolerance to secondary challenge to LPS[63,64]. Endotoxin tolerance has been linked to the pro-inflammatory MyD88-dependent transcriptional program, whereas TRIF- dependent genes were shown to be involved in the induction of endotoxin tolerance[54,63].

Another group of cytoplasmic PRRs that perform diverse immunological functions is the Nod-like receptors (NLR) family [65]. A subgroup of NLR, namely NLRP1, NLRP3 and NLRC4, and the PYHIN family member AIM2, examine the cytoplasm for danger signals and trigger the assembly of an inflammasome, a multiprotein complex[66,67]. Inflammasome formation requires the PRR as the sensor, and (in most cases) the adaptor apoptosis-associated speck-like protein (ASC) containing a caspase-recruitment domain (CASP), as well as the cysteine protease caspase-1. After assembly, the inflammasome triggers the proteolytic cleavage of dormant pro-caspase-1 into active caspase-1, which converts the cytokine precursors pro-IL-1β and pro-IL-18 into mature and biologically active IL-1β and IL-18, respectively[68,69]. While the production of most pro-inflammatory cytokines is primarily regulated at the

transcriptional level, secretion of IL-1β and IL-18 requires this additional proteolytic step. This two-step mechanism first requires stimulation through TLR or RLR, inducing the synthesis of IL1β and IL-18 as inactive precursors, which lack their signal peptide, as well as the inactive inflammasome components. In the second step, NLR-mediated inflammasome activation catalyzes the post-translational processing, required for the secretion and bioactivity.

Importantly, mature IL-1β is a potent pro-inflammatory mediator in many immune reactions, including the recruitment of innate immune cells to the site of infection and activation of adaptive immune cells.[70] Mature IL-18, on the other hand, is central for the production of interferon gamma (IFN-ɣ) and the potentiation of the cytolytic activity of NK- and T-cells [71]. Active caspase-1 is not only responsible for the cleavage of stated cytokines, but also induces a pro-inflammatory form of cell death, known as pyroptosis[72].

The best characterized inflammasome is the NLRP3-inflammasome. It comprises the NLR protein NLRP3, the adapter ASC, pro-caspase-1 and the serine-threonine kinase NEK7[73]. While all inflammasomes recognize certain pathogens, activation of the NRLP3 inflammasome can be triggered by numerous stimuli, chemically and structurally highly different. Thus, NLRP3 is most versatile, and also the most clinically implicated inflammasome.

The pro-inflammatory cytokine IL-1β is not only involved in immune reactions to infectious agents, but also in the development of many obesity-associated diseases, such as atherosclerosis, type II diabetes, and gouty arthritis[74]. Free fatty acids, usually elevated in plasma of obese people, have been proposed as one triggering event for NLRP3-inflammasome activation. Scientists already demonstrated that the saturated fatty acid palmitic acid (PA) has the capability to activate the NLRP3 inflammasome in murine macrophages[75].

1.4 Trained immunity and tolerance on monocytes and monocyte derived cells

Classically, immunological memory refers to an adaptive immune response, carried out by T- and B-lymphocytes, in response to secondary or tertiary infection with a pathogen. The immunological memory occurs after a primary (innate) immune

response against an antigen, after which a small number of memory T and B cells remain in the body and make up the cellular component of the immunological memory, which develop slowly but are very specific. Just recently, scientists challenged the dogma that only adaptive immunity can build immunological memory by studies that show that innate immune responses in invertebrates and plants, organisms that lack adaptive immune responses, can also elicit resistance to re-infection.

“Trained Immunity” is a term, introduced by *Mihai Netea*, that was established to describe the ability of the innate arm of the mammalian immune system to show enhanced responsiveness to re-infection with the same or a different pathogen[64]. It describes the phenomenon that innate immune cells such as monocytes, macrophages and natural killer cells can actually ‘remember’ pathogens and react with an enhanced response to a secondary infection with the same, as well as with a different pathogen, through mechanisms independent of adaptive immune responses[64]. In this context it is described that innate immune activation by infections or vaccinations leads to epigenetic changes, like histone modifications, and functional reprogramming of the immune cells[76]. The epigenetic rearrangements, which largely drive innate immune memory, generally are defined as sustained changes in transcriptional programs that lead to non-permanent changes in cell physiology but they do not involve permanent genetic changes like recombination or mutations. Trained immunity is shorter lived and less specific than classical memory but still is thought to push our immune cells to a stronger response to re-occurring pathogens, and thus typically to a faster recovery. For instance, *Netea* and colleges could show that binding of the surface receptor Dectin-1 to β-glucan, a cell wall component of the fungus *Candida albicans*, causes epigenetic changes in human monocytes that lead to a degree of training or memory in monocyte derived macrophages which evokes an increased release of inflammatory cytokines in response to a subsequent stimulation with LPS[77].

In contrast to the training obtained upon engagement of Dectin-1, *Netea* could also show that the stimulation of the membrane receptors TLR2, TLR4, and TLR5 by inflammatory doses of Pam3CSK4, LPS, and flagellin induced a long-term tolerant state in which monocytes produced fewer of the pro- inflammatory cytokines TNF-α and IL-6 upon re-stimulation than un-treated control cells did[77].

Considering the traditional assessment of the effects of tolerance as a hypo-inflammatory state while trained immunity results in an augmented production of pro-inflammatory cytokines, these two programs appear to be functional opposites.

1.5 Obesity and diet induced diseases

In the USA and Western countries, the replacement of the regular intake of healthy oils and fibers for a diet substantially based on high fat and high sugar content had severe consequences for public health. This change in dietary habits resulted in an epidemic of obesity with an worldwide prevalence of obese adults that has nearly tripled since 1975[78]. Speaking in numbers, 2016 more than 1.9 billion adults (≥ 18 years) were overweight (39 %), of which 650 million were obese (13 % of world population)[79]. Even 340 million children and adolescent aged 5 to 19 years, and 41 million children under the age of 5 were overweight or obese in 2016.[78,80] Currently, the weight classification of the world health organization (WHO) is based on the same body mass index (BMI) thresholds for adult males and females. Overweight is defined as a BMI equal to or more than 25 kg/m² and includes overweight (25 to <30 kg/m²) and obesity (≥ 30 kg/m²). Obesity in turn is subdivided into classes I (30 to <35 kg/m²), II (35.0 to <40 kg/m²) and III (≥ 40 kg/m²).[81]

The consequences of obesity are versatile and an approximate statistical prevalence of ~ 500 million people are suffering from its synergistic morbidities[82]. Already being overweight can lead to serious health consequences since the excess of macronutrients in the adipose tissue stimulates adipose tissue cells to release pro-inflammatory mediators such as TNF-α and IL-6 while downregulating the expression of adiponectin[83], which together with Leptin and Insulin regulates hunger and food intake. This leads to predisposition for a low-grade systemic inflammatory state and oxidative stress as well as for insulin resistance and an increase of hunger feeling. Inflammation is a risk factor for developing cardio vascular diseases (CVDs)[84] including atherosclerosis, metabolic syndrome, insulin resistance and diabetes mellitus.[85] Additionally, overweight is associated with diseases like depression, psoriasis, renal diseases and also some forms of cancer.[86–89]

1.5.1 Dietary fatty acids

Too much, too fatty, too salty, too sweet. In industrialized countries like Germany most diseases and afflictions are provoked by a small number of chronic diseases, all of which are correlated to disadvantageous dietary habits and an uncritical choice of eatables. Our eating behaviors do not fit our living and work behaviors. An increasing number of people work at the desk but are nourishing like doing hard physical work. The body constantly gets more than needed, especially too much fat. Thereby it has to be distinguished between healthy and unhealthy fats. Saturated fatty acids (SFA) are rather unhealthy while unsaturated fatty acids are indispensable for our body[90]. Saturated fatty acids are component of any animal products like butter, milk, meat and sausages. Moreover, they are component of hard vegetable oils like coconut fat, palm fat or other hardened vegetable oils, which are almost always part of sweet pastries or fried food[90]. Convenience meals and fast foods generally have high contents of saturated fats. It is well established that SFAs increase low-density lipoprotein (LDL) cholesterol, a strong risk factor for CVD[91].

Unsaturated fats are considered to be more health beneficial than saturated fats or trans fats and fall into two categories, mono-unsaturated (MUFA) and poly-unsaturated fatty acids (PUFA). MUFAs are associated with lowering LDL cholesterol and total cholesterol but at the same time increasing the production of the ‘good’ cholesterol, high-density-lipoprotein (HDL).[92–94] They have one double bond in the fatty acid chain with all of the remaining carbon atoms being single-bonded. MUFAs are usually liquid at room temperature and are found in olive oil, rapeseed oil, but also in vegetables like avocados, olives as well as in hazelnuts and macadamia nuts[90].

PUFAs are fats in which the constituent hydrocarbon chain possesses two or more carbon–carbon double bonds and they are of high importance for humans as our body is not able to synthesize them by its own. For instance, the PUFA linoleic acid (LA) plays an important structural role in cell membranes and gives rise to arachidonic acid, which is the major precursor of a series of bioactive metabolites called eicosanoids, which regulate a large number of physiological processes[95]. Essential PUFAs of a different structure with important health benefits include omega-3 fatty acids and omega-6 fatty acids. A PUFA is called omega-3 when the first double bond is located at the third carbon from the methyl group (CH_3) and omega-6 when the double bond is

at the sixth carbon of the chain from the same radical. Omega-3 fatty acids are primarily found in fish but can also be gained from non-fish sources by processing linoleic acid[96]. These fats are considered to be especially health beneficial as they are linked to improving immunity, rheumatoid arthritis, eye-sight, brain function, and heart health, as they lower both triglyceride levels and total cholesterol levels. Omega-6 fatty acids are also associated with reducing CVD risk by lowering LDL cholesterol levels, but they may also lower HDL levels.[97] Further, n-6 PUFAs exert mostly pro-inflammatory features, while n-3 PUFAs have anti-inflammatory and pro-resolving effects [98]. Therefore, the omega-6 fatty acids should be consumed in a balanced ratio with omega-3 fatty acids. Anthropological evidence suggests that the ratio human beings evolved eating was somewhere around 1:1, while the ratio today is about 16:1 (n-6:n-3)[99]. Good sources for PUFAs include fatty fish like salmon and herring, flaxseed oil, sesame oil, corn oil, sunflower seeds and sunflower oil as well as walnuts.

Other fats that can be found in Western diets are trans fats. Trans fats are a type of saturated fat that occur only in small amounts in nature but are widely created when food manufacturers want to extend the shelf life of foods containing fats by addition of a hydrogen to their chemical structure. The addition of the hydrogen makes the fats firmer and even more saturated, delaying rancidity and thus extending freshness. Trans fats are associated with increasing LDL and total cholesterol while lowering the good HDL cholesterol.[100] They are widely produced industrially from vegetable fats for use in margarine, snack food, frying fast foods and packaged baked goods. Trans fats occur also naturally and can be found in small amounts in beef, pork, butter and milk. These trans fats however have different effects from the man-made ones and are not associated with the same effects on cholesterol levels. Trans fats are in an intake-dependent manner consistently associated with increased risk of CVD.[90,100]

Taken together, fats are essential for health and need to be consumed every day. They are a good energy source and are a necessary nutrient to use fat-soluble vitamins (A, D, E, K)[101]. Further, fats play a huge role in metabolism, growth, bone protection, brain and nervous system function, as well as skin integrity[102,103]. But not all fats are the same or provide the same health benefits. High consumption of foods containing high amounts of saturated fats or trans fats may not only lead to obesity, but also to metabolic syndrome which is a constellation of hypertension, diabetes, dyslipidemia and fatty liver disease, which further increase the risk for CVD.[103]

The Mediterranean diet, in contrast to Western diet, is a diet inspired by the eating habits of Greece, Southern Italy, and Spain in the 1940s and 1950s and typifies a very balanced and healthy nourishment[105]. This diet is characterized by a low glycemic load, a high intake of healthy fats such as olive oil and fish oil, and low intake of processed meats, saturated fats, and trans fats. Mediterranean diet has been associated with several health benefits[104], including reduced total mortality, a reduced risk of selected cancers[105,106], cognitive impairments[107,108], all components of the metabolic syndrome[109], as well as a reduced risk for CVD[110].

1.5.2 Oleic acid (OA) and palmitic acid (PA) as representatives of unsaturated and saturated fatty acids in diet and their effect on insulin resistance

Dietary fats are an important energy source and the “United States Department of Agriculture (USDA) 2010 Dietary Guidelines for Americans” recommend daily total fat intake of 20% to 35% of energy intake, with saturated fatty acid (SFA) intake of <10% of energy and trans fatty acid intake as low as possible[111].

Fatty acids do not only differ in their saturation or unsaturation states but are also classified according to their length. Short-chain FAs have a chain length of 2 to 6 carbon atoms, medium-chain FAs contain between 7 and 12 carbon atoms, long-chain FAs have a length of 13 to 22 carbon atoms and the very-long-chain FAs go ahead with more than 22 carbon atoms. Long-chain fatty acids play an important role in the biological functions of cells. They serve as a source for metabolic energy, as substrates for cell membrane biogenesis and as precursors for several intracellular signaling molecules such as prostaglandins and leukotrienes[112]. Free fatty acids are generally derived from the breakdown of triglyceride molecules, which are released from adipose tissue and transported into the blood stream. Under conditions of metabolic dysfunction, cellular components of the innate immune system may be activated by excess FFAs, leading to pathologic consequences. For example, macrophages play a crucial role in the initiation of a chronic inflammatory state in obesity which may lead to several pathologic conditions like CVD and insulin resistance. In healthy individuals, plasma total FFA concentrations range from 200 – 600 µM[113,114] while under pathologic conditions such as obesity and diabetes levels can increase to 400-2000 µM, depending on the individual’s diet and variations in the serum insulin level[115,116].

Plasma free fatty acids released by adipose tissue reflect fat intake. Oleic acid (C18:1) and palmitic acid (C16:0) are the most abundant dietary and plasma FAs and represent 31% and 27% of total plasma FFA concentrations, respectively[117]. With their chain length they both belong to the long chain FAs but differ in their saturation state. Palmitic Acid is a saturated fatty acid with a 16-carbon backbone and is found naturally in palm oil and palm kernel oil, as well as in butter, cheese, milk and meat. Oleic acid is a mono-unsaturated omega-9 fatty acid that is the most widely distributed and abundant fatty acid in nature. Stearic acid (C18:0), which is the saturated counterpart to OA, is the second most occurring SFA in nature and can be derived from either animal fats or vegetable oils.[103,118]

The expansion of adipose tissue in obese individuals is associated with an expansion of non-esterified fatty acids (NEFAs), hormones, pro-inflammatory cytokines and other factors that are involved in the development of insulin resistance and Type II diabetes mellitus (T2DM). The SFA palmitic acid and the MUFA oleic acid contribute however differently to insulin resistance. Palmitic acid was reported to mediate insulin resistance and T2DM in three main mechanisms, namely (I) increased synthesis of deleterious complex lipids, (II) impaired function of cellular organelles and (III) receptor-mediated inflammation.

(I) When PA is increasingly internalized this FA exceeds its oxidative needs and is processed in deleterious non-oxidative metabolic pathways which leads to increased levels of diacylglycerol (DAG) and ceramide. As DAG activates novel protein kinase C (PKC)[119] the insulin signaling pathway is ultimately attenuated by phosphorylation of the insulin receptor substrate (IRS)-1 at serine residues, leading to impairment of insulin signaling. Further, inflammation may be provoked by certain PKC isoforms by activation of the pro-inflammatory signaling cascade inhibitor of NF-κB (IκB) kinase (IKK)b–NF-κB[119]. The increase in ceramide leads to activation of the NLRP3 inflammasome-mediated release of interleukin IL-1β and also leads to the activation of protein phosphatase 2A (PP2A) and PKC, which both attenuate the insulin signaling pathway[120].

(II) Excess palmitic acid can also affect functioning of mitochondria and ER which may result in the production of reactive oxygen species (ROS) and ER stress which further promotes pro-inflammatory responses and apoptosis due to activation of NF-κB, c-Jun N-terminal kinase (JNK), and NLRP3 inflammasome pathways.[121]

(III) PA is further described to activate proinflammatory pathways through membrane receptors such as TLR-4 leading to the activation of proinflammatory transcription factors such as NF-κB. Besides that, SFAs can modify the gut microbiota which leads to an increase in LPS levels after high fat intake, further enhancing TLR4 activation.[122,123]

On the contrary, studies of subjects that reduced their SFA intake and increased their MUFA intake resulted in a significant improvement of insulin sensitivity[124]. This advantageous effect of OA on insulin sensitivity may even explain the protective effects of the Mediterranean diet against both obesity and T2DM.

1.5.3 Free fatty acids and chronic inflammation

Metabolic homeostasis is hampered following excess nutrient intake during obesity and is linked to the induction of a chronic, inflammatory response with an interaction between metabolic (adipocytes) and immune cells, in particular macrophages. Metaflammation is the scientific term to describe this physiological state[125]. While there may be several mechanisms through which increased adiposity could lead to widespread inflammation, it is established that plasma FFA concentrations are significantly increased in close association with obesity[126], which is associated with the accumulation of immune cells such as macrophages and dendritic cells, that infiltrate the adipose tissue. Subsets of these accumulating myeloid cells express inflammatory markers and secrete pro-inflammatory cytokines that also comprise the response to LPS stimulation[127,128,129]. The saturated FFA palmitic acid has been shown to provoke a pro-inflammatory phenotype in cultured macrophages[1] while the MUFA oleic acid is rather described to triggers an anti-inflammatory M(IL4) like phenotype[2]. These pro-inflammatory macrophages trigger inflammatory signaling and stress responses that signal via TLR4 through JNK or IKKβ pathways. If over-nutrition persists, mechanisms that counteract inflammation (such as PPAR signaling) are suppressed, and the inflammation becomes chronic[130].

1.*6* The impact of fatty acid metabolism on myeloid cell differentiation

Metabolism provides not only energy to immune cells, but also actively influences diverse immune cell phenotypes. Fatty acid metabolism, particularly mitochondrial fatty

acid oxidation (FAO) emerges as an important regulator of innate immune cells. Catabolism of fatty acids, on the other hand, may even modulate the progression of disease, such as the development of obesity driven insulin resistance and T2DM.

In macrophages, the classical (M-IFN-ɣ) activation program has been noted to rely on glycolysis and later fatty acid synthesis (FAS)[131,132], while fatty acid oxidation has been implicated in the polarization of macrophages to the alternative (M-IL4) phenotype[133–135]. IL-4 stimulated anti-inflammatory macrophage polarization, for instance, increases FAO and the corresponding metabolic gene program, while inflammatory signals including LPS and IFN-ɣ, that are required to generate the classical inflammatory phenotypes, have been shown to drive FAS. Interestingly, cellular longevity is also thought to be supported by FAO[136,137].

Also, in moDC generation fatty acid metabolism seems to play an essential role as the nuclear receptor peroxisome proliferator activated receptor-ɣ (PPAR-ɣ), which is important in fatty acid metabolism, is significantly up-regulated in human monocyte-derived DCs induced by GM-CSF and IL-4 *in vitro* and largely affects cell maturation and function. It was described that fatty acid synthesis is essential for moDC differentiation while especially fatty acid oxidation seems to be essential for the expansion of $CD11b^+$ inflammatory DCs under allergic status in lung.[138,139]

Myeloid cells, like macrophages take up LDL, VLDL and oxidized lipoproteins via macro-pinocytosis, phagocytosis and scavenger receptor-mediated pathways[140]. Free cholesterol and fatty acids are generated following degradation of ingested lipids in the lysosome. Such cholesterol can be utilized to form lipid rafts. Accumulation of cellular cholesterol leads to activation of several transcription factors, including PPAR-ɣ, Liver X receptors (LXRs) and retinoid CX receptors (RXRs)[141,142] which subsequently regulate expression of their target genes including transporters such as ABCA1 and ABCG1 which regulate the efflux of free cholesterol and scavenger receptors[143–145]. Alternatively, passive efflux of free cholesterol can also occur via simple or facilitated diffusion[146].

Functionally, PPAR-ɣ has been described to control the inflammatory potential of myeloid cells by driving anti-inflammatory phenotype polarization and inhibiting pro-inflammatory gene expression including IL1-β, IL-6, TNF-α, IL-12 as well as iNOS[134,147,148]. For example, uptake of the fatty acids enabling FAO in M-IL4

phenotypes was shown to occur via the CD36 receptor which is induced by IL-4 and subsequent lysosomal lipolysis mediated by lysosomal acid lipase [149]. The oxidation of long-chain fatty acids in mitochondria requires transfer from the cytoplasm via acyl-coenzyme A (acyl-CoA). This is mediated by the coordinated action of the two enzymes carnitine palmitoyltransferase 1A and 2 (CPT1, CPT2).[133,150] CPT1A, the rate-limiting enzyme in mitochondrial long-chain fatty acid oxidation, generates acylcarnitines that can cross the mitochondrial membrane. Once inside, CPT2 removes the carnitine and initiates the oxidation of long-chain fatty acids to acetyl-CoA. This process yields in large amounts of acetyl-CoA, NADH and $FADH_2$ that are subsequently used in the TCA cycle and electron transport chain to generate ATP. The balance of fatty acid synthesis and fatty acid oxidation is regulated by the rate-determining metabolite in de novo fatty acid synthesis, malonyl-CoA, which can directly inhibit CPT1A activity.[150,151]

The current study sheds light on the direct effect of the saturated fatty acid PA and the unsaturated fatty acid OA on monocyte activation and differentiation based on the transcriptional profiles, giving rise to pro- or anti-inflammatory monocyte-derived cell functions. Further, the ability to develop a memory rendering the response to later bacterial infection, using LPS, was investigated.

2. Objectives

“Trained Immunity” describes the phenomenon that innate immune cells such as monocytes, macrophages and natural killer cells can actually ‘remember’ pathogens and react with an enhanced response to a secondary infection with the same, as well as with a different pathogen, through mechanisms independent of adaptive immune responses[64]. In this context it is described that innate immune activation by infections or vaccinations leads to epigenetic changes, like histone modifications, and functional reprogramming of the immune cells[76].

Also, dietary compounds like free fatty acids have been described to have an activating effect on myeloid-derived cells, however, depending on the saturation state into opposing directions.

In this study I investigated the direct effect of palmitic acid (saturated fatty acid), and oleic acid (unsaturated fatty acid), on the activation of monocyte-derived cells and their influence on trained immunity or tolerance upon re-stimulation with LPS. To analyze, how these factors influence monocyte-derived cell biology, RNA sequencing and enzyme-linked immunosorbent assay (ELISA) was performed. In a next level study, further insights into epigenetic modifications may be utilized by implemented techniques for Chromatin-Immunoprecipitation (ChIP) and Assay for Transposase-Accessible Chromatin (ATAC) followed by high throughput sequencing.

Illuminating the importance of dietary influences on the transcriptome and epigenome of immune cells as well as on their transcriptional memory may enable us to better understand the effects of diet leading to immunological diseases.

3. Materials

3.1. Chemicals and reagents

Agencourt AMPure XP beads	Beckman Coulter, Brea, USA
BSA	New England Biolabs, UK
Complete protease inhibitors	Hoffmann-La Roche, Basel, CH
Anti-CD61-Micobeads	MiltenyiBiotech, Bergisch Gladbach, DE
dATP	New England Biolabs, UK
dNTP solution	New England Biolabs, UK
Dynabeads protein G	Invitrogen Life Technologies, Karlsruhe, DE
EDTA	Calbiochem, San Diego, USA
EGTA	Calbiochem, San Diego, USA
Ethanol	Roth, Karlsruhe, DE
Fetal calf serum	Invitrogen LifeTechnologies, Karlsruhe, DE
Formaldehyde 16% (wt/vol)	Thermo Scientific, Massachusetts, USA
GeneRuler 1 kb Plus DNA Ladder	Thermo Scientific, Massachusetts, USA
Glutamax	Invitrogen Life Technologies, Karlsruhe, DE
Glycerol	Calbiochem, San Diego, USA
Glycine	Calbiochem, San Diego, USA
Glycogen	Roche Diagnostics GmbH, Mannheim, DE
HEPES buffer	Calbiochem, San Diego, USA
Klenow enzyme	New England Biolabs, UK
KOH solution	Sigma Aldrich, Taufkirchen, DE

Lithium chloride	Sigma Aldrich, Taufkirchen, DE
NEB buffer 2	New England Biolabs, UK
Pan Monocyte Isolation Kit	MiltenyiBiotech, Bergisch Gladbach, DE
Pancoll	PAA Laboratories GmbH, Pasching, AT
PBS	PAA Laboratories GmbH, Pasching, AT
PEG-8,000	Sigma Aldrich, Taufkirchen, DE

3.2. Cytokines and fatty acids

rh GM-CSF	Immunotools, Friesoythe, DE
rh M-CSF	Immunotools, Friesoythe, DE
Palmitic Acid	Sigma Aldrich, Taufkirchen, DE
Oleic Acid	Sigma Aldrich, Taufkirchen, DE
Stearic Acid	Sigma Aldrich, Taufkirchen, DE

3.3. Antibodies

Table 3.3.1: Antibody List for ChIP experiments

Antigen	Host	IgG Type	Company
H3K27Ac	Rabbit	Polyclonal	Abcam, Cambridge, UK
H3K27me3	Rabbit	Polyclonal	Merck Millipore, Billerica, USA
H3K4me1	Rabbit	Polyclonal	Abcam, Cambridge, UK
H3K4me3	Rabbit	Monoclonal	Merck Millipore, Billerica, USA
H3	Rabbit	Monoclonal	Merck Millipore, Billerica, USA
IgG	Rabbit	Polyclonal	Abcam, Cambridge, UK

Table 3.3.2: FACS-Antibody-Panel used for Monocyte Purity Check

Anibody	Stain	Clone	Company
CD61	PE	Y2/51	Miltenyi Biotech
CD19	APC/CY7	HIB19 (RUO)	BD Pharmingen
CD66b	FITC	G10F5	Biolegend
CD56	AlexaFluor647	B159	BD
CD14	Pac Blue	M5E2	Biolegend
CD16	BV605	3G8 (RUO)	BD
CD45	PerCp	HI30	Biolegend
CD123	PE CF594	7G3	BD
CD11c	PE/Cy7	3.9	Biolegend
CD3	BV510	OKT3	Biolegend

Table 3.3.3: FACS-Antibodies used for Life-Dead staining

Anibody	Stain	Catalog Number	Company
Annexin-V	FITC	556419	BD Pharmingen™
Propidium Iodide (PI)	PE	81845	Sigma Aldrich

3.4. PCR primers

Primers were designed with the Beacon Designer software and oligonucleotides were ordered from Sigma-Aldrich (Taufkirchen, DE).

3.4.1 RT- PCR primers for ChIP quality control

Semi-quantitative real time PCR experiments were performed with listed primers to validate performed ChIP-seq experiments. Primers were either designed to target sites with known associated HM enrichments as positive controls (pos.) or negative sites without corresponding target HM (neg.).

Table 3.4.1.1: Primer list for ChIP quality control qPCRs

Primer:	Sequence:	Value:
BMP2_fwd	5‘-CTCAGCACTCCGCATTTG-3‘	pos. control for H3K27me3 & neg. control of H3K4me3
BMP2_rev	5‘-CTCCCATCCAACGCTTAG-3‘	
GAPDH_MP_fwd	5’-TACTAGCGGTTTTACGGGCG-3’	pos. control for H3K4me3 & neg. control of H3K27me3
GAPDH_MP_rev	5‘-TCGAACAGGAGGAGCAGAGAGCGA-3‘	
H3K27Ac_GAPDH_fwd3	5’-AGGCTGGATGGAATGAAAGG-3’	pos. control for H3K27Ac
H3K27Ac_GAPDH_rev3	5‘-CAGGCGGAGGACAGGATG-3‘	
H3K4me1_GAPDH_fwd1	5‘-TGCTCTTGCTACTCTGCTCTG-3‘	pos. control for H3K4me1
H3K4me1_GAPDH_rev1	5‘-GGCTGTGTCCTCGTCTGG-3‘	
Neg Ctrl 1 H3K4me1/H3K27Ac fwd	5’-ATTATTGATGGAGAAATGTTG-3’	neg. control forH3K27Ac & H3K4me1
Neg Ctrl 1 H3K4me1/H3K27Ac rev	5’-ACTGTGGAATACCTAAGC-3’	

3.4.2 qPCR primers for fatty acid stimulation quality control

Quantitative PCR experiments were performed with listed primers to validate fatty acid uptake by monocytes. Primers were designed to target sites with known association to transcriptomic response to saturated and unsaturated fatty acid stimulation in monocytes.

Table 3.4.2.1: Primer list for quantitative PCRs of Trained Immunity Experiments

Primer:	Sequence:
hCCL3_fw #56	5‘-CAGAATCATGCAGGTCTCCAC-3‘
hCCL3_bw #56	5‘-GCGTGGTCAGCAGCAAGTG-3‘
hIL-1b_fw #78	5‘-TACCTGTCCTGCGTGTTGAA-3‘
hIL-1b_rev #78	5‘-TCTTTGGGTAATTTTTGGGATCT-3‘
hCCL4L2_fxd#20	5‘-CTTCCTCGCAACTTTGTGGT-3‘
hCCL4L2_rev#20	5‘-GCAGACTTGCTTGCCTCTTT-3‘
hIL8_fw #72	5‘-AGACAGCAGAGCACACAAGC-3‘
hIL8_bw #72	5‘-ATGGTTCCTTCCGGTGGT-3‘
hPON-2_fwd_#21	5‘-TCCACCTGCCACCTGATTA-3‘
hPON-2_rev_#21	5‘-AGCCAGACCATTGGGAAGTAT-3‘
hRCAN-1_fwd_#21	5‘-TGCGACCCCAGTCATAAACT-3‘
hRCAN-1_rev_#21	5‘-GCGTGCAATTCATACTTTTCC-3‘
hGAPDH_fwd#60	5‘-AGC CAC ATC GCT CAG ACA C-3‘
hGAPDH_rev#60	5‘-GCC CAA TAC GAC CAA ATC C-3‘

3.5 ATAC primers

Table 3.5.1: Pre-Annealing of Primer A with reverse and B with reverse for Tn5 loading:

Primer:	Sequence:
Tn5MErev	5‘-[phos]CTGTCTCTTATACACATCT-3‘
Tn5ME-A (Illumina FC-121-1030)	5‘-TCGTCGGCAGCGTCAGATGTGTATAAGAGACAG-3‘
Tn5ME-B (Illumina FC-121-1031)	5‘-GTCTCGTGGGCTCGGAGATGTGTATAAGAGACAG-3‘

3.5. Plastic ware

Amicon Ultra 0.5 ml Centrifugal Filters (Ultracel-50 K)	Merck Millipore, Darmstadt, DE
0,2 - 2 ml Eppendorf tubes	Eppendorf GmbH, Hamburg, DE
1.7 ml siliconized tubes	Sigma Aldrich, Taufkirchen, DE
Falcon 15 ml	Greiner bio-one, Frickenhausen, DE
Falcon 50 ml	Greiner bio-one, Frickenhausen, DE
LS columns	Miltenyi Biotech, Bergisch Gladbach, DE
Microtube, AFA fiber	Covaris, Woburn USA
Nunclon™ 94-well tissue culture plate	Thermo Scientific, Rockford, US
Nunclon™ 48-well tissue culture plate	Thermo Scientific, Rockford, US
Nunclon™ 12-well tissue culture plate	Thermo Scientific, Rockford, US
Nunclon™ 6-well tissue culture plate	Thermo Scientific, Rockford, US
Pipette filter tips, 10, 100, 200, 1000 µl	Starlab GmbH, Hamburg, DE
Pipette tips, 10, 200, 1000 µl	Greiner bio-one, Frickenhausen, DE
Pipettes 2, 5, 10 and 25 ml	Greiner bio-one, Frickenhausen, DE

Pre-Separation Filters	MiltenyiBiotech, Bergisch-Gladbach, DE
Sterile filter 22 µm	Sartorius, Hannover, DE
Syringe 50 ml	Braun, Melsungen, DE

3.6. Equipment

Auto MACS pro separator	MiltenyiBiotech, Bergisch Gladbach, DE
BD LSR II Flow cytometer	BD Biosciences, Heidelberg, DE
Centrifuge Type 5415	Eppendorf GmbH, Hamburg, DE
Centrifuge Type 5424	Eppendorf GmbH, Hamburg, DE
Centrifuge Type 5810R	Eppendorf GmbH, Hamburg, DE
Covaris S220	LGC Genomics, Berlin, DE
Eppendorf Concentrator Plus	Eppendorf GmbH, Hamburg, DE
HiScanSQ system	Illumina, Eidenhoven, NL
HiSeq 1500	Illumina, Eidenhoven, NL
Incubator Binder B series	Binder, Tuttlingen, DE
Incubator Binder C series	Binder, Tuttlingen, DE
LightCycler 480 PCR system	Roche diagnostics, Basel, Switzerland
Magnet MACS Multi Stand	MiltenyiBiotech, Bergisch Gladbach, DE
Mikroskope SM-LUX	Leitz, Wetzlar, DE
NanoDrop 2000	Thermo Scientific, Rockford, USA

Neubauer Chamber	Carl Roth Karlsruhe, DE
Odyssey® Infrared Imaging System	LI-COR Biosciences, Bad Homburg, DE
pH-meter	Knick, Berlin DE
Pipette Boy	IBS Integra Biosciences, CH
PowerPac HC Power Supply	Bio-Rad Laboratories, München, DE
Roller Mixer SRT 1	Stuart, Staffordshire, UKMettler-Toledo, Zwingenberg, DE
Shaker (type 3011)	GFL, Burgwedel, DE
TapeStation	Agilent Technologies, Santa Clara, USA
Water bath	Memmert, Schwabach, DE

3.7. Buffers and media

A-base addition buffer (iChIP)

6 µl 10x NEB buffer 2, 0.1 µl dATP (100 mM), 10.9 µl nuclease free water

Adapter ligation buffer (iChIP)

29 µl 2x DNA quick ligase buffer

Annexin-binding buffer

10 mM Hepes pH 7.4, 14 mM NaCl, 2.5 mM $CaCl_2$

Blocking Solution (IP)

0.5 % BSA in PBS

Chromatin release buffer (iChIP)

500 mM NaCl, 2% SDS, 2% Na-Deoxycholate, 2X Proteinase Inhibitor

Direct elution buffer (iChIP)

(0.5% SDS, 300 mM NaCl, 5 mM EDTA, 10 mM Tris Hcl pH 8.0)

End Repair Buffer (iChIP)

6.7 µl 10x T4 DNA ligase buffer, 0.67 µl BSA (10 mg/ml), 0.67 µl dNTP mix (10 mM), 16.96 µl nuclease free water

Fixative Solution (ChIP-Nexon)

1% Formaldehyde (Sigma Aldrich, 16 % Formaldehyde) in VLE-RPMI 1640 Medium

LiCl buffer (iChIP)

0.25 M LiCl, 0.5 % NP-40, 0.5 % sodium deoxycholate

Lysis Buffer (ATAC/IP/WB)

10 mM Tris-HCl (pH 7.4), 10 mM NaCl, 3 mM $MgCl_2$, 0.1 % IGEPAL-CA -630

MACS buffer

1 x PBS supplemented with 0.5 % BSA, 2 mM EDTA, pH=7.2 sterile-filtered

PBS-Tween (WB)

1 x PBS supplemented with 0.1 % Tween

RIPA buffer (iChIP/ IP)

10 mM Tris-Cl (Ph 7.6), 1 mM EDTA, 0.1 % SDS, 0.1 % sodium deoxycholate, 1 % Triton X-100

RIPA-NaCl buffer (iChIP)

0.3 M NaCl added to RIPA buffer

Tagmentation Buffer (5x) (ATAC)

50 mM TAPS-NaOH (ph 8.5), 25 mM $MgCl_2$, 50 % DMF (Attention: Precipitation -Make small amounts and start with DMF, then NaOH)

TE buffer (iChIP)

10 mM Tris (pH 8.0), 1 mM EDTA

TE/Triton X-100 buffer (iChIP)

0.2 % Triton X-100 added to TE-buffer

Tn5 Dialysis Buffer (2x) (ATAC)

10 mM HEPES-KOH (pH 7,2), 100 mM NaCl, 0.1 mM EDTA, 1 mM DTT, 0.1 % TRITON-X-100, 55 % Glycerol

2 x supplemented VLE-RPMI 1640 Medium

VLE-RPMI 1640 Medium (Merck), 20 % FCS, 2 % Na-Pyruvate, 2 % Glutamax, 2 % Pen/Strep, 30 U/ml GM-CSF, sterile filtered (0.45 µm filter)

3.8. Kits

Agencourt AMPure XP	Beckman Coulter GmbH, Krefeld, DE
CD61 Microbeads	MiltenyiBiotech, Bergisch Gladbach, DE
CD14 Microbeads	MiltenyiBiotech, Bergisch Gladbach, DE
KAPA SYBR FAST Roche LightCycler 480 2X qPCR Master Mix	KAPABiosystems, Wilmington, USA
Master Mix Maxima SYBR Green qPCR	Fermentas, GmbH, DE
Multiplex sequencing primer kit	Illumina, Eidenhoven, NL
Monocyte Isolation Kit II	MiltenyiBiotech, Bergisch Gladbach, DE
Pan Monocyte Isolation Kit	MiltenyiBiotech, Bergisch Gladbach, DE
QIAquick PCR Purification Kit	Qiagen, Hilden, DE
Tapestation DNA high sensitivity kit	Agilent Technologies, Santa Clara, USA

3.9. Software

Partek Genomics Suite Software

Cytoscape

Biolayout Express 3D

Prism

Corel Draw

R-Studio

4. Methods

4.1 PMBC isolation from buffy coats using ficol

Buffy coats from healthy donors were obtained from the Institute for Experimental Hematology and Transfusion Medicine of the University Hospital Bonn following protocols accepted by the institutional review board at the University of Bonn (local ethics vote no. 045/09). Informed written consent was provided for each specimen according to the Declaration of Helsinki.

To isolate peripheral blood mononuclear cells (PBMCs) from buffy coats the blood samples are diluted 1:2 with MACS-buffer and a Pancol density gradient centrifugation for 25 minutes at 1000 g is performed at RT (No Brake!). The leukocyte ring fraction is transferred to a new tube and cells are washed twice in MACS buffer at 200 g for 10 minutes at RT (thrombocyte wash).

4.2 Monocyte isolation by $CD14^+$ selection

The $CD14^+$ cells are magnetically labeled with CD14 Microbeads (Miltenyi Biotec) and by MACS separation column and in the presence of a magnetic MACS separator separated from the remaining PBMCs (see Kit instructions of “CD14 Microbeads human, Miltenyi Biotec”).

4.3 Monocyte isolation by negative depletion:

The Pan Monocyte Isolation Kit in combination with CD61 Microbeads (Miltenyi Biotech, respectively) were used for negative selection of classical (CD14++/CD16–), non-classical (CD16++/CD14+) and intermediate (CD16+/CD14++) monocytes. By this method, non-monocytes, such as T cells, B cells, NK cells, dendritic cells, basophils, and thrombocytes are indirectly magnetically labeled and depleted from the highly pure unlabeled monocytes using the AutoMACS program DepleteS.

The “Monocyte Isolation Kit II” is based on the same mechanism. With this Kit, non-monocytes like B-, T- and NK-cells are indirectly magnetically labelled using a cocktail of biotin-conjugated antibodies against CD3, CD7, CD19, CD56, CD123, Glycophorin A and CD16, as well as anti-Biotin Microbeads. This Kit was also used in combination with CD61 Microbeads (Miltenyi Biotech). The kits were used as intended by the manufacturer’s instructions.

4.4 Flow cytometry

Flow Cytometry describes a measuring technique which allows for cell type analysis of heterogenous cell populations by detection of cell surface markers and intracellular molecules. Thereby, the purity of isolated subpopulations as well as cell size and dimensions can easily be assessed. This is predominantly done by fluorescence intensity measurements by coupling specific fluorescently-labeled antibodies to cell surface or intracellular proteins or even to ligands like DNA.[152]

4.4.1 Purity check of monocytes:

The FACS-Antibody-Panel for the purity check is listed in **Table 3.3.2**. The purity of isolated Monocytes should lie approximately at 90 % when isolating via negative depletion.

4.4.2 Annexin-V-PI staining

The Annexin-V-Propidium-Iodide staining is an apoptosis-dead-cell staining which detects the externalization of phosphatidylserine in apoptotic cells via recombinant Annexin V, coupled to a fluorescent FITC-dye[153], and dead cells with propidium iodide[154] (see **Table 3.3.3**).

The cells are harvested and washed twice with PBS. Cell pellets are re-suspended in 50 µl of Annexin binding buffer (per 5 x 10^5 cells). 2,5 µl of Annexin-V-FITC is added and the cells are incubated for 15 minutes at room temperature, in the dark. Finally, 10 µl of PI (50 µg/ml) and 200 µl of Annexin binding buffer is added. The FACS measurement has to be realized in between the next 1-2 hours to minimize further cell death.

4.5 Presto-blue cell viability staining

The PrestoBlue assay is a reducing environment sensing cell viability assay. The reagent contains a cell-permanent compound which is blue in color and effectively non-fluorescent in solution. When PrestoBlue is added to the medium, viable cells take it up rapidly and due to their reducing environment, it is converted to an intensely red-fluorescent dye. This change can be detected by measuring fluorescence or absorbance.[155]

The PrestoBlue Cell Viability Reagent (Thermo Fischer) is used according to the manufacturer's instructions.

4.6 Cell fixation

Fixation is an essential step in processing histological sections from tissue biopsies to preserve them from decay. Tissue structure is determined by the shape and size of the macromolecules in the surrounding and inside of cells. Fixation helps to conserve cellular architecture and cell composition in tissue sections but also conserves proteins and other bio-active components in spatial relation to the cell. Any ongoing biochemical reactions are immediately terminated and the mechanical strength and stability of treated samples is increased due to the cross-linking capacity of formaldehyde. Thus, fixation is an essential process in studying tissue structures, cellular components or chromatin regulation.[156]

4.6.1 Formalin fixation (iChIP)

Cells are harvested and twice washed in 1 x PBS. The cells are centrifuged at 1200 rpm for 6 minutes and the cell pellets (up to 10^7 cells) are re-suspended in 9 ml of VLE-RPMI 1640 Medium. One milliliter of 10 % formaldehyde (Sigma Aldrich, 16 % Formaldehyde) is added drop by drop while shaking at medium speed and the cells are incubated in the fixation solution for ten minutes at room temperature. The reaction is stopped by the addition of 600 µl of 2.5M Glycine and incubation on ice for five minutes. Fixed cells are spun down at 1000 g for 4 minutes at 4°C. The cells are washed twice with ice cold PBS and finally snap frozen in liquid nitrogen and stored at – 80 °C for iChIP experiments.

4.6.2 Formalin fixation (ChIP-Nexon)

Cells are harvested, the medium is removed and the cells are re-suspended in 1-2 ml of fixative solution (per 1-5 mio. cells). The incubation time is 5 minutes at room temperature. The reaction is stopped by the addition of 1.25M Glycine (110 µl per ml of fixative solution) and direct centrifugation at 400 g for 5 minutes at 4°C. The supernatant is discarded and the cell pellet is rinsed twice with ice-cold PBS plus protease inhibitor cocktail (EDTA free Roche), centrifuged for 5 minutes at 4 degrees and the supernatant is removed. Finally, the fixed cell pellets are flash-freeze in liquid nitrogen and stored at – 80 °C for ChIP-Nexon experiments.

4.7 Immunoprecipitation (IP)

Immunoprecipitation (IP) is a biochemical pull-down-assay in which an antigen in a solution is concentrated using a specific antibody that is immobilized to a solid support such as magnetic protein-G/A coupled beads. IP is one of the most commonly used methods for the separation of proteins from tissue or cell lysates for the subsequent detection by western blotting or other biochemical assays.[157]

For the lysate preparation, cultured cells are harvested and twice washed in 1x PBS. The cells are centrifuged at 13,000 rpm for 10 minutes at 4 °C. For the lysis reaction the cell pellets are re-suspended in 40 µl of ice-cold lysis buffer per 10^7 cells and incubated on ice for 30 minutes. Thereafter cell lysates are centrifuged at the same settings as before and the supernatants containing the lysates are transferred to a new reaction tube while the tube containing the pellet is discarded.

For the IP reaction, the antibody of interest is coupled to the Dyna Protein G beads. At first, 50 µl of Dynabeads Protein G are blocked with 1 ml of ice-cold Blocking Solution. The beads are further washed twice with 1.5 ml of ice-cold blocking solution and finally re-suspended in 200µl of this solution. In a next step 5 µg of the specific antibody or the isotype control are added to the beads and are incubated over night at 4 °C on a rotator. At the next day the beads are washed three times in 1 ml of ice-cold Blocking Solution. Finally, the beads are re-suspended in 100 µl of the Blocking solution, the cell lysates are added and the solution is incubated over night at 4°C on a rotator. Now, the beads containing the immunoprecipitates need to be washed 3 times in 1 ml RIPA buffer and the antigen of interest is eluted from the beads by re-suspension in 20 µl

Laemmli Running Buffer, 5 µl of 5 x Laemmli Loading Buffer and boiling at 95 °C for 7 minutes. The samples are now ready for SDS-Page and Western Blotting.

4.8 ChIP-methods

Chromatin Immunoprecipitation followed by high throughput next generation sequencing (ChIP-seq.) has become a key technique in chromatin and epigenetic research.[158] The disadvantage of present ChIP-seq. methods is that they describe rather fine-tuned workflows which are optimized for specific experimental requirements. These methods often also have the drawback that the immunoprecipitation step is optimized for relatively high cell numbers making a problem when working with low cell number primary hematopoietic cell samples.

4.8.1 Indexing-first chromatin immunoprecipitation approach (iChIP)

The iChIP approach invented by David Lara-Astiaso et. al., 2014[159] pledges to be a highly sensitive ChIP approach with high sensitivity and reproducibility for small cell numbers. In this approach the barcoding is directly performed on the total cellular chromatin allowing multiple chromatin-barcoded samples to be pooled for immunoprecipitation. This step, according to the author, counteracts the low input enzymatic reactions performed in the conventional ChIP methods. The previously published high-throughput low cell iChIP protocol was adapted to create ChIP-seq data sets for histone modifications in low cell number experiments.

First the cells are harvested, washed in 1 x PBS and crosslinked with 1 % formaldehyde (Sigma Aldrich) for 10 minutes. Extracted nuclei of ~ 1 x 10^6 cells are lysed and the chromatin is sheared for 45 minutes in a Covaris S220 Device (Duty Factor: 2 %; Peak Incident Power 105 W; Cycles per Burst 200) producing chromatin fragments in the range of 50 – 500 bp. The TapeStation system (Agilent) is used for size confirmation. The sonicated material is immobilized on Protein G DynaBeads (Life Technologies) coated with antibody to H3 (Abcam; Millipore) and then indexed with Illumina sequencing compatible NEXTflex adapter oligonucleotides (Bio Scientific). The indexed chromatin is released from the H3 coated magnetic beads using antibody denaturing conditions (DTT, high salt and detergent) and then pooled with chromatin of other samples. Finally, ChIP is performed using 4 different polyclonal rabbit ChIP

antibodies for histone modifications, namely H3K4me1 (Abcam), H3K27Ac (Abcam), H3K4me3 (Millipore), H3K27me3 (Millipore) and a rabbit IgG control (Abcam). Therefore, the ChIP antibodies are first coated to magnetic protein G beads (Life Technologies) at room temperature for 1 hour and finally complexed to the barcoaded chromatin pool in an overnight reaction at 4 °C. The bead-bound immunocomplexes are washed with different salt buffers to remove non-specific antibody-protein complexes. The chromatin is de-cross-linked and RNA and proteins degraded in a 4 hours digestion step. The ChIPed chromatin is purified using SPRI AMPure XP beads (Beckman Coulter) and concentration and size recorded using the TapeStation (Agilent). To validate the success of performed iChIP experiments a qPCR measurement relative to unspecific IgG control signals is performed allowing relative enrichment calculations of the target samples.

4.8.2 NEXSON (nuclei extraction by sonication) - ChIP

The difference between the NEXON-ChIP and conventional ChIP methods lies in the lysis of cells and nuclei. This method was established by Laura Arrigoni et. al., 2015 [160] and as indicated by the name describes an ultrasound-based nuclei extraction method which is vastly effective across various organisms, cell types and numbers. The addition of the NEXON method in the ChIP workflow makes less sample-dependent adjustments possible. The authors even assure small cell number ChIPs (~10.000 cells) which can easily be processed without application of modified ChIP or library preparation protocols when performing NEXON first.

1 % formaldehyde (Sigma Aldrich) crosslinked Monocyte/Macrophage pellets are re-suspended in 1 ml of Farmham lab buffer supplemented with Complete Protease Inhibitor Cocktail EDTA-free (Roche), transferred into 12X12 AFA tubes (Covaris, 520081) and sonicated for 8 minutes in the Covaris instrument (S220) at Peak Incident Power 75 W, Duty Factor 2% and 200 Cycles per Burst. To see if the nuclei extraction worked out properly nuclei are checked under a phase contrast microscope. Then nuclei are transferred to a 1.5 ml low retention Eppendorf tube and pelleted down at 100 g for 5 minutes at 4°C. The pellets are then re-suspended in 130 µl of shearing buffer and transferred to 130 µl Microtubes. Shearing is performed for 20 minutes (dedicated) in the Covaris Instrument (S220) (Duty Factor: 2 %; Peak Incident Power

105 W; Cycles per Burst 200). The fragmented chromatin is finally transferred to a low retention 1.5 ml Microtube and centrifuged for 5 minutes at 10.000 g and 4 °C to pellet the insoluble debris. The supernatant containing the sheared chromatin is transferred to a fresh Eppendorf Tube and is further ChIP processed in the IPStar (Diagenode) using the iDeal ChIP-seq kit for Histones (Diagenode) and 4 different polyclonal/monoclonal rabbit ChIP antibodies for histone modifications (H3K4me1 (Abcam), H3K27Ac (Abcam), H3K4me3 (Millipore), H3K27me3 (Millipore)) as well as a rabbit IgG control (Abcam).

4.9 ATAC-sequencing

The Assay for Transposase Accessible Chromatin with high-throughput sequencing (ATAC-seq) was first described in 2013 as alternative advanced method for MNase-seq, FAIRE-Seq and DNase-Seq. This method is based on a process called tagmentation and allows to map chromatin accessibility genome-wide. The key player of this process is a mutant, hyperactive Tn5 transposase which simultaneously fragments accessible DNA and taggs it with sequencing adaptors. Regions of increased accessibility can be inferred by sequencing reads and regions of nucleosome position and transcription factor binding can be mapped.[161,162]

4.9.1 ATAC-procedure with in-house Tn5

Cultured cells are harvested, counted and 50,000 cells are centrifuged at 500 g for 5 minutes at 4°C. The cell pellets are washed once in 50 µl of cold 1 x PBS and again spun with the same setting as in the step before. The supernatant is discarded and the cell pellet is re-suspended in 50µl of ice-cold lysis buffer. The cell lysate is immediately centrifuged at 500 g for 5 minutes at 4°C. The supernatant is discarded and 20 µl of the transposition reaction mix (1 µl Tn5 + 4 µl 5x TAPS-DMF buffer + 15 µl H_2O) is added and gently mixed to the nuclei. The transposition reaction is incubated for 30 minutes at 37 °C. Following transposition, the chromatin is immediately purified using the Quiagen Min Elute Kit. The transposed DNA is finally eluted in 10 µl H_2O. The purified DNA is finally amplified by PCR using the following reagents and program.

Table 4.9.1.1: Reagents used for the Transposition Reaction

Reagent:	Volume:
Transposed DNA	10 µL
Nuclease Free H2O	10 µL
25µM Customized Nextera PCR Primer 1*	2.5 µL
25µM Customized Nextera PCR Primer 2*	2.5 µL
NEBNext High-Fidelity 2x PCR Master Mix (New England Labs Cat #M0541)	25 µL
	50 µL Total

* Barcode (change for each sample)

Table 4.9.1.2: PCR-Program for amplification of genomic DNA fragments

Temperature [°C]	Time	
(1) 72°C	5 min	
(2) 98°C	30 sec	
(3) 98°C	10 sec	x 11 cycles
(4) 63°C	30 sec	
(5) 72°C	1 min	
(7) Hold at 4°C		

The PCR products are purified using the Quiagen MinElute Kit and eluted in 12 µl H_2O. The Tape Station Device 2200 and Agilent High sensitivity D1000 stripes are used to validate tagmentation, correct amplification and sample concentration.

4.10 Western-blot

Western Blotting describes a technique to visualize specific proteins which previously have been separated by SDS-gel-electrophoresis. The separated proteins are

transferred to a nitrocellulose membrane by placing the SDS-gel next to the membrane and applying an electric current. Visualization of the target protein is enabled by binding of a specific antibody to the protein of interest and labeled secondary antibody binding.[163]

4.10.1 Wet blotting

For the lysis reaction the cell pellets are suspended in 40 µl of ice-cold lysis buffer per 10^7 cells and incubated on ice for 30 minutes. Thereafter cell lysates are centrifuged at 13,000 rpm for 10 minutes at 4°C and the supernatants containing the lysates are transferred to a new reaction tube. If necessary, the sample is filled up with Laemmli Running Buffer to 20 µl and 5 µl of 5 x Laemmli Loading Buffer is added before boiling at 95 °C for 5-7 minutes. The samples are now loaded on a 10 % SDS-Page gel and are run at 80 – 100 V. The proteins are blotted overnight at 25 mA on a 0.2 µm nitrocellulose membrane in a wet blotting procedure. The blotted membranes are washed three times for 10 minutes with 1 x PBS-Tween and then blocked for 1 hour in milk-solution (2.5 g milk powder in 50 ml PBS-Tween). After that the antibody is diluted according to the manufacturer's instructions in 3 ml of milk-solution and added to the membrane. Antibody coupling is performed overnight at 4°C. The next morning the membrane is washed tree times with PBS-Tween and 1 µl of the secondary anti-rabbit Licor antibody is added in 5 ml of Licor-buffer : PBS (1:1). The membranes are incubated for 1 – 2 hours at RT on a rotator. Finally, excess antibody is washed away with PBS-Tween and the membrane is scanned on the LI-COR Odyssey device.

4.11 Trained immunity experiments

4.11.1 Donor information

Buffy coats from three healthy donors were obtained from the Institute for Experimental Hematology and Transfusion Medicine of the University Hospital Bonn following protocols accepted by the institutional review board at the University of Bonn (local ethics vote no. 045/09). Informed written consent was provided for each specimen according to the Declaration of Helsinki.

Table 4.11.1.1: Donor Information

Donor-Nr.:	Blood Group:	Age:	BMI [kg/m^2]:
1	0-positive	32	22.1
2	B-positive	31	22.2
3	A-positive	29	25.2

4.11.2 Fatty acid preparation and culturing of cells

1,143 x 10^6 cells were suspended in 1 ml pure VLE-RPMI 1640 Medium (Merck) and later 1:2 diluted with 2 x Medium containing supplements (control) and palmitic or oleic acid.

2 x Control Medium

- 0.8 % EtOH

2 x Fatty Acid Medium:

- 200 µM OA/PA + 0.8 % EtOH

Figure 4.11.2.1: Scheme of Fatty-Acid-Medium preparation.

Before The 2 x medium is 1:1 diluted with the cells in pure VLE-RPMI 1640 Medium it is heated up to 55 °C to make sure that the fatty acids are equally dissolved.

Cell samples (RNA-seq. (Quiazol), PFA-fixed, Formaline fixed, and Tn5 transposase treated) were collected for all conditions and donors at days 0, 1, 4 and 5. The Monocytes (Day 0) were checked for purity (see purity check FACS-staining).

4.12 RNA isolation from monocytes and cDNA synthesis

4.12.1 RNA isolation from monocytes for quality control qPCR

Up to 1 x 10^7 Monocytes are lysed in 1 ml QIAzol Lysis reagent and incubated for 5 minutes at room temperature to allow complete dissociation of nucleoprotein complexes. For phase separation 200 µl of chloroform is added, thoroughly mixed and incubated for 3 minutes at room temperature. The samples are centrifuged at 12000 rcf for 10 minutes at 4°C. The aqueous phase is transferred to a new reaction tube, 1:1 diluted with isopropanol and incubated for at least 3 hours at -20°C. The sample is thawed and for 10 minutes incubated at room temperature before it is centrifuged again at 12000 rcf for 5 minutes at 4°C. The supernatant is removed and the pellet is washed two times with 80 % Ethanol. The Ethanol is removed and the pellet is re-suspended in 100 µl H_2O (nuclease free) and 300µl of 100 % Ethanol as well as 10 µl of 3M Na-Ac is added. The mixture is again incubated at -20 °C overnight, thawed and centrifuged at maximum speed (16000 rcf) for 30 minutes. The supernatant is completely removed and the pellet is washed two times with 300 µl of 80 % Ethanol. The RNA pellet is dried until no Ethanol remains and dissolved in ddH_2O at 55 °C. Purity and concentration are determined spectroscopically using the Nanodrop 2000 device (Thermo Scientific).

4.12.2 cDNA synthesis by reverse transcription

For cDNA synthesis a reverse transcription (RT)- PCR is applied to the isolated RNA samples. Here the Transcriptor First Strand cDNA Synthesis Kit (Roche) was used according to the manufacturer's instructions.

Table 4.12.2.1: Reaction setup for annealing of Anchored Oligo(dT)15 primers

Component	Amount
RNA input	500 ng
Anchored Oligo(dT) 50 µM	1 µL
Nuclease free H20	to 13µL

Table 4.12.2.2: Program used to anneal Anchored Oligo(dT)15 primers

Step	Temperature	Duration	Number of Cycles
Anchored Oligo(dT)15 annealing	65 °C	10 min	1

Table 4.12.2.3: Reaction setup for annealing of Anchored Oligo(dT)15 primers

Component	Amount
Sample input	13 µL
Transcriptor RT buffer, 5x concentrated	1 µL
Protector RNase Inhibitor	0.5 µL
dNTPs (10mM)	2 µL
Transcriptor Reverse Transcriptase	0.5 µL

Table 4.12.2.4: Reaction setup for reverse transcription of mRNA

Step	Temperature	Duration	# Cycles
Reverse Transcription	55 °C	30 min	1
Inactivation of RT	85 °C	5 min	1
Cooling	4 °C	∞	1

4.13 Semi-quantitative real-time PCRs

4.13.1 Validation of trained immunity pre-experiments using the LightCycler® 480 probes master

Validation of trained immunity experiments is done by visualization of transcriptomic changes in specific marker genes upon fatty acid stimulation using the Light Cycler 480 Probes Master system (Roche) which is based on TaqMan probes. TaqMan probes are hydrolysis probes that are designed to increase RT-PCR specificity. The TaqMan probe principle is based on 5' exonuclease chemistry which uses a fluorogenic probe and fluorophore-based detection of a specific PCR product as it accumulates during PCR.

4 µl of cDNA is added to the Master Mix for the RT-PCR reaction (see **Table 4.13.1.1**). The qPCR samples are all run as duplicates in 96-well plates using the LightCycler 480 II device (Roche). The standard program used is listed in **Table 4.13.1.2**. Nuclease free water is used as negative control and GAPDH is used as housekeeping gene. Data are analyzed by $2^{-\Delta\Delta CT}$ method.

Table 4.13.1.1: Real-Time PCR setup using the LightCycler® 480 Probes Master

Component	Amount
LightCycler® 480 Probes Master	5 µL
Primer Mix (forward and reverse 10µM each)	0.2 µL
Probe	0.1 µL
Nuclease free water	0.7 µL

Table 4.13.1.2: Reaction setup for Real-Time PCR using LightCycler® 480 Probes Master

Step	Temperature	Duration	Number of Cycles
Initial denaturation	95°C	5 min	1
Denaturation	95°C	10 sec	45
Primer annealing	60°C	30sec	
Amplification	72°C	1 sec	
Cooling	20 °C	30 sec	1

4.13.2 Validation of ChIP quality using the maxima SYBR green/fluorescein qPCR master

Validation of ChIP-seq quality was done by semi-quantitative real time PCR using the Maxima SYBR Green/Fluorescein qPCR Master Mix kit (Fermantas).

Table 4.13.1.3: Reaction setup for Real-Time PCR using the Maxima SYBR Green/Fluorescein qPCR Master Mix

qRT-PCR reaction mix Type	Amount
Maxima SYBR Green qPCR MM (2x)	12.5 µl
Forward primer (10µM)	0.75 µl
Reverse primer (10µM)	0.75 µl
Water	10 µl
ChIP DNA (Diluted 1:5)	1 µl

The qPCR samples were all run as duplicates in 96-well plates using the LightCycler 480 II device. The standard program used is listed in **Table4.13.1.4**.

Table 4.13.1.4: Standard RT-qPCR program for ChIP validation.

Type	Temperature [°C]	Time	Cycles
Initial denaturation	95	10 min.	1
Denaturation	95	15 sec.	40
Annealing	60	30 sec.	
Extension	72	30 sec.	

Relative PCR enrichment values of positive (Pos) against negative (Neg) target sites were calculated using the ΔΔCT method. ChIP-results were graphed as ratios of specific ChIP-antibody enrichment values (S) to unspecific IgG-antibody enrichment values. The visualization shows the relative enrichment.

$$\Delta Ct = Ct(S) - Ct(IgG)$$

$$\Delta\Delta Ct = Ct(Pos) - Ct(Neg)$$

$$Relative\ enrichment = 2 - \Delta\Delta C$$

4.14 Enzyme linked immunosorbent assay (ELISA)

Enzyme-linked immunosorbent assay is a method for the determination of antigen or antibody concentration in solution. In an ELISA, an antigen is immobilized to a solid surface and then complexed with an antibody that is linked to an enzyme. Detection is accomplished by assessing the conjugated enzyme activity via incubation with a substrate to produce a measurable product.

Levels of soluble TNF (R&D) and IL-6 (Sanquin) in the supernatants of each sample of the trained immunity experiment were measured with ELISA kits in accordance to the manufacturer's instructions. All ELISA assays were performed by the group of *M.G. Netea (Mihai)* Professor, Faculty of Medical Sciences, Radboud University.

4.15 RNA-sequencing

4.15.1 Isolation of RNA following sequencing

The RNA isolation procedure of RNA-seq. samples and all downstream steps were performed by the help of Michael Kraut and Heidi Theis.

For each condition approximately 0.5 x 10^6 cultured cells are lysed in Quiazol (Quiagen). Total RNA is extracted using the miRNeasy Micro kit (Quiagen), quantification and quality assessment is done by Tape Station (Agilent) analysis. The next step is the library preparation including cDNA synthesis, adapter (Illumina) ligation and amplification. For quantification and quality assessment of the libraries Tape Station (Agilent) measurements and KAPA Illumina Quant PCRs are performed using the LightCycler 480 II device. When libraries pass the quality- and quantification-standards they are pooled and for normalization issues a second KAPA Illumina Quant PCR is done. The cDNA libraries are then denatured and clustered on a flow cell (Illumina) using a cBlot machine (Illumina). Finally, the pooled libraries are sequenced in a single-read 75 bp sequencing run on the HiSeq1500 (Illumina) using the TrueSeq SBS kit v3 (Illumina). Base calling, demultiplexing and BCL to FASTQ data conversion was done by Dr. Kristian Haendler using the CASAVA v1.8 software (Illumina). Kallisto Software 0.43.0, a program for quantifying abundances of transcripts from RNA-Seq data, was utilized

for *very* fast RNA-Seq quantification based on pseudo-alignment (done by Kathrin Klee). Subsequently, the annotated data are normalized with the DESeq2 package (Love, M. I., Huber, W. & Anders, S., 2014)[164] by computing a size factor for each sample. The size factor is calculated by taking the median of ratios of each sample to the reference sample. We use the default parameter recommended by the Bioconductor DESeq2 workflow for RNA-Seq data (https://www.bioconductor.org/help/workflows/rnaseqGene/), a package for the statistical software R v3.4.1 (https://cran.r-project.org/bin/windows/base/old/3.4.1/).

For visualization purposes, normalized read counts below 1 are set to 1 (flooring) to allow the usage of logarithmic scales during the comparison of differentially activated monocyte-derived cells. Genes with normalized RNA-seq values ≥ 10 are defined as expressed. Independent sequencing samples were created for 3 donors. Finally, Partek Genomics Suite (PGS) 6.6 was used for data evaluation.

4.16 Bioinformatic data analysis

4.16.1 Identification of differentially expressed genes

In Partek Genomics Suite 6.6 Analysis of Variance (ANOVA) models were applied to define differentially expressed (DE) genes. Differences between two comparable groups or conditions are determined by setting certain Fold Change (FC) and False Discovery Rate (FDR, Benjamini and Hochberg, 1995)[165] adjusted p-value cutoffs. The corresponding cutoffs are given in the respective results paragraphs. The most variable genes were determined in ANOVA models to compare the variations throughout the conditions, i.e. genes with most significant p-values.

To visualize the structure within the data, we carried out principal component analysis (PCA) of all present genes and hierarchical clustering on the 1,000 genes with the greatest variance within the data set, with default settings in PGS, based on P values according to the expression values of the samples across the conditions. PCA is a mathematical technique that transforms a number of correlated variables into a smaller number of uncorrelated variables, called principal components. The first principal component accounts for as much of the

variability in the data as possible, and each subsequent component accounts for as much of the remaining variability as possible.
Hierarchical clustering is a useful method to visualize how samples group together based on similarity of features.
Venn diagrams display the number of overlapping and distinct genes between selected DE-gene lists.

4.16.2 Coregulation networks and comparative bioinformatics

To describe the structure within the data sets, I performed Co-expression network analysis based on Pearson's correlation coefficients using BioLayout Express 3D (*Theocharidis et al.*, 2009)[166]. I determined ANOVA model-defined DE-genes for each condition at each extraction time point (24 hours, 96 hours and 116 hours) as input for the network analysis. I visualized the network in Cytoscape and colored the nodes within the network, representing the genes, according to their fold change among two conditions. The difference in expression relative to the overall mean, determined by the group fold change (GFC) of the respective condition, is indicated by color-coding of the respective nodes.

For GO-Enrichment analysis (GOEA) the open-source software package ClusterProfiler (Yu, G., Wang, L.-G., Han, Y. & He, Q.-Y., 2012)[167] for functional enrichment analysis was used. If not differently stated, GO terms were considered significantly enriched with a Bonferroni-corrected p-value ≤ 0.05.

Kyoto Encyclopedia of Genes and Genomes (KEGG)[168] enrichment analysis (*Kanehisa, Furumichi, Tanabe, Sato, & Morishima*, 2017)[169] on DE genes found between the different conditions was also performed with ClusterProfiler with a background set of all present genes. If not differently stated, terms were considered significantly enriched with a Bonferroni-corrected p-value ≤ 0.05.

The PANTHER (protein annotation through evolutionary relationship) classification system (http://www.pantherdb.org/) is a comprehensive system that combines gene function, ontology, pathways and statistical analysis tools.[170] The PANTHER website was used to browse and query gene functions of determined DE-genes.

5. Results

5.1 Set-up of trained immunity experiment

Western diet is characterized by a high intake of omega-6 and saturated fatty acids, a low intake of omega-3 fatty acids and the consumption of too much sugar and salt. It is known that high-fat Western diets correlate with chronic inflammatory diseases like atherosclerosis and the activation and polarization of myeloid-derived cells plays an essential role in the development and progression of such diseases.[171]

Previous studies have shown that saturated and unsaturated fatty acids can polarize myeloid-derived cells into inflammatory- and anti-inflammatory phenotypes, respectively.[2,121] We suggest that the cells are not only phenotypically polarized by ingredients of our diet, but also are capable of developing a memory.

To determine these biological questions, the following experimental trainings settings were established.

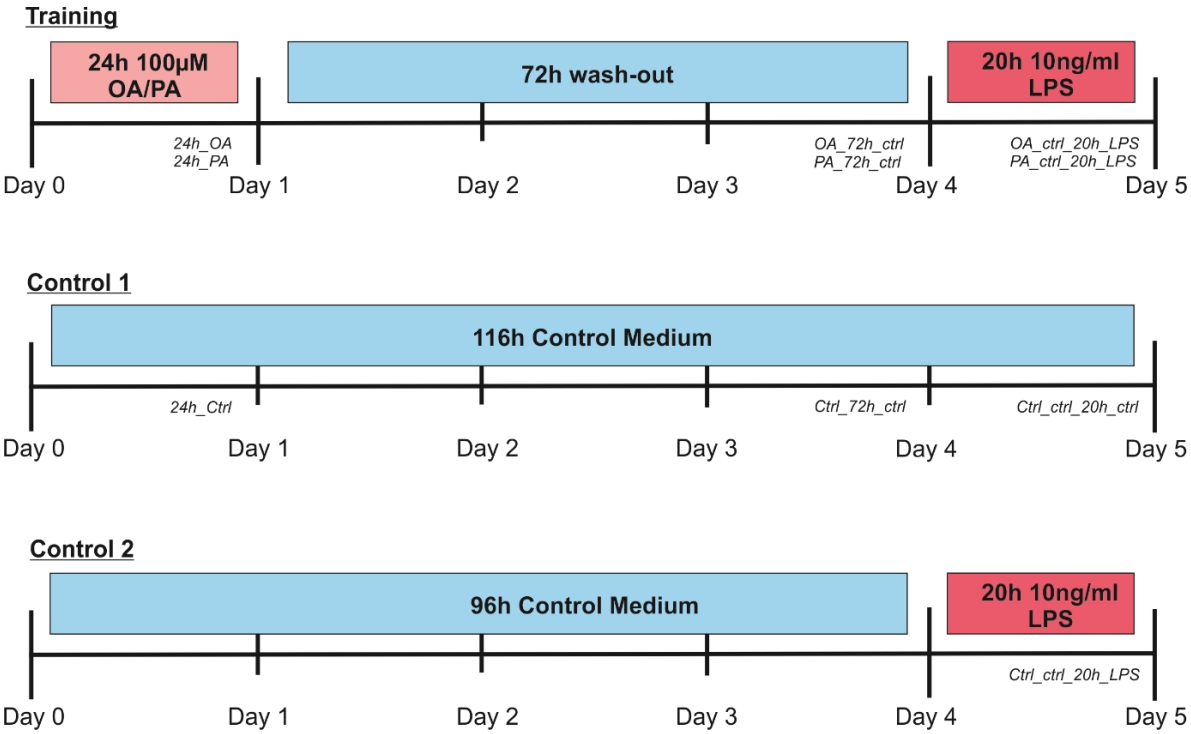

Figure 5.1.1: Scheme of set-up of trained immunity experiment giving rise to the different experimental conditions and control treatments. Sample names are stated in italic and will be kept through this work.

In the main experiment, the freshly isolated monocytes are stimulated for 24 hours either with 100 µM oleic acid, 100 µM palmitic acid or simply with control medium. The stimulation phase is followed by a three days wash-out phase, where the cells are cultured in identical supplemented VLE-RPMI Medium (see *3.7 Buffers and Media*). Finally, the cells are re-stimulated with 10 ng/ml LPS for further 20 hours to determine the potency of the cells to retain prior information and changing behavior. Control 1 is cultured for the whole time in supplemented VLE-RPMI Medium. The transcriptome of cultured cells was analyzed after 24 hours, 96 hours (day 4) and after 116 hours, at day 5.

5.1.1 Set-up of standard conditions

To set-up the standard conditions of the trained immunity experiment, fatty acid solubility, toxicity on freshly isolated monocytes, as well as cell survival over the time of the experiment, under the different stimulation conditions, was tested and optimized.

At the outset of set-up of the trained immunity experiment cells were stimulated with oleic acid (C18:1cis9) or stearic acid (C18:0) as representatives for the unsaturated and saturated fatty acids found in Mediterranean or Western diet, respectively.
Since oleic acid and stearic acid are both very abundant in diet and structurally very similar, we first intended to investigate the effect of these FFAs on the transcriptome of monocyte-derived cells. However, as oleic acid and palmitic acid (C16:0) make up the more representative fatty acids in Mediterranean and Western diet, and are the most prominent fatty acids utilized in the body, we later decided to replace SA with PA for ultimate cell priming. Since stearic acid at concentrations of 100 µM is described to be even more harmful to lymphocytic cells than palmitic acid[172] and in total, the cytotoxicity of these saturated fatty acids was reported to be similar[173], evaluated standard conditions for dose determination were transferred to PA treatments. Hence, settings from pre-experiments were overtaken and a test-run was performed.

In the first set of experiments, an adequate fatty acid concentration for appropriate cell survival and responses was determined. Many working groups work with fatty acid concentrations of 250 µM when stimulating myeloid-derived cells for 24 hours. However, as our goal was to stimulate the cells with the most activating FFA concentrations, the highest transcriptional response to the marker genes CCL3, IL-8

and CCL4L2 was determined for monocytes cultured for 24 hours in medium with FFA concentrations lying between 300 µM and 50 µM. The marker genes were determined from previous RNA-seq. data of SA and OA stimulated macrophages[174] and RT-qPCRs from extracted cellular mRNAs were performed.

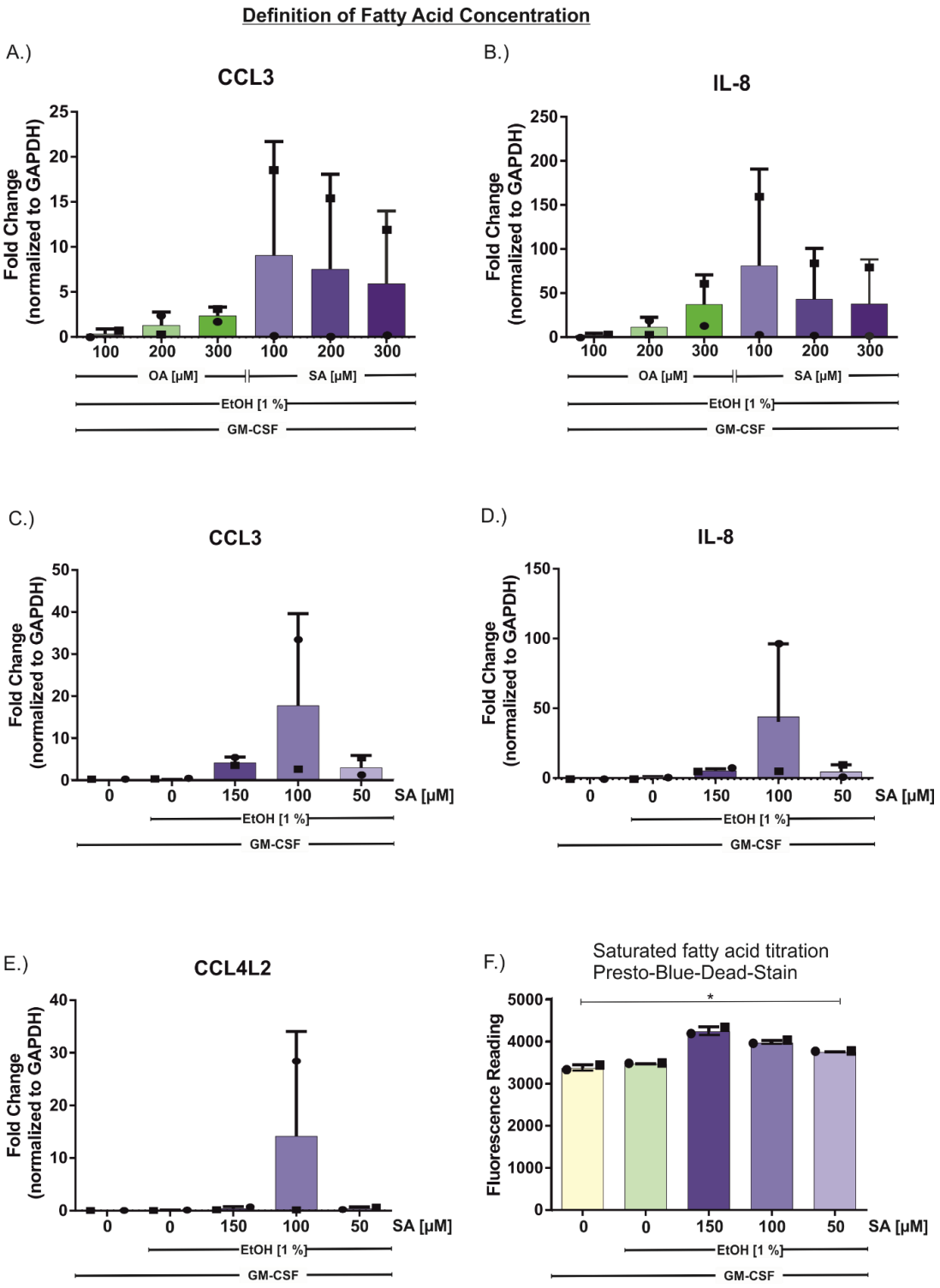

Figure 5.1.1.1: Definition of fatty acid concentrations for adequate cell survival and response to stimulus. In the described experiments, cells were cultured in VLE-RPMI 1640 Medium containing 500 U/ml GM-CSF. A.) & B.) Titration of oleic- and stearic acid concentrations based on RT-qPCR results from isolated myeloid cell derived mRNA after 24h stimulation. The read-out is the upregulation of the marker genes IL-8 and CCL3 (n=2). C.), D.) & E.): Titration of saturated fatty acid concentrations based on RT-qPCR results from isolated myeloid cell derived mRNA after 24h stimulation. The read-out is the upregulation of the marker genes CCL3, IL-8 and CCL4L2, respectively (n=2). F.) Presto-Blue-Dead-Cell staining of myeloid-derived cells stimulated with increasing stearic acid concentrations, compared to control (n=2). *p < 0.05 (Repeated measures one-way ANOVA). ■ – Donor A; ● – Donor B (different Donors in A.)/B.) and C.)-F.)).

When investigating CCL3 and IL-8 mRNA levels (**Figure 5.1.1.1 A.)** and **B.)**), the strongest response to SA is achieved at a concentration of 100 µM. With increasing SA concentrations, a decrease of respective mRNA levels can be observed. In case of OA cultures, the effect is vice versa and significantly lower as seen for SA. Since the toxic effect of saturated fatty acids on myeloid-derived cells is much higher as the effect of unsaturated fatty acids, SA concentrations were taken as dose determining factor. The high deviations in expression levels between the cells of tested human donors was seen in all repeated test samples and is induced by the versatility of human genetic information and by environmental influences.

To determine the ideal saturated fatty acid concentration for the trained immunity experiment, SA concentrations were further split into smaller entities of 150 µM, 100 µM and 50 µM and the inherent effect of 1 % EtOH, used to solve FAs, was also tested and compared to a control just containing the supplemented culture medium. **Figure 5.1.1.1 C.)**, **D.)** and **E.)** show the evaluated qPCR results of this experiment. For each tested gene transcript, it could be shown that 1 % EtOH has almost no effect on transcriptional levels of macrophage inflammatory markers compared to the zero control or SA stimulated cells. The results of this experiment indicate that the effect of SA on myeloid-derived cells is constantly highest at a concentration of 100 µM. Higher as well as lower SA concentrations lead to meaningful lower CCL3, IL-8 and CCL4L2 mRNA levels. 150 µM and 50 µM SA seem to have almost no effect on CCL4L2 expression levels, while with 100 µM SA stimulation mean mRNA levels are ~15 times increased. The huge deviations in calculated FCs in samples of different donors are the result of different genetic and environmental backgrounds of the human donors.

With the presto-blue assay the toxicity of applied SA concentrations compared to zero control and the 1 % EtOH control was tested. Examining **Figure 5.1.1.1 F.)** it can be seen that 1 % EtOH has just a very low cytotoxic effect on cultured myeloid-derived cells, when compared to the zero control. In case of SA stimulated cells, the cytotoxicity increased with increasing SA concentrations. Hence, fatty acid concentrations for the trained immunity experiment were set to 100 µM saturated- and unsaturated fatty acid, respectively.

Since all influencing factors, despite the fatty acids, should be kept as low as possible in the trained immunity experiment, and M- and GM-CSF depending on the dose,

themselves have been shown to have effects on myeloid-derived cells[175&176], the minimum concentration of these factors for proper cell survival was determined by titration.

In the first dose-defining experiment (**Figure 5.1.1.2 A.)** to **D.)**) the viability of cells cultured in medium without any colony stimulating factor (CSF), with M-CSF concentrations between 50 U/ml and 6.25 U/ml and with GM-CSF concentrations between 500 U/ml and 12.5 U/ml were tested. The viability of cells was measured over three days in 24 hours intervals as well as after six days.

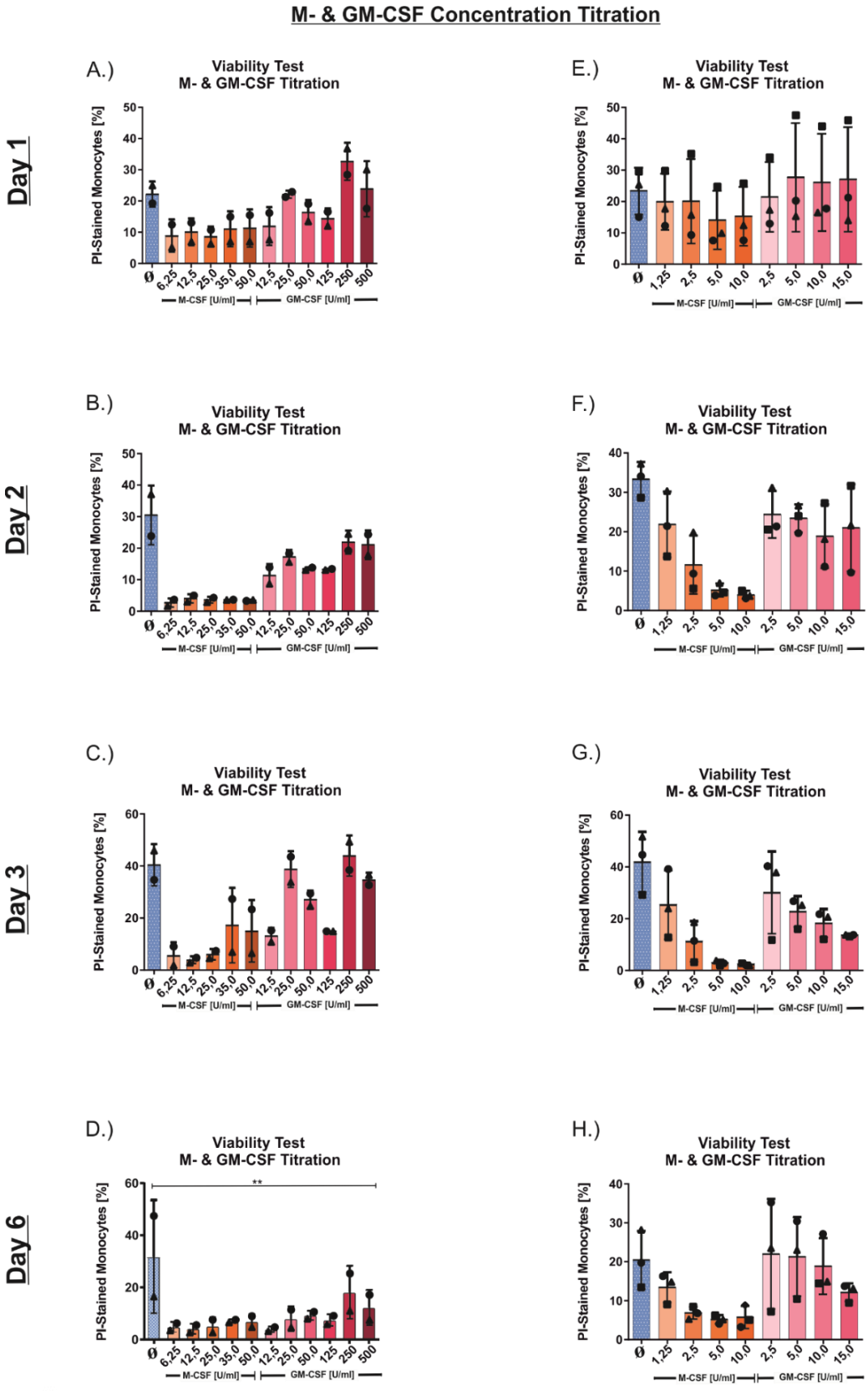

Figure 5.1.1.2: Pre-definition of adequate M-CSF and GM-CSF concentrations in medium for optimal cell survival with preferably low concentrations of the colony stimulating factors. Cell death measured by propidium iodide staining and FACS analysis after cell cultivation in medium containing M-CSF concentrations ranging from 6.25 U/ml to 50 U/ml and GM-CSF concentrations ranging from 12.5 U/ml to 500 U/ml after A.) 24 hours, B.) 48 hours, C.) 72 hours of culture and D.) 144 hours of culture. A.) –

D.) n=2. The same was done repeated with cultures containing M-CSF concentrations ranging from 1.25 U/ml to 10 U/ml and GM-CSF concentrations ranging from 2.5 U/ml to 15 U/ml after E.) 24 hours, F.) 48 hours, G.) 72 hours of culture and H.) 144 hours of culture. E.) – H.) n=3. *p < 0.05 (Repeated measures one-way ANOVA). If not marked by an *, comparisons were not significant. ▲ – Donor A; ● – Donor B; ▲ Donor C (in both experimental settings cells of different donors were taken and experiments were performed at different time points).

As indicated in **Figure 5.1.1.2**, culturing myeloid-derived cells in medium not containing any CSF highly reduces the viability of these cells, especially when compared to cultures containing low concentrations of M- or GM-CSF. In case of M-CSF, there is a trend of increasing viability with decreasing M-CSF concentrations. However, there is some unsteadiness between the time points at concentrations of 12.5 U/ml M-CSF. Investigating cell viability of GM-CSF cultures in **Figure 5.1.1.2 A.)** to **D.)**, we see a fluctuating viability of cells with decreasing GM-CSF concentrations. At concentrations of 500 U/ml, 250 U/ml and 25 U/ml cell viability is highly reduced at all measured time points, while concentrations of 125 U/ml, 50 U/ml and 12.5 U/ml rather seem to have a positive effect on cell survival. The lowest GM-CSF concentration (12.5 U/ml) in this experiment has constantly the best survival effect on tested monocytes at all tested time points.

Since both, M- and GM-CSF cultures, seemed to have the best survival effect on myeloid-derived cells with lowest concentrations tested, a second test run with even lower concentrations was performed (**Figure 5.1.1.2 E.)** – **H.)**). Here, cell viability at M-CSF concentrations between 10 U/ml and 1.25 U/ml and GM-CSF concentrations between 15 U/ml and 2.5 U/ml were tested.

M-CSF cultures with 5 U/ml show best viability levels at day 1 and day 6, but constantly afford high viability to the cells. A similar high viability is detectible in cultures with 10 U/ml M-CSF, with highest viability values at days 2 and 3. The cultures with very low M-CSF concentrations, namely 2.5 U/ml and 1.25 U/ml display at all tested time points two to five times less viable cells as cultures containing 5 or 10 U/ml M-CSF (see **Figure 5.1.1.2 E.)** to **F.)**).

In GM-CSF cultures (see **Figure 5.1.1.2 E.)** to **H.)**) highest viability of present cells after one day of culturing (**E.)**) is detectible in the 2.5 U/ml GM-CSF cultures. 3 to 4 % less viable cells are detectible in cultures containing 10 U/ml and 15 U/ml GM-CSF. A similar cell loss is seen in the zero control while 5 U/ml GM-CSF lead to lowest viability

of present cells. At the second day of culturing, the viability of present cells was reshuffled. Here, cells cultured with 10 U/ml GM-CSF are with 20 % dead cells most viable while at the later time points the cultures containing 15 U/ml GM-CSF undercut the viability in 10 U/ml cultures by approximately one third, giving best results for viability. In contrast, the 2.5 U/ml GM-CSF cultures show sustained the lowest effect on cell survival when evaluating test cultures at day two, three and six (see **Figure 5.1.1.2 F.)**, **G.)** & **H.)**). Taken together, it can be said that myeloid-derived cells are most viable when either cultured in medium containing 5 U/ml M-CSF or 10-15 U/ml GM-CSF.

Although the viability of cells cultured in medium containing M-CSF is much higher compared to GM-CSF, we decided to culture the monocytes in GM-CSF, bringing them in a state in which they rather differentiate into inflammatory than anti-inflammatory phenotypes. M-CSF exhibits a mostly homeostatic expression pattern, whereas GM-CSF is a product of cells activated during inflammatory or pathologic conditions[175].

Although the previous experiment showed that 1 % EtOH in the culture medium has just a very low cytotoxic effect on cultured monocytes, we intended to decrease the EtOH concentration further by at least 50 % but still needed to ensure proper fatty acid dissolution and uptake. As read-out, the fold change of PON2 mRNA levels over expression levels of the house-keeping gene GAPDH was selected. PON2 was used as marker gene since triglyceride accumulation in macrophages upregulates PON2 expression and may act as cellular antioxidant that protects myeloid-derived cells from oxidative stress[177].

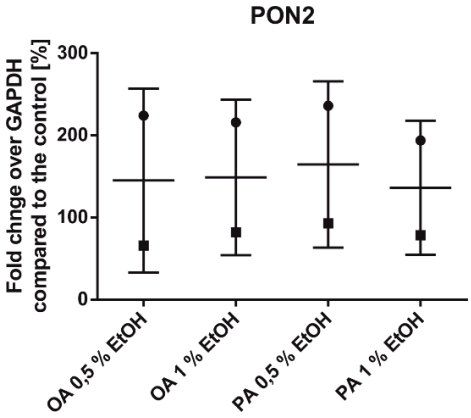

Figure 5.1.1.3: Optimization of ethanol concentration for optimal cell survival and fatty acid solubility. The culture media were supplemented and contain 5 U/ml M-CSF (n=2). Repeated measures one-way-ANOVA. Data were not significant with a p-value of 0,4117. Percental increase of PON2 expression over GAPDH compared to control over GAPDH; Control = 100 %. ● – Donor X; ■ – Donor Y;–mean value.

The expression of PON2 was in total not very high when examining the fold change over GAPDH. The cells of different donors responded with different high PON2 expression levels and in case of OA stimulation divergent expression levels in relation to EtOH concentrations are detectible between cells of different donors. In case of 24h OA stimulation there is a small difference in mean PON2 expression between 0.5 % and 1 % EtOH concentrations, with 1 % EtOH cultures giving the higher level. Here it has to be considered that cells of different donors have the tendency to react with different strength and also in different ways to certain influencing factors. In case of PA cultures, we see a consistent increase of PON2 expression in 0.5 % EtOH containing PA cultures. Since PA is less well dissolvable than OA, the reactions seen in PA stimulated cells were taken as the limiting factor and to reduce EtOH cell toxicity further, we reduced the concentration in both conditions even to 0.4 %. This concentration was tested in a pre-run of the final experiment.

To guarantee adequate cell numbers for the planned sequencing experiments at each intermediate step and at the end of the training experiment a pre-run, defining the number of cells that need to be plated at the beginning of the experiment, was performed. With the help of counting beats for flow cytometry, cell loss between starting and end-point of each experimental condition, was calculated. The percental cell loss over the experimental time is visualized in **Figure 5.1.1.4**.

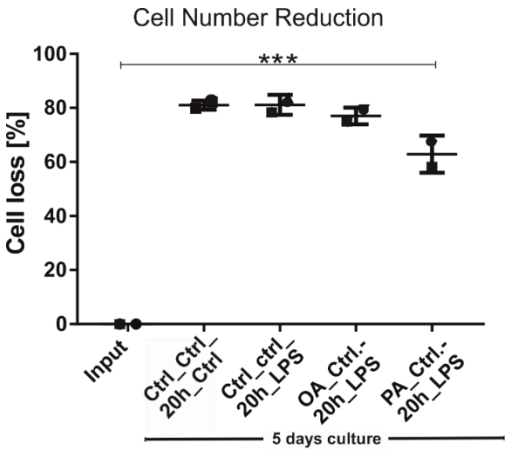

Figure 5.1.1.4: Definition of cell loss over time in the different experimental conditions (n=2). Ordinary one-way-ANOVA was used for significance prediction (*** $p \leq 0.0005$). ● – Donor X; ■ – Donor Y.

In total, **Figure 5.1.1.4** shows that we have an overall cell loss of approximately 80 % in the zero as well as in the LPS control. Interestingly, the cell loss of the 24h OA-

primed cells is slightly less and the PA-primed cells exhibit even 10 % less dead cells after LPS stimulation compared to both controls.

The cell number for each experimental condition was set to a number that adjusts 80 % of cell loss after five days of culturing.

Also, the isolation procedure of CD14/CD16 positive monocytes may, depending on the technique used, influence the cells for instance via activation by positive selection. To minimize influencing factors, we compiled methods of monocyte selection by negative depletion. In a first experiment I attempted to deplete all CD19, CD56 and CD3 positive cells from PBMCs by gradient centrifugation isolated.

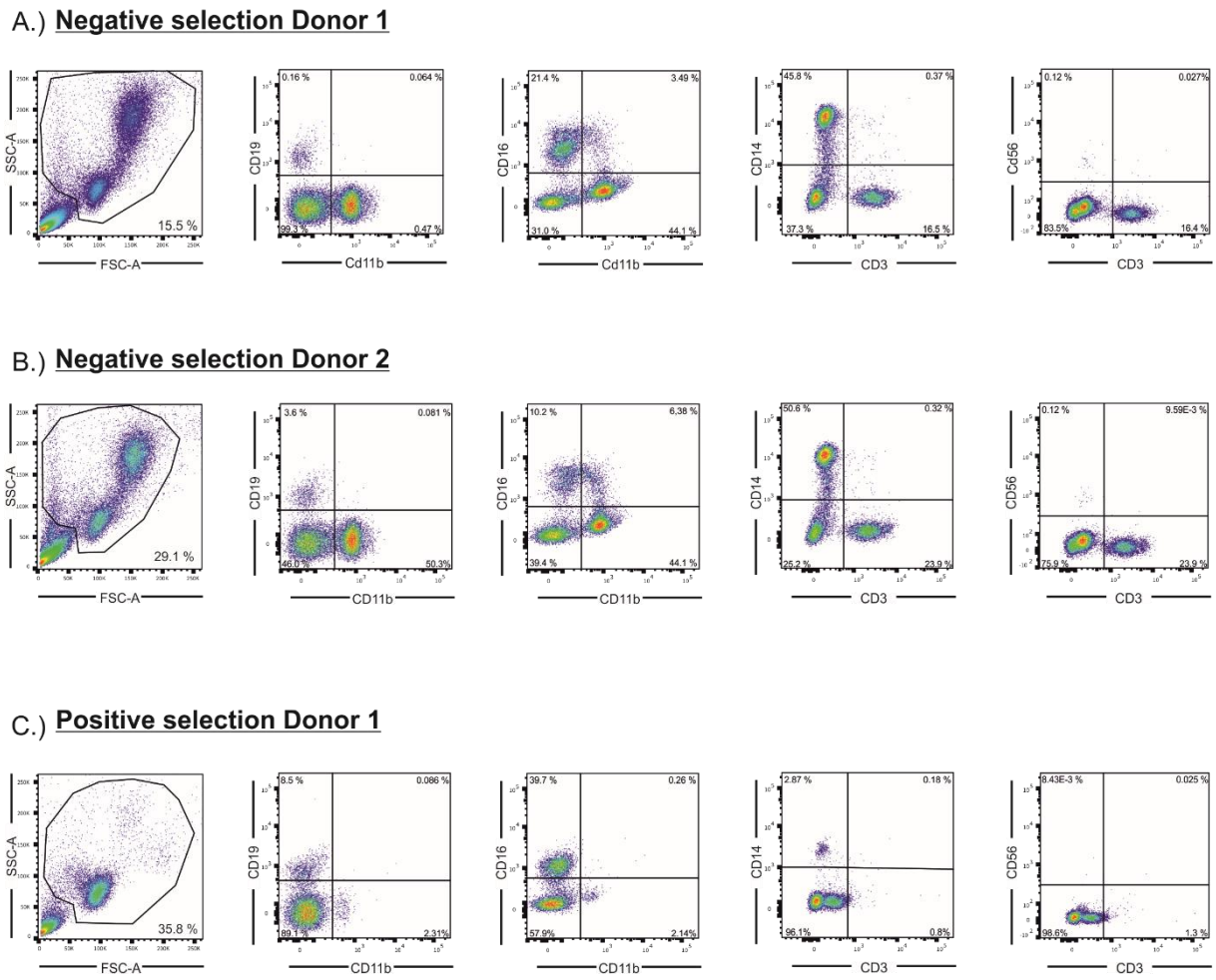

Figure 5.1.1.5: Monocyte Isolation by depletion of $CD19^+$, $CD56^+$ and $CD3^+$ cells. A.) Negative depletion fraction of Donor 1, B.) Negative depletion fraction of Donor 2 and C.) CD56, CD19 and CD3 positive isolation fraction.

As visualized in **Figure 5.1.1.5 A.)** and **B.)**, this method was not very successful. Although this isolation procedure was repeated with different antibody-coated microbead concentrations (20µl microbeads/10^7 cells & 25µl microbeads/10^7 cells) the purification of myeloid-derived cells was not effective. While CD56 positive NK-cells were almost fully depleted, the cell fraction was still contaminated by 2-4 % of CD19 and 16 – 24 % of CD3 positive cells. The CD14 and CD16 positive cells made up ~45 – 50 % and 16.5 - 25 %, respectively. A high load of cell debris and platelet contaminations is indicated by the SSC – FSC fraction that was not gated.
Since an increase in CD3 and CD19 microbead concentrations would rise costs further, we decided to resort to a purchasable kit alternative.

Two different monocyte isolation kits from Miltenyi Biotec were tested and compared. The “Pan Monocyte Isolation Kit” is an indirect magnetic labelling system for the isolation of untouched monocytes from human PBMCs. With this kit classical ($CD14^{++}CD16^{-}$), intermediate ($CD14^{++}CD16^{+}$) and non-classical ($CD14^{+}CD16^{++}$) monocytes can be enriched.

The “Monocyte Isolation Kit II” is based on the same mechanism. With this kit, non-monocytes like B-, T- and NK-cells are indirectly magnetically labelled using a cocktail of biotin-conjugated antibodies against CD3, CD7, CD19, CD56, CD123, Glycophorin A and CD16, as well as anti-biotin microbeads.

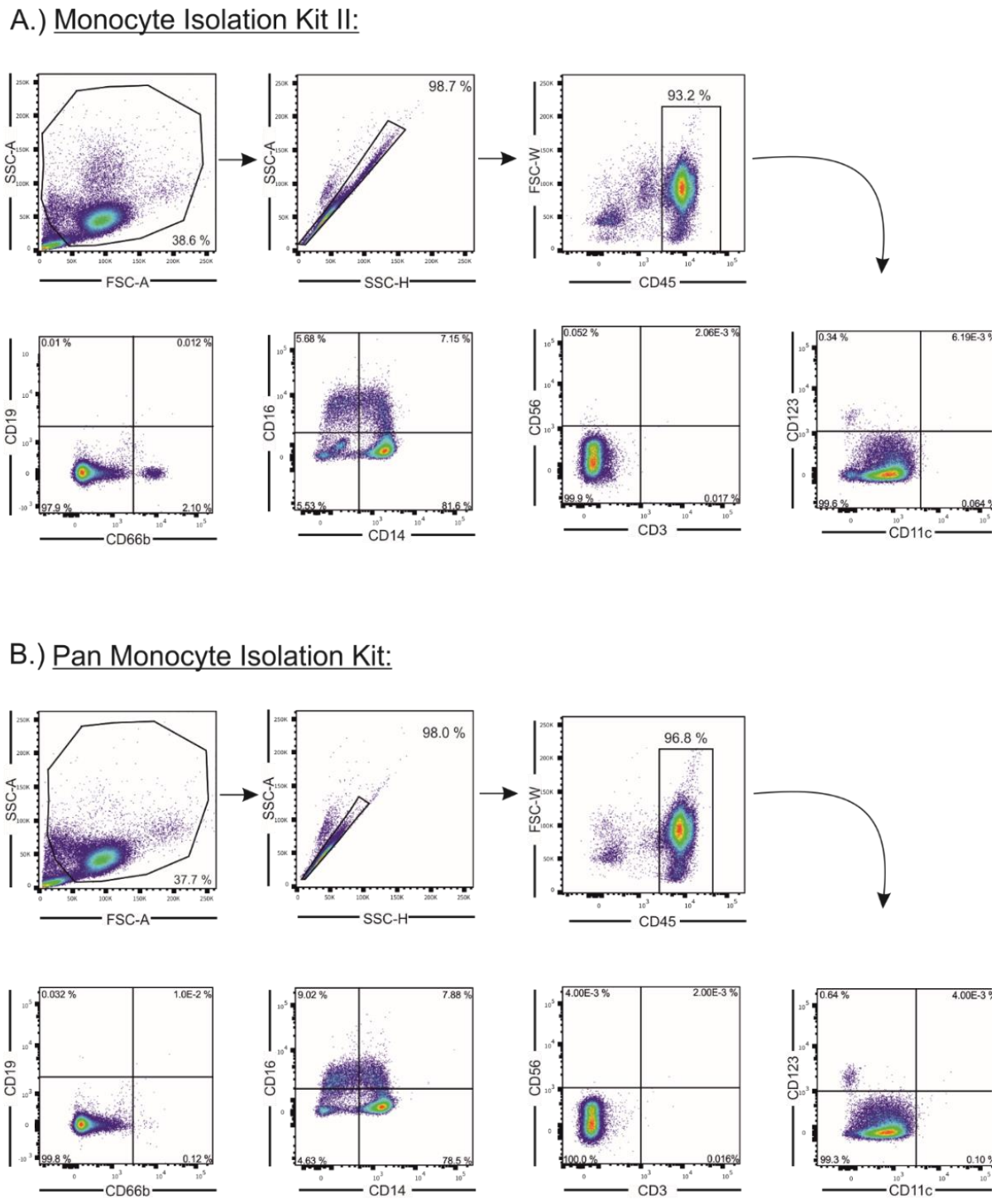

Figure 5.1.1.6: Monocyte isolation by negative depletion. A.) Monocyte Isolation Kit II (Milteniy Biotech) versus B.) Pan Monocyte Isolation Kit (Miltenyi Biotech).

As can be seen from **Figure 5.1.1.6 A.)** and **B.)**, the gated, CD45 positive cell fraction is highly pure with only 5.56 % of $CD14^{--}/CD16^{--}$ cells when using the Monocyte Isolation Kit II, and 4.63 % of $CD14^{--}/CD16^{--}$ cells when using the Pan Monocyte Isolation Kit.

In this experiment, we got 81.6 % of classical ($CD14^{++}CD16^{-}$), 7.15 % of intermediate ($CD14^{++}CD16^{+}$) and 5.68 % of non-classical ($CD14^{+}CD16^{++}$) monocytes using the Monocyte Isolation Kit II and 78.5 % of classical ($CD14^{++}CD16^{-}$), 7.88 % of intermediate ($CD14^{++}CD16^{+}$) and 9.02 % of non-classical ($CD14^{+}CD16^{++}$) monocytes when applying the Pan Monocyte Isolation Kit. This trend was confirmed by monocyte isolation from PBMCs of several further donors at different time points (minimum n=2).

However, with both methods, the initial gating of cells (SSC-A vs FSC-A) comprised highest 40 % of cell number (in majority of cases markedly less). Microscopic examination of isolated cells showed a high number of very small, but not moving cells, which due to their lens-shaped structure were suggested to be platelets. A fluorescent anti-CD61-antibody staining confirmed this suggestion. Therefore, tested monocyte isolation kits were supplemented by CD61 MicroBeads (Miltenyi Biotec).

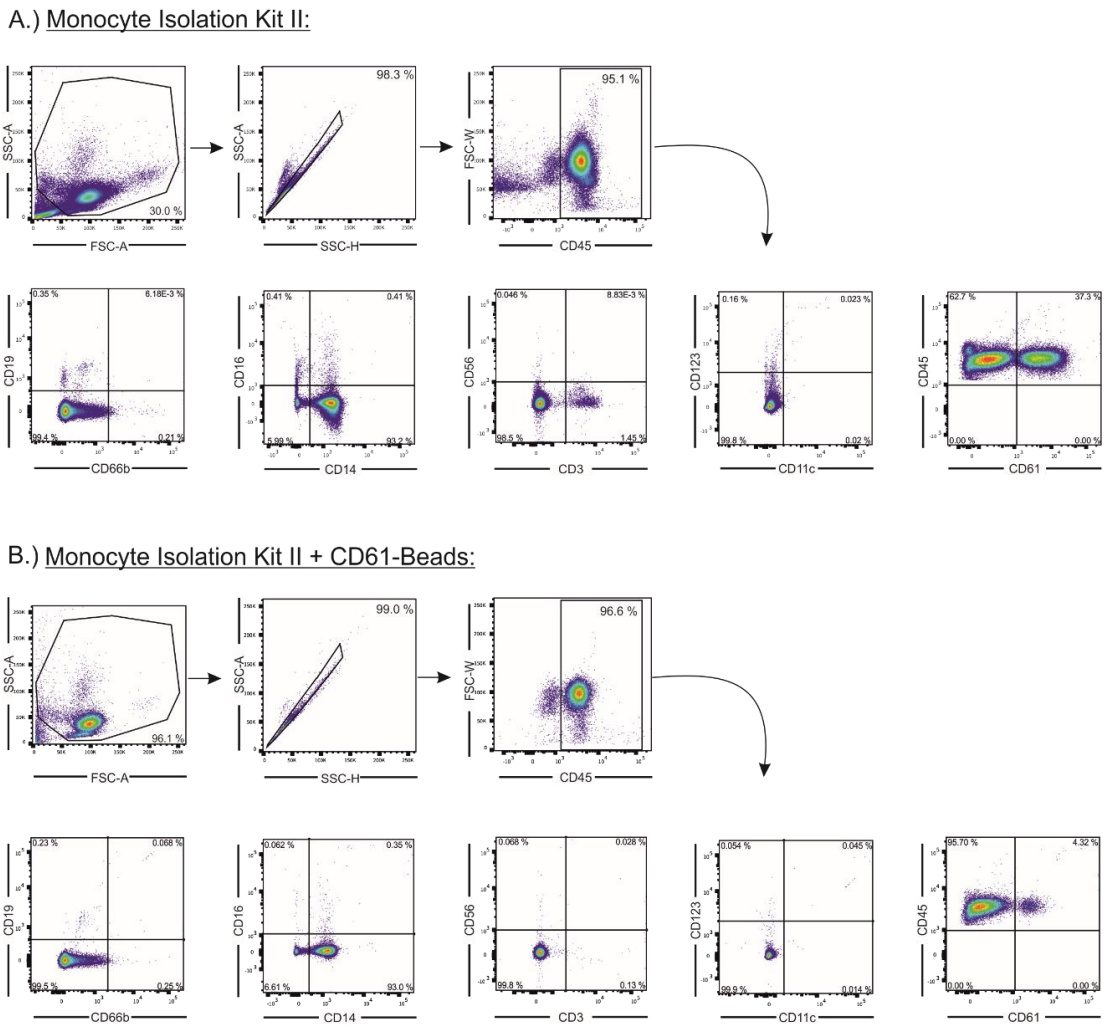

Figure 5.1.1.7: Monocyte isolation by negative depletion. A.) Untouched monocyte isolation using the Monocyte Isolation Kit II alone, or B.) in combination with anti-CD61 MicroBeads (Miltenyi Biotec).

Figure 5.1.1.7 shows the purity of monocytes isolated (**A.)**) by the Monocyte Isolation Kit II alone, or (**B.)**) in addition with CD61 microbeads. When comparing the percentage of cells gated in the first SSC-A versus FSC-A gate in **Figure 5.1.1.7 A.)** and **B.)**, it gets obvious that the addition of CD61 microbeads caused a huge reduction of contaminating cells. The gated population compassing the monocyte fraction in **Figure 5.1.1.7 A.)** represents just 30 % of measured cells, while with addition of CD61 microbeads (**B.)**) the monocyte fraction increased to more than 96 %. The assumption that a great number of contaminating cells is CD61 positive was confirmed by comparison of the CD45 vs CD61 gating in **Figure 5.1.1.7 A.)** and **B.)**. Monocyte isolation without addition of CD61 microbeads led to a 37.3 % $CD61^{+}$-cell contamination, while only 4.32 % of the gated population was CD61-positive when replenishing the monocyte isolation Kit with CD61 microbeads.

In total, it can be said that both, the Monocyte Isolation Kit II, as well as the Pan Monocyte Isolation Kit in combination with CD61 microbeads, mediate highly pure monocyte separation. Since the Pan Monocyte Isolation Kit is the successor of the Monocyte Isolation Kit II, allowing the isolation of classical, intermediate and non-classical monocytes from PBMCs, we decided to use this technique for untouched monocyte isolation.
Using the combination of the Pan Monocyte Isolation Kit and CD61 microbeads, a purity between 85-95 % could constantly be achieved.

5.2. Chromatin immuno-precipitation followed by sequencing (ChIP-seq.)

5.2.1 Indexing-first chromatin immunoprecipitation approach (iChIP)

The iChIP method was published by David Lara-Astiaso *et. al.*, 2014[159] who demonstrate histone ChIP-seq. results from samples of down to 500 cells. The particular on this approach is that barcoding is directly performed on the total cellular chromatin which allows multiple chromatin-barcoded samples to be pooled for immunoprecipitation. This step, according to the author, counteracts low input enzymatic reactions performed in the conventional ChIP methods.

To implement this method in our laboratory, the settings for chromatin shearing were optimized to our device (Covaris 220) and all intended ChIP antibodies were tested on human and murine chromatin samples.

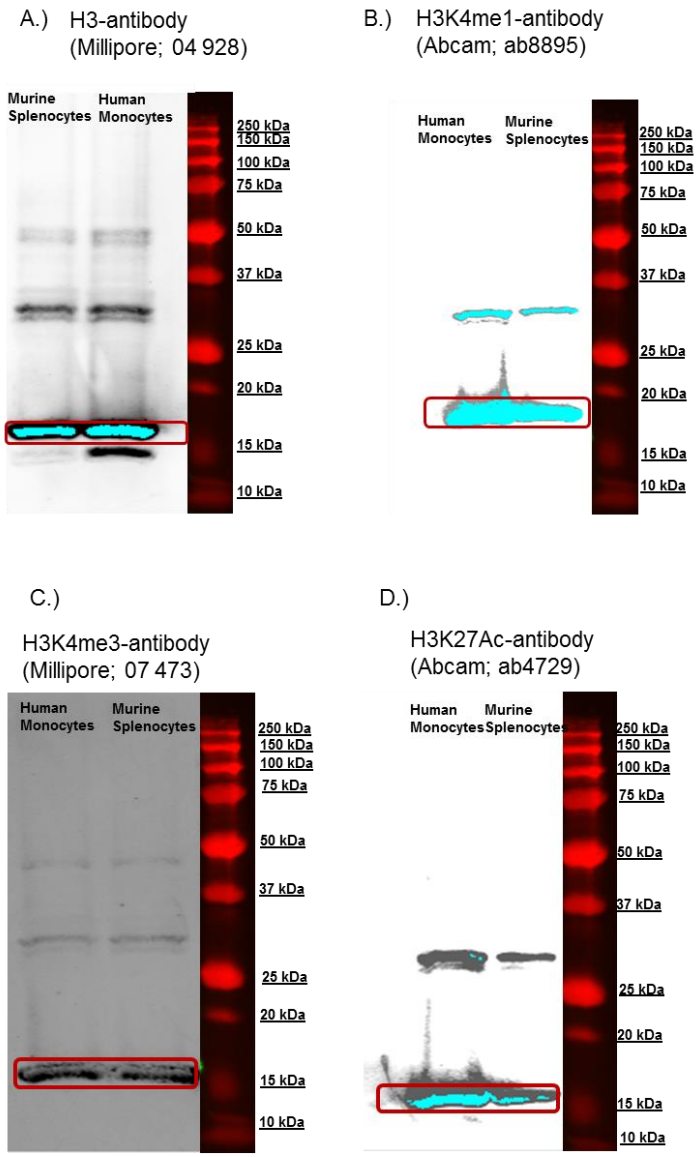

Figure 5.2.1: Histone ChIP antibody test with chromatin of human and murine cells. Direct Immunoprecipitation samples were taken for western blotting. As primary antibodies for western blotting the described antibodies were taken, respectively. A.) Anti-H3-pan-antibody-test (Millipore). B.) Anti-H3K4me1-antibody-test (Abcam). C.) Anti-H3K4me3-antibody-test (Millipore). D.) Anti-H3K27Ac-antibody-test (Abcam).

The western blots done on immunoprecipitated chromatin samples (see **Figure 5.2.1**) show that the ChIP-antibodies bind to their respective human and murine antigen.

The first iChIP test run, performed on 0.5 million cells per ChIP resulted in a very low anti-H3K4me1-antibody bound chromatin enrichment (**Figure 5.2.2 A.)**). To spot the source of chromatin loss, intermediate samples were taken after each critical step of the iChIP procedure starting with chromatin of 2 x 10^6 cells (see **Figure 5.2.2 B.)**). **Figure 5.2.2 C.)** represents the amount of chromatin that was set in and put out at each important intermediate iChIP step. Chromatin concentrations were determined using the Tape Station 200 device (Agilent). Comparing the quantity of chromatin that was set in for the H3-ChIP and the amount of chromatin that was bound by the anti-H3-antibody, it can be seen that only ~2.74 % of input 1 chromatin was bound by the anti-H3-antibody. This already indicates a huge loss of chromatin at this step of the iChIP procedure. In contrast to that, in the second step of the iChIP ~13.43 % of Input 3 chromatin was bound by the anti-H3K4me1-antibody-coupled-beads.

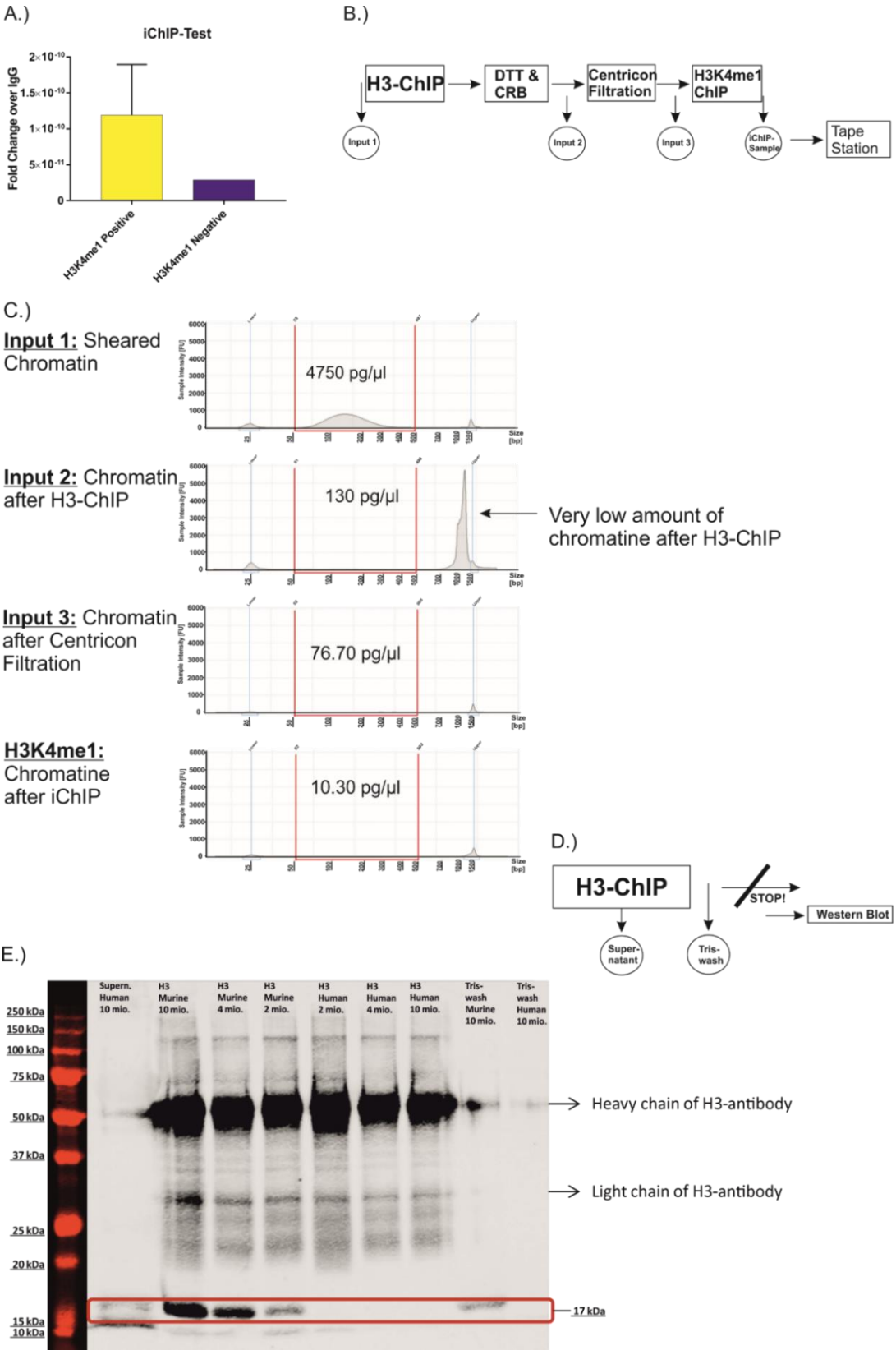

Figure 5.2.2: Verification of chromatin loss in the iChIP procedure. A.) First iChIP test run using chromatin of 0.5 x 10^6 cells per ChIP. B.) Scheme of intermission time points of the iChIP method for the identification of the source of chromatin loss. C.) Tape Station measurement results of intermediate iChIP samples. D.) Scheme of intermission time points of the iChIP method, stopped after the H3- ChIP. E.) Western blot of intermediate H3-ChIP samples of human and murine origin. Chromatin of 2 x 10^6, 4 x 10^6 and 10 x 10^6 cells was used in this experiment.

To find the source of chromatin loss in the first part of the iChIP procedure, a second intermission study was performed. Here, chromatin of human and murine samples using different cell numbers (10 x 10^6, 4 x 10^6 and 2 x 10^6), were taken into account. The time points of intermediate sample collection are visualized in **Figure 5.2.2 D.)**. H3-proteins were split from the antibody-bound-beads by denaturation and present H3-proteins were visualized by western blotting. As indicated by the light band of the first slot of the western blot, the supernatant of the 10 x 10^6 human cell sample still contained traces of the H3-protein, while in none of the human H3-ChIP samples H3 could be visualized. In contrast, in the murine H3-ChIP samples, H3 was bound and could be visualized in all cell number samples. However, in the intermediate Tris-wash sample H3 could also be visualized which assures for chromatin loss at this washing step. In total, the cell numbers taken to visualize the source of chromatin loss are far higher as the cell numbers that we want to investigate in our low cell number ChIP procedure. Further, the iChIP procedure should also be performable on human samples, which with the given H3-antibody was not successful. Therefore, the iChIP technique was not established in our laboratory.

5.2.2. Nuclei extraction by sonication (NEXSON) chromatin preparation method for ChIP-seq

The NEXON technique established by ultrasound-based nuclei extraction was published by Laura Arrigoni *et. al.*, 2015 [160], and is said to harmonize ChIP-seq. workflows across cell types and conditions as it allows to gain chromatin from properly isolated nuclei. Our intention was to establish a small cell number ChIP-seq. method, which fully eliminates the need for extensive optimization and sample-dependent adjustments. Therefore, we tried to include the NEXON in our ChIP-seq. workflow.

The ChIP-Nexon method was tested in combination with the IP-Star device (Diagenode). In the test experiments ~ 300.000 cells were taken per reaction.

The first step of establishment of the mentioned technique was the definition of shearing time for perfect cell lysis and chromatin fragmentation. The shearing time for monocyte lysis was set to 8 minutes (see ChIP-Nexon Method) since appropriate cell lysis could be ascertained by microscopic visualization of nuclei and cell wall appearance. Chromatin shearing was tested by setting the duration to 15 minutes, 20

minutes and 30 minutes (**Figure 5.2.2.1 A.), B.)** and **C.)**, respectively), aiming for DNA fragmentation in the sizes of 50 bp to 750 bp. TapeStation measurements were done to visualize and compare the shearing performance.

Validating the chromatin size obtained with the different shearing durations, it is visible that after 20 minutes of shearing the chromatin size is of best quality. Thus, the Nexon part was standardized to 8 minutes cell lysis and 20 minutes chromatin shearing for monocytes.

Optimization of Monocyte and Chromatine Shearing

A.)
Monocyte Lysis: 8 minutes shearing
Chromatine Fragmentation: 15 minutes shearing

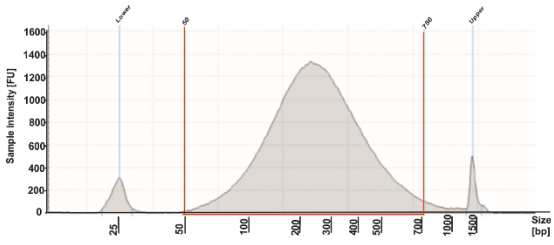

From [bp]	To [bp]	Average Size [bp]	Conc. [pg/µl]	Region Molarity [pmol/l]	% of Total
50	750	277	10500	76700	98.06

B.)
Monocyte Lysis: 8 minutes shearing
Chromatine Fragmentation: 20 minutes shearing

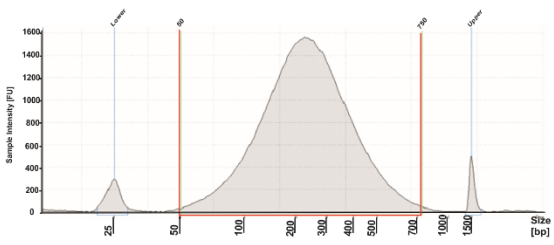

From [bp]	To [bp]	Average Size [bp]	Conc. [pg/µl]	Region Molarity [pmol/l]	% of Total
50	750	256	13200	103000	99.27

C.)
Monocyte Lysis: 8 minutes shearing
Chromatine Fragmentation: 30 minutes shearing

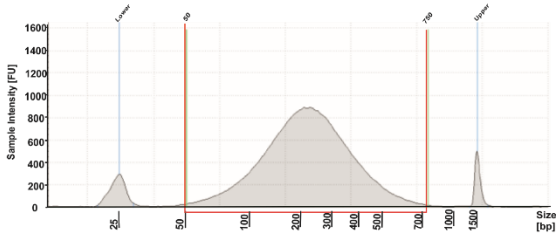

From [bp]	To [bp]	Average Size [bp]	Conc. [pg/µl]	Region Molarity [pmol/l]	% of Total
50	750	243	6780	55600	99.07

ChIP-Nexon-Test using the IP-Star (Diagenode)

D.)

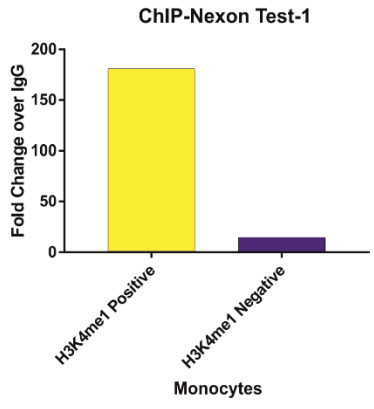

E.)

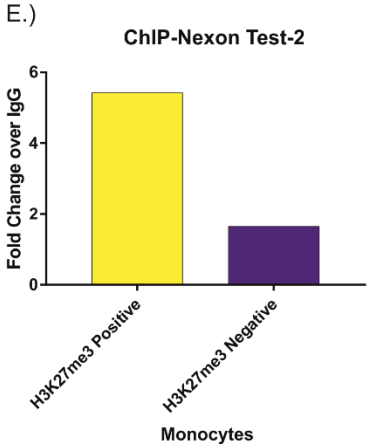

Figure 5.2.2.1: ChIP-Nexon optimization on monocytic samples. A.), B.), C.): Chromatin fragment size and amount verification after cell lysis and chromatin shearing by sonification using the Tape Station device. Monocyte lysis was always performed by sonification for 8 minutes A.) Chromatin shearing for 15 minutes. B.) Chromatin shearing for 20 minutes. C.) Chromatin shearing for 30 minutes. D.) & E.): ChIP-Nexon test run with chromatin of ~333.000 monocytes using the IP-Star device (Diagenode). This experiment was performed by the Bachelor student Lee Xian See.

The first test Nexon-ChIP run, using chromatin of monocytes from three different donors, was performed using anti-H3K4me1 and anti-H3K27me3-antibodies. These antibodies bind to enhancer sides and to a specific chemical modification of the DNA-

packaging protein histone H3 which is commonly associated with repression of expression of nearby genes, respectively. As visualized in **Figure 5.2.2.1 D.)** and **E.)**, the H3K4me1 ChIP was successful with a calculated fold change over the IgG control ChIP of ~180, while the calculated fold change of the H3K27me3 ChIP lies at about 5.5. As this was the expected result, the ChIP-Nexon method was shown to work effectively and was established as standard ChIP-seq. procedure in our laboratory.

5.3 Assay for transposase-accessible chromatin with high throughput sequencing (ATAC-Seq.)

ATAC-seq was first described by Buenrostro J.D. *et. al.*, 2013 as an alternative and advanced method for MNase-seq, FAIRE-Seq and DNase-Seq. This method is based on a process called tagmentation and allows to map chromatin accessibility genome-wide. The key player of this process is a mutant, hyperactive Tn5 transposase which simultaneously fragments accessible DNA and taggs it with sequencing adaptors. Regions of increased accessibility can be inferred by sequencing reads and regions of nucleosome position and transcription factor binding can be mapped.[161,162]

To reduce costs for the ATAC reaction we cooperated with Professor Dr. Matthias Geyer from the Department of Structural Immunology at the University of Bonn. He supplied us with self-produced, hyperactive Tn5, containing classical E54K and L372P missense mutations (but wild type M56) and comprising a C-terminal intein tag and a chitin-binding domain (CBD). Using a chitin-column they purified the in-house Tn5 protein from *E.coli* transfected with pTXB1-Tn5ES (as described by Picelli *et. al*., 2014[178]). To activate the in-house Tn5 transposase, it needs to be loaded with an equimolar mixture of pre-annealed primers (see *3.5 ATAC Primers*), containing hyperactive mosaic end (ME) sequences. This step can be done at two different time points, either on-column loading, which is done in the chitin-column prior to Tn5 purification, or after column purification, in an extra performed loading step. We first tried to load the Tn5 after column purification as we thought that the inactive Tn5 might be better storable. However, to prevent dimerization and dimer extension during subsequent PCR amplifications of tagmented DNA, residual, unbound primers needed to be removed in an extra step, after Tn5 loading. To optimize the purity of the activated Tn5 product, two purification techniques were tested against each other and

tagmentation capabilities were tested using genomic DNA of ~50.000 RAW 264.7 cells per reaction.

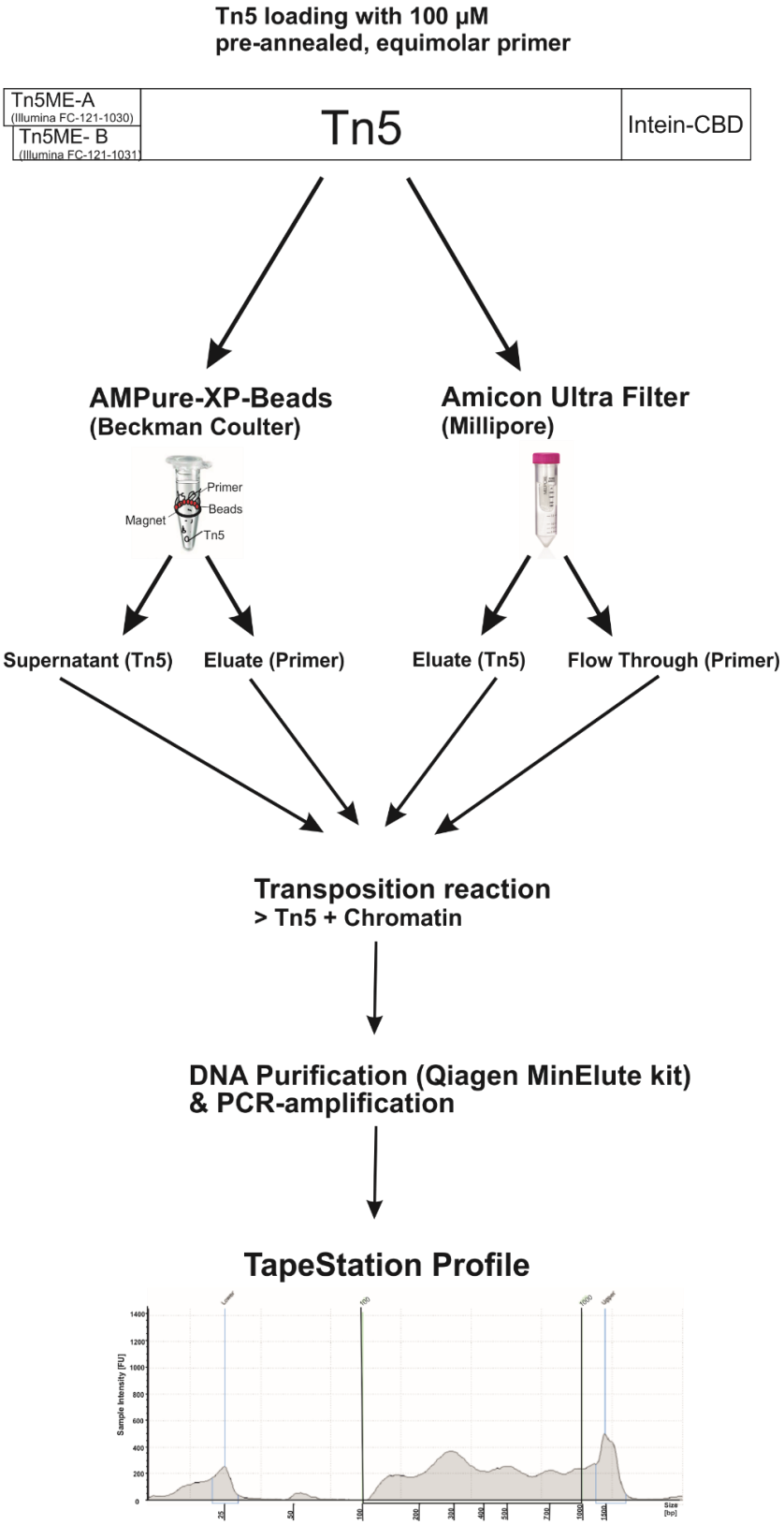

Figure 5.3.1: Tn5 activation and purification. Scheme of experimental set-up. Microtube pictures were modified for the scheme from web pages[179,180].

In a first phase we used Agencourt AMPure-XP beads (Beckman Coulter) and Amicon Ultra Filters (Millipore) as purification methods (see **Figure 5.3.1**) for excess primer removal according to manufacturer's instructions. To assert that no activated Tn5 is lost during the purification process we tested both, the filter eluate and bead supernatant fractions (active Tn5 expected) and filter flow-through and bead eluate fractions (residual primer, but no active Tn5 expected) for their capability to actively perform a tagmentation reaction on genomic DNA. Post tagmentation, all reactions were purified using the MinElute Kit (Quiagen) and PCR amplified (see *4.9.1 ATAC-sequencing with in-house Tn5*) for 11 cycles. Amplified tagmentation products as well as residual primers and primer-dimers were visualized by Agilent High Sensitivity D1000 assays on a TapeStation 2200 system. As positive control a tagmentation profile generated with commercially available Tn5 (Illumina) was assayed while the purification control reaction was performed with unpurified, loaded Tn5. **Figure 5.3.2** shows the profiles of the High Sensitivity D1000 assays.

Tn5 expected **Tn5 not expected**

A.) AMPure-XP-Beads Eluate B.) AMPure-XP-Beads Supernatant

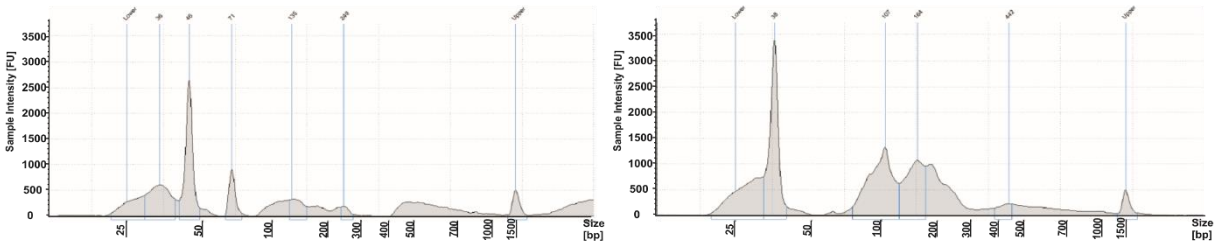

C.) Amicon Ultra Filter Eluate D.) Amicon Ultra Filter Flow-Through

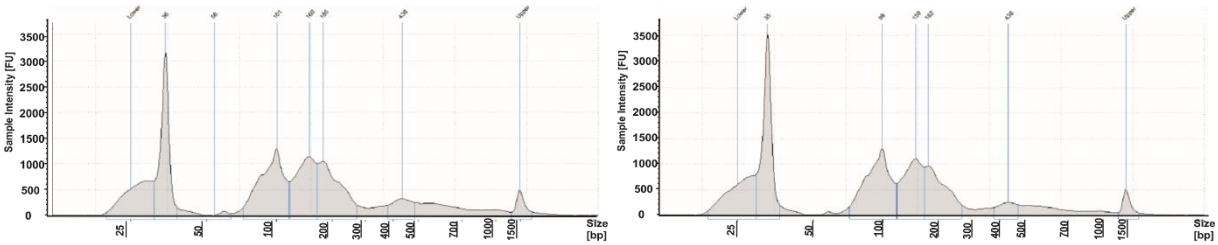

F.) Illumina Tn5 E.) 100 µM equimolar primer

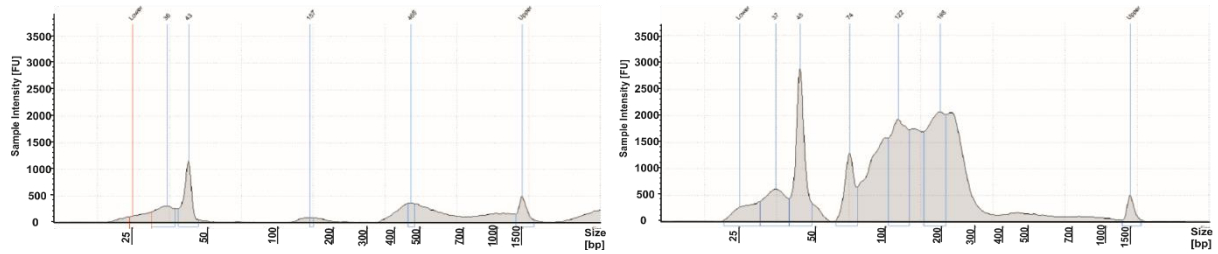

Figure 5.3.2: Comparison of two different approaches to remove excess primers from loaded Tn5. Agilent High Sensitivity D1000 TapeStation assay profiles of tagmented and PCR amplified genomic DNA from 50.000 RAW 264.7 cells are used as indicator for Tn5 tagmentation activity and protein purity. In A.) and B.) amplification products of tagmentation reactions performed with supernatant or eluate from 2.5-fold Agencourt AMPure-XP-bead (Beckman Coulter) purified Tn5 are visualized, respectively. C.) and D.) show profiles from tagmentation reactions performed with the Amicon ultra 0.5 ml centrifugal filters C.) eluate and D.) flow-through. E.) shows a tagmentation profile after amplification generated with commercially available Tn5 (Illumina). The negative control profile depicted in F.) was generated with only 100 µM equimolar pre-annealed primer in place of loaded Tn5 during the tagmentation reaction with subsequent amplification. Experiment was performed together with the PhD student Maren Köhne.

During the purification process of activated Tn5, residual primers and primer-dimers precipitate to the surface of the paramagnetic-particles and can be discarded, leaving the supernatant containing the purified Tn5. **Figure 5.3.2 A.)** and **B.)**, shows that the reaction performed with the supernatant as well as the one performed with the bead

eluate contain a high peak with oligonucleotides of ~50 bp, indicating that excess loading primer removal was not complete. When comparing the TapeStation assay pattern of PCR products from the tagmentation reaction performed with unpurified Tn5 (**Figure 5.3.2 F.)**), similarities in the full patterns can be recognized in both bead clean-up fractions (**A.)** & **B.)**) showing that the bead clean-up was not successful. Nevertheless, comparing it to the DNA pattern of the positive control reaction, performed with the commercially available transposase (Illumina) (**Figure 5.3.2 E.)**), one can see similarities in tagmented gDNA patterns. This indicates that the in-house Tn5 was activated and able to at least tagment the gDNA partially. The tagmentation patterns of all reactions look however suboptimal which probably was coursed by too abundant amplification and overloading of the high sensitivity screen tapes.

Interestingly, also in the Illumina sample a peak at the size of ~43 bp is detectable, indicating dimer formation of residual primers from DNA amplification after the tagmentation reaction. These residual primers usually get lost at a later purification step using the Qiagen Min elute kit (see *4.9.1 ATAC with in-house Tn5*).

The Amicon Ultra Filter (Millipore) purification was done directly after Tn5 activation by primer loading. Both, the eluate, intended to contain the activated Tn5, as well as the flow-through intended to contain excess primers were tested in tagmentation reactions (**Figure 5.3.2 C.)** and **D.)**). Remarkably, both samples look very similar in their patterns, showing residual primer-dimer contaminations as well as large amplification fragments, indicating Tn5 leakage through the filter. Since the tested sample purification techniques did not bring the desired results, we conferred with the group of Prof. Dr. Geyer and decided to perform an on-column purification as described by Picelli *et. al.*, 2014[178].

The on-column purification was performed by Ann-Katrin Greifenberg from the Geyer group, who activated the Tn5 by loading it with equimolar, pre-annealed primers directly on the chitin-column. Thus, allowing excess un-loaded oligonucleotides to be discarded with the flow-through before releasing the -Tn5 from the column by DTT induced cleavage of the intein-CBD tag (see Picelli *et. al.*, 2014[178]).

To verify that not only purification, but also primer annealing and thus Tn5 activation was successful, we assessed the functionality of the assembled Tn5 through its ability to tagment high-molecular-weight genomic DNA into 400 – 500 bp fragments.

Therefore, tagmentation samples of reactions performed with 100/200 ng gDNA (murine lymphocytes) using the in-house Tn5, were loaded on an agarose gel (1% Type LE, in TAE buffer). As negative controls, 500 ng of un-tagmented and un-amplified DNA and 100 ng (right) / 200 ng (left) of un-tagmented but PCR amplified DNA was also assessed.

A.) Agarose-Gel of Tn5 transposed and un-transposed gDNA

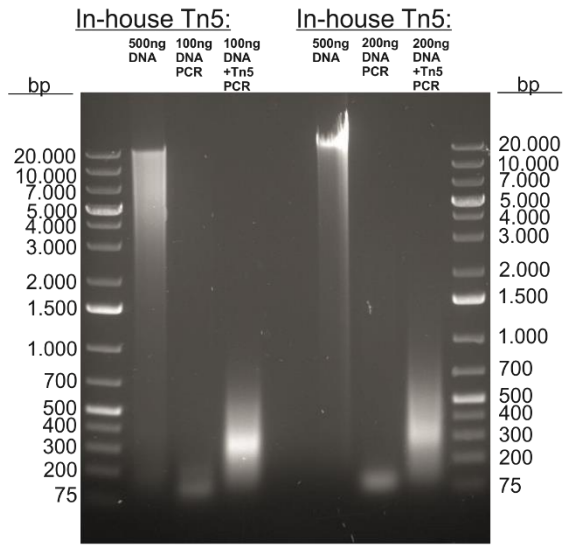

B.) 100 ng gDNA PCR amplified

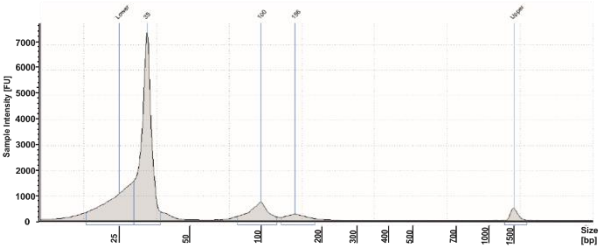

C.) 100 ng gDNA + Tn5 (in-house) PCR amplified

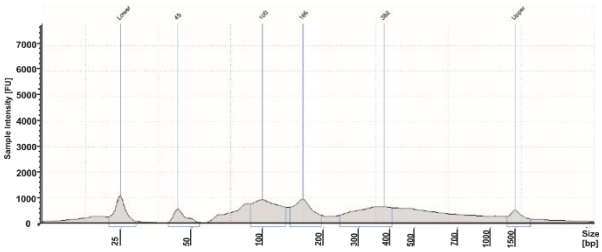

Figure 5.3.3: In house Tn5 activity test. A.) Gel picture of in-house Tn5 transposed and un-transposed, non-PCR and PCR-amplified pre-amplified DNA. Gene Ruler 1kb DNA Plus Ladder, 1% Agarose. B.)-C.) Visualization of fragment size of PCR amplified genomic DNA (5 ng) by Tape Station High Sensitivity measurement. C.) and of in-house Tn5 tagmented 5 ng genomic DNA, PCR amplified. Experiment was performed together with the PhD student Maren Köhne.

In **Figure 5.3.3 A.)**, it can be seen that the PCR amplified tagmentation samples are fragmented in the range of ~100 bp – 1.000 bp with the highest concentration at about 250 – 400 bp. The un-tagmented gDNA is visualized at the left side (500 ng DNA) of the gel, representing the negative control for the respective tagmentation reactions. In both cases un-tagmented gDNA is ~20 kb in size. The PCR products of the un-

tagmented gDNA are with ~75 bp very short and represent excess primers and primer-dimer.

The TapeStation D1000 high sensitivity assay profiles of the PCR amplified gDNA sample (**Figure 5.3.3 B.)**) and the in-house Tn5 tagmented and PCR amplified gDNA sample (**Figure 5.3.3 C.)**) further confirm the size distribution of the loaded samples and thus the desired activity of in-house Tn5.

Since the in-house Tn5 was proven to be functional after column purification, the optimal working conditions for the tagmentation reaction needed to be assessed. Thereby we geared to the settings described by Picelli et. al., 2014[178] and by the Nextera Illumina kit. We set the reaction temperatures to 55°C or 37°C, the reaction time to 30 minutes or 10 minutes and the optimal amount of Tn5 was tested using 0.5 µl, 1 µl or 5 µl Tn5 per reaction. For each reaction, chromatin of ~200.000 RAW264.7 cells was used.
Hereby, it should be considered that the perfect DNA size range for library preparation of later ATAC-samples lies between 100 bp and 1000 bp. In **Figure 5.3.4**, the percental amount of 100 bp – 1000 bp fragments is visualized for each test condition.

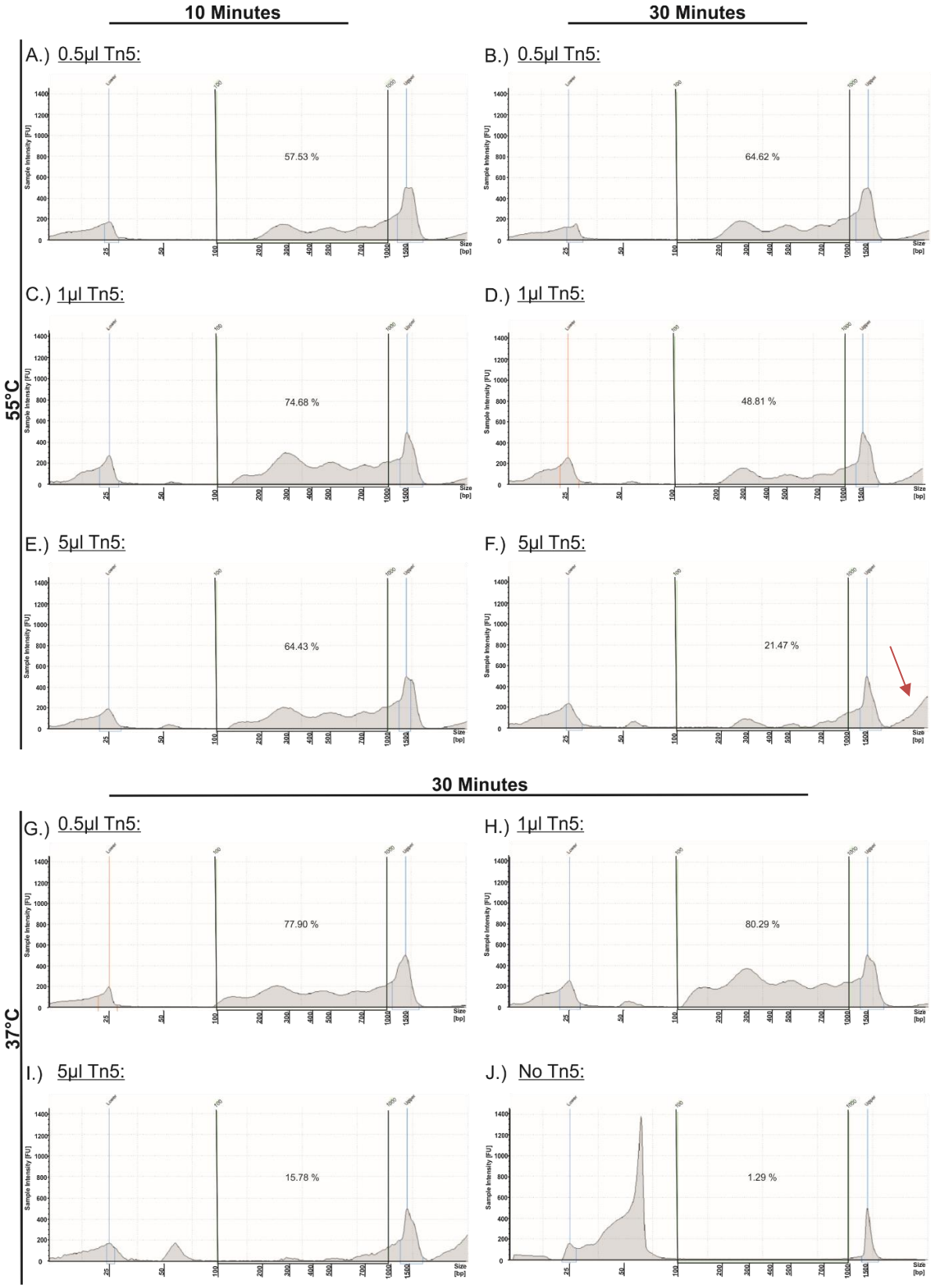

Figure 5.3.4: Optimization of tagmentation reaction time and temperature. A.) – F.) visualizes DNA fragment size after tagmentation at 55°C. Samples visualized in A.), C.) and E.) were incubated with varying amounts of in-house Tn5 (stated above each figure) for 10 minutes, while those visualized in B.), D.) and F.) are incubated for 30 minutes. Samples visualized in G.) – J.) are incubated at 37°C for 30 minutes. The in-house Tn5 concentrations used in the different reactions are given for each figure. Experiment was performed together with the PhD student Maren Köhne.

Investigating the DNA size distribution after tagmentation, visualized in **Figure 5.3.4** it gets visible that tagmentation worked best with 1 µl Tn5 at 37°C and 30 minutes incubation time (**Figure 5.3.4 H.)**) and with 0.5 µl Tn5 and incubation at 37°C for 30 minutes (**Figure 5.3.4 G.)**) with 80.29 % and 77.90 %, respectively. As indicated by the red arrow in **Figure 5.3.4 F.)**, at 55°C, with all varying conditions, there is also DNA of larger fragment size, which can't be fully visualized by the High Sensitivity 1000 Tape (Agilent). With a reaction time of 30 minutes at 37°C and 0.5 or 1 µl Tn5 (**Figure 5.3.4 I & H.)**) this is almost not detectible. Due to the test result we set our standard conditions for the tagmentation reaction to 1 µl Tn5 and an incubation time of 30 minutes at 37°C.
The NEXON-ChIP-seq. technique was implemented as standard procedure in our laboratory.

5.4 Trained immunity experiment on monocytes

Western diet is characterized by a high intake of omega-6 and saturated fatty acids, a low intake of omega-3 fatty acids and the consumption of too much sugar and salt.[181] In this study, we investigated the effect of the saturated fatty acid palmitic acid and the unsaturated fatty acid oleic acid on immune cells, namely monocytes. Thereby, the direct as well as long term effects (after 3 days wash-out) of the fatty acids on monocyte-derived cells was determined. In addition to that, the ability of memory development due to polarization of monocytes by OA and PA was assessed by later stimulation with LPS.

5.4.1 Main experiment

Classical ($CD14^{++}CD16^{-}$), intermediate ($CD14^{++}CD16^{+}$) and non-classical ($CD14^{+}CD16^{++}$) monocytes were isolated by negative depletion from PBMCs of previously Donor-selected buffy coats (see **Table 4.11.1.1**). The purity of isolated cells was validated by FACS analysis using the antibodies listed in **Table 3.3.2**.

Purity Check

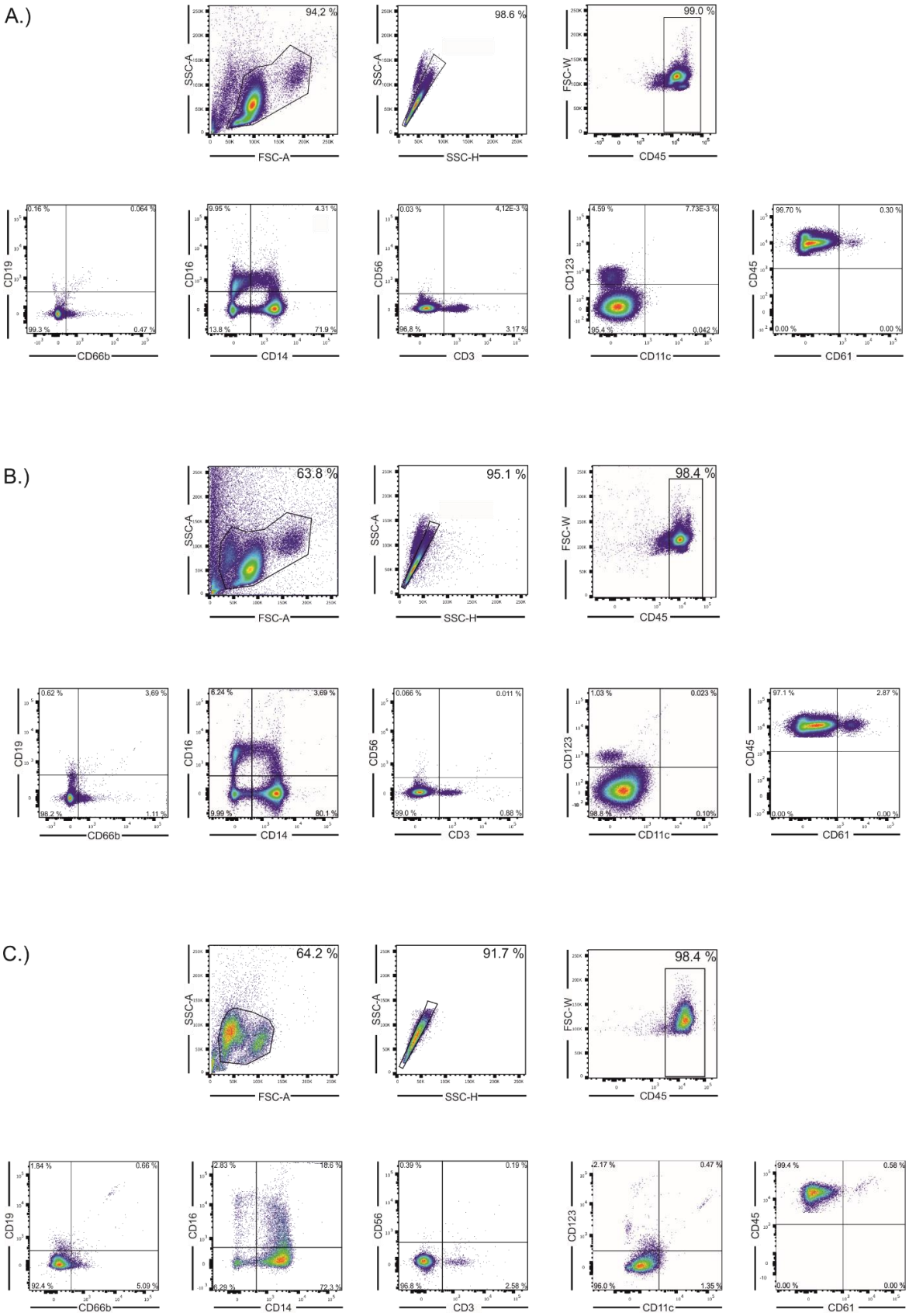

Figure 5.4.1.1: Purity check of negatively depleted, CD14/CD16 positive cells from human buffy coats. Visualized is the gating strategy used for the purity check. A.) shows the purity of cells Isolated from Donor 1, B.) from Donor 2 and C.) Donor 3.

Figure 5.4.1.1 shows the gating strategy and statistical distribution of bound surface markers. The CD16-CD14 gate illustrates that the isolated cells of Donor 1 (**Figure 5.4.1.1 A.)**) are to more than 86 %, of Donor 2 (**Figure 5.4.1.1 B.)**) to 90 % and of Donor 3 (**Figure 5.4.1.1 C.)**) to more than 93 % $CD14^+$, $CD16^+$ or $CD14^+$ and $CD16^+$ positive. The cells of Donor 1 (**Figure 5.4.1.1 A.)**) are to 3.17 % CD3 positive and have a 0.3 % platelet impurity. Donor 2 (**Figure 5.4.1.1 B.)**) has with 0.67 % of CD19 positive B-cells, with 0.88 % of CD3 positive T-cells and with 2.87 % of CD61 positive platelets in the gated area still a purity of ~90 %. The contaminating cells in the cell sample of Donor 3 (**Figure 5.4.1.1 C.)**) consist to 1.54 % of CD19 positive B-cells, to 5.09 % of CD66b positive granulocytes or eosinophils, to 2.59 % of CD3 positive T-cells, to 0.58 % of CD61 positive platelets and to 0.45 % of CD123 and CD11c double positive dendritic cells.

Validating the statistical distribution of surface markers of isolated cells from all three donors (**Figure 5.4.1.2**), it can be said that the isolation of *classical, intermediate and non-classical monocytes* was successful, possessing a mean percentage of 91.14 %.

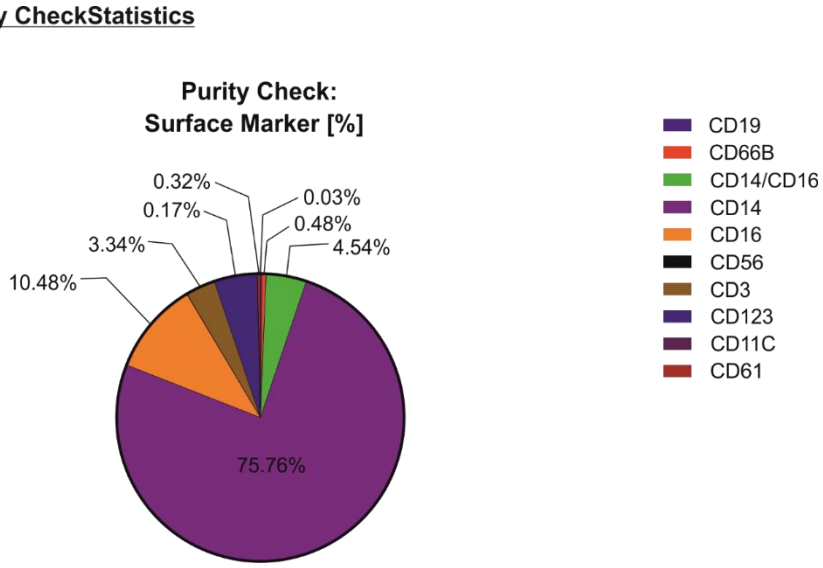

Figure 5.4.1.2: Statistical distribution of surface markers of freshly isolated myeloid-derived cells.

Since the monocyte isolation was successful, cells from each donor were cultured according to the experimental setup (see **Figure 5.5.1**). To assure that the fatty acids in the medium were well dissolved and ingestible by monocytes, 20 hours control and palmitic acid cultured cells of all three donors were harvested for RT-qPCR

measurements of mRNA content. Due to cell number restrictions we decided to check only for PA cultures as PA is less well dissolvable than OA. As markers we used IL1B, CCL3 and RCAN-1 which have been shown to be upregulated upon PA stimulation in other studies[182]. As described previously, CCL3 is important in immune responses to infection and inflammation as it induces the synthesis and release of other pro-inflammatory cytokines such as interleukin-1 (IL-1), IL-6 and TNF-α from macrophages[183].

Interleukin-1β is a pro-inflammatory cytokine involved in many obesity-associated diseases in a NLRP3-dependent way. In recent studies palmitate (C16:0) demonstrated its ability to induce IL-1β secretion in human macrophages[184].

RCAN-1 is expressed in lesional macrophages and studies have shown that RCAN-1 plays a role in atherosclerosis progression as atherosclerotic plaques show an up-regulated RCAN-1 expression profile[185].

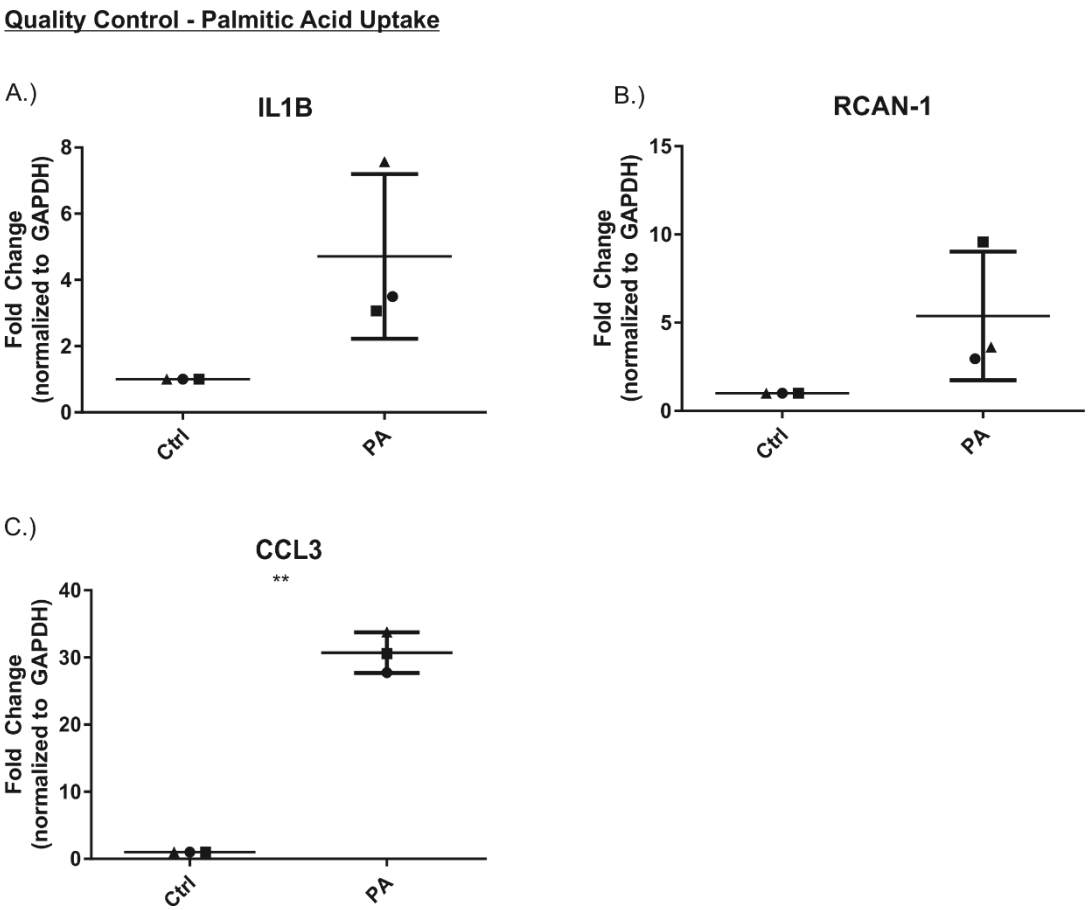

Figure 5.4.1.3: Quality control of fatty acid uptake. RT-qPCR results of 20 hours PA and control medium cultured cells (n=3). A.) IL1B up-regulation due to palmitic acid uptake. B.) Upregulation of RCAN-1 transcripts in response to PA uptake. C.) CCL3 up-regulation in response to PA uptake. p* ≤ 0.05, p** ≤ 0.005, p*** ≤ 0.0005 (Student's t-test) ▲ – Donor 1; ● – Donor 2; ■ – Donor 3.

In **Figure 5.4.1.3** the fold change of specific transcripts of described genes over GAPDH, normalized to the control, is depicted. The fold change in PA stimulated samples is for IL1B between 2.5 and 7.5 times and for CCL3 between 28 and 34 times higher as in control samples. Either RCAN-1 signals are ~3 to 9 times higher as in control cultures. The cells respond to PA uptake with the upregulation of tested inflammatory marker genes, however the different donors induced totally different expression levels for IL1B and RCAN-1. In case of CCL3 a closer transcriptional relationship can be seen, showing a p-value ≤ 0.005.

The toxicity of culture conditions and the resulting cell viability was flow cytometrically measured by AnnexinV-PI staining. AnnexinV-FITC binds to membrane phosphatidylserine from the inner side of the plasma membrane of apoptotic cells and Propidium Iodine (PI) intercalates with reachable DNA strands of dead cells.[154,186]

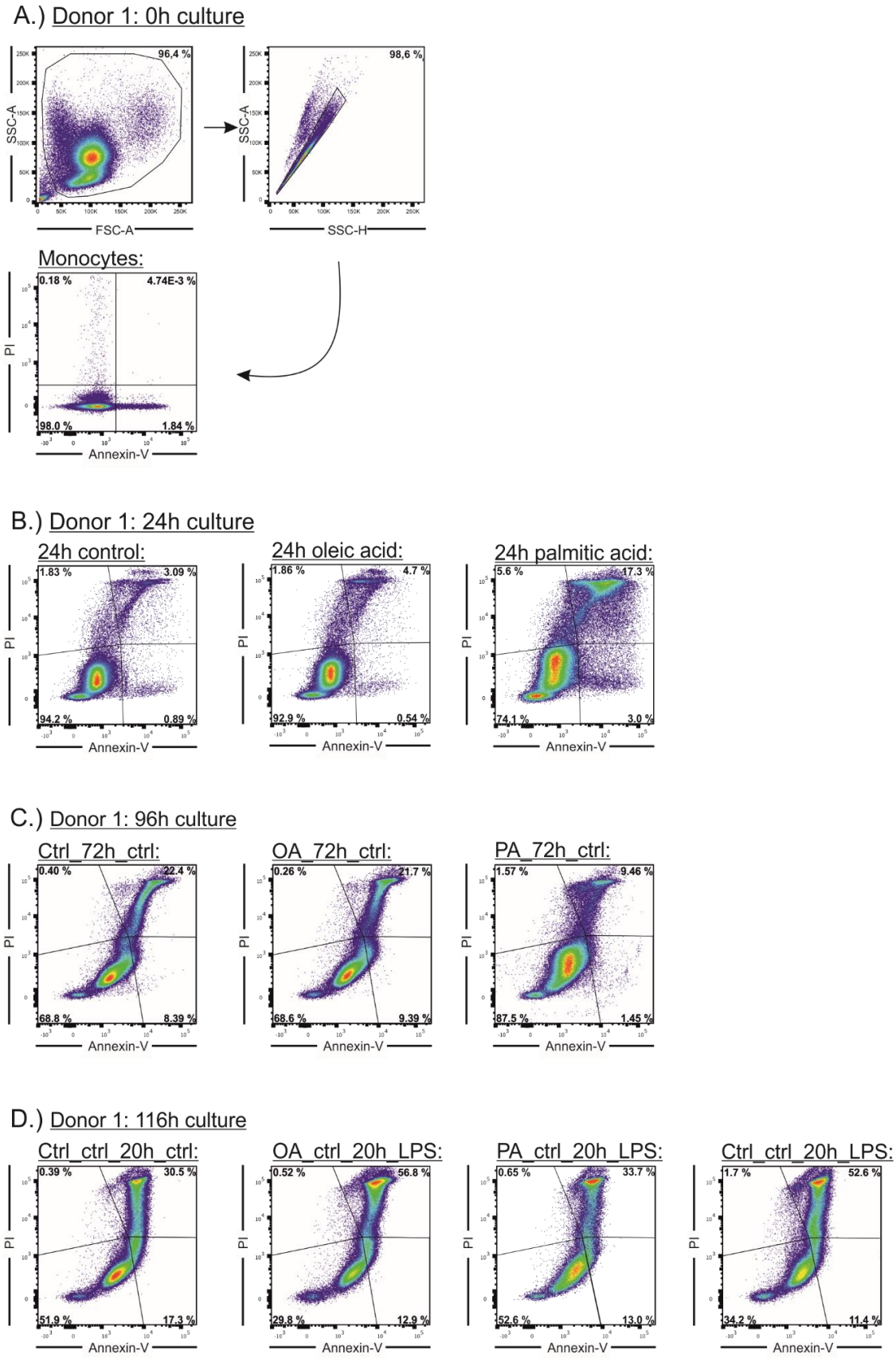

Figure 5.4.1.4: Cell survival after training. A.) Gating strategy and AnnexinV-PI staining of freshly isolated monocytes. B.) AnnexinV-PI staining of 24 hours fatty acid stimulated monocytes. C.) AnnexinV-PI staining after 24h stimulation followed by 72 hours of wash-out. D.) AnnexinV-PI staining after re-stimulation with LPS.

Figure 5.4.1.4 visualizes the gating strategy of performed flow cytometric measurements. The dead-cell/apoptosis measurements are visualized for all conditions at each intermediate time point for Donor 1. The statistical cell survival of all donors and single conditions taken together are visualized in **Figure 5.4.1.5**.

Figure 5.4.1.5: Percental cell survival at the different time points of training based on AnnexinV-PI staining.

Figure 5.4.1.5 shows the mean statistical distribution of viable, apoptotic and dead cells. Approximately 2.5 % of freshly isolated monocytes are Annexin-V and PI positive while about 97.5 % of isolated cells are viable (**Figure 5.4.1.5 A.)**). After 24 hours of culturing in control, oleic acid or palmitic acid medium (**Figure 5.4.1.5 B.)** - **D.)**) the viability of present cells in 24h_Ctrl and 24h_OA samples are with 20.37 % dead cells and ~76 % viable cells, and 21.9 % dead cells and ~75 % viable cells, respectively, very similar. The viability of 24h_PA stimulated cells however is with ~41 % dead cells and 4.68 % in apoptosis running cells rather diminished and makes up only ~54 % viable cells.

After the three-day wash-out period the viability of OA_72h_Ctrl primed and Ctrl_72h_Ctrl cells is with ~67.5 % viable-, ~20 % dead- and 12.73 % apoptotic cells, and with ~73.3 % viable-, 16 % dead- and 10.38 % apoptotic cells, respectively, still quite similar. Best viability of present cell is perceived in PA_72h_Ctrl cultures, which, at this time point, contain ~80 % viable, ~17.5 % dead and 2.41 % apoptotic cells.

At day 5 of culturing, after the 20 hours LPS stimulation, the viability of present cells in the PA_ctrl_20h_LPS and the Ctrl_ctrl_20h_LPS samples is now very similar. Ctrl_ctrl_20h_LPS has in total about 52.5 % viable cells, ~35 % dead cells and ~12 % are apoptotic. The PA_ctrl_20h_LPS cultures show even ~59 % viable cells, ~31 % dead cells and ~10 % of apoptotic cells. In contrast, the OA_ctrl_20h_LPS cultures have a mean viability of just ~37 %, while ~48 % of cells are dead and further 15.57 % of cells are running into apoptosis. The Ctrl_Ctrl-20h_Ctrl cultures, lacking the 20 hours LPS stimulation, show 47.83 % viable cells, ~37 % dead cells and also 15.59 % of apoptotic cells. In summary it can be said that at the end of the experiment PA-primed cells show the highest viability of present cells after PA_Ctrl_20h_LPS cultivation whereas OA-primed cells show lowest viability after OA_Ctrl_20h_LPS stimulation. Interestingly, the viability of Ctrl_Ctrl_20h_LPS cultures is 4.5 % higher as in Ctrl_Ctrl_20h_Ctrl cultures which didn’t get the strong inflammatory LPS signal for the last 20 hours.

The morphology of freshly isolated monocytes and cultured monocyte-derived cells was observed at each step of the training experiment.

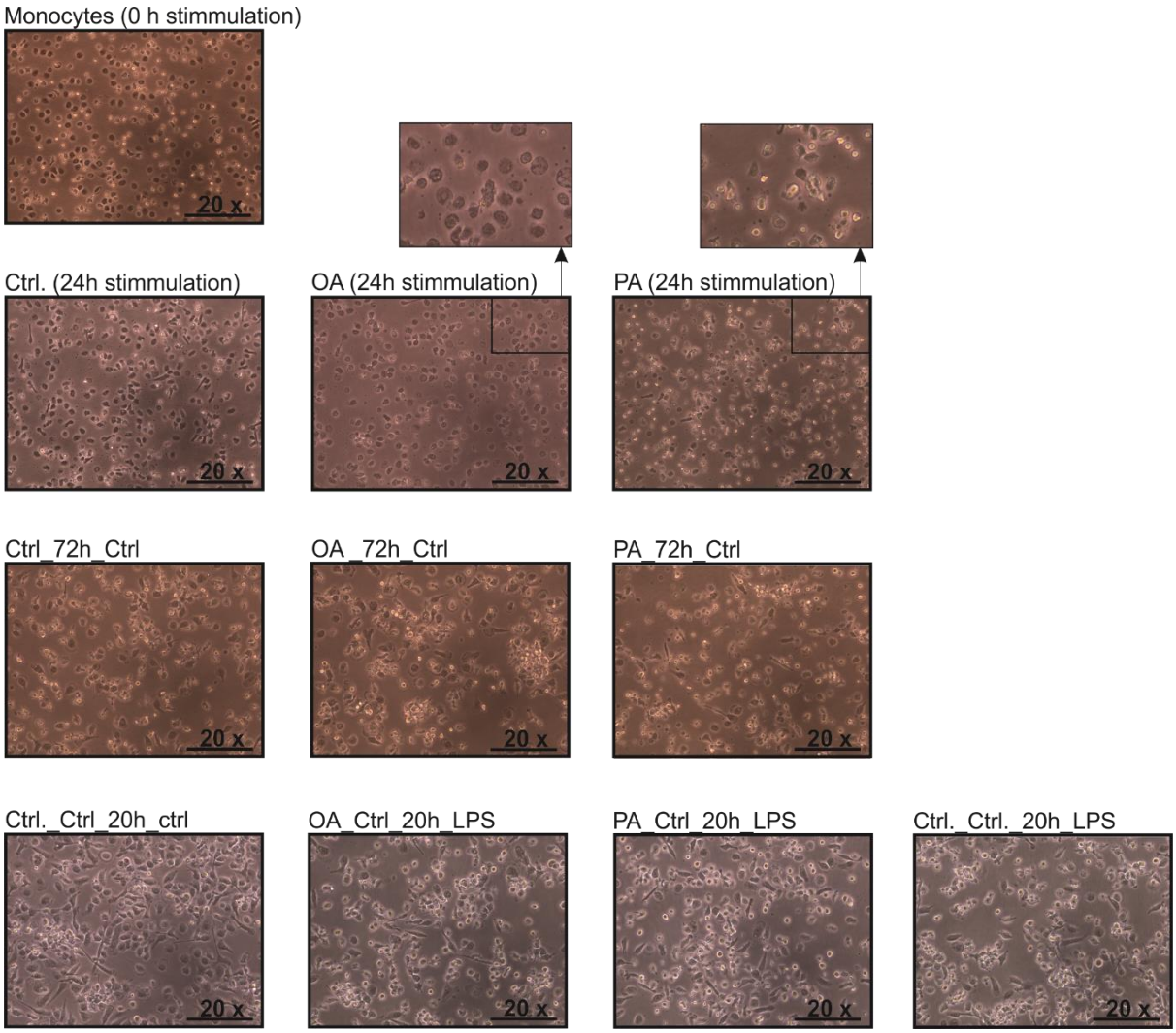

Figure 5.4.1.6: Cell morphology of cultured cells at each step of the trained immunity experiment.

As expected, freshly isolated monocytes are round in shape and not adherent, indicating that cells are non-activated. After 24 hours the cells cultured in 24h_Ctrl medium start to lose their roundish shape and get adherent. The 24h_OA stimulated cells are very similar in appearance, but in addition, taken up lipid droplets are indicated in the zoomed-in picture (**Figure 5.4.1.6**). In accordance with the Annexin-V-PI results, 24h_PA stimulated cells seem to be more activated and less viable compared to 24h_Ctrl and 24h_OA simulated cells. The zoomed-in picture of 24h_PA shows cells containing granules as well as cell debris in the surrounding medium.

Examining the cell morphology of 96 hours cultures it seems that the three days wash-out of stimuli let the cells of different priming culture conditions appear phenotypically similar again. The cells in each of the cultures appear to be activated and viable. After

116 hours of culturing, the Ctrl_Ctrl_20h_LPS stimulated cells seem phenotypically strongly activated, but still appear similar to the Ctrl_Ctrl_20h_Ctrl (without LPS).

RNA-sequencing analysis

RNA-sequencing analysis is an important tool to understand the way certain factors may influence the transcriptome of a cell. In this part of the study we analyzed the direct and long-term effect of oleic and palmitic acid on the transcriptome of monocyte-derived cells.

5.5 Transcript analysis of monocyte-derived cells after 24 hours of training

To enable a detailed analysis of the effect of OA and PA on monocyte re-programming and differentiation, we generated genome-wide transcriptome data by RNA-sequencing of 24h_OA and 24h_PA stimulated monocytes as well as on a 24h_Ctrl. As outlined in the following sections, extensive bioinformatics analysis on described mRNA data was performed.

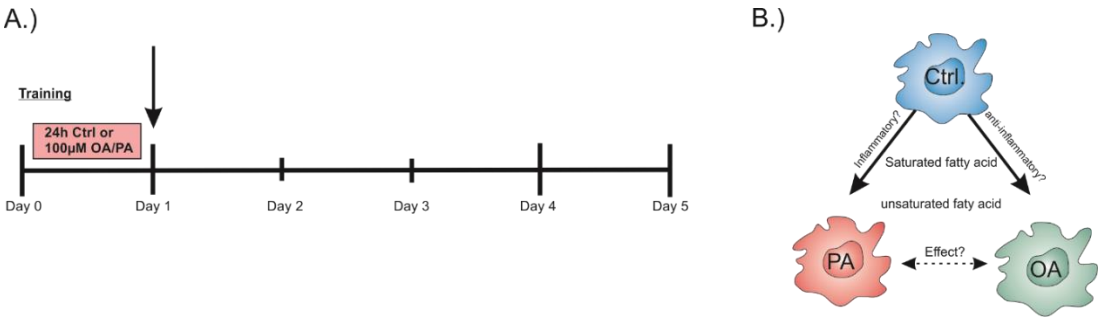

Figure 5.5.1: Schematic visualization of experimental set-up and biological questions. A.) Experimental Set-Up. The arrow is pointed on the time point of experimental conditions analyzed. B.) Scheme describing the biological questions addressed after 24 hours of cultivation.

In **Figure 5.5.1 A.)** the time point of mRNA extraction is visualized by an arrow. The biological questions that were addressed are schematically visualized in **B.)**. Which direct effect does the saturated fatty acid palmitic acid and the unsaturated fatty acid oleic acid have on monocytes? Do they drive monocyte differentiation? Are the monocyte-derived cells driven towards an inflammatory or anti-inflammatory phenotype?

5.5.1 Data preprocessing

The RNA-seq. data were processed as described in the Methods section (see *4.16 Bioinformatic data analysis*). After normalization, the read counts were imported into Partek Genomics Suite V6.6 (PGS) and floored by setting all lower read counts to at least 1. After rejecting the low expressed transcripts, the 24 hours sample data comprised 11.702 transcripts. These genes were retained for further analyses.

5.5.2 Dimensionality reduction

As it has been reported that the biological effects of saturated and unsaturated fatty acids on immune cells are different[187], we first intended to determine the direct effect of oleic acid and palmitic acid on human monocytes. Both, the saturated fatty acid PA and the unsaturated fatty acid OA make up the most abundant fatty acids in diet and also are most concentrated as free fatty acids in serum.[118]

The high-throughput data achieved from the 24 hours cultures consist of thousands of genes (variables) which make up thousands of dimensions. However, to visualize the fundamental structure within this dataset the dimensionality was reduced by performance of a 3D Principle Component Analysis on all genes.

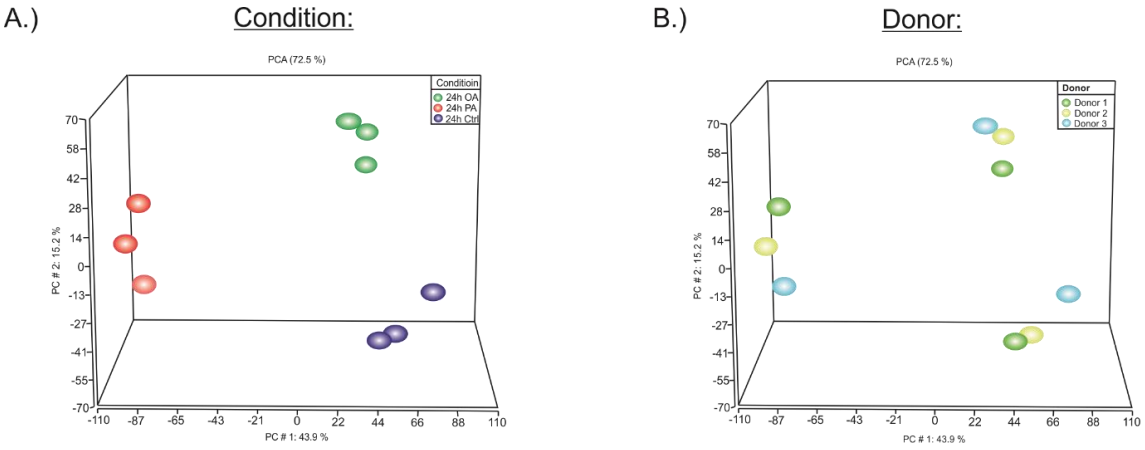

Figure 5.5.2.1: Principal component analysis A.) 3D-PCA of control and OA-, PA- treated monocyte culture mRNA samples. B.) 3D-PCA taking the donor into account.

PCA was used to understand the transcriptional similarities and differences between the different stimulated monocytes (**Figure 5.5.2.1 A.)**). The donors were taken into

account to determine if the origin of cells has an influence on the cluster formation (**Figure 5.5.2.1 B.)**). As expected, the 24 hours samples cluster separately according to the stimulus they got, with 24h_OA treated cultures clustering closer to the 24h_Ctrl than the 24h_PA cultures. Since in each cluster transcripts of all three donors are represented, a donor effect can be excluded.

5.5.3 Variance analysis

Differentially expressed (DE) genes were defined by Analysis of Variance (ANOVA) models by setting certain fold change (FC) thresholds and False Discovery Rate[165] adjusted p-value cutoffs to determine differences between two conditions. The corresponding cutoffs used for the 24 hours expression comparisons were as follows: FC ≥ 2 or ≤ -2 and p-value with FDR ≤ 0.05.
To identify common response genes after the fatty acid stimulations, an ANOVA model was applied.

5.5.4 Statistical ANOVA model to describe differentially expressed genes

The ANOVA-model was used to determine the 1000 most variable and differentially expressed (DE) genes between the three conditions (see **Figure 5.5.4.1**).

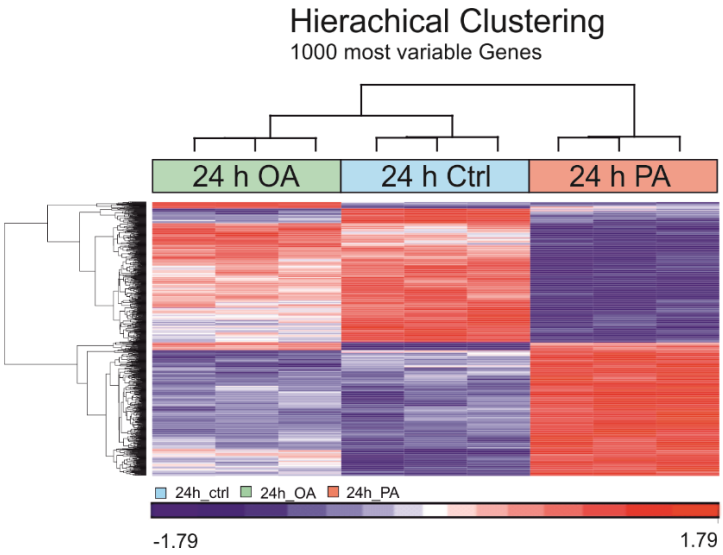

Figure 5.5.4.1: Transcriptional fingerprint of human monocytes after 24 hour oleic and palmitic acid treatment. Heatmap of the top 1000 genes being most variable across the dataset. Log2-expression values were z-transformed and scaled (-1.79 (blue) to 1.79 (red)).

While the up- and down-regulated genes of 24h_Ctrl and 24h_OA cultures to a great extend cluster together, the clustering of 24h_PA stimulated cells appears to be regulated in the opposite direction. Meaning, genes that are upregulated in the 24h_OA and 24h_Ctrl samples, are mainly down-regulated in 24h_PA stimulated cells, and vice versa.

Venn Diagrams

Figure 5.5.4.2: The direct effect of saturated and unsaturated fatty acids on monocyte differentiation and transcriptional characteristics. The Venn-diagrams visualize the comparison of shared up- and down-regulated genes. Differentially expressed genes (FC ≥ 2; p-value ≤ 0.05 with FDR).

Taking the Venn diagrams (**Figure 5.5.5.2**) into account, this trend is further approved. Only 40 DE-genes of the dataset overlap between 24h_OA and 24h_PA cultures. Twenty of these genes are up- and 20 genes are down-regulated (see Appendix **Table 8.1**). As already indicated in the hierarchical clustering, in 24h_PA stimulated cells, much more genes are differentially expressed compared to 24h_Ctrl as indicated for 24h_OA stimulated cells. In 24h_PA stimulated monocytes, in total 872 genes were differentially expressed, while in 24h_OA samples only 61 genes were verifiable when compared to 24h_Ctrl cultures. The products of overlapping DE-genes between 24h_OA and 24h_PA cultures that were up-regulated are for instance involved in fatty acid metabolic processes like lipid uptake and transport (LDLR, ACSL1, PLIN2), in response to external stimuli, receptor mediated endocytosis and lysozyme composition (ADGRE3, CMRF35, CTSL, respectively) as well as in signal induced proliferation (S1PA1L2) and cell differentiation (ETS2). Overlapping DE-genes that were down-regulated comprise such whose gene products are involved in response to stress or toxic substances, signal transduction, receptor mediated endocytosis and immune system response, response to IFN-ɣ as well as in antigen processing and presentation (GPX3, NDRG2, CD206, IRF4, CD1A).

Gene and pathway involvement information of this section was taken from http://www.pantherdb.org/ and https://www.genecards.org/ [188,189].

5.5.5 Functional interpretation of transcript analysis

To assess the functionality of the genes transcribed and to link prior knowledge to our data, we performed a gene ontology enrichment analysis using ClusterProfiler[167]. GO-terms were considered significantly enriched with a Bonferroni corrected p-value ≤ 0.05 and p-adjust cutoff of 0.2. The size of the dots represents the gene ratio, which indicates the ratio of the DE-gene number to the total gene number in a certain pathway. The color of the dots represents the range of p-values and thus indicates the significance. By application of an R-genome suite script for GO-enrichment analysis, a dot plot visualization of overexpressed genes in sets of genes that are up- or down-regulated in 24h_OA or 24h_PA stimulated cell samples compared to 24h_Ctrl or to each other was developed.

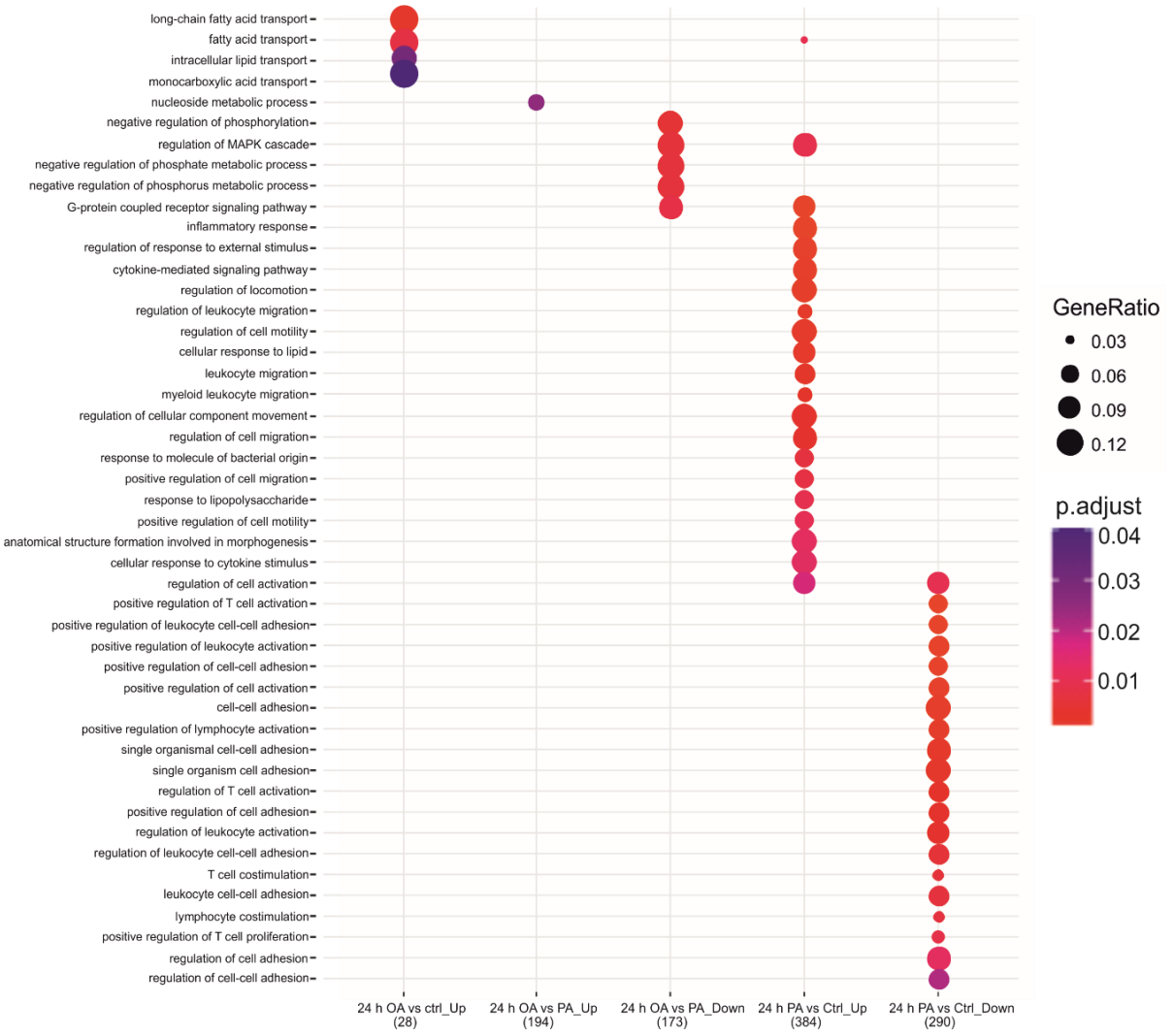

Figure 5.5.5.1: Saturated and unsaturated fatty acids induce transcriptomic changes in monocytes. GO-term-enrichment analysis of up- and down-regulated genes from the total set of DE-genes in the 24 hours dataset. Under the description of comparisons on the X-axis the number of genes is shown. The Y-axis shows the GO terms. The gene ratio indicates the ratio of the differentially expressed gene number to the total gene number in a certain pathway. The size and color of the dots represent the gene number and the range of p-values, respectively.

As described in **Figure 5.5.5.1**, most DE-gene products upregulated in 24h_OA samples compared to 24h_Ctrl participate in fatty acid/lipid transport and monocarboxylic acid transport. The enrichments in 24h_OA samples compared to 24h_PA samples code for proteins involved in nucleoside metabolic processes, which describe processes taking place in RNA or DNA synthetic progressions, which is crucial for proliferating cells[190,191]. Processes that are up-regulated in 24h_PA compared to 24h_OA samples are mainly described by 'negative regulation of phosphate metabolic processes', as well as 'regulation of MAPK cascade' and 'G-protein coupled receptor signaling cascade'. Phosphorylation plays a crucial role in metabolic reprogramming, which has emerged as a critical regulator of immune cell

activation, important to modulate the effector functions of activated macrophages[192]. The terms ‘regulation of MAPK cascade’ and ‘G-protein coupled receptor signaling cascade’ either describe processes that are highly involved in myeloid cell differentiation and polarization, microbial elimination, inflammation and resolution, as well as in macrophage-mediated pathologies.[193,194]

In addition, KEGG (Kyoto Encyclopedia of Genes and Genomes) pathway enrichment analysis was performed with defined DE-genes of the 24 hour samples, using ClusterProfiler. The KEGG enrichment analysis of pre-defined DE-genes was performed by Dr. Thomas Ulas (LIMES-Institute, University of Bonn).

KEGG is a database resource that integrates genomic, chemical and systemic functional information. In particular, gene catalogs from completely sequenced genomes are linked to higher-level systemic functions of the cell, the organism and the ecosystem.[168] Thereby the gene ratio indicates the ratio of the DE- gene number to the total gene number in a certain pathway. The p-value represents the probability of observing an event by random chance. Significance is determined by setting a threshold, here 0.05. If the p-value is less than 0.05, pathway X is considered significant because the chance of randomly observing the same result is less than 5%.

A.) 24h_OA vs 24h_Ctrl - Expression

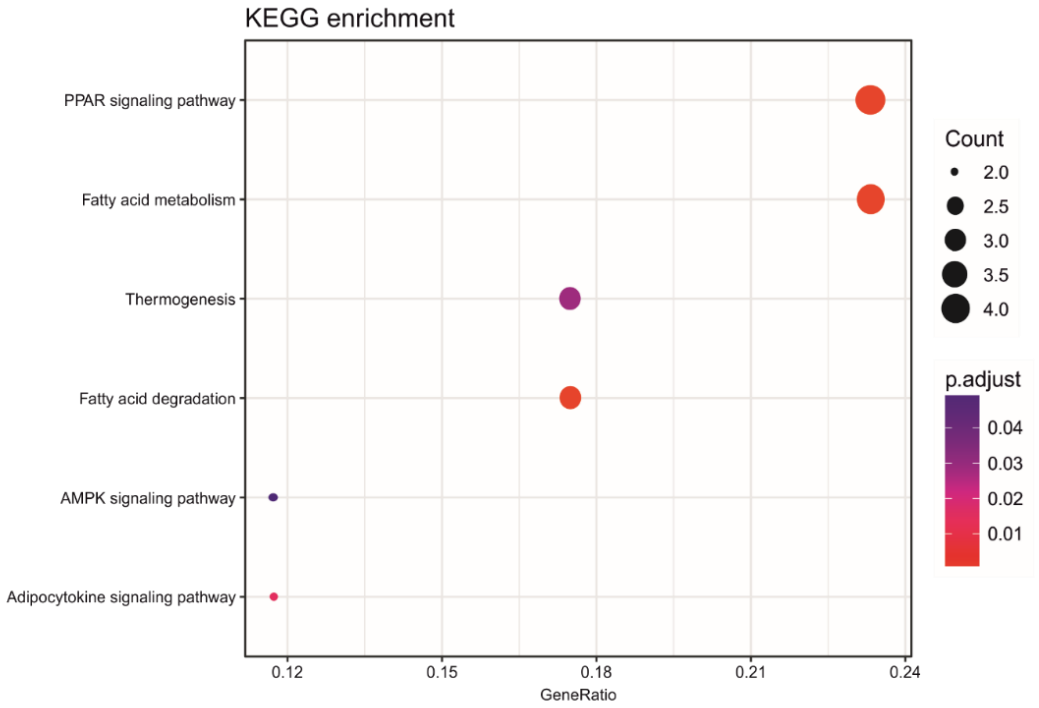

B.) 24h_PA vs 24h_Ctrl - Expression

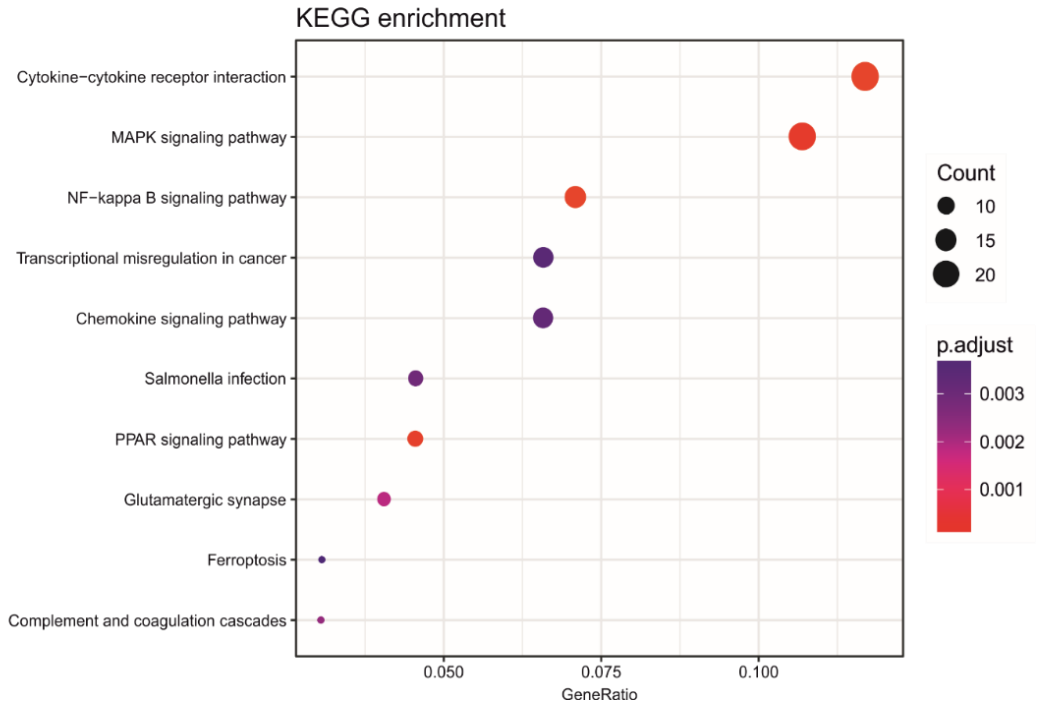

C.) 24h_PA vs 24h_OA - Expression

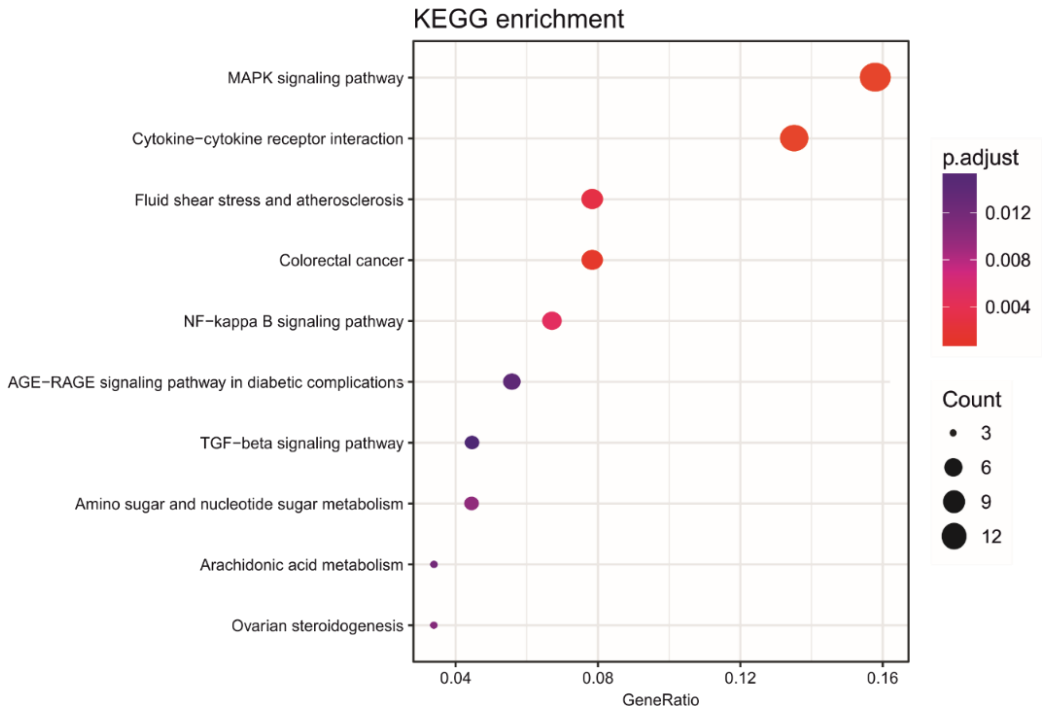

Figure 5.5.5.2: KEGG-enrichment analysis. Scatterplot of enriched KEGG pathways for DE-genes up-regulated in 24 hours OA and PA-primed monocyte-derived cells. The gene ratio indicates the ratio of the differentially expressed gene number to the total gene number in a certain pathway. The size and color of the dots represent the gene number and the range of p-values, respectively. A.) Represents pathways upregulated in 24h_OA stimulated monocytes compared to 24h_Ctrl cells. B.) Shows pathways to which up-regulated DE-genes of 24h_PA versus 24h_Ctrl cultures contribute, while in C.) pathways are visualized that are upregulated in 24h_PA stimulated monocytes when compared to 24h_OA cultures. DE-genes were defined by fold changes of ≥ 2 and p-values ≤ 0.05.

Figure 5.5.5.2 A.) shows KEGG pathways of DE-genes established by comparison of 24h_OA and 24h_Ctrl cultures. The gene count is quite low however, this is also true for the number of differentially expressed genes (32) set in for analysis. ‘PPAR signaling pathway’ and ‘Fatty acid metabolism’ are the terms with highest gene counts (4 genes) and gene ratios. ‘Thermogenesis’ and ‘Fatty acid degradation’ are the pathways comprising second most DE-genes (3 genes) with a gene ratio of 0.18. In ‘AMPK signaling pathway’ and ‘Adipocytokine signaling pathway’ two DE-genes are involved, respectively. The gene ratios are accordingly relatively low (< 0.12).

In **Figure 5.5.5.2 B.)** KEGG pathways of up-regulated DE-genes in 24h_PA stimulated monocytes compared to 24h_Ctrl, are described. Here the gene counts of genes involved in described pathways are higher as seen for 24h_OA cultures, but also the number of implicated DE-genes were much higher (518). The gene ratios are with

highest ~0.12 quite low. The pathways with highest gene ratios comprise ‘Cytokine-cytokine receptor interaction’ and ‘MAPK signaling pathway’ (> 20 genes involved). Also, the ‘NF-kappa B signaling pathway’, ‘Transcriptional mis-regulation in cancer’ and ‘Chemokine signaling pathway’ have comparably high gene counts (≤ 15 genes involved). Pathways with lower gene ratios (≤ 10 genes involved) include ‘Salmonella infection’, ‘PPAR-signaling pathway’, ‘Glutamatergic synapse’, ‘Ferroptosis’ and ‘Complement and coagulation cascade’.

Ferroptosis is a type of programmed cell death driven by loss of activity of the lipid repair enzyme glutathione peroxidase 4 (GPX4) and subsequent accumulation of lipid-based reactive oxygen species, particularly lipid hydroperoxides. This process is genetically and biochemically distinct from other forms of regulated cell death such as apoptosis, unregulated necrosis, and necroptosis.[195] Ferroptosis activation also often plays a regulatory role on growth of tumor cells in the human body which might explain the pathway involvement in ‘Transcriptional mis-regulation in cancer’. Ferroptosis could explain the high cell death rate in the 24h_PA cultures.

Figure 5.5.5.2 C.) shows pathways that are up-regulated in 24h_PA compared to 24h_OA stimulated monocytes. 226 DE-genes were taken under investigation. Located pathways with highest gene counts and gene rations were defined as ‘MAPK signaling pathway’ and ‘Cytokine-cytokine receptor interaction’. DE-genes that either were up-regulated are integrated in ‘Fluid shear stress and atherosclerosis’ and ‘Colorectal cancer’, showing a gene ratio of 0.08. Further pathways up-regulated in 24h_PA stimulated cells encompass ‘NF-kappa B signaling pathway, ‘AGE-RAGE signaling pathway in diabetic complications’, ‘TGF-β signaling pathway’ and ‘Amino sugar and nucleotide metabolism’. The pathways are listed with decreasing gene counts and gene ratios. In this plot the p-values are all below 0.05 and thus pathways are most significant because the chance of randomly observing the same result is less than 5%.

5.5.6 Co-expression network analysis

To define differences and similarities in transcript expression among the conditions, I performed Co-expression network analysis based on Pearson’s correlation coefficients. I used BioLayout Express3D (BioLayout), which is a powerful tool for the

visualization and analysis of network graphs. A Pearson's correlation coefficient cutoff of 0.88 was used to determine similarity between the individual expression profiles. The set of the 50 most up-and 50 most down-regulated genes (highest/lowest fold change) between 24h_OA and 24h_Ctrl, 24h_PA and 24h_Ctrl and 24h_OA and 24h_PA cultured monocyte-derived cells were later filtered for p-values of ≤ 0.05 and a fold changes of ≥ 2 / ≤ -2 in one of the comparisons using the ANOVA table. Of the previously selected genes, 141 passed the filtering and where used as input for the network analysis.

The network was visualized in Cytoscape. The nodes within the network represent the expressed genes and their connection to eachother. The difference in expression relative to the overall mean, determined by the group fold change (GFC) of the respective condition, is indicated by color-coding of the respective nodes. Bluish colored nodes indicate that expression of the respective gene is down-regulated, while reddish nodes indicate that expression of the respective gene is up-regulated when compared to the overall expressed mean.

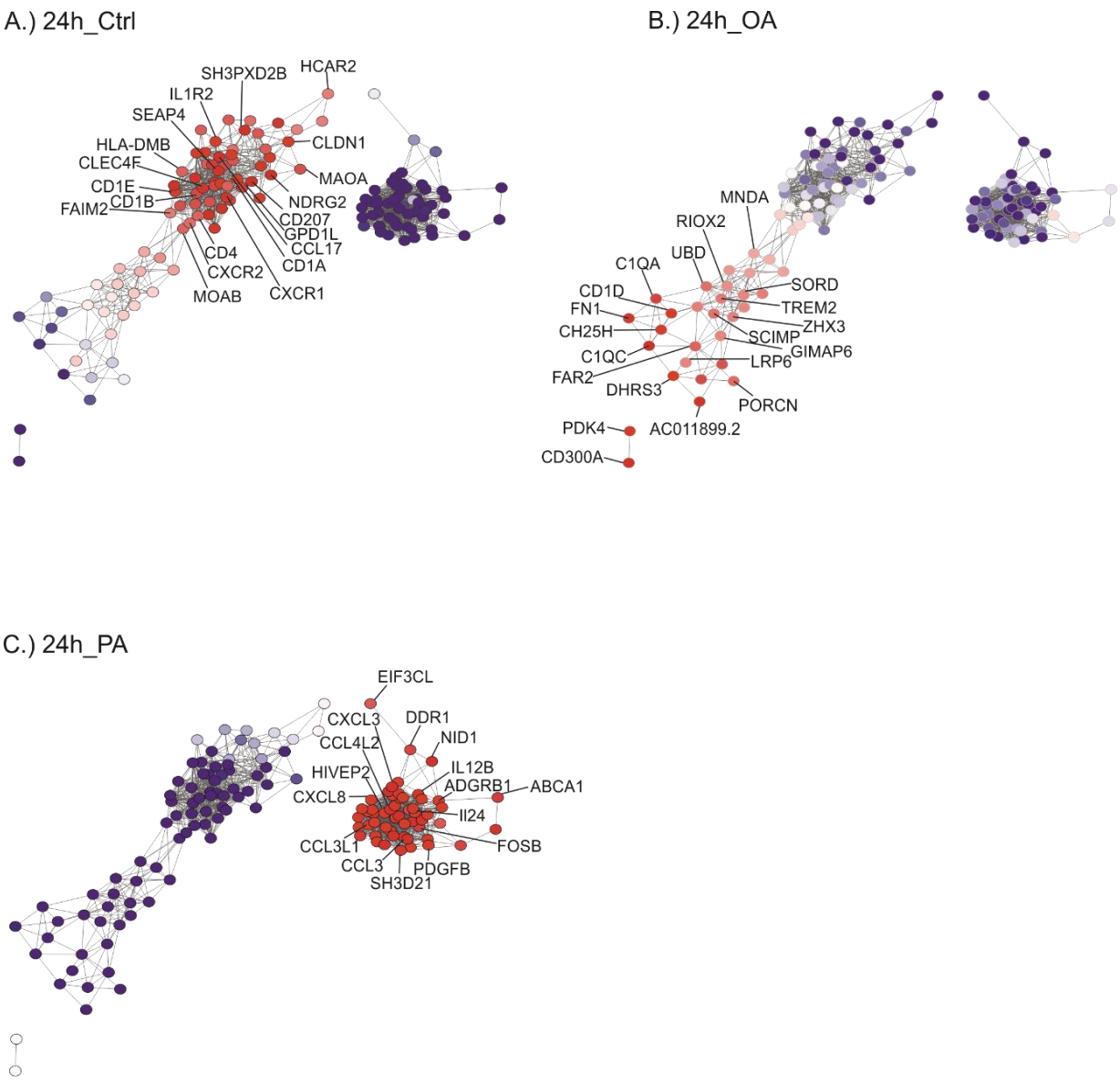

Figure 5.5.6.1: Palmitic acid and oleic acid induced transcriptomic changes in myeloid-derived cells. Visualization of co-expressed genes in monocytes after 24 hour treatment with oleic acid, palmitic acid and control medium. Differences in expression relative to the overall mean is indicated by color-coding of the respective nodes. The network is based on the top 50 highest and lowest differentially expressed genes (p-value ≤0.05) between OA and control, PA and control and OA and PA stimulated cells after 24 hours of culturing. The Pearson's correlation coefficient cutoff was set to 0.88. The network consists of 136 nodes and 1339 edges.

Comparing the overall color distribution of the network, it is demonstrated that 24h_PA-primed cells (**Figure 5.5.6.1 C.)**) down-regulate all of the visualized genes that are up-regulated in the control cells or 24h_OA stimulated cells, and vice versa. This is only partially true when comparing the network coloration of 24h_OA-primed cells with the 24h_Ctrl (**Figure 5.5.6.1 A.)** & **B.)**). Here, at least some genes are regulated in the same direction and are just slightly up-regulated (rose color).

Genes that are up-regulated in 24h_PA stimulated cells code for molecules involved in cell migration and proliferation (PDGFB, FOSB), for pro-inflammatory mediators and inflammatory response genes such as IL12B, CCL3L1, CCL4L2 and CXCL8, CCL3, HIVEP2 and genes involved in endocytosis and apoptosis like SH3D21, ADGRB1 and IL24. Additionally, the ABC1A gene, which codes for a protein functioning as cholesterol efflux pump in the cellular lipid removal pathway is up-regulated[196].

In case of 24h_Ctrl cultures, mainly genes that code for molecules involved in lipid and glycolipid binding, presentation and activation of T-cells (CD1A/B/E), involved in immunomodulatory and inflammatory processes (CCL17, CXCR1, CD4, IL1R2, HLA-DMB), in dendritic cell differentiation (CD207, CLEC4F, NDRG2), in the regulation of lipid metabolism (GPD1L) as well as proteins that play a role in adipocyte development and metabolism (STEAP4, HCAR2, SH3PXD2B), are strongly expressed.

In 24h_OA stimulated cells, genes which products are involved in cell adhesion and migration processes (FN1) and differentiation (PORCN), that participate in antigen presentation (CD1D, SCIMP), or are involved in leukocyte recruitment to inflammatory sides (CXCR2), such that participate in immune complex formation (C1QC, C1QA, CH25H), and such that function in immune response by triggering the production of constitutive inflammatory cytokines (TREM2) and other proteins that participate in the innate immune response (UBD), are up-regulated. As mentioned in the introduction, TREM2 is also associated with an atherosclerosis-specific population of inflammatory macrophages[46].
On the other hand, under the influence of 24h_OA also inflammation counter acting proteins, like CD300A and ASB13, are differentially expressed.
Further, genes are up-regulated, that code for molecules involved in metabolic processes, like FAR2, which catalyzes the reduction of saturated but not unsaturated C16 and C18 fatty acyl-CoA to fatty alcohols.

As previously mentioned, some few network genes that are up-regulated in both, 24h_Ctrl and 24h_OA stimulated cells could be identified. Proteins encoded by these genes comprise such involved in important metabolic pathways (MAOB-dopamine, SORD-glucose), or are involved in receptor-mediated endocytosis of lipoprotein and protein ligands (LRP6). MNDA is one of the proteins that play a role in the monocyte specific response to interferons. ZHX3, a protein associated with transcriptional repression is also differentially expressed. In both conditions genes coding for proteins

involved in cell survival, like FAIM2, GIMAP6 and RIOX2 are elevated. Considering the coloration of the network nodes, it can be seen that most of the described genes are stronger expressed in the 24h_OA network (**Figure 5.5.6.1 B.)**) compared to the 24h_Ctrl network (**Figure 5.5.6.1 A.)**).

Gene and pathway information of this section were taken from http://www.pantherdb.org/ and https://www.genecards.org/ [188,189].

5.6 Transcriptional analysis of monocyte-derived cells after wash-out of training stimuli

After wash-out of fatty acid stimuli, genome-wide transcriptome data from isolated mRNA contents of the monocyte-derived cells were generated and extensive bioinformatics analysis was performed.

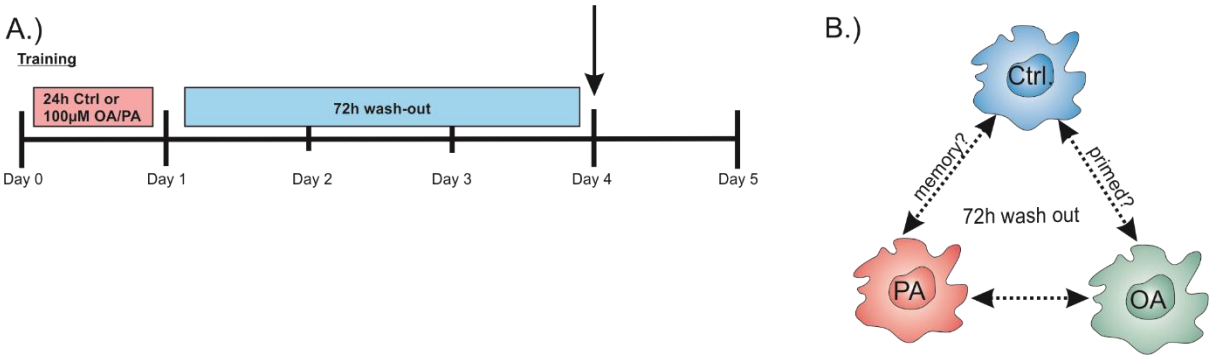

Figure 5.6: Macrophage activation after a three-day wash-out period. A.) Experimental set-up. The arrow is pointed on the time point of experimental conditions analyzed. B.) Scheme describing the biological questions addressed after 24 hours fatty acid stimulation followed by a 72 hours wash-out period.

At this step of analysis, the mRNA samples of 96 hours cultures were examined. **Figure 5.6 A.)** schematically visualizes the time point of mRNA extraction. The biological questions that were addressed is visualized in **B.)**: Did the 24h_OA and 24h_PA stimulations have a lasting effect on the transcriptome of OA_72h_Ctrl and PA_72h_Ctrl monocyte-derived cells? Which characteristics did these cells develop in response to the given influences?

5.6.1 Data preprocessing

The 96 hours samples were pre-processed the same way as described for the 24 hours samples.

After pre-processing the 96 hours sample dataset comprised 11.819 transcripts. These genes were retained for further analysis.

5.6.2 Dimensionality reduction

High-throughput data were visualized as principal components to show the structures and cluster formation after the three days wash-out period.

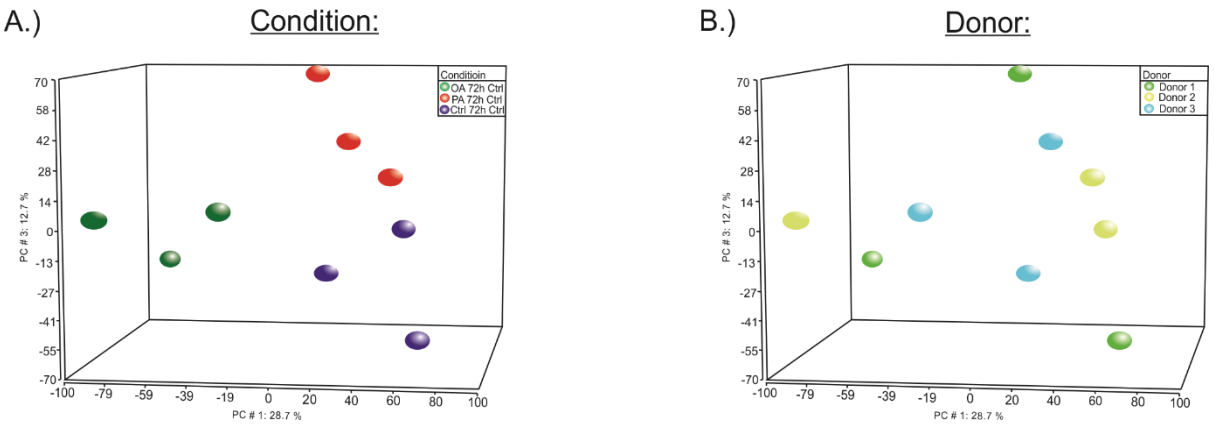

Figure 5.6.2.1: Transcriptional similarities of control and OA- or PA- primed cells after wash-out. A.) 3D-Principal Component Analysis (PCA) of transcriptional patterns of the pre-primed monocyte cultures. B.) 3D-Principal Component Analysis (PCA) taking the donor into account.

The PCA based on the expression data obtained from OA_72h_Ctrl, PA_72h_Ctrl and Ctrl_72h_Ctrl monocyte-derived cells of the 3 male human donors are visualized in **Figure 5.6.2.1 A.)** and **B.)**, respectively. Interestingly, the 96 hours cultures still possess transcriptomes that even after three days of stimuli wash-out build separate clusters, in accordance to the priming stimulus they received. However, compared to the 24 hours clusters, the 96 hours samples group closer together, representing a closer transcriptional similarity between the different conditions. Here, PA_72h_Ctrl and Ctrl_72h_Ctrl transcription profiles cluster closer together while OA_72h_Ctrl

cultures build a more separated cluster. Investigating **Figure 5.6.2.1 B.)** it can be seen that a donor effect is not detectible.

5.6.3 Variance analysis

Differentially expressed genes where defined by ANOVA-models by setting certain fold change (FC) thresholds and False Discovery Rate[165] adjusted p-value cut-offs to determine differences between two conditions. To identify common response genes an ANOVA model was applied.
The corresponding cutoffs used for the 96 hours samples were as follows:
FC ≥ 1.5 or ≤ -1.5 and p-value with FDR ≤ 0.1.

5.6.4 Statistical ANOVA model to describe differentially expressed genes

The ANOVA-model was used to determine the 1.000 most variable and differentially expressed (DE) genes between the three conditions.

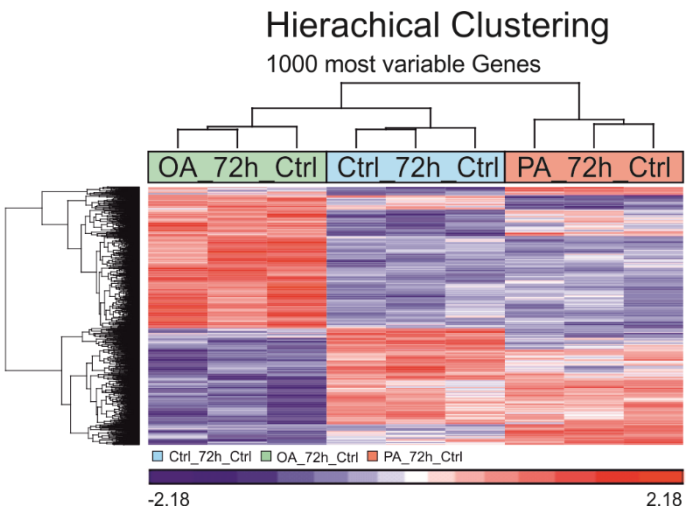

Figure 5.6.4.1: The transcriptional effect of PA and OA on monocyte-derived cells after a 72 hour wash-out period. Heatmap of the top 1000 genes being most variable across the dataset. Log_2-expression values were z-transformed and scaled (-2.18 (blue) to 2.18 (red)).

Figure 5.6.4.1 shows the hierarchical clustering of the 1000 most variable genes across the 96 hours sample dataset. Remarkably, this time expression patterns of up- and down-regulated genes of Ctrl_72h_Ctrl and PA_72h_Ctrl cultures overlap to great

extents, while the expression profiles of OA_72h_Ctrl cells are largely regulated opposed.

This trend is further approved when validating the number of DE-genes determined for OA_72h_Ctrl and PA_72h_Ctrl cultures compared to Ctrl_72h_Ctrl (**Figure 5.6.4.2**). Comparison revealed 171 DE-genes for OA_72h_Ctrl versus Ctrl_72h_Ctrl while only 3 DE-genes (METRN, NDFIP2, CENPW) could be determined under same cutoff conditions comparing PA_72h_Ctrl and Ctrl_72h_Ctrl expression profiles. Only 1 DE-gene in the 96 hours dataset is overlapping between OA_72h_Ctrl and PA-72h_Ctrl cultures, namely METRN.

Under the same cutoff conditions 124 DE-genes could however be determined between transcriptomes of OA_72h_Ctrl and PA_72h_Ctrl. In this comparison 59 DE-genes were proportionally up-regulated in OA_72h_Ctrl cultures while 65 were comparatively up-regulated in PA_72h_Ctrl cultures.

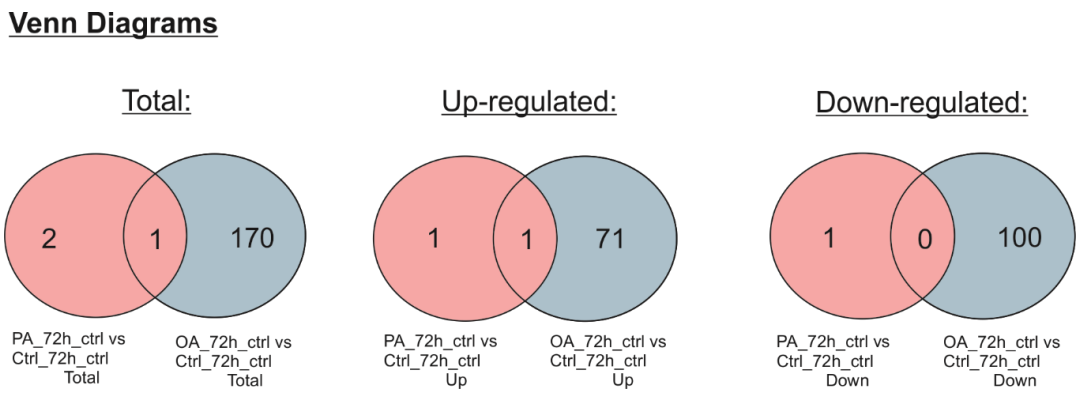

Figure 5.6.4.2: Visualization of shared up- and down-regulated genes after wash-out. Venn-diagrams showing the number of overlapping genes in OA- and PA- primed cells after wash-out, compared to the control. Differentially expressed genes were determined by following cutoffs: FC ≥ 1.5 or ≤ -1.5 and p-value ≤ 0.1 with FDR.

5.6.5 Functional interpretation of transcript analysis after wash-out

To assess the functionality of expressed genes and to link prior knowledge to our data, I performed a gene ontology enrichment analysis using the ClusterProfiler[167] classification system. GO-terms were considered significantly enriched with a Bonferroni corrected p-value of ≤ 0.7 and p-adjust cutoff of 0.2. A dot plot visualization of overexpressed genes in OA or PA-primed wash-out samples compared to control or to each other is shown in **Figure 5.6.5.1**.

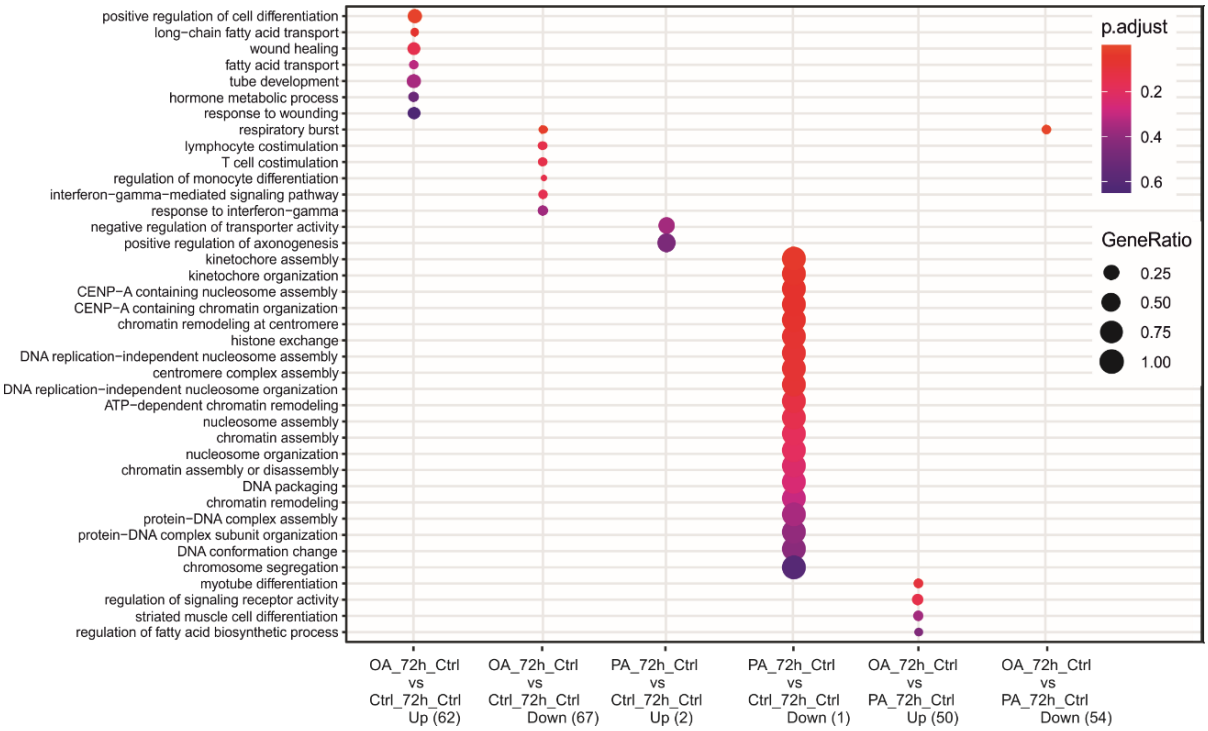

Figure 5.6.5.1: GO-term-enrichment analysis of up- and down-regulated differentially expressed genes compared to the total set of genes in the dataset. The corresponding cutoffs used for the 96 hours samples were as follows (OA_72h_ctrl vs Ctrl_72h_ctrl: FC ≥ 2 or ≤ -2; p-value ≤ 0.1 with FDR // PA_72h_ctrl vs Ctrl_72h_ctrl: FC ≥ 1.5 or ≤1.5; p-value ≤ 0.1 with FDR // OA_72h_ctrl vs PA_72h_ctrl: FC ≥ 2 or ≤ -2 and p-value with FDR ≤ 0.1).

Terms that describe involvement of up-regulated DE-genes in OA_72h_Ctrl when compared to Ctrl_72h_Ctrl samples include ‘positive regulation of cell differentiation’, ‘long-chain fatty acid transport’, ‘wound healing’, ‘tube development’ and ‘hormone metabolic process’. These terms describe fatty acid metabolic processes however with a low gene ratio but quite high significance. Higher gene ratios could be observed for processes involved in the induction of restoration and differentiation of the cells, which might be induced by seizure of the stimulus. The terms that describe the tendency of down-regulated DE-genes in OA_72h_Ctrl samples when compared to Ctrl_72h_Ctrl include ‘respiratory burst’, ‘lymphocyte/T-cell co-stimulation’, ‘regulation of monocyte differentiation’, and ‘IFN-ɣ-mediated signaling pathway’. Here, terms describing phagocytic processes as well as adaptive immune cell activation are prevalent. Although a high number of DE-genes were determined in this comparison, the gene ratios in GOEA are rather low.

GO-terms describing functional involvement of DE-genes up-regulated in OA_72h_Ctrl compared to PA_72h_Ctrl cultures comprise ‘myotube differentiation’, ‘striated muscle cell differentiation’, ‘regulation of signaling receptor activity’, as well as ‘regulation of

fatty acid biosynthetic process'. Conspicuously, the term regulation of signaling receptor activity has the highest gene ratio and fatty acid biosynthetic processes, although with low gene ratio and relatively high p-value, still play a role. Down-regulated DE-genes in OA_72h_Ctrl compared to PA_72h_Ctrl samples were described to play a role in 'respiratory burst'. Phagocytic processes thus seem to play a larger role in PA_72h_Ctrl and Ctrl_72h_Ctrl cultures.

GO-terms determined for the two up-regulated DE-genes in PA_72h_Ctrl samples compared to Ctrl_72h_Ctrl encompass 'negative regulation of transporter activity' and 'positive regulation of axonogenesis'. In both cases the gene ratios are with 0.5 and 0.75 quite high but the significance is with $p \geq 0.3$ relatively low. Interestingly, in this comparison only one gene is down-regulated but this gene counts for a number of GO-terms like 'kinetochore organization', 'CENP-A containing nucleosome/chromatin assembly/organization', 'histone exchange' or 'chromatin remodeling'.

5.6.6 Co-expression network analysis

Co-expression network analysis was performed using a network created from DE-genes (FC ≥ 1.5 or ≤ - 1.5 and p-value ≤ 0.1 with FDR) between OA_72h_Ctrl versus Ctrl_72h_Ctrl, OA_72h_Ctrl versus PA_72h_Ctrl and PA_72h_Ctrl versus Ctrl_72h_Ctrl. In Biolayout 3D we used a Pearson's correlation coefficient cutoff of 0.91 to determine similarity between the individual expression profiles. The network is build-on 214 nodes and 1888 edges. As usual, the difference in expression relative to the overall mean, determined by the group fold change (GFC) of the respective condition, is indicated by color-coding of the respective nodes. Bluish colored nodes indicate that the expression of the respective gene is down-regulated, while reddish nodes indicate that the expression of the respective gene is up-regulated when compared to the overall expressed mean.

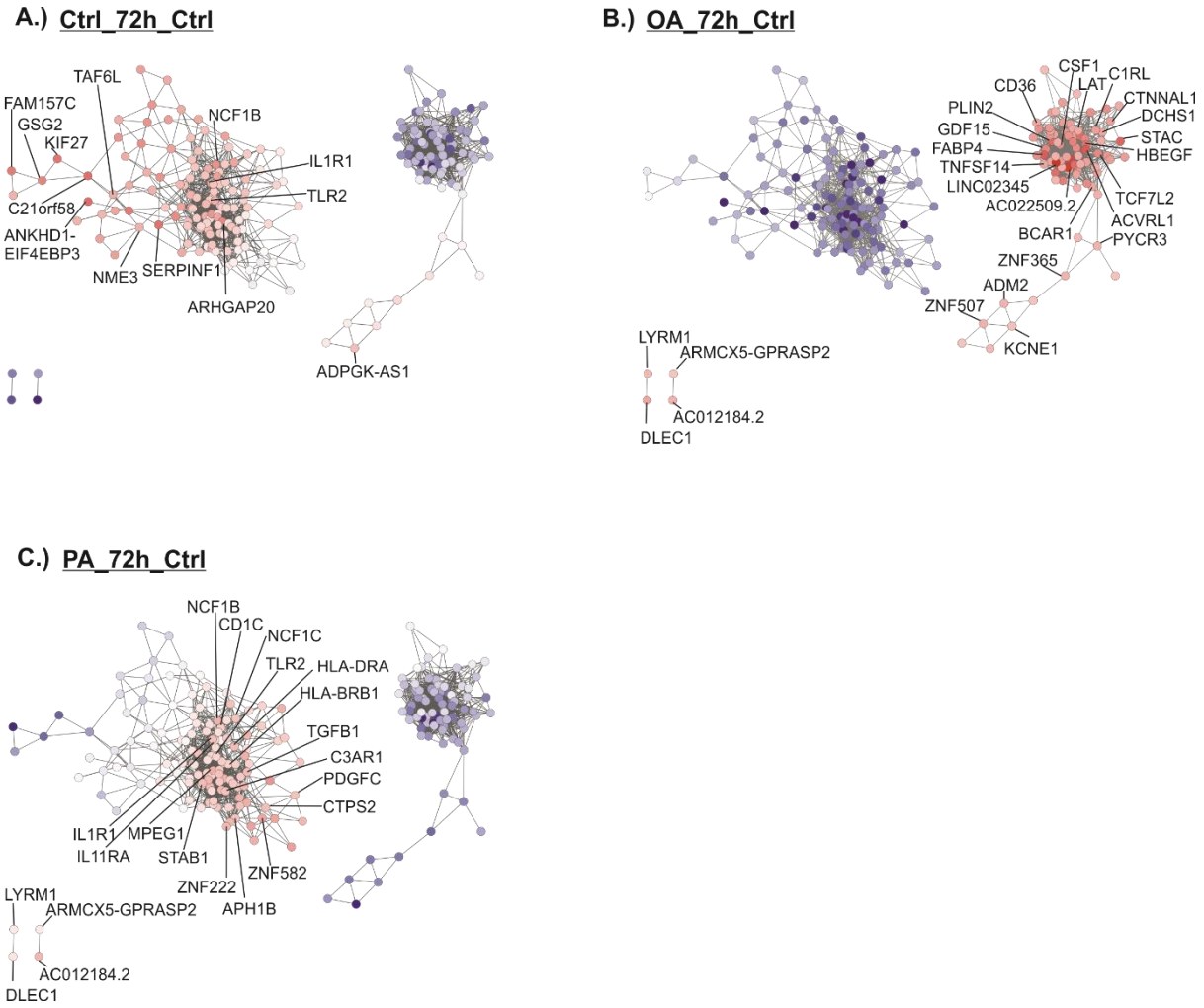

Figure 5.6.6.1: Saturated and unsaturated fatty acid priming has a lasting transcriptional effect on the transcriptome of myeloid-derived cells. A.) - C.) Visualization of co-expressed genes in saturated and unsaturated fatty acid primed monocytes after a 72 hours wash-out period. Differences in expression relative to the overall mean are indicated by color coding of the respective nodes. The network was constructed from all DE-genes between OA_72h_Ctrl versus Ctrl_72h_Ctrl, OA_72h_Ctrl versus PA_72h_Ctrl and PA_72h_Ctrl versus Ctrl_72h_Ctrl with fold change of ≥ 1.5 / ≤ -1.5 and p-value ≤ 0.1. The Pearson's correlation coefficient cutoff was set to 0.91. The Network consists of 214 nodes and 1888 edges.

Comparing the overall color distribution of the network representing the expression in OA_72h_Ctrl or PA_72h_Ctrl cultures, it gets visible that also after 72 hours of wash-out OA-primed cells down-regulate almost all of the visualized genes that are up-regulated in the Ctrl_72h_Ctrl and PA_72h_Ctrl cells. The investigated DE-genes make up two big separate network clusters. The left cluster is shared by genes which expression is up-regulated in Ctrl_72h_Ctrl and PA_72h_Ctrl cultures with intersecting genes being in both conditions just moderately expressed. This is shown by the slightly rose coloration of the intersecting nodes. Genes located at the lower right border of the left cluster are slightly up-regulated in PA_72h_Ctrl cultures while rather neutrally

expressed in Ctrl_72h_Ctrl cells. These nodes visualize the specific gene marks of PA_72h_Ctrl cultures. PA_72h_Ctrl cultures share just four up-regulated genes with OA_72h_Ctrl at the lower left side of the network. These genes comprise LYRM1, DELEC1, ARMCX5-GPRASP2 and AC012184.2, which are visualized as two separate clusters, each consisting of two nodes. Only AC012184.2 is equally high expressed in both conditions. Some few genes at the tail structure of the right, big cluster are slightly up-regulated in OA_72h_Ctrl and to some extent also in Ctrl_72h_Ctrl cells.

Concisely, expression data of the 96 hours samples demonstrate that the 24 hours fatty acid priming even after 72 hours of fatty acid subtraction have a lasting effect on monocyte-derived cell expression patterns which in this visualization is contrary regulated between OA and PA-primed cell samples with PA_72h_Ctrl cultures showing a higher degree of coincidence to Ctrl_72h_Ctrl cultures than to OA_72h_Ctrl cultures.

5.7 Transcriptional analysis of monocyte-derived cells after re-stimulation

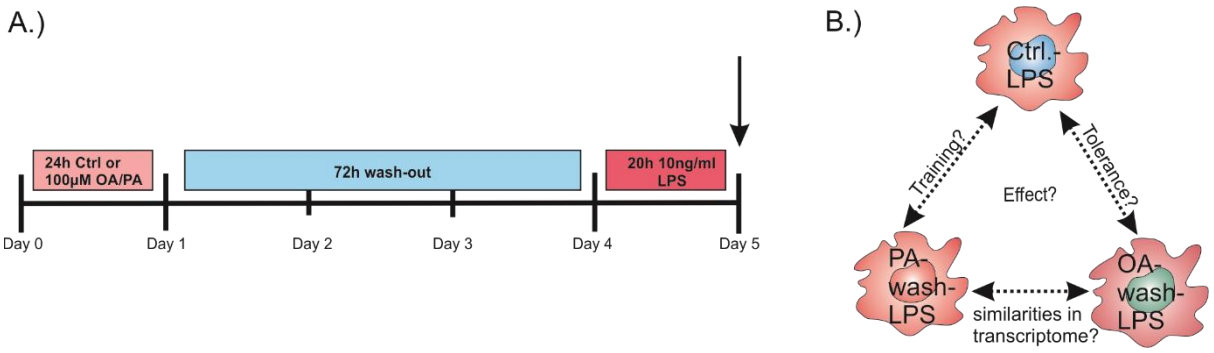

Figure 5.7.1: Re-stimulation of OA and PA trained myeloid-derived cells. A.) Set-up of trained immunity experiment. The arrow is pointed on the time point of experimental condition analyzed. B.) Scheme describing the biological questions addressed to the fatty acid pre-primed monocytes after LPS re-stimulation.

As in the previous RNA-sequence analysis section, **Figure 5.7.1 A.)** describes the time point of mRNA extraction by the pointing arrow. The biological questions that were addressed are schematically visualized in **B.)**. Does contact to dietary components like palmitic and oleic acid influence the transcriptome of monocyte-derived cells irreversibly? Do these cells develop a memory which allows them to be more tolerant or to react faster and stronger to a danger signal like LPS?

5.7.1 Data preprocessing

The 116 hours samples were pre-processed the same way as described for the other time points.

After pre-processing the 116 hours sample data comprised 11.865 transcripts. These genes were retained for further analysis.

5.7.2 Dimensionality reduction

High-throughput expression data were processed and visualized as principal components to show the structures and cluster formation after re-stimulation with LPS.

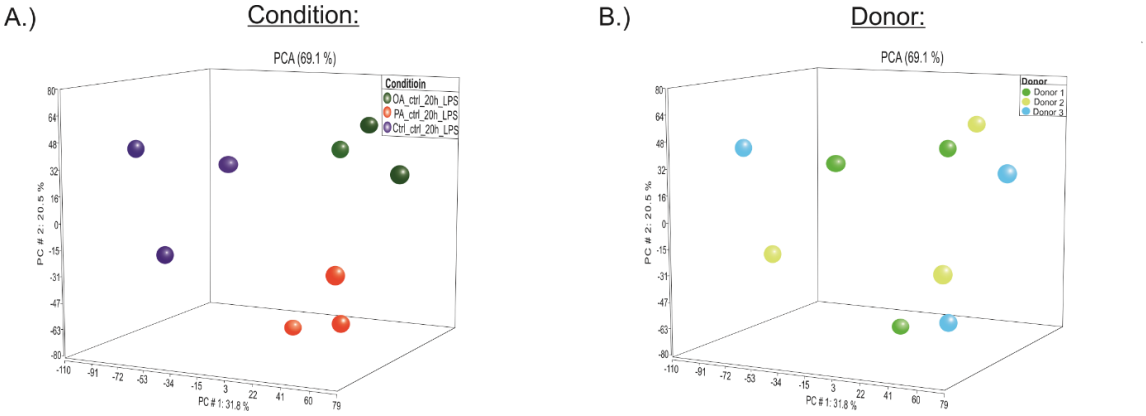

Figure 5.7.2.1: Transcriptional comparisons of control and OA- or PA- trained cells after LPS re-stimulation. A.) 3D-principal component analysis (PCA) of transcriptional patterns of the pre-primed and LPS stimulated monocyte cultures. B.) 3D-principal component analysis (PCA) taking the donor into account.

The PCA based on the conditions (**Figure 5.7.2.1 A.)**) of 116 hours samples still shows the formation of clear clusters, although the cells were cultured for the last 92 hours under the same culture condition with final contact to LPS.
Figure 5.7.2.1 B.) shows that this trend is not influenced by the parentage of cells.

5.7.3 Variance Analysis

DE- genes where defined by ANOVA-models. The corresponding cutoffs used for the 116 hours conditions were as follows:
FC ≥ 1.5 or ≤ -1.5 and p-value with FDR ≤ 0.05.

5.7.4 Statistical ANOVA model to describe differentially expressed genes

The ANOVA-model was also used to determine the 1.000 most variable and differentially expressed (DE) genes between the three/four conditions.

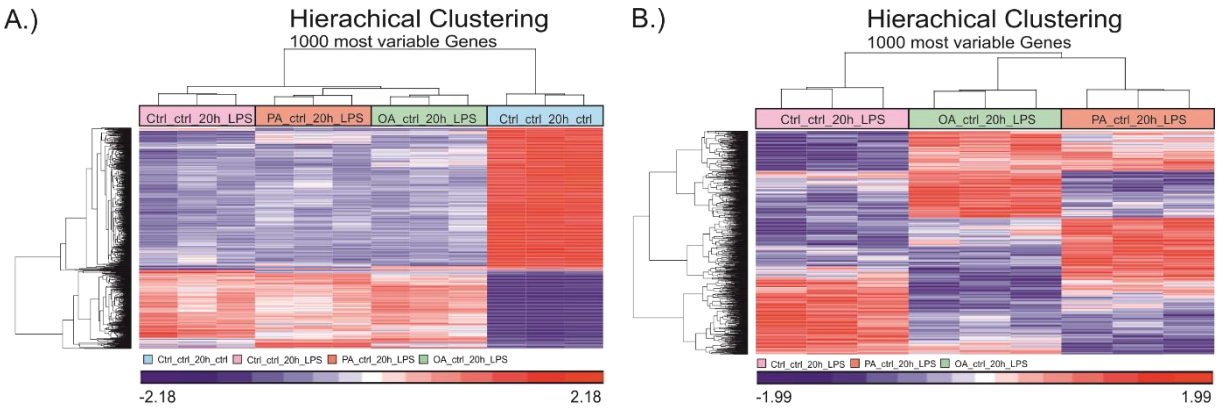

Figure 5.7.4.1: Oleic acid and palmitic acid both have a long-lasting effect on monocyte-derived cells. Hierarchical clustering showing the 1000 most variable genes of fatty acid trained cells and controls with and without final LPS stimulation. A.) Heatmap of the top 1000 genes being most variable across the dataset including Ctrl_ctrl_20h_ctrl. Log_2-expression values were z-transformed and scaled (-2.18 (blue) to 1.99 (red)). B.) Heatmap of the top 1000 genes being most variable across the dataset (without Ctrl_ctrl_20h_ctrl). Log_2-expression values were z-transformed and scaled (-1.99 (blue) to 1.99 (red)).

Figure 5.7.4.1 A.) shows a hierarchical clustering of the 1000 most variable genes across the complete 116 hours sample dataset, while in **B.)** Ctrl_Ctrl_20h_Ctrl data are withdrawn to allow a closer look on the real effect of fatty acid priming.

The hierarchical clustering of the 1000 most variable genes across the full 116 hours sample dataset shows that the difference of expression patterns between Ctrl_Ctrl_20h_Ctrl and the samples that finally were LPS stimulated is so strong that the 24 hours priming effect of OA and PA stimulations was masked by the LPS effect itself. Therefore, RNA-sequence analysis of 116 hours samples does not include the zero control Ctrl_Ctrl_20h_Ctrl.

In **Figure 5.7.4.1 B.)** expression patterns of the up- and down-regulated genes in Ctrl_Ctrl_20h_LPS, OA_Ctrl_20h_LPS and PA_Ctrl_20h_LPS samples appear very different. Although the cells cultured under different priming conditions were cultured for the last 92 hours in the same culture environment and finally all got in contact with the same amount of LPS, the expression patterns of the 1000 most variable genes vary heavily between the conditions.

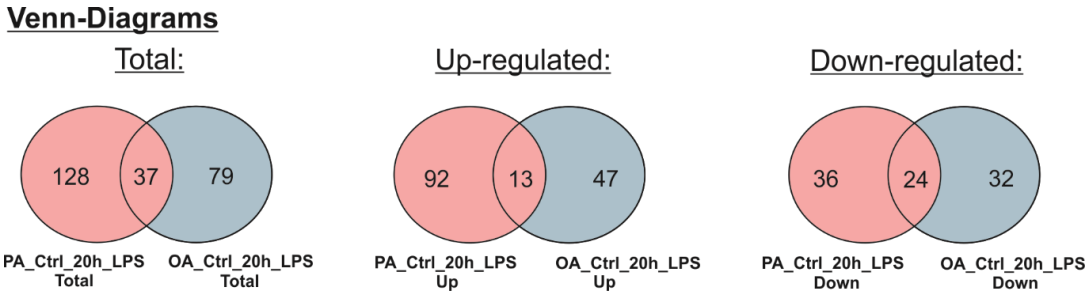

Figure 5.7.4.2: Monocyte-derived cells develop a specialized memory upon interaction with saturated and unsaturated fatty acids which origin in different transcriptional outcomes upon stimulation with LPS. Venn-diagrams visualizing the comparison of shared up- and down-regulated genes between OA_Ctrl_20h_LPS and PA_Ct6rl_20h_LPS. Differentially expressed genes were defined by comparison to Ctrl_Ctrl_20h_LPS, a FC ≥ 1.5/ ≤ - 1.5 and p-value ≤ 0.05 with FDR.

Venn diagrams showing the number of overlapping DE-genes between OA_Ctrl_20h_LPS and PA_Ctrl_20h_LPS are visualized in **Figure 5.7.4.2**. DE-genes were defined by comparisons with Ctrl_Ctrl_20h_LPS expression patterns. Considering the total number of DE-genes of the two conditions, it gets clear that 24 hours PA and OA priming forces the cells into a state of divergent transcriptional response to LPS compared to Ctrl_Ctrl_20h_LPS and to each other. The variant effect in LPS response is however stronger for PA-primed cultures as seen for OA-primed cultures, which is visualized by the number of determined DE-genes. In PA_Ctrl_20h_LPS samples, in total 165 genes, and in OA_Ctrl_20h_LPS samples, 116 genes were differentially expressed (FC +/-1.5; p-value with FDR ≤ 0.05) compared to Ctrl_Ctrl_20h_LPS. Of the 37 overlapping DE-genes, 13 are up-regulated while 24 are down-regulated (see Appendix **Table 8.3**). The functional involvement of up-regulated genes may be described by GO-terms like ‘detoxification’ (FAM213B, GSTM1), ‘metabolic process’ (ADCY3, AK1, FAM213B, GSTM1, HYAL3, MAP4K2, SPATA18, SYNJ2, TEAD3, UCHL3), ‘cellular process’ (ADCY3, AK1, FAM213B, GLIPR1, GSTM1, HYAL3, MAP4K2, SIRPB1, SPATA18, SYNJ2, TEAD3, UCHL3), ‘reproductive process’ (ADCY3, HYAL3, TEAD3) and ‘immune system process’ (GLIPR1, MAP4K2, SIRPB1). Involvement of products of overlapping down-regulated transcripts can be described by GO-terms like ‘immune system process’ and ‘response to stimulus’ (BCL2L11, CD1E, CST3, CST7, DEGS1, HLA-DOA, NDRG1, TSPAN14, UBD), ‘pigmentation’ (BCL2L11), ‘detoxification’ (CLIC2) and ‘biological adhesion’ (BCL2L11, STAB1). Here, it should be considered that CST7 and CD1E are genes that are upregulated when monocytes differentiate into DCs[197,198]. Since these genes are down-regulated in OA_Ctrl_20h_LPS and PA_Ctrl_20h_LPS compared to

Ctrl_Ctrl_20h_LPS, it is indicated that Ctrl_Ctrl_20h_LPS monocyte-derived cells are differentiating into moDCs.

Gene and pathway information of this section were taken from http://www.pantherdb.org/ and https://www.genecards.org/ [188,189].

Comparing the transcriptomes of OA_Ctrl_20h_LPS versus PA_Ctrl_20h_LPS, 82 DE-genes could be determined of which 32 are up- and 50 are down-regulated.

5.7.5 Functional interpretation of transcript analysis

As before, we performed a gene ontology enrichment analysis with the 116 hours samples, using the ClusterProfiler[167] classification system. GO-terms were considered significantly enriched with a Bonferroni corrected p-value of ≤ 0.05 and p-adjust cutoff of 0.1. A dot plot visualization of overexpressed genes in the OA_ctrl_20h_LPS or PA_ctrl_20h_LPS stimulated samples compared to Ctrl_ctrl_20h_LPS or to each other is shown in **Figure 5.7.5.1**.

Figure 5.7.5.1: GO-term-enrichment analysis of up- and down-regulated DE-genes of fatty acid trained monocyte-derived cells after re-stimulation with LPS. GO-terms were considered significantly enriched with a Bonferroni corrected p-value of ≤ 0.05 and p-adjust cutoff of 0.1.

The GO-enrichment analysis is visualized in **Figure 5.7.5.1**. ‘Fatty acid metabolic process’ is the only GO-term appearing for up-regulated DE-genes in OA_Ctrl_20h_LPS samples compared to Ctrl_Ctrl_20h_LPS, with a gene ratio of 0.15. When compared to PA_Ctrl_20h_LPS instead of to Ctrl_Ctrl_20h_LPS samples, much more GO-terms, taking only 26 up-regulated DE-genes into account, are predicted. These terms describe processes involved in ‘small molecule biosynthetic processes’, the ‘regulation of triglyceride, lipid, sterol and cholesterol transport’, the ‘regulation of lipid localization’, as well as in ‘acylglycerol and triglyceride homeostasis’.
The term that describes the tendency of functional involvement of down-regulated DE-genes in OA_Ctrl_20h_LPS compared to PA_Ctrl_20h_LPS samples is termed ‘negative regulation of lipid transport’, which goes along with the up-regulated processes.

GO-terms describing product involvement of up-regulated DE-genes in PA_Ctrl_20h_LPS, compared to the Ctrl_Ctrl_20h_LPS comprise ‘complement activation, classical pathway’, ‘lipid biosynthetic process’ (large gene ratio) and ‘humoral immune response mediated by circulating immunoglobulin’. The gene ratio for ‘lipid biosynthetic process’ is with 0.20 comparably high and also significant with a p-value of 0.02. Conspicuously, the terms describing the gene product involvement of down-regulated DE-genes in PA_Ctrl_20h_LPS cultures compared to Ctrl_Ctrl_20h_LPS encompass several processes involved in the inflammatory response of myeloid-derived cells and in the initiation of adaptive immune responses. Predicted GO-terms for this condition comprise ‘response to IFN-ɤ’, ‘antigen processing and presentation of peptide antigen via MHC class II’, ‘positive regulation of leukocyte activation’, ‘cytokine-mediated signaling pathway’, ‘positive regulation of cell adhesion’, and many more. Since genes whose products are involved in such processes are down-regulated in PA_Ctrl_20h_LPS cultures it is suggested that PA priming sets monocyte-derived cells into a state of tolerance to LPS.

In addition to GO-term analysis, KEGG enrichment analysis was performed using pre-defined DE-genes of the 116 hours samples. The KEGG-enrichment analysis was performed by Dr. Thomas Ulas (LIMES-Institute, University of Bonn). Settings described for 24 hours samples were overtaken. The cutoffs of included DE-genes were set to FC ≥ 2 and p-value ≤ 0.05.

A.) OA_ctrl_20h_LPS vs Ctrl_ctrl_20h_LPS - Expression

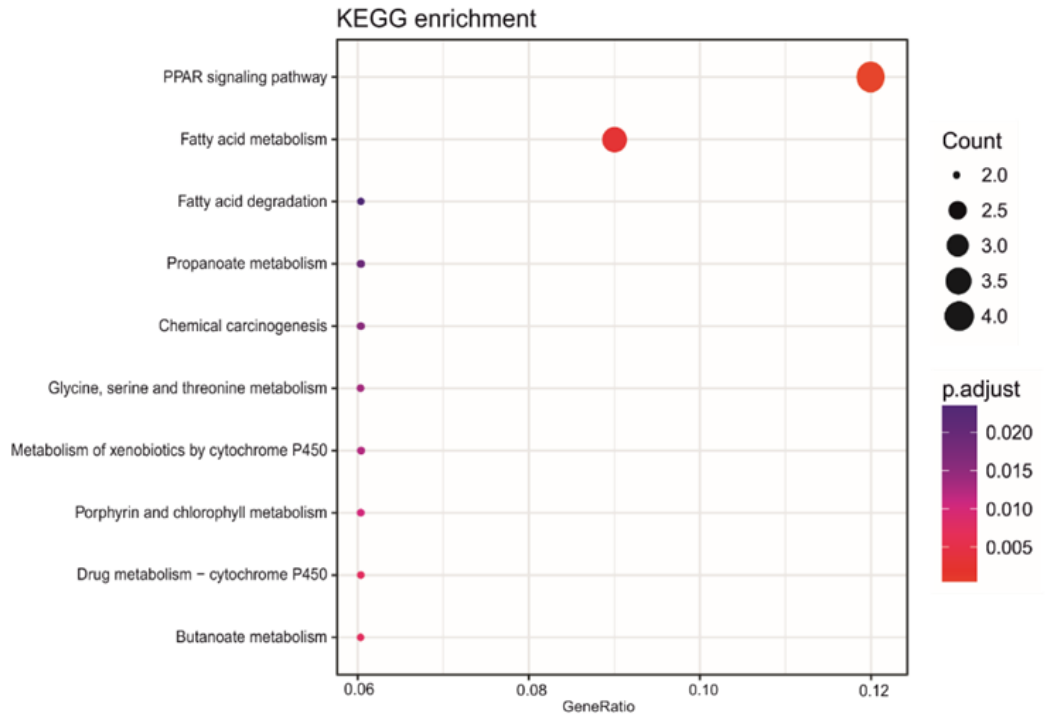

B.) PA_ctrl_20h_LPS vs Ctrl_ctrl_20h_LPS - Expression

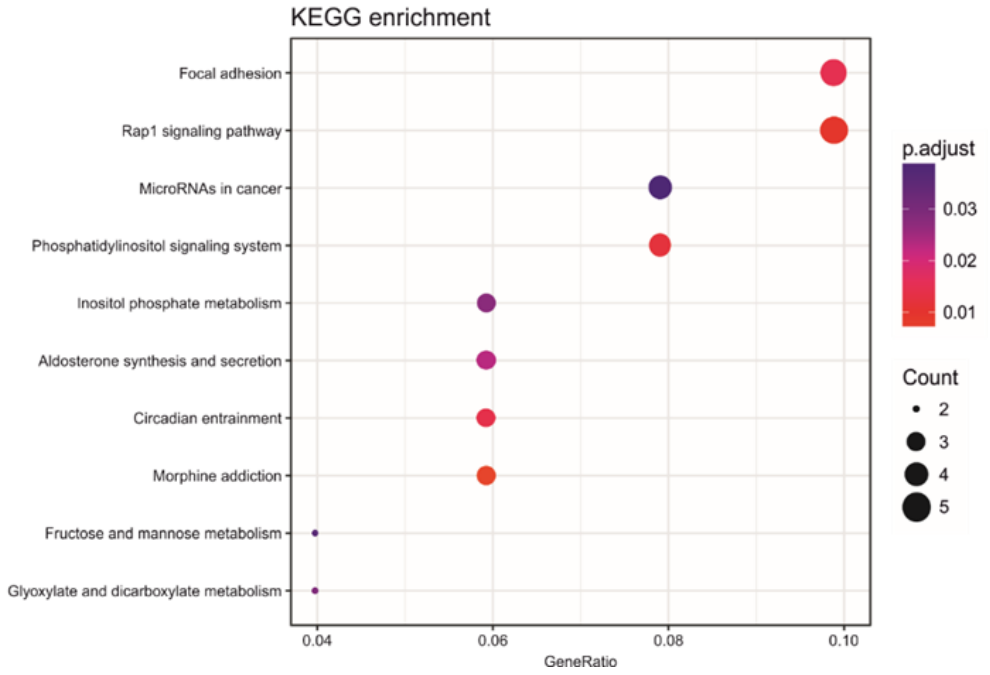

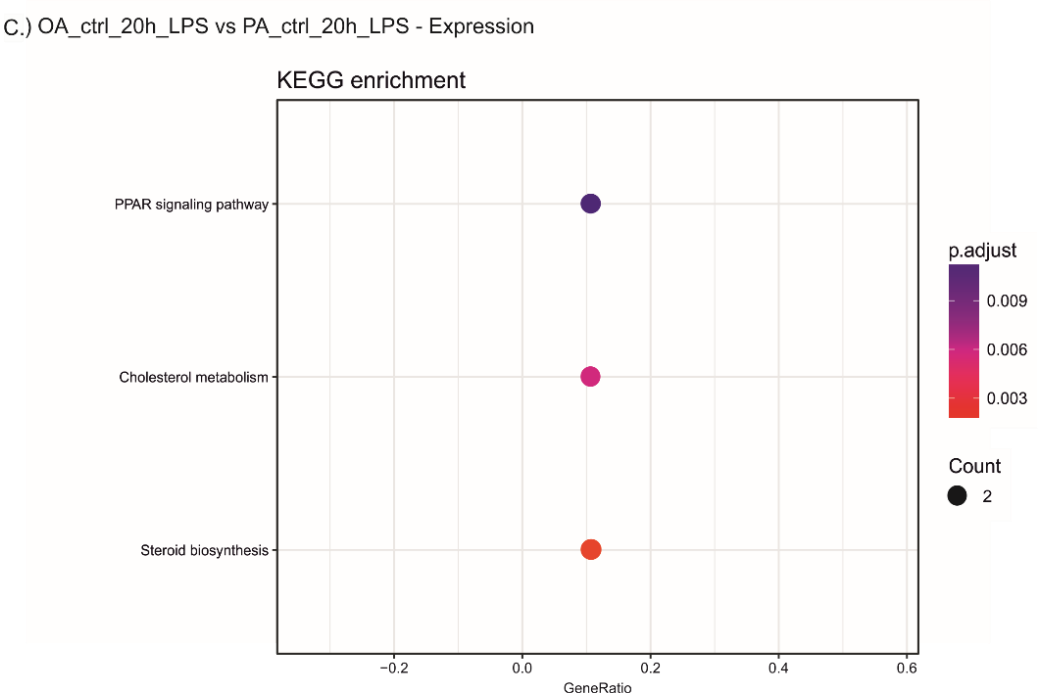

Figure 5.7.5.2: KEGG-enrichment analysis. Scatterplot of enriched KEGG pathways for DE-genes up-regulated in OA_Ctrl_20h_LPS and PA_Ctrl_20h_LPS monocyte-derived cells. The gene ratio indicates the ratio of the differentially expressed gene number to the total gene number in a certain pathway. The size and color of the dots represent the gene number and the range of p-values, respectively. A.) Represents pathways upregulated in OA_Ctrl_20h_LPS stimulated monocyte-derived cells compared to Ctrl_Ctrl_20h_LPS cells. B.) Shows pathways to which up-regulated DE-genes of PA_Ctrl_20h_LPS versus Ctrl_Ctrl_20h_LPS cultures contribute, while in C.) pathways are visualized that are upregulated in OA_Ctrl_20h_LPS monocyte-derived cells when compared to PA_Ctrl_20h_LPS cultures. DE-genes were defined by fold changes of ≥ 2 and p-values ≤ 0.05.

Figure 5.7.5.2 A.) shows KEGG pathways of up-regulated DE-genes established by comparison of OA_Ctrl_20h_LPS and Ctrl_Ctrl_20h_LPS cultures. The gene count is quite low although the number of up-regulated differentially expressed genes (60) set in for analysis was quite high. Likewise, as in 24 hours OA stimulated monocyte-derived cells, ‘PPAR signaling pathway’ and ‘Fatty acid metabolism’ are the terms with highest gene counts (4 genes), gene ratios and significance (p-adjust ≤ 0.005). In the remaining pathways described for this comparison, the gene counts and gene ratios are with two genes involved and a gene ratio of 0.06 relatively low. Pathway descriptions of genes with p-adjust lying between 0.015 and 0.02 are ‘fatty acid degradation’, ‘propanoate metabolism’, ‘chemical carcinogenesis’, ‘glycine, serine and threonine metabolism’ and ‘metabolism of xenobiotics by cytochrome P450’. The pathways assumed with higher significance (p-adjust between 0.01 and 0.005) include ‘porphyrin and chlorophyll metabolism’, ‘drug metabolism – cytochrome P450’ and ‘butanoate metabolism’.

In **Figure 5.7.5.2 B.)** KEGG pathways determined for up-regulated DE-genes in PA_Ctrl_20h_LPS compared to Ctrl_Ctrl_20h_LPS monocyte-derived cells, are described. Here the gene counts of gene products involved in described pathways are with ≤ 5 slightly higher as visualized for OA_Ctrl_20h_LPS cultures, but the number of implicated up-regulated DE-genes was also much higher (105). The gene rations are with highest ≤ 0.1 quite low. The pathways with highest gene ratios and gene counts comprise 'Focal adhesion' and 'RAP1 signaling pathway'. 'Micro RNAs in cancer' and 'phosphatidyl inositol system' both count 4 DE-genes involved and a gene ratio of 0.08. Pathways described with gene ratios of 0.06 and three genes implicated are described as 'inositol phosphate metabolism', 'aldosterone synthesis and secretion', 'circardian entrainment' and 'morphine addiction'. The pathways given with lower gene ratios (0.04) and involvement of 2 genes include 'fructose and mannose metabolism' and 'glyoxylate and dicarboxylate metabolism'.

Figure 5.7.5.2 C.) shows pathways that are up-regulated in OA_Ctrl_20h_LPS compared to PA_Ctrl_20h_LPS cultures. In this comparison only 32 DE-genes were taken under investigation. Here, involvement of three pathways could be determined with gene ratios of 0.1 and two genes involved, respectively. Implied pathways are the 'PPAR signaling pathway', 'cholesterol metabolism' and 'steroid biosynthesis'.

5.7.6 Co-expression network analysis

Co-expression network analysis was performed using a network created from 100 genes possessing the highest and 100 genes possessing the lowest fold change in the following comparisons: OA_ctrl_20h_LPS vs Ctrl_ctrl_20h_LPS, PA_ctrl_20h_LPS vs Ctrl_ctrl_20h_LPS and OA_ctrl_20h_LPS vs PA_ctrl_20h_LPS. These 600 genes were filtered for FC ≥ 2 and ≤ -2 as well as for p-values ≤ 0.05. In Biolayout 3D we used a Pearson's correlation coefficient cutoff of 0.85 to determine similarity between the individual expression profiles. The network was build-on 280 nodes and 4028 edges.

Up- and down-regulated DE-genes are visualized by the color-coding of the group fold change (GFC) of the respective condition. As usual, bluish colored nodes indicate that the expression of the respective gene is down-regulated, while reddish nodes indicate

that the expression of the respective gene is up-regulated when compared to the overall expressed mean.

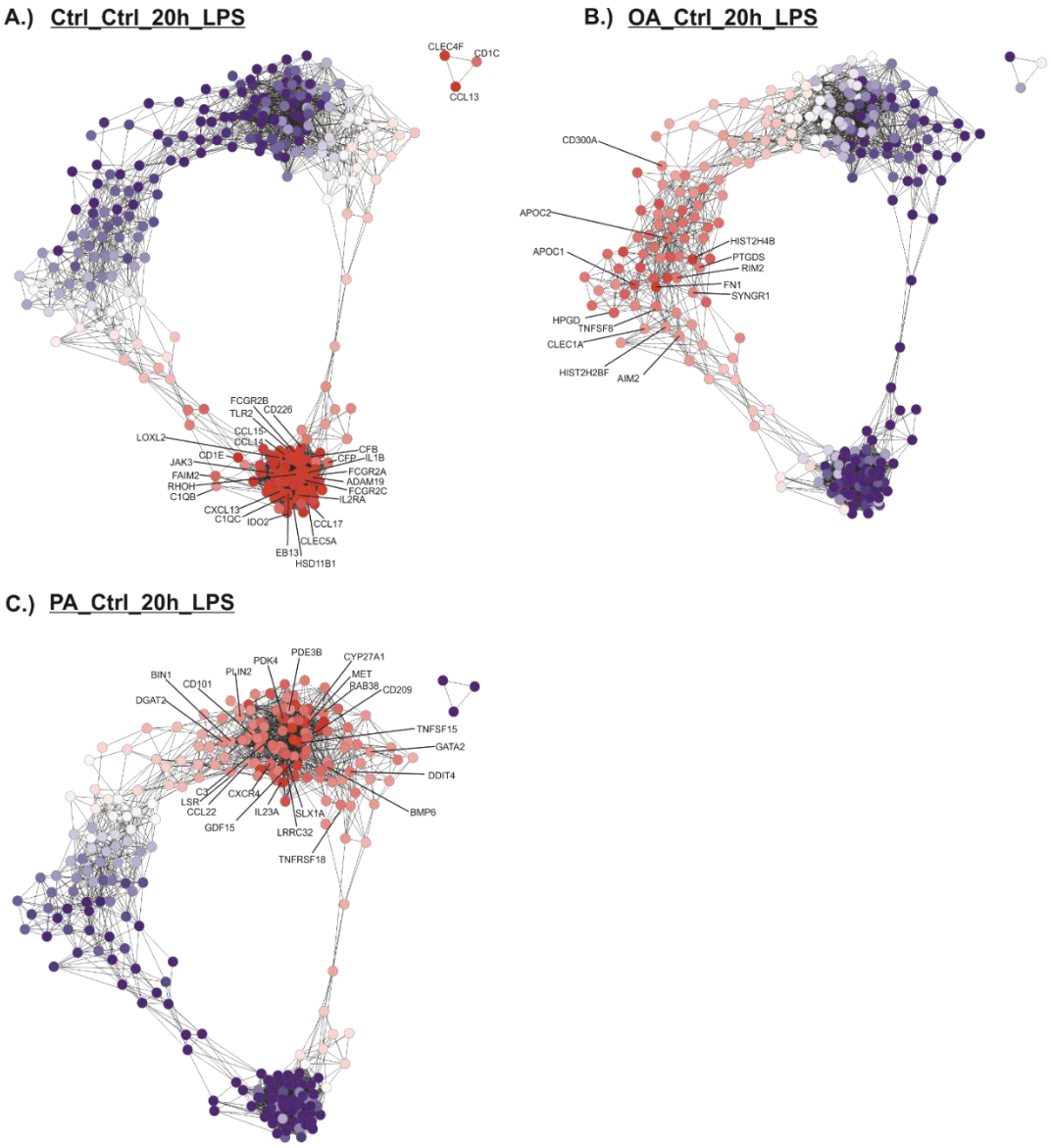

Figure 5.7.6.1: Co-expression network analysis of fatty acid pre-primed and LPS-re-stimulated monocyte-derived cells.
Visualization of co-expressed genes in saturated and unsaturated fatty acid pre-primed monocytes, followed by a 72 hours wash-out period and a 20 hours LPS re-stimulation. Pictured are differences in expression relative to the overall mean. This is indicated by the color coding of the respective nodes. The network is based on the top 100 highest and lowest differentially expressed genes (and final filtering for p-value ≤ 0.05 & FC ≤-2/≥2) between OA_Ctrl_20h_LPS and Ctrl_Ctrl_20h_LPS, PA_Ctrl_20h_LPS and Ctrl_Ctrl_20h_LPS and OA_Ctrl_20h_LPS and PA_Ctrl_20h_LPS stimulated cells after 116 hours of culturing. The Pearson's correlation coefficient cutoff was set to 0.85. The Network consists of 277 nodes and 3504 edges.

Comparing the overall color distribution of the network it gets visible that the expression patterns changed completely between the three different culture conditions. Genes that

are up-regulated in Ctrl_Ctrl_20h_LPS are almost completely down-regulated in the fatty acid-primed samples. This is however also true when comparing the expression pattern of network genes in OA_ctrl_20h_LPS and PA_ctrl_20h_LPS. In total, it can be said that the expression pattern of selected network genes switches completely between the conditions and have almost no overlap. Therefore, this network is perfect to describe the variance in expressed genes and cell programs turned-on or off due to previous OA or PA priming.
The typical and unique LPS response of tested monocyte-derived cells is presented by red colored nodes in **Figure 5.7.6.1 A.)**. Genes specifically up-regulated in response to LPS by OA_Ctrl_20h_LPS cultures are visualized as red nodes in **Figure 5.7.6.1 B.)**, and those of PA_Ctrl_20h_LPS cultures are shown in **Figure 5.7.6.1 C.)**.

In Ctrl_ctrl_20h_LPS genes that are up-regulated comprise such involved in complement activation (C1QB, C1QC, CFB and CFP), in the inflammatory response (IL2RA, FFAR2, CCL15-CCL14, FCGR2A, ADAM19, Jak3, CD1E, CCL13, CCL17, CXCL13, CLEC5A, MAP1LC3A, FCGR2B, TLR2, EB13, FCGR2C, UBD, IDO2) and genes that are involved in the stress response of myeloid-derived cells, including DUSP1, HSD11B1 and SESN3. Under these conditions, also genes coding for proteins that are involved in cellular survival are up-regulated. These genes comprise RHOH and FAIM2. Moreover, genes that code for proteins that control or induce differentiation and function of granulocytes and macrophages (CSF2RA and ABCA9) are either expressed. In addition to that, genes whose products are involved in activation (CREB5) or co-repression (LOXL2) of transcription are up-regulated upon LPS stimulation. LOXL2, a gene coding for a protein that functions as specific tag for epigenetic transcriptional activation by mediating deamination of trimethylated Lys4 of histone H3 (H3K4me3) was either up-regulated.

In case of OA_Ctrl_20h_LPS monocyte-derived cells, genes that are specifically up-regulated include C5, a gene coding for a protein involved in the membrane-attack-complex and many further genes that code for proteins involved in different actions of the innate immune-response and inflammation (PGD2, HPGD, SYNGR1, CLEC1A, FN1, AIM2, TNFSF8). Further, genes that code for proteins involved in the negative regulation of macrophage mediated inflammation (FAM213A and CD300A), involved in transcription regulation and chromosome as well as genome stability (HIST2H4B,

HIST2H2BF, RIM2) are differentially expressed. Also, genes coding for proteins involved in lipoprotein metabolism (APOC1 and APOC2), are increasingly transcribed.

Network genes specifically up-regulated in PA_Ctrl_20h_LPS cultures include C3 which plays a central role in the activation of the complement system and many other pro-inflammatory mediators like IL23A, TNFRSF15, TNFRSF18, GDF15, CD209, CCL22, RAB38 and CXCR4. In addition to those, also genes coding for proteins involved in suppression of extensive immune-system activation, including CD101, playing a role as inhibitor of T-cell proliferation and LRRC32, which is a T-regulatory cell activation marker, are up-regulated. BIN1, a gene coding for a protein involved in the activation of a caspase-independent apoptotic process might be counter acted by the increased expression of gene products involved in proliferation and survival (DDIT4 & MET). Further, proteins that play a role in lipid metabolism and adipocyte development (PDK4, CYP27A1, DGAT2, PLIN2, PDE3B) or the clearance of triglyceride-rich lipoprotein from blood (LSR), are highly expressed. Up-regulated genes that play a role in the regulation of gene expression and transcription factor binding include GATA2, GDF15 and BMP6. SAX1A, an important regulator of genome stability, is either differentially expressed.

5.8 Transcriptomic analysis of the complete trained immunity dataset

5.8.1 Data preprocessing

The complete dataset comprising all time-points of the trained immunity experiment was pre-processed the same way as described before.

After pre-processing the data comprised 10.830 transcripts. These genes were retained for further analysis.

Upon PAMPs and DAMPs recognition, TLRs recruit TIR domain-containing adaptor proteins such as MyD88 and TRIF, which initiate signal transduction pathways that terminate in the activation of NF-κB, IRFs, or MAP kinases to regulate the expression of chemokines, cytokines, and type I IFNs which ultimately protect the host from microbial infection[8]. As described in the introduction, LPS but also saturated fatty acids have been described to induce pro-inflammatory processes in myeloid cells. In both cases inflammatory processes are induced by TLR4 (in case of SFAs also TLR2/TLR6)

activation[199]. To investigate if rather MyD88- or TRIF-dependent responses were triggered by the stimuli set at the different time points of investigation, expression network analysis using genes downstream of MyD88- and of TRIF- pathway, respectively, was performed. Gene-lists for MyD88- and TRIF-dependent downstream genes were taken from the following publication: *Thomas Ulas et. al.*: S100 alarmin-induced innate immune programming protects newborn infants from sepsis; Nature Immunology; June 2017[200].

Figure 5.8.1.1 shows the MyD88-dependent TLR4 signaling module network for each condition at each time point of investigation. Co-expression network analysis was performed using 43 genes downstream of the MyD88-dependent TLR4 pathway. In Biolayout 3D, we used a Pearson's correlation coefficient cutoff of 0.70 to keep higher correlation between the conditions. The network was build-on 37 nodes and 151 edges. Up- and down-regulated DE-genes are visualized by the color-coding of the group fold change (GFC) of the respective condition. As usual, bluish colored nodes indicate that the expression of the respective gene is down-regulated, while reddish nodes indicate that the expression of the respective gene is up-regulated when compared to the overall expressed mean.

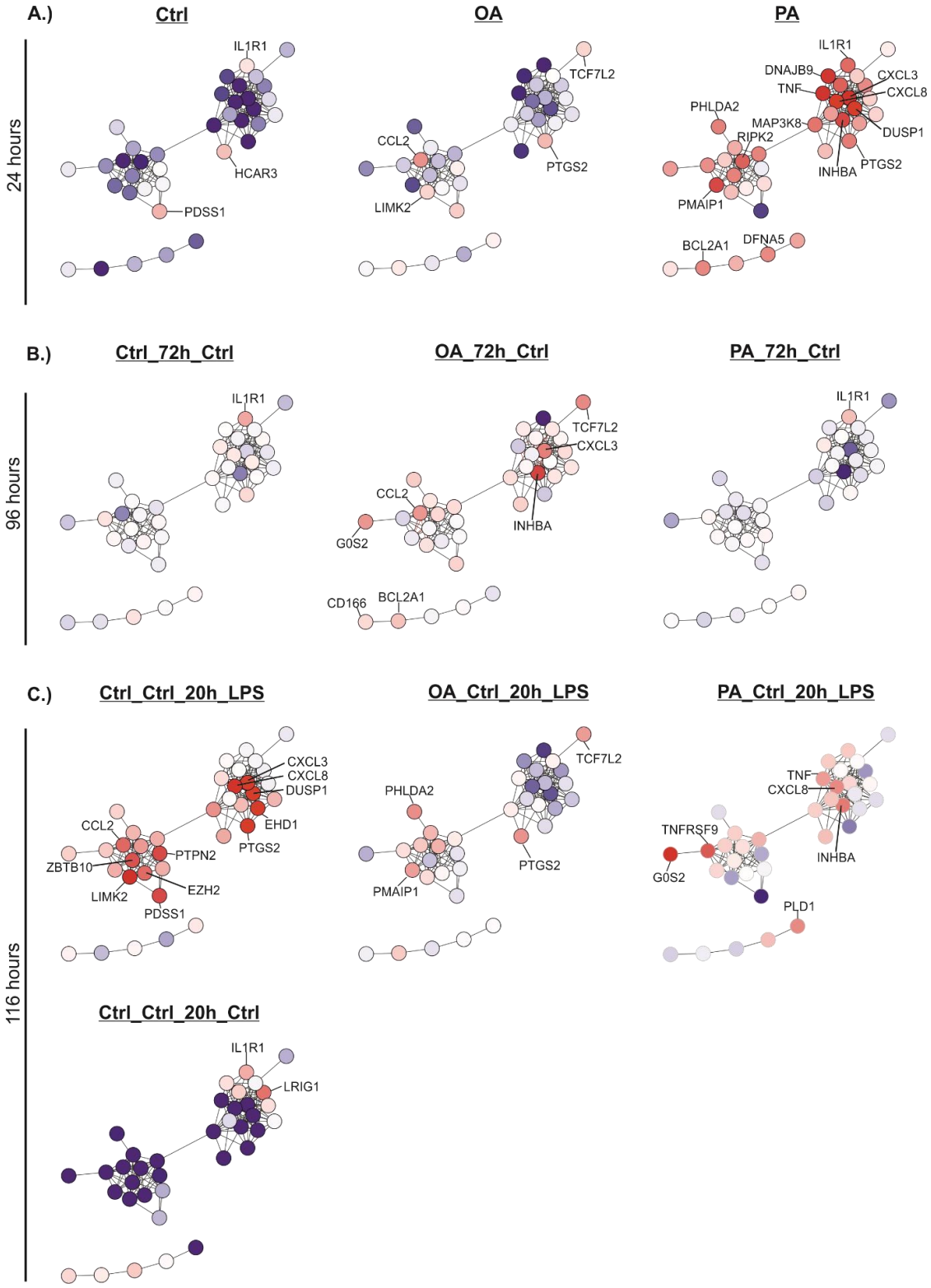

Figure 5.8.1.1: Transcriptomic changes in palmitic acid and oleic acid primed monocyte-derived cells before and after re-stimulation with LPS and the corresponding activation of MyD88-dependent gene programs. A.) Expression patterns of MyD88-dependent downstream genes in 24 hours samples. B.) Expression patterns of MyD88-dependent downstream genes in 96 hours samples, after wash-out of priming fatty acids. C.) Expression patterns of MyD88-dependent downstream genes in 116 hours samples after final LPS stimulation.
In Biolayout 3D a Pearson's correlation coefficient cutoff of 0.70 was used to keep higher correlation between the conditions. The network was build-on 37 nodes and 151 edges. Visualized are group fold changes (GFCs) of expression means (n=3).

In **Figure 5.8.1.1 A.)** the network representing the expression pattern of the 24 hours samples are visualized. In the control network only three downstream genes of the MyD88-dependent pathway are slightly up-regulated. These comprise IL1R1, HCAR3 and PDSS1. After 24 hours of OA stimulation, monocyte-derived cells also have just slight up-regulation of few network genes, these comprise CCL2, PTGS2, TCF7L2, LIMK2 and PDSS1. In case of 24 hours PA stimulation the cells up-regulate almost all of the MyD88-dependent downstream network genes. Only PTPN2 and PDSS1 are slightly down-regulated. Genes that are highly up-regulated include PMAIP1, TNF, DNAJB9, IL1R1, CXCL3, CXCL8, DUSP1 and INHBA.

In **Figure 5.8.1.1 B.)** the expression patterns of the 96 hours samples are visualized. After the three days of wash-out the expression patterns of the Ctrl_72h_Ctrl and PA_72h_Ctrl appear very similar. Here, the expression patterns of all network genes, besides IL1R1, are quite neutral or even down-regulated. In OA_72h_Ctrl however, more MyD88-dependent TLR4 pathway genes than after 24 hours OA stimulation, are up-regulated. Genes with a relatively high GFC for OA_72h_Ctrl involve INHBA, CXCL3, TCF7L2, CCL2 and G0S2.

In the 116 hours networks, after LPS stimulation, we see a clearly different expression patterns of MyD88-dependent TLR4 pathway genes in Ctrl_Ctrl_20h_LPS, OA_Ctrl_20h_LPS and PA_Ctrl_20h_LPS stimulated cells. Most downstream pathway genes are up-regulated in the Ctrl_Ctrl_20h_LPS samples. Genes with strong GFCs encompass PTPN2, CCL2, ZBTB10, LIMK2, PDSS1, EZH2, PTGS2, EHD1, DUSP1, CXCL8 and CXCL3. In OA_Ctrl_20h_LPS only some few network genes are slightly up-regulated. The genes with highest GFCs in these samples include PHLDH2, PMAIP1, PTGS2 and TCFL2. The few network genes that are up-regulated in PA_Ctrl_20h_LPS on the other hand involve G0S2, TNFRSF9, PLD1, INHBA, CXCL8 and TNF. Also, in the Ctrl_Ctrl_20h_Ctrl samples some few MyD88-dependent TLR4 pathway genes are up-regulated while the remaining are strongly down-regulated. The two genes with strongest GFCs are LRIG1 and IL1R1.

In total, it can be said, that in the MyD88-dependent TLR4 network expression patterns of 24h_PA and Ctrl_Ctrl_20h_LPS cultures are most comparable (**Figure 5.8.1.1A.)**).

The MyD88-dependent network represents just genes downstream of the MyD88-dependent activation of TLR4. Therefore, I further assessed normalized gene counts

of MyD88 itself as well as of its adaptor protein TIRAP and final expression of IL1B and TNF in response to MyD88-dependent TLR4 activation. **Figure 5.8.1.2** visualizes normalized counts of the complete dataset for each condition and at each time point of cell investigation.

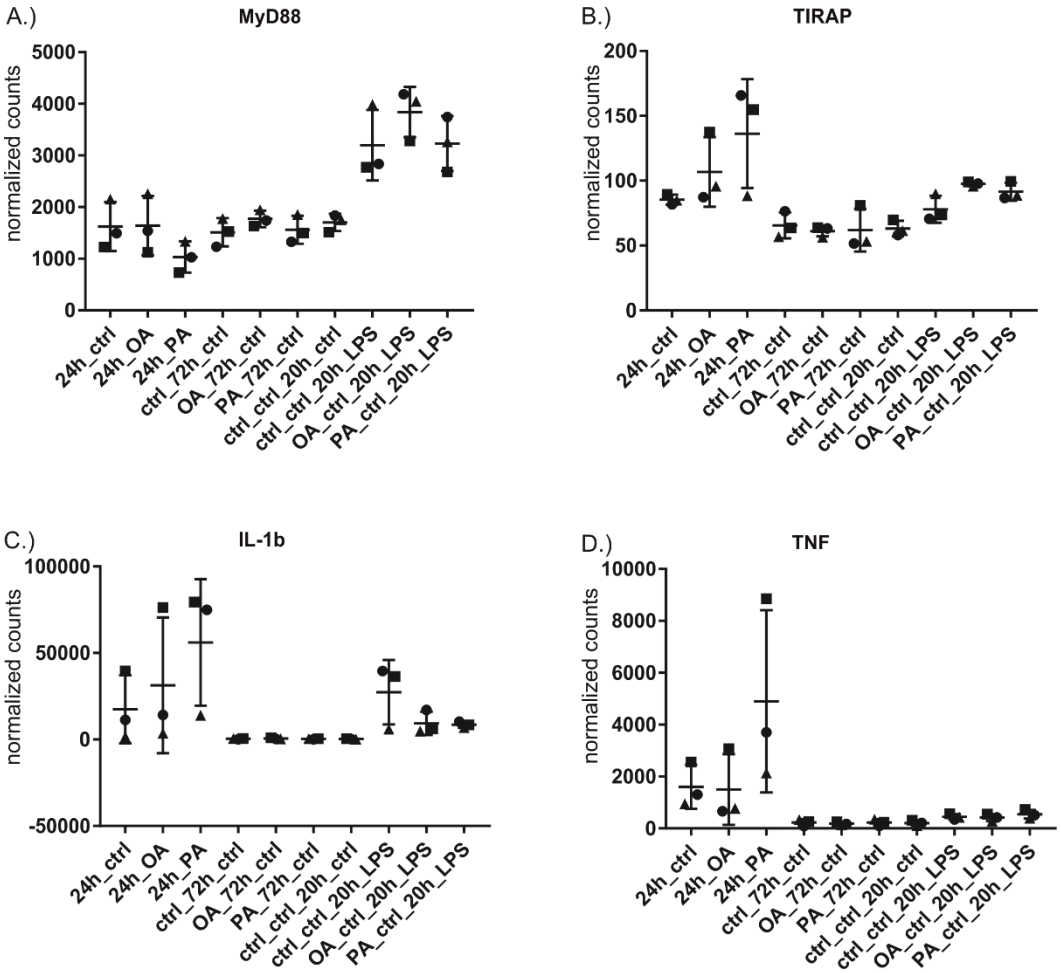

Figure 5.8.1.2: Direct MyD88, adapter and TLR4 activation product expression. Normalized expression counts of complete dataset count table. A.) Normalized expression counts of MyD88 gene. B.) Normalized expression counts of the gene coding for the MyD88 adapter protein TIRAP. C.) Normalized expression counts of IL1B, a gene expressed in response to MyD88-dependent TLR4 activation. D.) Normalized expression counts of TNF, a gene expressed in response to MyD88-dependent TLR4 activation. ▲ – Donor 1; ● – Donor 2; ■ – Donor 3. Ordinary One-Way ANOVA was used for significance measurements. Data were not significant.

Investigating normalized counts of the 24 hours samples, it gets visible that 24h_OA and 24h_Ctrl samples have a similar mean count number of about 1.600 while the mean count number of 24h_PA samples is with ~ 1.000 counts much lower. The expression of the MyD88 adapter protein gene TIRAP is however contrarily regulated.

Here, the mean number of counts is highest in 24h_PA samples which goes in hand with mean IL1B and mean TNF expression. In 24h_OA samples normalized TIRAP counts are lower as in 24h_PA samples however increased compared to 24h_Ctrl cultures. This is also true for mean IL1B expression, while mean TNF counts equal those of 24h_Ctrl samples.
In 96 hours samples, mean MyD88 expression counts are for all three conditions similarly high as in 24h_Ctrl and 24h_OA cultures with OA_72h_Ctrl being a bit higher in number as Ctrl_72h_Ctrl and PA_72h_Ctrl cultures, which lie in the range of ~1.500 counts. Mean count numbers of the adapter protein gene lie with approximately 70 counts all in the same range. IL1B and TNF are with count numbers of close to zero not notably expressed.

Investigating normalized count numbers of the 116 hours samples it gets visible that Ctrl_Ctrl_20h_Ctrl samples equal the mean count number of wash-out samples after 96 hours of culturing. The samples finally stimulated with LPS for 20 hours in contrast all show increased count numbers for MyD88 and IL1B expression. Mean count numbers for MyD88 are with ~3.900 counts highest in OA_Ctrl_20h_LPS. Ctrl_Ctrl_20h_LPS and PA_Ctrl_20h_LPS have equally high mean count numbers of ~3.200. Expression of the adapter protein gene TIRAP are a bit increased compared to 96 hours samples and lie between ~75 and ~100 counts with Ctrl_Ctrl_20h_LPS having fewest and OA_Ctrl_20h_LPS highest counts. In PA_Ctrl_20h_LPS TIRAP counts are slightly less as in OA_Ctrl_20h_LPS samples. Interestingly, IL1B expression shows the highest mean count number of ~27.500 in Ctrl_Ctrl_20h_LPS while mean counts in OA_Ctrl_20h_LPS and PA_Ctrl_20h_LPS lie below 10.000. TNF expression is not very high compared to 24 hours samples and mean counts lie at ~ 450 in Ctrl_Ctrl_20h_LPS, ~ 420 in OA_Ctrl_20h_LPS and ~ 545 in PA_Ctrl_20h_LPS cultures. Although not easily detectible in the figure projection due too high scaling of 24 hours samples, TNF expression shows almost hundred counts more in PA_ctrl_20h_LPS compared to Ctrl_Ctrl_20h_LPS and thus is over-expressed in this condition.

When count numbers are getting high, vast deviations between the single donors can be observed. This is typical for human samples as different genetic background and environmental conditions impact the cells.

Figure 5.8.1.3 shows the TRIF-dependent TLR4 signaling module network for each condition at each time point of investigation. Co-expression network analysis was performed using 37 genes downstream of the TRIF-dependent TLR4 pathway. In Biolayout 3D we used a Pearson's correlation coefficient cutoff of 0.77 to keep higher correlation between the conditions. The network was build-on 36 nodes and 357 edges. As usual up- and down-regulated DE-genes are visualized by the color-coding of the group fold change (GFC) of the respective condition.

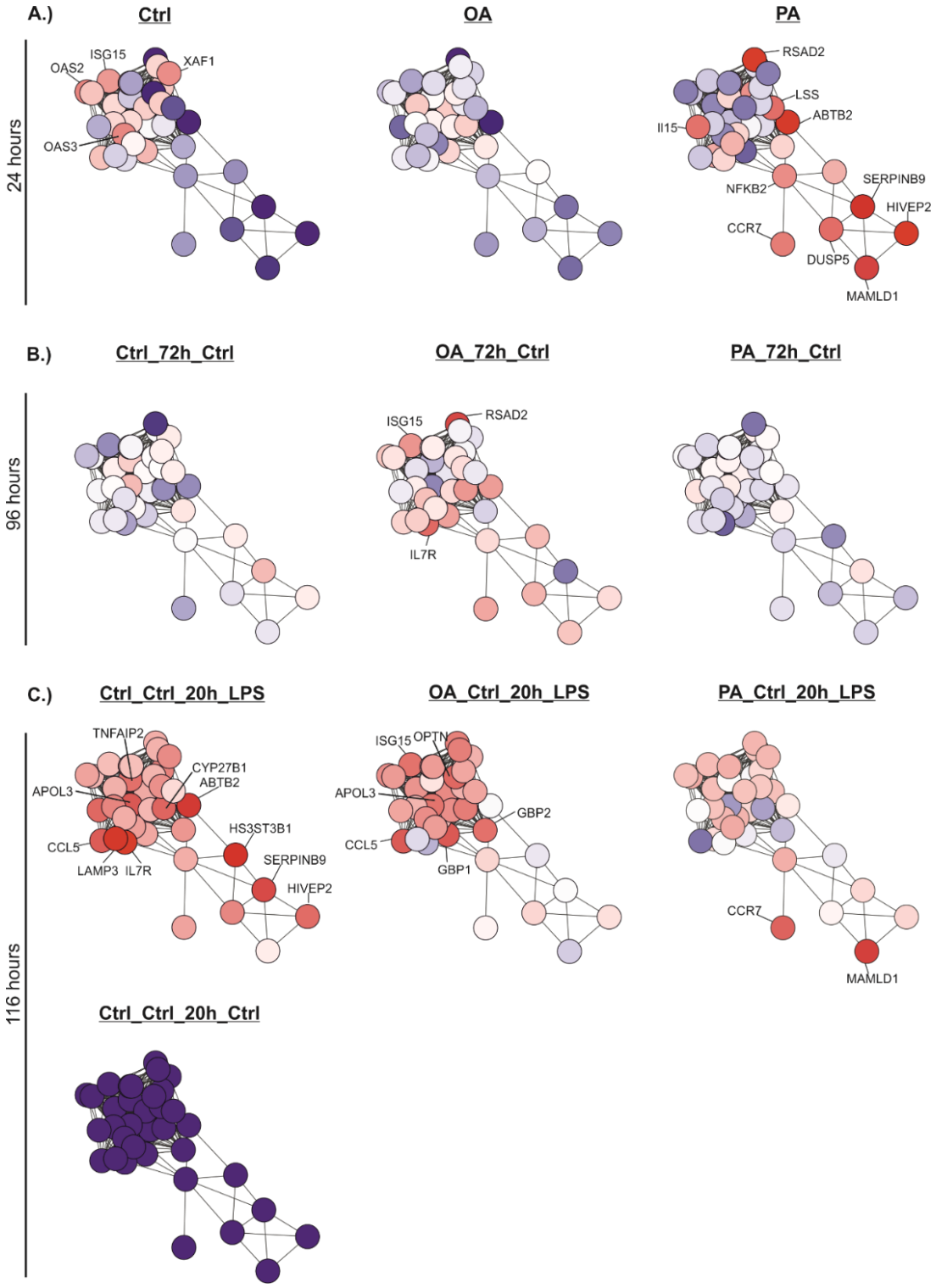

Figure 5.8.1.3: Transcriptomic changes in palmitic acid and oleic acid primed monocyte-derived cells before and after re-stimulation with LPS and the corresponding activation of TRIF-dependent gene programs. A.) Expression patterns of TRIF-dependent downstream genes in 24 hours samples. B.) Expression patterns of TRIF-dependent downstream genes in 96 hours samples, after wash-out of priming fatty acids. C.) Expression patterns of TRIF-dependent downstream genes in 116 hours samples after final LPS stimulation. The network was built on 36 nodes and 357 edges. In Biolayout 3D a Pearson's correlation coefficient cutoff of 0.77 was used to keep higher correlation between the conditions. Visualized are group fold changes (GFCs) of expression means (n=3).

In **Figure 5.8.1.3 A.)** the relative expression patterns of 24 hours samples are visualized. It is noticable that even in the control much more network genes are slightly up-regulated compared to the MyD88-dependent TLR4 pathway network. Genes with a relatively high GFC include OAS2, OAS3, ISG15 and XAF1. In 24h_OA cultures only some few network genes are weakly up-regulated. The 24h_PA stimulation in contrast had a stronger effect in sense of TRIF-dependent pathway gene activation. Here for several network genes the GFC is high. These genes include MAMLD1, HIVEP2, SERPINB9, ABTB2 and RSAD2. Genes that are moderately up-regulated include LSS, IL15, DUSP5, CCR7 and NFKB2.
As in the MyD88-dependant TLR4 pathway gene network, after the three days wash-out phase, the expression patterns of TRIF-dependant pathway network genes of Ctrl_72h_Ctrl and PA_72h_Ctrl samples are rather weak and similar in patterns. In OA_72h_Ctrl samples much more network genes are slightly up-regulated with RSAD2, ISG15 and IL7R showing highest GFCs.

In the 116 hours networks (**Figure 5.8.1.3 C.)**), after LPS stimulation, in the Ctrl_Ctrl_20h_LPS sample all TRIF-dependent network genes are up-regulated. Some just slightly, others appear in deep red and represent a high GFC for these genes. Highly expressed network genes in Ctrl_Ctrl_20h_LPS comprise ABTB2, IL7R, HS3ST3B1, LAMP3, IL15, APOL3, SERPINB9, CCL5 and CYP27B1.

The network visualizing GFCs of OA_Ctrl_20h_LPS cultures appears similar in the expression pattern as Ctr_Ctrl_20h_LPS with the difference that IL7R, LAMP3, ABTB2, HS3ST3B1 and SERPINB9 are rather down-regulated. In the network representing the expression patterns of PA_Ctrl_20h_LPS stimulated cells, most network genes are expressed moderate or neutrally. However, CCL5, APOL3, TNFAIP2, CYP27B1 and HS3ST3B1 are slightly down-regulated while MAMLD1 and CCR7 appear in deep red and represent highly expressed genes. In the Ctrl_Ctrl_20h_Ctrl samples all TRIF-dependent TLR4 pathway network genes are strongly down-regulated.

As the TRIF-dependent network also just represents genes downstream of the TRIF-dependent activation of TLR4, we further assessed normalized gene counts of TRIF itself as well as of its adaptor protein TRAM and final expression of CCL5 in response to TRIF-dependent TLR4 activation. No expression data could be found for CXCL10, CD80 or IFNB1 in the complete processed dataset.

Figure 5.8.1.4 visualizes normalized counts of the complete dataset for each condition and at each time point of cell investigation.

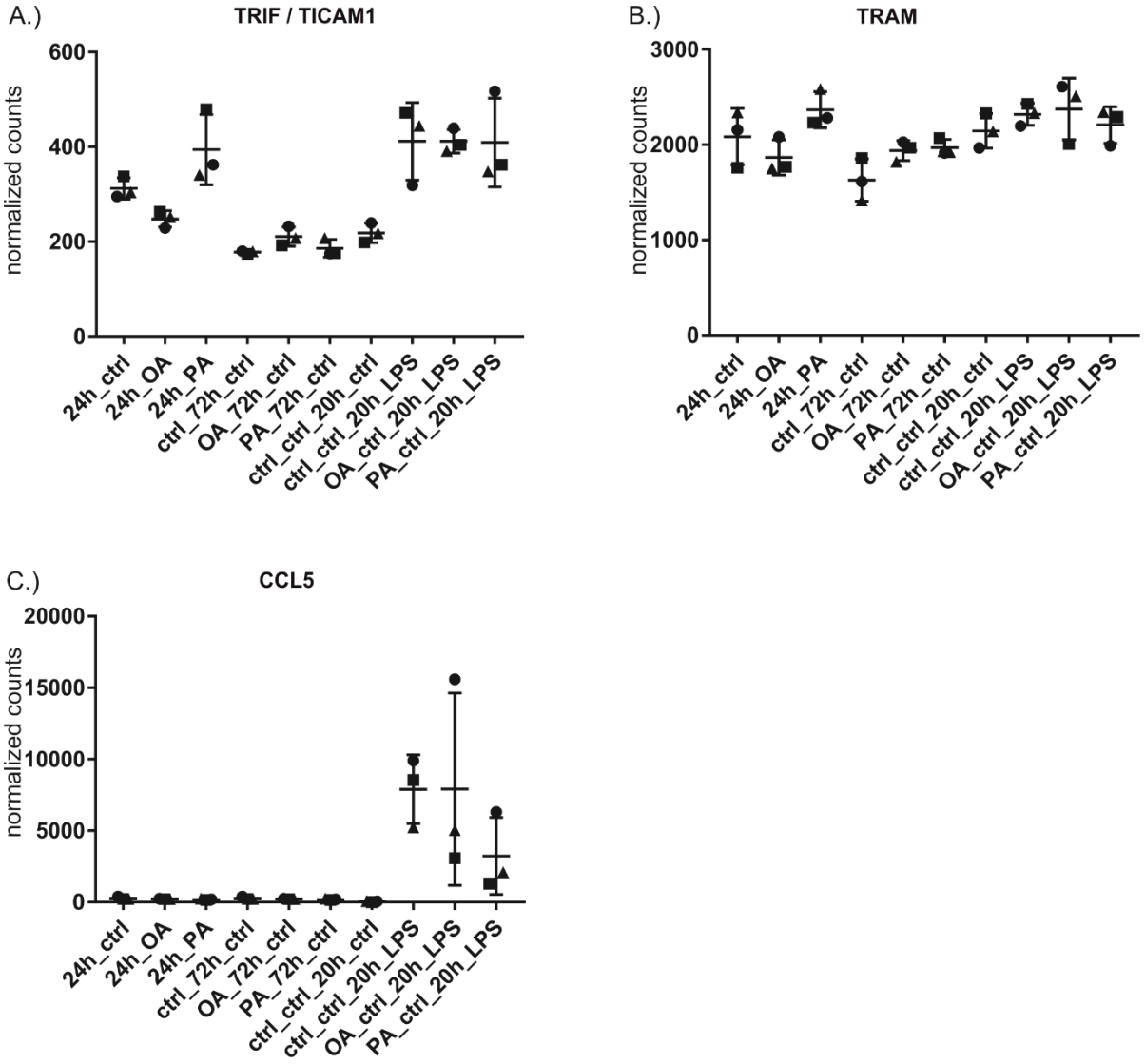

Figure 5.8.1.4: Direct TRIF, adapter and product expression. Normalized expression counts of complete dataset count table were used for analysis. A.) Normalized expression counts of TRIF (also called TICAM1) gene. B.) Normalized expression counts of the gene coding for the TRIF adapter protein TRAM. C.) Normalized expression counts of CCL5, a gene expressed in response to TRIF-dependent TLR4 activation. ▲ – Donor 1; ● – Donor 2; ■ – Donor 3. Ordinary One-Way ANOVA was used for significance measurements. Data were not significant.

Figure 5.8.1.4 A.) shows the relation of TRIF (TICAM1) counts determined for each condition. Investigating normalized counts of the 24 hours samples, it gets visible that 24h_PA has with ~ 400 the highest mean count number. The 24h_Ctrl samples have a mean count of ~ 310 while 24h_OA samples have with ~ 250 counts the lowest mean expression of TRIF. Although much higher counts, the expression of the adapter

protein gene TRAM goes inherent with the trend seen for TRIF expression. Normalized count numbers in 24h_Ctrl samples lie at ~2.085, in 24h_OA samples at ~1.865 and in 24h_PA samples at 2.365 counts. CCL5 expression in 24 hours samples however differs from that trend. Here the mean number of counts is with ~275 highest in 24h_Ctrl samples, second highest with ~220 counts in 24h_OA and lowest with ~ 200 counts in 24h_PA samples.

In the 96 hours samples mean TRIF expression counts are for all three conditions similar high with OA_72h_Ctrl giving with 210 highest counts. PA_72h_Ctrl samples have 185 and Ctrl_72h_Ctrl ~175 mean normalized counts. Mean count numbers of the adapter protein TRAM however show similarly high values for PA_72h_Ctrl and OA_72h_Ctrl with ~1.970 and ~1.940, respectively. The Ctrl_72h_Ctrl samples have lower mean counts of 1.630 for TRAM. In case of CCL5 expression, levels go down after the wash-out period and also lie very close together with OA_72h_Ctrl giving highest with 70 counts and PA_72h_Ctrl and Ctrl_72h_Ctrl lying slightly lower with 57 and 58 counts, respectively.

As seen for MyD88 dependent gene counts, normalized count numbers of the Ctrl_Ctrl_20h_Ctrl samples equal the mean count number of wash-out samples after 96 hours of culturing in each of the gene counts.

The samples finally stimulated with LPS for 20 hours, in contrast, all show increased count numbers for TRIF and CCL5 expression, compared to the other time points. Mean count numbers for TRIF equal each other and all lie around 410 counts. This trend can also be seen for the expression of the adapter protein gene TRAM. Normalized count numbers are with ~2.375 counts highest in OA_Ctrl_20h_LPS samples. Ctrl_Ctrl_20h_LPS samples show with ~2.320 counts a similar mean value. PA_Ctrl_20h_LPS shows lowest mean expression values with 2.210 counts.

Interestingly, CCL5 expression shows the lowest mean count number of ~ 3.230 in PA_Ctrl_20h_LPS while mean counts in OA_Ctrl_20h_LPS and Ctrl_Ctrl_20h_LPS both lie around 7.900 counts.

As seen before, with increasing count numbers huge deviations between the single donors can be observed. This is typical for human samples as different genetic background and environmental conditions impact the cells.

Another network was constructed to examine NLRP3-inflammasome activation for each tested condition at each time point of investigation. The network was constructed of twelve genes that are part of NLRP3-inflammasome activation and resulting IL18 or IL1B expression. In Biolayout 3D a Pearson's correlation coefficient cutoff of 0.73 was taken to keep high correlation between the conditions. The network was build-on 12 nodes and 12 edges. Up- and down-regulated DE-genes are visualized by the color-coding of the group fold change (GFC) of the respective condition, taking the complete dataset into account. Color coding was done as usual indicating the expression compared to the overall expressed mean at each time point of investigation from an expression table processed for the complete dataset.

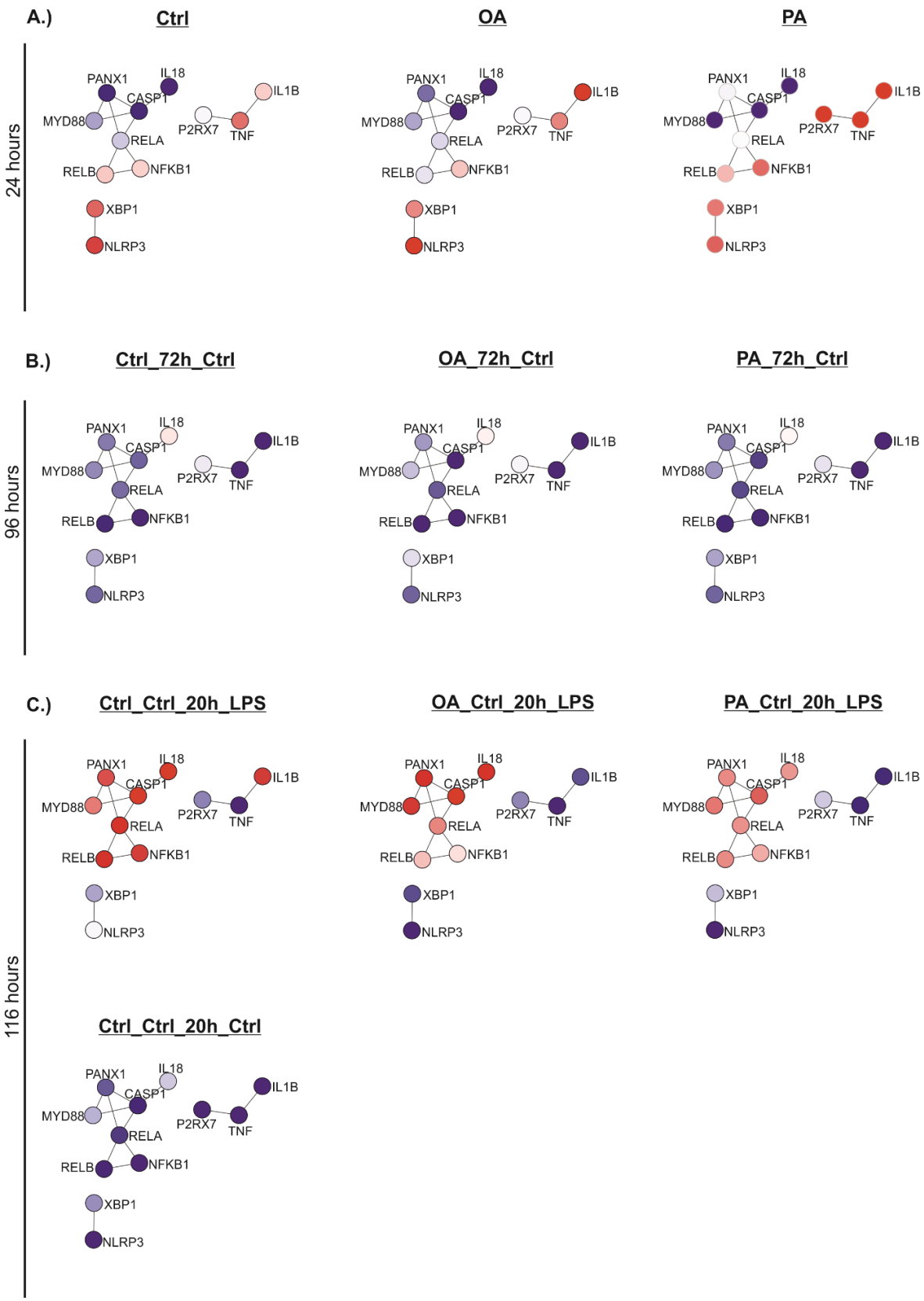

Figure 5.8.1.5: NLRP3-Inflammasome activation network. Visualization of co-expressed genes in saturated and unsaturated fatty acid pre-primed monocytes, followed by a 72 hours wash-out period and finally a 20 hours LPS stimulation. Pictured are differences in expression relative to the overall mean of the samples taken at the same time point. This is indicated by the color coding of the respective nodes. The Pearson's correlation coefficient cutoff was set to 0.73. The Network consists of 12 nodes and 12 edges (n=3).

The NLRP3 inflammasome is an important innate immune pathway that regulates at least two host responses to protect against infections. One is the secretion of the pro-inflammatory cytokines IL-1β and IL-18 and the other one the induction of pyroptosis of infected cells.[201] NLRP3 inflammasome activation is also involved in many obesity-associated diseases, such as T2DM, atherosclerosis, and gouty arthritis, through its ability to induce IL-1β release. The molecular link between obesity and inflammasome activation is still unclear, but free fatty acids have been proposed as one triggering event.[65] Here, I analyzed NLRP3-inflammasome activation in respect to IL1-β and IL-18 expression using a network applied to the complete experimental dataset, setting expression values in relation to each other. TLR4, MyD88 and REL-like domain containing proteins (RELA, RELB and NFKB1) for NF-κB activation were integrated into the network to allow evaluation of direct involvement in NLRP3 activation. NLRP3 activation involves the formation of a multiprotein scaffold complex, including NLRP3 and caspase-1, which is required for caspase-1 activation and subsequent cleavage and release of mature IL-1β and IL-18. In primary macrophages, potassium ion flux and the membrane channel pannexin 1 (PANX1) have also been suggested to play roles in inflammasome activation, therefore mentioned gene transcripts were integrated.[202]

The NLRP3 inflammasome plays an important role in the cellular defense against invading pathogens and is also reported to be expressed in macrophages facing free saturated fatty acids. To determine if this holds true for our conditions and whether the toll-like receptor 4 (TLR4), myeloid differentiating factor 88 (MyD88), or nuclear factor-kappa B (NF-κB) pathways are involved in the regulation of NLRP3 expression upon PA stimulation a network visualizing corresponding expression patterns is shown in **Figure 5.8.1.5**.

After 24 hours of culturing event in the 24h_Ctrl samples the expression of NLRP3 and XBP1 is markedly up-regulated. Also, expression of TNF and IL1B as well as RELB and NFKB1 are slightly up-regulated. The expression patterns of 24h_OA stimulated monocyte-derived cells looks very similar to the control patterns, however with a much stronger expression of IL1B and downregulation of RELB. After 24 hours of PA treatment, cells strongly express R2RX7, TNF and IL1B. RELB is comparably up-regulated as in 24h_Ctrl samples and NFKB1 is stronger expressed while NLRP3 is up-regulated to a lesser degree. In all the conditions we also see an upregulation of

NF-κB-complex genes. In 24h_PA and 24h_Ctrl cultures RELB and NFKB1 and in 24 hours OA samples only NFKB1 is up-regulated, indicating hetero- and homodimer complex formation for NF-κB activation, respectively. However, caspase 1 expression is strongly down-regulated in all conditions. One explanation would be that the NLRP3-inflammasome was not activated and no mature IL-1β proteins could be formed.
After the wash-out period the expression patterns of network genes of each of the conditions appear similar. As visualized in **Figure 5.8.1.5 B.)** besides IL18, which is rather neutrally expressed, all other network genes are down-regulated to a similar extend.
After final LPS stimulation (**Figure 5.8.1.5 C.)**) the Ctrl_Ctrl_20h_LPS control shows high expression of RELA, RELB and NFKB1 as well as moderate up-regulation of MYD88 and high up-regulation of PANX1, CASP1, IL18 and IL1B genes. NLRP3 is neutrally expressed. In OA_Ctrl_20h_LPS samples RELA, RELB and NFKB1 are moderately and MYD88, PANX1, CASP1, IL18 are highly expressed, while IL1B and NLRP3 genes are down-regulated. The PA_Ctrl_20h_LPS samples show moderate up-regulation of RELA, RELB, NFKB1 PANX1, CASP1, IL18 genes with CASP1 showing strongest expression. Here, IL1B and NLRP3 are strongly down-regulated. In the Ctrl_Ctrl_20h_Ctrl all network genes are down-regulated when compared to the group mean of all 116 hours samples. IL1B expression is an LPS-specific response which seems to be inhibited by fatty acid priming whereby the effect of OA and PA priming on monocyte-derived cells seems to be equally strong. The expression patterns of the NLRP3-inflammasome network again indicates that monocyte-derived cell exposure to dietary fatty acids renders the fate of the cells and has a lasting influence on expression patterns in response to later infection.

Venn diagrams showing the number of overlapping DE-genes of different treatments and time points, are visualized in **Figure 5.8.1.6**. DE-genes (see description **Figure 5.8.1.6**) were defined by comparisons with the respective time-point control. Normalization and determination of DE-genes was done for all time points separately, as described before (see section **5.4.1 – 5.4.3**).

A.) **OA-Primed Cells:**

B.) **PA-Primed Cells:**

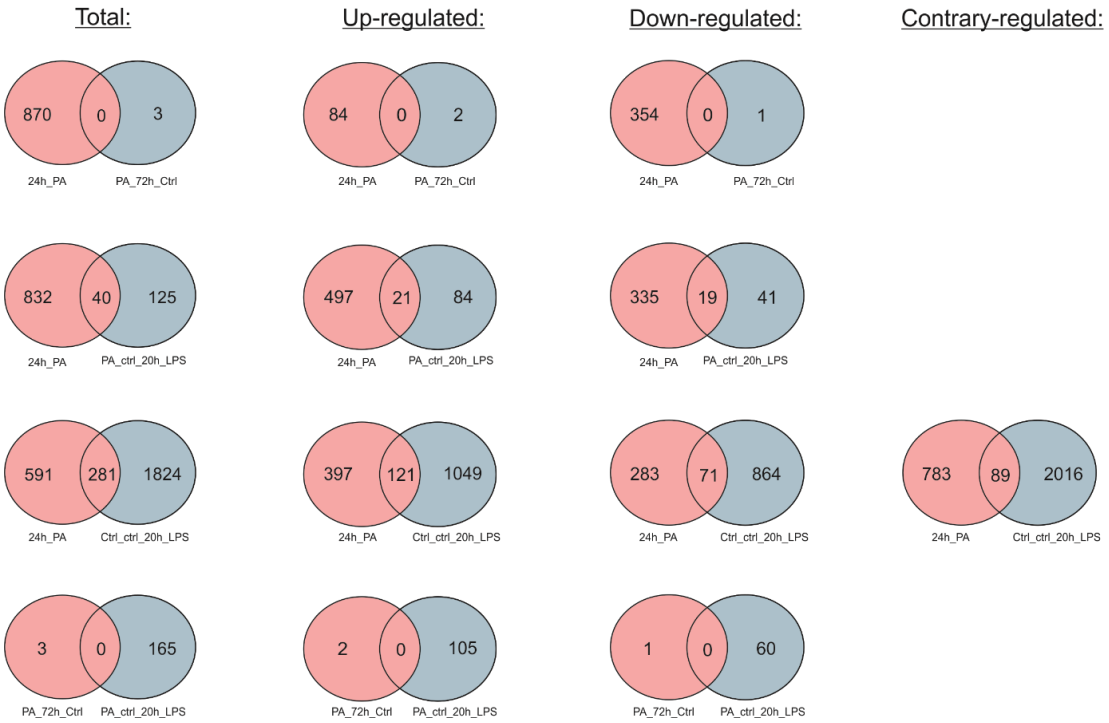

Figure 5.8.1.6: Comparison of overlapping differentially expressed genes at different time points between cells with the same priming condition. A.) Overlap of DE-genes between 24 hours OA stimulated cells and OA_72h_ctrl or OA_ctrl_20h_LPS stimulated cells, respectively. B.) Overlap of DE-genes between 24 hours PA stimulated cells and PA_72h_ctrl or PA_ctrl_20h_LPS stimulated cells, respectively. Differentially expressed genes (24 hours samples: FC ≥ 2 or ≤ -2; p-value ≤ 0.1 with FDR // 72 hours samples: FC ≥ 1.5 or ≤ -1.5; p-value ≤ 0.1 with FDR // 116 hours samples: FC ≥ 1.5 or ≤ -1.5; p-value ≤ 0.05 with FDR).

As can be seen from **Figure 5.8.1.6 A.)**, in expression patterns of oleic acid pre-stimulated cells, there is not much overlap in DE-genes when comparing 24 hours, 96 hours and 116 hours OA-primed samples with each other. In 24h_OA and OA_72h_Ctrl no gene overlaps. In 24h_OA and OA_Ctrl_20h_LPS two DE genes overlap, however, only one is expressed in the same direction. Again, no DE-gene overlaps in OA_72h_Ctrl versus OA_Ctrl_20h_LPS. When comparing 24h_OA DE-genes with Ctrl_Ctrl_20h_LPS DE-genes we find an overlap of 25 genes, however not all of them are regulated in the same direction. Eight up-regulated genes do overlap, while five overlapping genes are down-regulated in both samples. Further twelve DE-genes are overlapping but are up-regulated in the one and down-regulated in the other condition.

In case of PA-primed samples (**Figure 5.8.1.6 B.)**), in total a much greater overlap of DE-genes in the different conditions could be determined. For 24h_PA versus PA_72h_Ctrl no DE-gene overlaps, however, 40 DE-genes are overlapping between 24h_PA and PA_Ctrl_20h_LPS. They are all regulated in the same direction, namely 21 are up- and 19 down-regulated. Conspicuously even 281 DE-genes are overlapping between 24h_PA and Ctrl_Ctrl_20h_LPS. 192 DE-genes, of which 121 are up-regulated and 71 are down-regulated, are regulated in the same direction. The remaining 89 DE-genes are regulated in contrary directions. PA_72h_Ctrl and PA_Ctrl_20h_LPS do not overlap in their DE-gene patterns.

5.8.2 Enzyme linked immunosorbent assay (ELISA) for determination of secreted TNF and IL-6 levels and expression data evaluation

TNF and IL-6 ELISA-tests were performed on culture media of all conditions and at each intermediate time point of the trained immunity experiment (in collaboration with L. Joosten, Radboud University, Nijmegen).

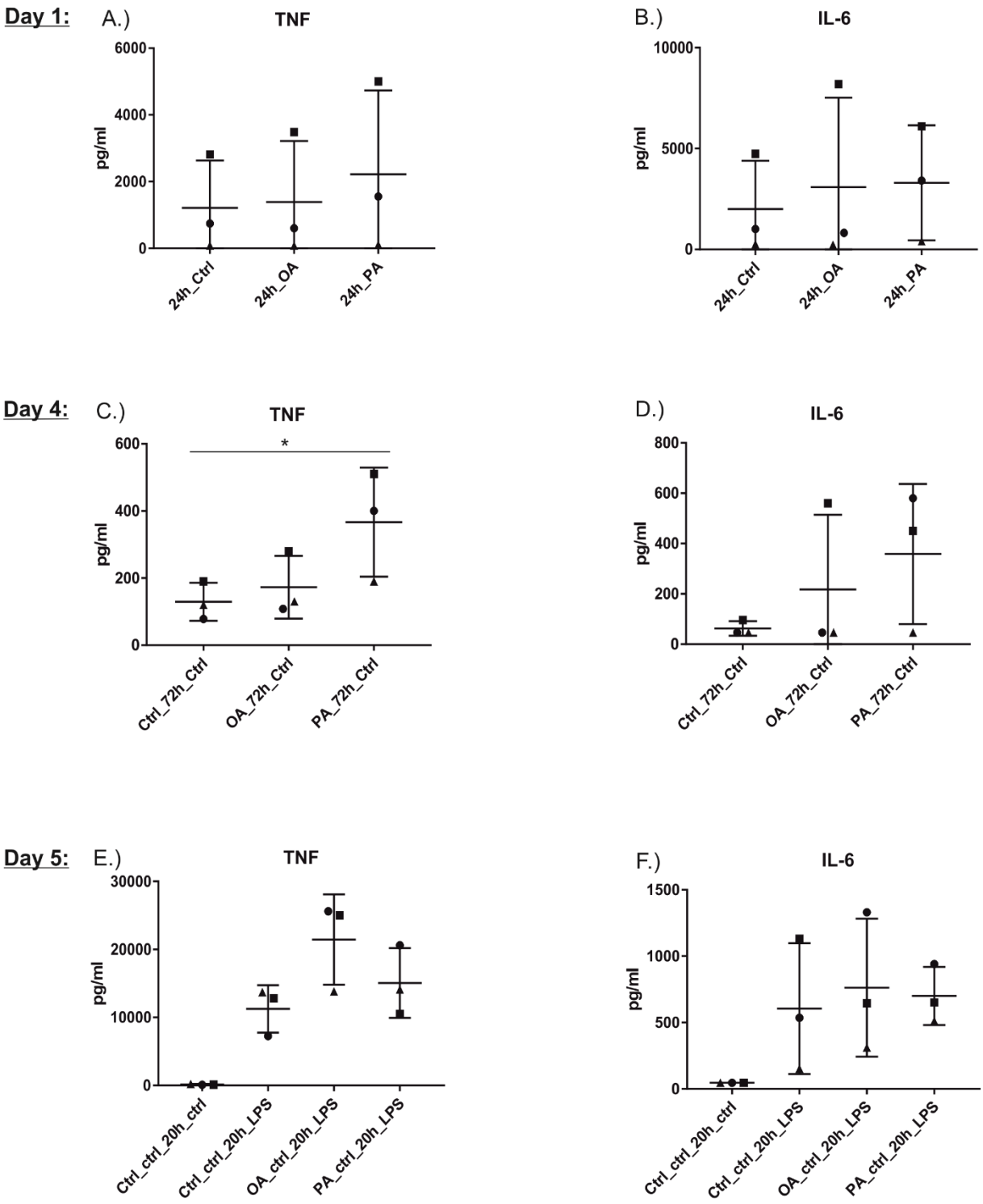

Figure 5.8.2.1: Oleic acid and palmitic acid induced trained immunity in monocyte-derived cells upon re-stimulation with LPS. Supernatants from each culture condition and time point was taken for TNF and IL-6 enzyme-linked-immunosorbent-assays A.) TNF-ELISA-data of 24 hours samples. The data have a p-value of 0.1830 and are statistically not significant. B.) IL6-ELISA-data of 24 hours samples. The data have a p-value of 0.5135 and are statistically not significant. C.) TNF-ELISA-data of 96 hours samples. The data are significant with a p-value of 0.0422. D.) IL6-ELISA-data of 96 hours samples. The data have a p-value of 0.3278 and are statistically not significant. E.) TNF-ELISA-data of 116 hours samples. The data are significant with a p-value of 0.0101 F.) IL6-ELISA-data of 116 hours samples. Ordinary one-way ANOVA was used for significance measurements. The data have a p-value of 0.1201and are statistically not significant. ▲ – Donor 1; ● – Donor 2; ■ – Donor 3.

Investigating **Figure 5.8.2.1**, it gets visible that the tendency of mean TNF and IL-6 concentrations in media of the same condition is of similar strength after 24 hours and 96 hours of culturing. After 24 hours of culture (**Figure 5.8.2.1 A.)** & **B.)**), cells treated with palmitic acid produce by far more TNF and IL-6 as the 24h_Ctrl cultures when investigating mean concentrations. However, the TNF ELISA-values of 24h_OA cultures only slightly exceed the concentrations found in 24h_Ctrl medium, while mean IL-6 concentrations are similar to those found after 24 hours in culture medium of 24h_PA stimulated cells. At day 4 (**Figure 5.8.2.1 C.)** & **D.)**) the same trend is observed, however, the mean IL-6 concentrations found in the culture media are more than ten times less as those observed at day 1. Also, the detected TNF concentrations are at least five times reduced after the wash out period. Interestingly, at day 5, the previously described expression trend changed, inducing highest TNF (~21.466 pg/ml) and IL-6 (~760 pg/ml) secretion by OA-primed cells after LPS stimulation. However, PA-primed cells still secrete more TNF and IL-6 after PA_Ctrl_20h_LPS stimulation as Ctrl_Ctrl_20h_LPS, with ~15.000 versus ~12.000 pg/ml TNF and 605 versus 700 pg/ml IL-6, respectively (**Figure 5.8.2.1 E.)** & **F.)**).

Conspicuously, the different donors react at all time points with totally different concentrations of secreted TNF and IL-6. Thereby the donors described by the triangle and the circle (Donor 1 and 2, respectively) lie in the majority of cases much closer together in the amounts of secretions. Hereby, it hast to be recognized that Donor 3 (rectangle) has with 25.2 kg/m^2 the highest BMI and by definition is overweight.

Statistical significance could only be determined for TNF measurements at day 4 and day 5. For statistically relevant results, more samples should be taken in account.

Also, gene expression data of TNF and IL-6 were visualized as count number graphs. Comparing TNF/IL-6 ELISA and expression data, it is visible that these in some conditions differ from each other when correlated. Expression data were taken from expression tables processed for each single time point of investigation, namely 24 hours, 96 hours and 116 hours, respectively, separately (**Figure 5.8.2.2**).

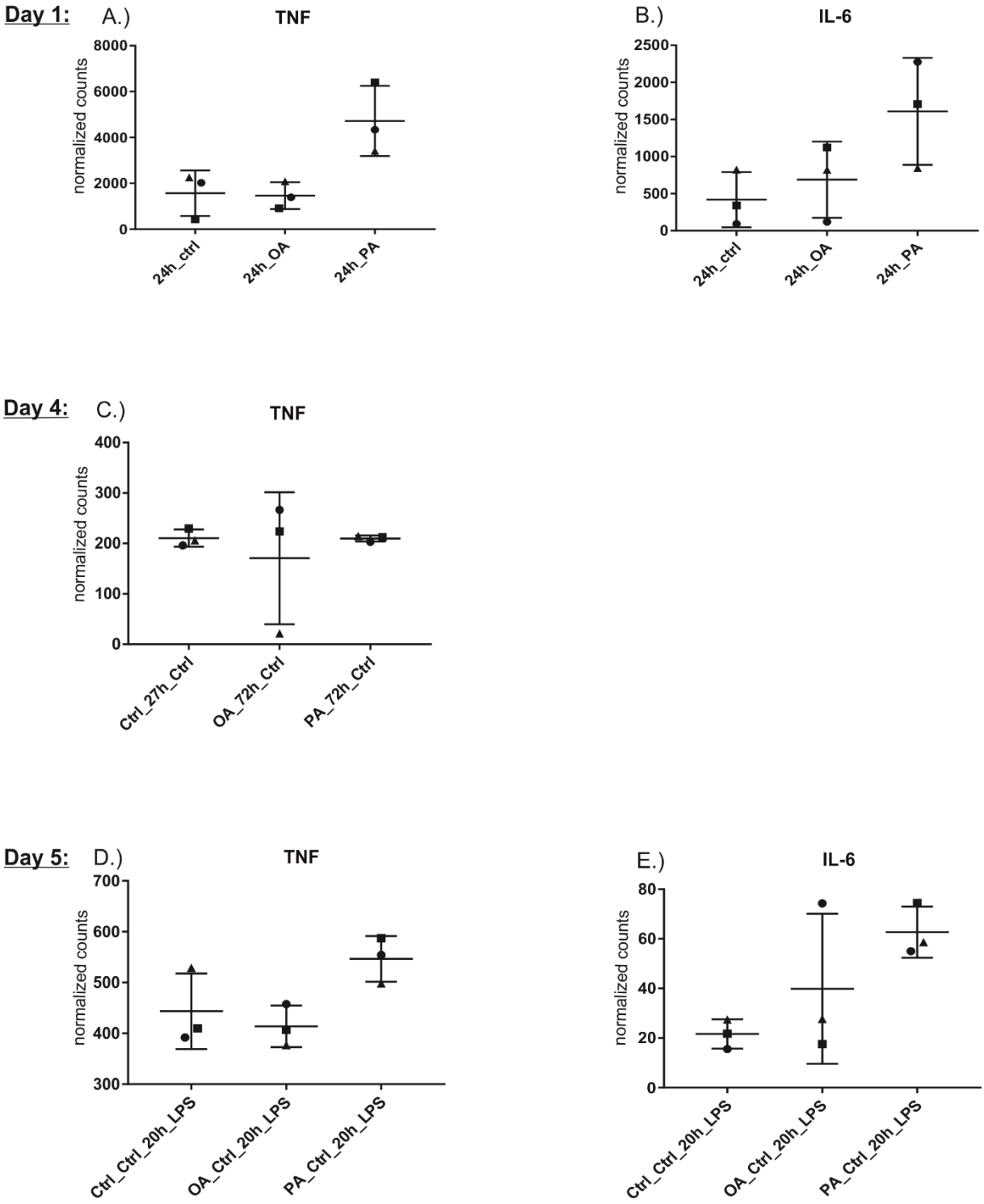

Figure 5.8.2.2: Expression count analysis for identification of oleic acid and palmitic acid induced trained immunity in monocyte-derived cells upon re-stimulation with LPS. Expression values of each condition and time point was taken for TNF and IL-6 expression analysis A.) TNF-expression-data of 24 hours samples. The data have a p-value of 0,1380and are statistically not significant. B.) IL6-expression-data of 24 hours samples. The data have a p-value of 0,2251 and are statistically not significant. C.) TNF-expression-data of 96 hours samples. The data are significant with a p-value of 0,6618. D.) TNF-expression-data of 116 hours samples. The data are significant with a p-value of 0,2006 E.) IL6-expression-data of 116 hours samples.
The data have a p-value of 0.2352 and are statistically not significant. For each graph ordinary one-way ANOVA was used for significance measurements. ▲ – Donor 1; ● – Donor 2; ■ – Donor 3.

Expressed TNF and IL-6 mRNA counts of 24 hours samples in total are quite high compared to the other visualized time points. For TNF we got similar high expression counts in 24h_Ctrl and 24h_OA samples, while mean TNF expression in 24h_PA samples is with ~ 5.000 counts more than two times higher. Mean IL-6 expression counts of 24h_PA samples are with ~1.700 counts also highest. The 24h_Ctrl samples have in mean just ~400 counts and 24h_OA samples approximately 750 counts. In the 24 hours stimulations, we see a big variance in expression values between the donors under same conditions.

In the 96 hours samples dataset, only expression values for TNF could be determined. After wash-out of the stimuli expression values decreased to less than 350 counts. Here, we found similar expression levels in Ctrl_72h_Ctrl and PA_72h_Ctrl cultures The different donors of Ctrl_72h_Ctr and PA_72h_Ctr samples react also very similar, while in case of OA_72h_Ctr Donor 1 shows only a very low number of read counts and Donor 2 reacts with a higher number of TNF counts compared to the other stimulations. Thus, the mean expression of TNF in OA_72h_Ctrl samples is lower as in PA_72h_Ctr and Ctrl_72h_Ctr. Interestingly, huge variance in expression values between the donors is just seen in OA_72h_Ctrl.

After LPS stimulation in the 116 hours dataset, TNF and IL-6 expression compared to 24 hours samples is also much decreased. Here, TNF lies in the range of less than 600 counts and IL-6 goes even down to less than 80 counts.

For both cytokines PA_Ctrl_20h_LPS samples show highest count numbers with ~550 counts for TNF and ~70 counts for IL-6. Mean TNF values of OA_Ctrl_20h_LPS samples lie even below those of Ctrl_Ctrl_20h_LPS samples with 400 and 450 counts, respectively. In case of IL-6 mean expression values of OA_Ctrl_20h_LPS samples lie around 40 and those of Ctrl_Ctrl_20h_LPS around 25 counts. Here it has to be considered that high variance between the donors can be seen in OA_Ctrl_20h_LPS samples with Donor 2 showing a much higher count number as the other two donors.

6. Discussion

Cardiovascular disease (CVD) is the number one cause of death and disability worldwide[203]. Poor diet, moreover, is a leading risk factor for CVD[203,204]. Therefore, dietary improvements have the potential to significantly reduce the prevalence of CVD[205].

In this study I investigated the effect of diet induced regulation and activation of human monocyte-derived cells. Thereby I focused on the influence of the saturated and the unsaturated fatty acids PA and OA, as representatives of Western and Mediterranean diet, on the activation and transcriptomic regulation of monocyte-derived cells. Further, the influence of the representative dietary fatty acids OA and PA, in terms of training and tolerance, upon later re-stimulation with LPS was validated.

To set up experimental conditions, fatty acid solubility, direct inflammatory response to OA and PA, M-CSF and GM-CSF supplementation as well as cell survival over time was investigated and conditions were optimized. I decided to isolate monocytes from healthy male donors by negative depletion to avoid cell activation by anti-CD14 antibody binding. To keep possible influencing factors low, the ethanol content, necessary to solubilize FFAs, was reduced to a minimum of 0.4 % in the final medium and GM-CSF concentrations were kept as low as possible for suitable cell survival.

The final experiment was set up with highly pure, freshly isolated human monocytes of healthy male donors.

6.1 Transcript analysis of monocytes after 24 hours training

Monocytes circulate in the bloodstream for up to 5 days. Alongside, immunological imprinting of either immunosuppression or innate immune memory determines the functional fate of monocytes and monocyte-derived cells.[206]

In this part of the study we addressed the question which direct effect the saturated fatty acid palmitic acid and the unsaturated fatty acid oleic acid have on monocytes after 24 hours of culturing. I analyzed their direct effects on monocyte polarization and differentiation.

The PCA, visualizing transcriptomic differences between monocytes cultured for 24 hours in either OA, PA or control medium shows that both, OA and PA, have a direct

effect on the transcriptome of tested cells which separate in clearly defined clusters. The Hierarchical Clustering of the 1000 most variable genes as well as DE-gene analysis demonstrate however, that the transcriptomic differences between 24h_PA treated and control cells is much higher as for 24h_OA treated and control cells. In fact, transcriptional analysis of 24h_OA stimulated monocytes and 24h_Ctrl cells just gives rise to 61 DE-genes. Up-regulated DE-genes in 24h_OA samples play a role in long-chain fatty acid transport and the activation of lipid metabolic processes. An anti-inflammatory effect of OA on monocyte-derived cells was ascertained from KEGG enrichment analysis. Here, 'PPAR signaling pathway' was the term appearing with most gene counts and highest significance. Peroxisome proliferator-activated receptors (PPARs) are nuclear hormone receptors that are activated by fatty acids and their derivatives. PPARs bind fatty acids and eicosanoids. There are three subtypes of PPARs, namely PPAR-α, -β/δ, and -ɤ, whereby PPAR-α plays a role in the clearance of circulating or cellular lipids via the regulation of gene expression involved in lipid metabolism in liver and skeletal muscle. PPAR-β/δ is involved in lipid oxidation and cell proliferation and PPAR-ɤ promotes adipocyte differentiation to enhance blood glucose uptake[207]. As described in the introduction, the PPAR-signaling pathway is associated with a M-IL4-like anti-inflammatory phenotype[148].

In contrast to 24h_OA stimulated monocytes, GOEA and KEGG pathway analysis of 24h_PA stimulated monocytes document that these cells highly express pro-inflammatory mediators and inflammatory response genes. These findings go in hand with prior literature, for instance explained by Palomer *et. al.*, 2018, who review mechanistic insights into the beneficial effects of oleic acid compared with palmitic acid on insulin resistance and T2DM, including its anti-inflammatory actions, and its capacity to inhibit endoplasmic reticulum (ER) stress[208].

In our experimental set up, a higher activation state of 24h_PA treated monocyte-derived cells is specified by GO-terms like 'regulation of MAPK cascade' and 'G-protein coupled receptor signaling cascade' as these processes are highly involved in myeloid cell differentiation and polarization, microbial elimination, inflammation and resolution, as well as in macrophage-mediated pathologies.[193,194]

The high number of overlapping DE-genes (192 genes) between 24h_PA stimulated and Ctrl_Ctrl_20h_LPS stimulated monocyte-derived cells as well as the GOEA of the

24h_PA samples, exhibiting the term ‘response to lipopolysaccharide’, code for the high inflammatory potential of PA. Preceding studies described already that PA has a similar effect on macrophage polarization as LPS. Thereby, it has been described that the signaling mechanism induced by SFAs is mediated by TLR4 activation.[60,209] TLR4 is the best characterized of all PRRs and the earliest evidence linking TLR4 to lipid-induced inflammation can be backdated to the time it was identified as receptor for LPS[210]. Osborn and Olefsky, 2012[211] hypothesized that long-chain SFAs are TLR4 agonists as the major constituent of LPS responsible for its immunostimulatory activity is the lipid A (LPA) region, which contains numerous saturated fatty acyl-chains that are required for binding to and activating TLR4. Lancaster *et al*., 2018, however demonstrated that the inflammatory fatty acid palmitate is actually not a direct TLR4 agonist but that long-chain SFA-induced inflammatory signaling is completely TLR4-dependent and that TLR4-dependent priming is necessary for long-chain SFAs to activate inflammatory signaling in macrophages. Though, TLR4 is required for palmitate-induced inflammation through TLR4-dependent priming and altered cellular metabolism.[212]

Underlining the hypothesis that SFAs do force the activation of TLR4, we could show that only 24h_PA stimulated monocytes activated almost all of the MyD88-dependent downstream genes (see **Figure 5.8.1.1 A.)**) while in 24h_OA and 24h_Ctrl cultures downstream genes were comparably down-regulated. These results were strengthened by corresponding MyD88, TIRAP and final IL1B and TNF expression data and by the evaluation of TNF ELISA data, which showed increased values in 24h_PA stimulated monocytes compared to 24h_OA and 24h_Ctrl monocyte-derived cells. In line with former publications, we can conclude that even if PA is not a direct TLR4 agonist, it forces the activation of MyD88-dependent TLR4 activation in monocyte-derived cells, which is not indicated by OA stimulations. TRIF-dependent TLR4 activation was in neither case exhibited since CCL5 expression was down-regulated and as low as in the control situation.

The NLRP3 inflammasome is an important innate immune pathway that regulates at least two host responses to protect against infections. One is the secretion of the pro-inflammatory cytokines IL-1β and IL-18 and the other one the induction of pyroptosis of infected cells.[201] The NLRP3 inflammasome is involved in many obesity-associated diseases, such as T2DM, atherosclerosis, and gouty arthritis, through its ability to

induce IL-1β release[213]. In this study we also could show that PA stimulation leads to over-expression of NLRP3 and IL1B in monocyte-derived cells. These findings fit very well to data from A. Christ *et. al*., 2018 who demonstrated that Western diet, high in SFAs, induced systemic inflammation, myeloid progenitor proliferation and re-programming in myeloid cells which again depended on NLRP3 inflammasome activation. They interpreted that NLRP3 mediates trained immunity following Western diet in myeloid cells of tested mice.[214] As previously stated, with our 24h_PA experiment we also could show that monocyte-derived cells stimulated with PA for 24 hours highly express NLRP3 and the inactive form of IL1β, but intense activation of the NLRP3 inflammasome was not indicated since the gene CASP1 coding for the IL1β activating enzyme caspase 1 was not notably upregulated.
Laurent L'homme *et. al.*, 2013 reported that UFAs like oleate and linoleate do not activate the NLRP3 inflammasome and instead rather reveal an anti-inflammatory property through preventing inflammasome activation by SFAs.[184] Unexpectedly, the NLRP3 network data of 24h_OA stimulated monocytes show also high expression of NLRP3 and IL1B, however, in line with published results, NLRP3-inflammasome activation was again not indicated since CASP1 expression was equally down-regulated as described for 24h_PA cultures. These results give space for speculations and indicate no necessary involvement of NLRP3 inflammasome activation in PA induced inflammatory signaling in monocyte-derived cells. The inclusion of secreted IL-1β values would now give the full picture and clear information about actual NLRP3-inflammasome activation.

The monocyte isolation procedure and transfer to culturing medium which induced stress signals to the cells may be an explanation for increased expression of NLRP3 components in all 24h conditions. TNF, which is secreted in high amounts in all 24h samples compared to 96h samples (see **Figure 5.8.2.1 A.) & C.)**) is described to be an important transcriptional regulator of NLRP3 inflammasome components in murine inflammasomopathies[215] and might also be the reason for over-expression of these components in all 24h cultured monocyte-derived cells.

In line with former publications, the complete expression data profile of 24h_OA cultures indicates that OA highly induces fatty acid metabolic processes in monocyte-derived cells, most pronounced in fatty acid oxidation, which drive the cells towards an anti-inflammatory M-IL4 like phenotype[208]. 24h_PA cultured monocyte-derived

cells in contrast developed into pro-inflammatory phenotypes, initiating innate immune responses similar to those described to be induced by LPS activated macrophages, while fatty acid metabolic processes seem to play a minor role. Surprisingly, the overall picture of the 24h_Ctrl cultures exhibited expression profiles of activated monocyte-derived cells with typical moDC characteristics (see **Figure 5.5.6.1 A.)** (CD207, CLEC4F, NDRG2)) while 24 hours fatty acid stimulations either indicated monocyte-derived cells with typical macrophage characteristics, however with divergent polarizations.

Interestingly, TREM2, a gene coding for a receptor protein which was found to be highly expressed on one of two atherosclerosis-specific macrophage populations described by Cochain *et. al.*, 2018, was up-regulated in 24h_OA stimulated monocytes[46]. Cochain *et. al.*, 2018 described that Trem2^{high} macrophages appear to be endowed with specialized functions in lipid metabolism and catabolism and presented a gene expression signature reminiscent of osteoclasts, suggesting a lesion calcification. Moreover, Trem2 expression was detected in human lesional macrophage populations which were also present in advanced stages of atherosclerosis.[46] These typical characteristics go in line with our findings of 24h_OA stimulated monocyte-derived cells.

That 24h_PA stimulated monocyte-derived cells evolved not only pro-inflammatory, but also pro-atherosclerotic characteristics is not surprising and either proposed by the overexpression of the ABC1A gene (**Figure 5.5.6.1**). The gene product of ABC1A has been described to promote cholesterol efflux to extracellular acceptors *in vitro* and *in vivo* (reverse cholesterol transport) and to influence atherosclerosis in mice[216].

A probable conclusion from these data would be that in atherosclerotic lesions either inflammatory and anti-inflammatory acting myeloid-derived cells do play a likewise important role, facilitating the simultaneous progression and resolution of atherosclerotic plaques. Atherosclerosis and Diabetes are diseases which stand in close proximity to overweight and excess saturated fatty acid consumption, thus it is not surprising that monocytes stimulated with high amounts of palmitic acid produce gene products that are crucial for such complications.

6.2 Transcript analysis of monocyte-derived cells after wash-out of the fatty acid stimuli

After activation of the innate immune system, innate immune cells may undergo long-term functional reprogramming.

Hence, we were questioning if either OA or PA can induce certain long-term changes in monocyte-derived cells, and if so, which changes are inherent to the condition?

Thereby, PCA and hierarchical clustering of the 1000 most variable genes show already a clear differentiation of monocyte-derived cells after medium exchange and 3 days of cultivation, resulting in similar transcriptomes of cells from PA_72h_Ctrl and Ctrl_72h_Ctrl cultures but clearly distinct transcriptomes of monocyte-derived cells from OA_72h_Ctrl cultures.

A first indication of cellular programs activated in monocyte-derived cells from OA_72h_Ctrl cultures are given by GO-term analysis of up-regulated DE-genes compared to Ctrl_72h_Ctrl cultures. This analysis revealed not only terms like ‘positive regulation of cell differentiation’, but also ‘long-chain fatty acid transport’ and ‘wound healing’. The longer inhabitation and metabolization of OA by monocyte-derived cells may thereby effectively drive the cells towards an anti-inflammatory M-IL4 like phenotype. This trend is further approved by GO-terms of down-regulated DE-genes which almost all describe mechanisms involved in phagocytic processes and adaptive immune cell activation.

The expression network (**Figure 5.6.6.1**), which visualizes the DE-genes with highest and lowest group fold change of all 96 hours sample comparisons, also shows a high coincidence of expressed genes in Ctrl_72h_Ctrl and PA_72h_Ctrl cultures.
Genes being neutrally expressed in Ctrl_72h_Ctrl cultures but slightly up-regulated in PA_72h_Ctrl code for instance for proteins involved in T-cell activation (e.g. HLA-DRA), in the Notch signaling pathway (APH1B), in the interleukin signaling pathway (e.g. IL11RA) and in inflammation mediated by chemokine and cytokine pathway (e.g. C3AR1), or in angiogenesis (e.g. PDGFC). These pathway involvements show that PA, although washed-out for three days, has a lasting albeit low pro-inflammatory and phagocytic effect on monocyte-derived cells.
Interestingly, the aberrations from transcriptomes of Ctrl_72h_Ctrl cells might in part be constituted in the repression of CENPW in PA_72h_Ctrl cells. CENPW is a gene

coding for a protein involved in ‘kinetochore organization’, ‘CENP-A containing nucleosome/chromatin assembly and organization’, ‘histone exchange’ and ‘chromatin remodeling’. CENPW is a component of the hetero-tetrameric CENP-T-W-S-X complex that binds and supercoils DNA, and plays an important role in kinetochore assembly and function. It is one of the inner kinetochore proteins, which is required for normal chromosome organization and normal progress through mitosis.[189,217,218] As CENPW binds specifically to histone H3-containing nucleosomes at the centromere, down-regulation of this gene-product may lead to less coiled chromatins and thus might indicate histone based epigenetic changes induced in PA_72h_Ctrl cultures that may not only have a direct effect on the transcriptome but also may prepare the cell for a faster reaction to emerging hazards. In line with this observation the deviation in expressed and secreted values of the inflammatory marker TNF and IL-6 (see **Figure 5.8.2.1** & **Figure 5.8.2.2**) may be considered. We see that cells of all wash-out samples transcribe similar mean amounts of TNF mRNA while the secreted fractions differ and are by far higher in PA_72h_Ctrl as in OA_72h_Ctrl and Ctrl_72h_Ctrl. Such aberrations might be explained by epigenetic modifications initiated by the priming condition leading to post transcriptional modifications and/or post-translational processing of important gene products like TNF. Such modifications have a huge impact on the fate of cells and expression values alone cannot reflect the actual state of a cell. Further, down-regulation of CENPW indicates that PA_72h_Ctrl monocyte-derived cells proliferate less than Ctrl_72h_Ctrl cells.

Although there is no overlap of DE-genes from 24h_OA and OA_72h_Ctrl cultures, DE-gene analysis of OA_72h_Ctrl transcriptomes either show M-IL4 like anti-inflammatory cell differentiation. Up-regulated genes in OA_72h_Ctrl include several that participate in the Wnt-, in the TGF-β-, in the PPAR- as well as in the Rap1 signaling pathway. Wnt-signaling is involved in mechanisms of proliferation and differentiation and expression of Wnt ligands by macrophages has been associated with M-IL4-like anti-inflammatory phenotypes[219]. TGF-β signaling is also involved in controlling expression of genes characteristic for alternatively activated macrophages[220] and as described in the previous section, PPARs are nuclear hormone receptors that are activated by fatty acids and their derivatives and their signaling pathways are either associated with an M-IL4-like phenotype[148]. The Repressor activator protein 1 (Rap1) pathway is involved in signaling connected to metabolism and contributes to body

weight regulation[221]. However, in pro-inflammatory macrophages, Rap1 also promotes cytokine production via NF-κB activation favoring a pro-inflammatory environment which may contribute to the development and progression of atherosclerosis[222].

All these aspects together indicate that after OA seizure investigated OA_72h_Ctrl monocyte-derived cells further differentiated into an anti-inflammatory regeneration mode, still facing towards an M-IL4-like phenotype. On the other hand, the seizure of PA led to a large reduction of pro-inflammatory gene transcripts in PA_72h_Ctrl monocyte-derived cells which appear with a comparatively low-grade pro-inflammatory phenotype, with related expression profiles as seen in Ctrl_72h_Ctrl monocyte-derived cells. As mentioned before, transcriptomic data do not give the full picture of the cellular phenotype. Although expression data of OA_72h_Ctrl monocyte-derived cells indicate a more anti-inflammatory phenotype, either TNF as well as IL-6 ELISA-data show higher secretion of both inflammatory marker proteins than Ctrl_72h_Ctrl cells. Applying further techniques like ChIP-Nexon-seq., ATAC-seq. and a broader panel of secreted cytokines via ELISA would give us a closer view on the real state of the cells.

6.3 Transcript analysis of monocytes after training

In the past decade, myeloid and lymphoid lineage cells of the innate immune system have been shown to display long-term changes in their functional program through metabolic and epigenetic reprogramming in response to primary exposure to certain PAMPs or DAMPs[64,76,206]. Reprogramming causes these cells to be either hyperresponsive or hyporesponsive, resulting in a changed immune response to secondary stimuli. This innate immune memory, which has been termed ‘trained immunity’[206], may even be activated by dietary fatty acids. Recently, ‘trained immunity’ was confirmed *in vivo* in a murine model of western type diet,[214] where high fat diet induced persistent pro-inflammatory changes in bone marrow derived myeloid cells. These findings go in hand with the association of monocyte-derived macrophages of patients with established atherosclerosis, displaying a trained phenotype after *ex vivo* stimulation[223]. In serum of atherosclerosis animal models and in humans at cardiovascular risk, the presence of abnormal high levels of circulating aldosterone (hyperaldosteronism) is a common disorder[224]. Lately, cardiovascular researchers could show that aldosterone induces trained immunity *in vitro*, which is dependent on epigenetically mediated up-regulation of fatty acid synthesis. They demonstrated that

aldosterone promoted enrichment of the transcriptionally permissive H3K4me3 modification at promoters of genes central to the fatty acid synthesis pathway.[225]
These findings not only provide an explanation for the detrimental cardiovascular effects of aldosterone but also may hint to the regulation of diet induced dysregulations via ‘trained immunity’.

In this study we addressed the question if typical dietary fatty acids like the unsaturated fatty acid OA and the saturated fatty acid PA may reprogram monocyte-derived cells in a way making them hyper- or hyporesponsive to secondary infection with the bacterial endotoxin LPS.

That priming of monocytes with either OA or PA had a definite effect on the metabolic activity of monocyte-derived cells, even after wash-out, was already indicated from the previous section. Interestingly, PCA of cellular transcriptomes after secondary stimulation with LPS shows that both fatty acids provoke a changed immune response in monocyte-derived cells which leads to the activation of different transcriptional programs in response to LPS (**Figure 5.7.2.1 B.)**).

As shown by the Hierarchical Clustering of the 1000 most variable genes (**Figure 5.7.4.1 A.))**, taking the Ctrl_Ctrl_20h_Ctrl into account, the overall response to LPS is really strong and a high number of response transcripts do overlap between the conditions. Investigating however the 1000 most variable genes between the conditions re-stimulated with LPS (**Figure 5.7.4.1 B.)**), it is visible that depending on the priming condition absolutely varying transcriptional programs are displayed.
Having this awareness, I now focused on the metabolic differences that were traceable due to priming with the different dietary fatty acids.
On transcriptomic basis it is indicated that OA priming induces long lasting fatty acid metabolic processes which even show dominance after LPS stimulation (see **Figure 5.7.5.1 & Figure 5.7.5.2)**. These lipid metabolic processes are strongly linked to an anti-inflammatory M-IL4 like phenotype in macrophages[226] which are comparably down-regulated in PA_Ctrl_20h_LPS monocyte-derived cells.
However, compared to Ctrl_Ctrl_20h_LPS stimulated monocyte-derived cells several transcripts whose products are involved in pro-inflammatory processes are even down-regulated in PA_Ctrl_20h_LPS cultures. These processes are mainly involved in the activation of adaptive immune responses and are described by GO-terms like ‘antigen processing and presentation of peptide antigen via MHC class II’ and ‘positive

regulation of leukocyte activation' (see **Figure 5.7.5.1**). On the other hand, DE-genes that are up-regulated in PA_Ctrl_20h_LPS compared to the Ctrl_Ctrl_20h_LPS also code for proteins involved in 'complement activation, classical pathway' and 'humoral immune response mediated by circulating immunoglobulin'. Processes that are also highly pro-inflammatory. KEGG enrichment analysis replenished the listing of process involvement by 'focal adhesion', 'Rap1 signaling pathway' and 'aldosterone synthesis and secretion'. Thereby, focal adhesion describes the initiated cell migration along the connective endothelium following cellular signals to the infected biological tissue[227]. When Rap1 is released into the cytoplasm it induces the production of pro-inflammatory cytokines via NF-κB signaling in macrophages, which also stands in correlation with the development and progression of atherosclerotic lesions[222]. Further, 'aldosterone synthesis and secretion' was demonstrated to play a role in transcriptomes of PA_Ctrl_20h_LPS compared to Ctrl_Ctrl_20h_LPS stimulated monocyte-derived cells. This correlation may indicate a connection between PA- and aldosterone- induced, and FAS inherent 'trained immunity' in monocyte-derived cells.

Another explanation for the activation of different pro-inflammatory response mechanisms in Ctrl_Ctrl_20h_LPS and PA_Ctrl_20h_LPS cultures may be the cellular differentiation state. That CD1E and CST7 (see **Figure 5.7.4.2** & **Figure 5.7.6.1**) are up-regulated in Ctrl_Ctrl_20h_LPS compared to PA_Ctrl_20h_LPS and OA_Ctrl_20h_LPS cultures indicates that these cells differentiated into moDCs[197,228], while PA_Ctrl_20h_LPS and OA_Ctrl_20h_LPS stimulated monocytes rather appeared to differentiate into monocyte-derived macrophages with a reverse activation state.

However, as at least 37 DE-genes do overlap in OA_Ctrl_20h_LPS and PA_Ctrl_20h_LPS, some fatty acid induced LPS specific cellular programs do also overlap in these monocyte-derived cell populations. Of the overlapping up-regulated genes among others, some count for pro- and others for anti-inflammatory products. The gene-product of FAIM213B for example is a negative regulator of macrophage mediated inflammation by inhibition of inflammatory cytokine production, probably by suppression of the MAPK signaling pathway[188]. However, the gene product of MAP4K2, which is also up-regulated in both conditions, has been shown to specifically activate MAP-kinases[188], describing the tightly regulated response of monocyte-derived cells to danger signals like LPS.

Taking the specifically regulated transcripts of the typical and unique LPS response of Ctrl_Ctrl_20h_LPS, OA_Ctrl_20h_LPS and PA_Ctrl_20h_LPS, visualized in the Co-expression network (**Figure 5.7.6.1**), into account, it gets clear that cells of the myeloid lineage are never fully pro- or anti-inflammatory and depending on training and differentiation state can display a number of different programs in response to a particular danger signal.

In case of OA_Ctrl_20h_LPS stimulated monocyte-derived cells, genes that are specifically up-regulated include such that code for proteins involved in different actions of the innate immune response and inflammation (PGD2, HPGD, SYNGR1, CLEC1A, FN1, AIM2, TNFSF8), as well as in the negative regulation of macrophage mediated inflammation (FAM213A and CD300A). As previously mentioned, also genes coding for proteins involved in lipoprotein metabolism, including APOC1 and APOC2 are overexpressed. In 2010, scientists showed that APOC1 is not only involved in lipoprotein metabolism but also strongly binds to LPS, and thereby enhances the LPS-induced TNF-α response *in vitro* (RAW 264.7 macrophages) and *in vivo* (C57Bl/6 mice). *In vitro* studies showed additionally that the stimulating effect of APOC1 on the LPS response resembles that of LPS-binding protein and depends on CD14/TLR-4 signaling.[229,230] On transcriptomic level OA_Ctrl_20h_LPS monocyte-derived cells, seemed rather to balance the inflammatory response to LPS by their anti-inflammatory potential, compared to PA_Ctrl_20h_LPS. TNF and IL-6 ELISA data however, gave another picture. Secreted levels of these factors where highest in OA_Ctrl_20h_LPS cultures. This phenomenon of 'training' might go inherent with the lipid metabolic processes, induced by OA priming, which not only drive monocyte-derived cells into a M-IL4 like phenotype but also with involvement of APOC1, induce hyperresponsiveness to LPS by activation of TRIF-dependent TLR4 signaling (see **Figure 5.8.1.3 C.)**).

In PA_Ctrl_20h_LPS samples up-regulated network genes also include not only products that count for pro-inflammatory mediators but also such that are involved in suppression of extensive immune-system activation, like CD101 and LRRC32. These gene products play specific roles in inhibition of adaptive immune cell proliferation and regulatory T-cell activation[231,232]. In this stimulation situation also survival signals are pronounced, which might be the explanation for the increased survival of present cells in PA_Ctrl_20h_LPS samples (see **Figure 5.4.1.5**) compared to the other conditions.

Although also in this condition several inflammation counter acting proteins are transcribed, after LPS stimulation mean TNF and IL-6 ELISA data are higher as in the Ctrl_Ctrl_20h_LPS situation even though co-expression networks indicate strong activation of either MyD88- and TRIF-dependent TLR4 activation as well as high expression of NLRP3 inflammasome components like IL-18, IL1B and Casp1 in this condition. In line with that, investigating the involvement of products of specifically up-regulated genes in Ctrl_Ctrl_20h_LPS (**Figure 5.7.6.1 A.)**), we see a strong involvement in 'complement activation', in the 'inflammatory response to LPS' and in the 'stress response' of myeloid-derive cells. Surprisingly, overexpressed genes code also for proteins involved in macrophage differentiation and in activation (CREB5) or co-repression (LOXL2) of transcription. LOXL2 thereby mediates the post-translational oxidative deamination of lysine residues on target proteins leading to the formation of deaminated lysine. It specifically mediates deamination of trimethylated Lys-4 of histone H3 (H3K4me3), a specific tag for epigenetic transcriptional activation. Since LOXL2 removes an active epigenetic mark it generally acts as a transcriptional repressor.[233] The here explained repressor function might somehow be responsible for the comparably low mean secretion of TNF and IL-6 in Ctrl_Ctrl_20h_LPS cultures, markers used to measure 'trained immunity' by TLR ligands like LPS as second stimuli.[77] The established histone ChIP-Nexon technique would now be a reasonable choice to analyze which genes are specifically co-repressed in this condition, especially as in Ctrl_Ctrl_20h_LPS cultures either MyD88- and TRIF-dependent TLR4 activation was specified and most pronounced under the conditions.

The comparatively reduced MyD88- and TRIF-dependent TLR4 activation in PA_Ctrl_20h_LPS and reduced MyD88-dependent TLR4 activation in OA_Ctrl_20h_LPS cultures upon LPS stimulation is contradictory to the higher secretion of TNF and IL-6. However, the gene product of MAP4K2, which is up-regulated in both conditions, has been shown to specifically activate MAP-kinases[189], describing the tightly regulated response of monocyte-derived cells to danger signals like LPS. The MAPK pathway has a vital function in TLR4 signaling and subsequently the production of pro-inflammatory mediators[234].

The NLRP3 inflammasome network (see **Figure 5.8.1.5**), either indicated highest activation state under Ctrl_Ctrl_20h_LPS conditions with high Casp1, IL18, IL1B and neutral NLRP3 expression. In case of OA_Ctrl_20h_LPS and PA_Ctrl_20h_LPS

Casp1 and IL18 were also highly expressed, however, the expression of IL1B and NLRP3 was intensely down-regulated. IL1B expression is an LPS specific response which seems to be down-regulated due to fatty acid priming whereby the effect of OA and PA priming, in respect to this observation, seems to be similar strong. The expression patterns of the NLRP3-inflammasome network again indicate that monocyte-derived cell exposure to dietary fatty acids renders the fate of the cells and has a lasting influence on expression patterns, especially in response to secondary stimulation with LPS.

In studies with human samples it has always to be considered that cells of different donors can react totally different, with different strength and even with completely divergent specificity to one and the same factor. We could see this in both, ELISA and expression data although we equalized gender and approximated BMI and age of the donators. Due to differences in genetic background, environmental and nutritional influences, as well as activity state of the donors, totally different peculiarities are expectable. We all are unique, so are our cells.

Although from this study we got an idea of which effects are to expect in sense of monocyte training by oleic and palmitic acid, respectively, for a statistically more relevant evaluation of the training effect, a higher number of cell donators and epigenetic analysis techniques like ChIP-Nexon-seq. and ATAC-seq. would be reasonable for a next level study.

6.4 Resume

Over all it can be said, that exposure of monocytes to the dietary fatty acids OA and PA leads to differential activation of monocyte-derived cells towards a rather anti- or pro-inflammatory phenotype, respectively. After 24 hours of culturing expression and ELISA data led to the same interpretation. Here, gene expression data indicated that either 24h_Ctrl, 24h_OA and 24h_PA cultures differentiated into different phenotypes, with 24h_Ctrl cultures showing pro-inflammatory moDC characteristics, 24h_PA cultures showing pro-inflammatory characteristics, with attributes also described for macrophages found in atherosclerotic lesions, and 24h_OA cultures showing anti-inflammatory characteristics with a specific signature (TREM2) described to be significant for one specific population of atherosclerosis-specific macrophages[46]. In the onset of the training experiment expression and ELISA data partially facilitated divergent interpretations which give rise to post transcriptional modifications of evaluated mRNA contents or post-translational processing of resulting protein contents, which might also be initiated by epigenetic modifications of regulatory genes. Also, deviating long-term effects due to OA and PA priming could be achieved, especially when taking the LPS response into account. Here, expression data strongly suggest the initiation of ‘immunological tolerance’ in OA pre-stimulated cultures, while TNF and IL-6 ELISA-data strongly indicate a ‘training’ effect in this condition. In PA_Ctrl_20h_LPS cultures a ‘training’ effect is even indicated by TNF and IL-6 ELISA-data, compared to the Ctrl_Ctrl_20h_LPS, however to a lesser extend as shown for OA_Ctrl_20h_LPS cultures. As ‘trained immunity’ is till now only defined by TNF and IL-6 secretion levels, we could clearly show a training effect induced by both fatty acids, however, with a stronger effect induced by OA priming. It seems logical, that in humans that privilege a healthy, Mediterranean diet PAMP’s are faster resolved, due to a stronger and faster response to the infecting agent as in people who stress their immune cells continuously by diets rich in SFA. However, with this theory the stronger TNF and IL-6 response to LPS due to FA priming compared to Ctrl_Ctrl_20h_LPS cannot be explained.

The given results might on the one hand be explained by divergent differentiation of monocytes due to the different priming conditions in the first 24 hours, giving rise to different monocyte-derived cell functions. On the other hand, epigenetic modifications of cellular chromatins are highly indicated by the described long-term effect of OA in OA_72h_Ctrl and OA_Ctrl_20h_LPS cultures. Another indication for epigenetic

modifications is the highly deviating LPS response of PA_Ctrl_20h_LPS and Ctrl_Ctrl_20h_LPS cells although for PA_72h_Ctrl and Ctrl_72h_Ctrl cultures only 3 DE-genes could be determined.

With this study we got already an idea of how monocyte-derived immune cells are poled due to the different dietary fatty acids they were exposed to. We could show which different cellular programs were displayed in PA and OA pre-treated cells in response to the danger signal LPS. In a next level study, insights into indicated epigenetic modifications in chromatins of tested cells could simply be deepened using the established ChIP-Nexon technique. In addition, open chromatin and transcription factor binding sites could be defined using ATAC-seq. The application of these novel techniques could help to better understand how dietary factors sustainably shape the fates of our immune cells and may even lead to the development of new atherosclerotic plaque resolving medications.

Acknowledgements

Foremost, I would like to express my sincere gratitude to my advisor Professor Dr. Joachim Schultze for the support of my Ph.D. study and research, and for his immense knowledge. His guidance helped me in the time of research and data analysis.

Besides my advisor, I would like to thank Professor Dr. Marc Beyer for his open ear and estimations in critical experimental questions.

I also want to thank Dr. Thomas Ulas, who introduced me to the first steps in RNA-seq.-analysis and supported me when I had a question.

Furthermore, I want to thank Dr. Anna Aschenbrenner for her competent support in the realization of several cell culture pre-experiments and her aid in upcoming scientific questions. Also, I want to thank Olympia Papantonopoulou and Dr. Anna Aschenbrenner for their help in the performance of the main free fatty acid experiment, which would not have been realizable without their help.

I would like to thank Maren Köhne, who was either actively involved in the establishment of ATAC reactions with the new *in-house* Tn5 which was supplied by Professor Dr. Matthias Geyer and his working group. In this context, I also want to thank Professor Dr. Matthias Geyer and his working group for their commitment and the good collaboration.

My sincere thanks also go to the Ph.D. students of the Genomics and Immunoregulation group at the LIMES Institute, for the many constructive discussions, their help in the lab and beyond. Especially, Olympia Papantonopoulou, Sander Tuit, Saskia Mayer, Lisa Schmidleithner, Maren Köhne and Arik Horne did not only support me in scientific issues but also gave me new motivation in difficult situations. Thank you for that!

The Ph.D. students Jonas Schulte-Schrepping, Kevin Baßler, Patrick Günther and Stefanie Warnat-Herresthal supported me whenever I needed help in performing the bioinformatics analysis. As I had no previous experience in bioinformatic RNA-seq. analysis, their help was of great importance for me. Thank you all for your patience.

I also want to mention the technical assistants Heidi Theis, Maren Schell and Michael Kraut, who organized the laboratories and taught me the standard procedures of the lab. Heidi Theis was especially dedicated in the assistance of comprehensive cell culture experiments. Thank you for your support.

Last but not least I want to thank my family and friends for encouraging me in all of my pursuits and inspiring me to follow my way. I am especially grateful to my parents, who supported me emotionally and financially. I always knew that you believed in me and wanted the best for me.

Thank you

References

1. Laine, P. S. *et al.* Palmitic acid induces IP-10 expression in human macrophages via NF-κB activation. *Biochem. Biophys. Res. Commun.* **358,** 150–155 (2007).

2. Camell, C. & Smith, C. W. Dietary Oleic Acid Increases M2 Macrophages in the Mesenteric Adipose Tissue. *PLoS One* **8,** (2013).

3. Santoni, G. *et al.* Danger- and pathogen-associated molecular patterns recognition by pattern-recognition receptors and ion channels of the transient receptor potential family triggers the inflammasome activation in immune cells and sensory neurons. *J. Neuroinflammation* **12,** 21 (2015).

4. Iwasaki, A. & Medzhitov, R. Toll-like receptor control of the adaptive immune responses. *Nature Immunology* (2004). doi:10.1038/ni1112

5. Capella, M. Inmunidad Innata. *Inmunol. Básica* **16,** 1–7 (2008).

6. Mandrup-Poulsen, T. *et al.* Cytokines and the endocrine system. I. The immunoendocrine network. *Eur. J. Endocrinol.* **133,** 660–71 (1995).

7. Dowling, J. K. & Mansell, A. Toll-like receptors: the swiss army knife of immunity and vaccine development. *Clin. Transl. Immunol.* **5,** e85 (2016).

8. Kawasaki, T., Kawai, T., Kutikhin, A. G. & Trendelenburg, G. Toll-like receptor signaling pathways. Frontiers in Immunology 5, 1 (2014).

9. Kawai, T. & Akira, S. Signaling to NF-??B by Toll-like receptors. *Trends Mol. Med.* **13,** 460–469 (2007).

10. Janeway, C. *Immunobiology 5 : the immune system in health and disease*. Garland Pub (2001).

11. Ziegler-Heitbrock, L. *et al.* Nomenclature of monocytes and dendritic cells in blood. *Blood* **116,** e74-80 (2010).

12. Geissmann, F., Manz, M. G., Jung, S., Sieweke, M. H. & Ley, K. Development of monocytes, macrophages and dendritic cells. *Science (80.).* **327,** 656–661 (2010).

13. Davies, L. C., Jenkins, S. J., Allen, J. E. & Taylor, P. R. Tissue-resident macrophages. *Nat. Immunol.* **14,** 986–995 (2013).

14. Gordon, S. & Taylor, P. R. Monocyte and macrophage heterogeneity. *Nat. Rev. Immunol.* **5,** 953–964 (2005).

15. Yang, J., Zhang, L., Yu, C., Yang, X.-F. & Wang, H. Monocyte and macrophage differentiation: circulation inflammatory monocyte as biomarker for inflammatory diseases. *Biomark. Res.* **2,** 1 (2014).

16. Auffray, C. *et al.* Monitoring of blood vessels and tissues by a population of monocytes with patrolling behavior. *Science* **317,** 666–70 (2007).

17. Wong, K. L. *et al.* Gene expression profiling reveals the defining features of the classical, intermediate, and nonclassical human monocyte subsets. *Blood* **118,** e16-31 (2011).

18. Rô Me Cros, J. *et al.* Human CD14 dim Monocytes Patrol and Sense Nucleic Acids and Viruses via TLR7 and TLR8 Receptors. *Immunity* **33,** 375–386 (2010).

19. Jakubzick, C. *et al.* Minimal Differentiation of Classical Monocytes as They Survey Steady-State Tissues and Transport Antigen to Lymph Nodes. *Immunity* **39,** 599–610 (2013).

20. Mosig, S. *et al.* Different functions of monocyte subsets in familial hypercholesterolemia: potential function of CD14 + CD16 + monocytes in detoxification of oxidized LDL . *FASEB J.* **23,** 866–874 (2009).

21. Zawada, A. M. *et al.* SuperSAGE evidence for CD14++CD16+ monocytes as a third monocyte subset. *Blood* **118,** e50-61 (2011).

22. Jakubzick, C. V, Randolph, G. J. & Henson, P. M. Monocyte differentiation and antigen-presenting functions. *Nat. Publ. Gr.* **17,** (2017).

23. Tamoutounour, S. *et al.* Origins and Functional Specialization of Macrophages and of Conventional and Monocyte-Derived Dendritic Cells in Mouse Skin. *Immunity* **39,** 925–938 (2013).

24. Bain, C. C. *et al.* Resident and pro-inflammatory macrophages in the colon represent alternative context-dependent fates of the same Ly6Chi monocyte precursors. **6,** (2013).

25. Rivollier, A., He, J., Kole, A., Valatas, V. & Kelsall, B. L. Inflammation switches the differentiation program of Ly6Chi monocytes from antiinflammatory macrophages to inflammatory dendritic cells in the colon. *J. Exp. Med.* **209,** 139–55 (2012).

26. Schlitzer, A. *et al.* Identification of cDC1- and cDC2-committed DC progenitors reveals early lineage priming at the common DC progenitor stage in the bone marrow. *Nat. Immunol.* **16,** 718–728 (2015).

27. Lavin, Y. *et al.* Tissue-resident macrophage enhancer landscapes are shaped by the local microenvironment. *Cell* **159,** 1312–1326 (2014).

28. Malyshev, I. & Malyshev, Y. Current Concept and Update of the Macrophage Plasticity Concept: Intracellular Mechanisms of Reprogramming and M3 Macrophage 'Switch' Phenotype. *Biomed Res. Int.* **2015,** 1–22 (2015).

29. Sica, A. & Mantovani, A. Macrophage plasticity and polarization: in vivo veritas. *J. Clin. Invest.* **122,** 787–95 (2012).

30. Gomez Perdiguero, E. *et al.* Tissue-resident macrophages originate from yolk-sac-derived erythro-myeloid progenitors Most haematopoietic cells renew from adult haematopoietic stem cells (HSCs). *Nature* **518,** (2015).

31. Guilliams, M. *et al.* Alveolar macrophages develop from fetal monocytes that differentiate into long-lived cells in the first week of life via GM-CSF. *J. Exp. Med.* **210,** 1977 (2013).

32. Ginhoux, F. & Jung, S. Monocytes and macrophages: developmental pathways and tissue homeostasis. *Nat. Publ. Gr.* **14,** (2014).

33. Merad, M., Sathe, P., Helft, J., Miller, J. & Mortha, A. The Dendritic Cell Lineage: Ontogeny and Function of Dendritic Cells and Their Subsets in the Steady State and the Inflamed Setting. *Annu. Rev. Immunol.* **31,** 563–604 (2013).

34. Guilliams, M. *et al.* Dendritic cells, monocytes and macrophages: a unified nomenclature based on ontogeny. *Nat. Rev. Immunol.* **14,** 571–8 (2014).

35. See, P. *et al.* Mapping the human DC lineage through the integration of high-dimensional techniques. *Science* **356,** eaag3009 (2017).

36. Dhodapkar, M. V & Dhodapkar, K. M. Recent advances and new opportunities for targeting human dendritic cells in situ. *Oncoimmunology* **3,** e954832 (2014).

37. Schraml, B. U. *et al.* Genetic tracing via DNGR-1 expression history defines dendritic cells as a hematopoietic lineage. *Cell* **154,** 843–58 (2013).

38. Helft, J. *et al.* Dendritic Cell Lineage Potential in Human Early Hematopoietic Progenitors. *Cell Rep.* **20,** 529–537 (2017).

39. Bao, M. & Liu, Y.-J. Regulation of TLR7/9 signaling in plasmacytoid dendritic cells. *Protein Cell* **4,** 40 (2013).

40. Swiecki, M. & Colonna, M. The multifaceted biology of plasmacytoid dendritic cells. *Nat. Rev. Immunol.* **15,** 471–85 (2015).

41. Tussiwand, R. *et al.* Klf4 expression in conventional dendritic cells is required for T helper 2 cell responses. *Immunity* **42,** 916 (2015).

42. Persson, E. K., Scott, C. L., Mowat, A. M. & Agace, W. W. Dendritic cell subsets in the intestinal lamina propria: Ontogeny and function. *Eur. J. Immunol.* **43,** 3098–3107 (2013).

43. Schlitzer, A. & Ginhoux, F. Organization of the mouse and human DC network. *Curr. Opin. Immunol.* **26,** 90–99 (2014).

44. Sander, J. *et al.* Cellular Differentiation of Human Monocytes Is Regulated by Time-Dependent Interleukin-4 Signaling and the Transcriptional Regulator NCOR2. *Immunity* **47,** 1051–1066.e12 (2017).

45. Collin, M. & Bigley, V. Human dendritic cell subsets: an update. *Immunology* **154,** 3–20 (2018).

46. Cochain, C. *et al.* Single-Cell RNA-Seq Reveals the Transcriptional Landscape and Heterogeneity of Aortic Macrophages in Murine Atherosclerosis. *Circ. Res.* **122,** 1661–1674 (2018).

47. Wu, L. *et al.* RelB is essential for the development of myeloid-related CD8alpha- dendritic cells but not of lymphoid-related CD8alpha+ dendritic cells. *Immunity* **9,** 839–47 (1998).

48. Caesar, R., Tremaroli, V., Kovatcheva-Datchary, P., Cani, P. D. & Bäckhed, F. Crosstalk between Gut Microbiota and Dietary Lipids Aggravates WAT Inflammation through TLR Signaling. *Cell Metab.* **22,** 658–668 (2015).

49. Jialal, I., Kaur, H. & Devaraj, S. Toll-like Receptor Status in Obesity and Metabolic Syndrome: A Translational Perspective. *J. Clin. Endocrinol. Metab.* **99,** 39–48 (2014).

50. Bell, J. K. *et al.* Leucine-rich repeats and pathogen recognition in Toll-like receptors. *Trends Immunol.* **24,** 528–33 (2003).

51. Botos, I., Segal, D. M. & Davies, D. R. The structural biology of Toll-like receptors. *Structure* **19,** 447–59 (2011).

52. Broad, A., Kirby, J. A., Jones, D. E. J. & Applied Immunology and Transplantation Research Group, A. I. and T. R. Toll-like receptor interactions: tolerance of MyD88-dependent cytokines but enhancement of MyD88-independent interferon-beta production. *Immunology* **120,** 103–11 (2007).

53. Thompson, M. R., Kaminski, J. J., Kurt-Jones, E. A. & Fitzgerald, K. A. Pattern recognition receptors and the innate immune response to viral infection. *Viruses* **3,** 920–40 (2011).

54. Yamamoto, M. *et al.* Role of Adaptor TRIF in the MyD88-Independent Toll-Like Receptor Signaling Pathway. *Science (80-.).* **301,** 640–643 (2003).

55. Hoebe, K. *et al.* Upregulation of costimulatory molecules induced by lipopolysaccharide and double-stranded RNA occurs by Trif-dependent and Trif-independent pathways. *Nat. Immunol.* **4,** 1223–1229 (2003).

56. Lien, E. & Golenbock, D. T. Adjuvants and their signaling pathways: beyond TLRs. *Nat. Immunol.* **4,** 1162–1164 (2003).

57. Kröncke, K. D., Fehsel, K., Suschek, C. & Kolb-Bachofen, V. Inducible nitric oxide synthase-derived nitric oxide in gene regulation, cell death and cell survival. *Int. Immunopharmacol.* **1,** 1407–20 (2001).

58. Hill, B. G., Dranka, B. P., Bailey, S. M., Lancaster, J. R. & Darley-Usmar, V. M. What part of NO don't you understand? Some answers to the cardinal questions in nitric oxide biology. *J. Biol. Chem.* **285,** 19699–704 (2010).

59. Fessler, M. B., Rudel, L. L. & Brown, J. M. Toll-like receptor signaling links dietary fatty acids to the metabolic syndrome. *Curr. Opin. Lipidol.* **20,** 379–85 (2009).

60. Nicholas, D. A. *et al.* Palmitic acid is a toll-like receptor 4 ligand that induces human dendritic cell secretion of IL-1β. *PLoS One* **12,** e0176793 (2017).

61. Lancaster, G. I. *et al.* Evidence that TLR4 Is Not a Receptor for Saturated Fatty Acids but Mediates Lipid-Induced Inflammation by Reprogramming Macrophage Metabolism. *Cell Metab.* 1–15 (2018). doi:10.1016/j.cmet.2018.03.014

62. Wu, T.-T., Chen, T.-L. & Chen, R.-M. Lipopolysaccharide triggers macrophage activation of inflammatory cytokine expression, chemotaxis, phagocytosis, and oxidative ability via a toll-like receptor 4-dependent pathway: Validated by RNA interference. *Toxicol. Lett.* **191,** 195–202 (2009).

63. Biswas, S. K. & Lopez-Collazo, E. Endotoxin tolerance: new mechanisms, molecules and clinical significance. *Trends Immunol.* **30,** 475–487 (2009).

64. Netea, M. G., Latz, E., Kingston, H. G., Mills, L. A. & Neill, J. O. '. Innate immune memory: a paradigm shift in understanding host defense. *Nat. Publ. Gr.* **16,** (2015).

65. Davis, B. K., Wen, H. & Ting, J. P.-Y. The Inflammasome NLRs in Immunity, Inflammation, and Associated Diseases. *Annu. Rev. Immunol.* **29,** 707–735 (2011).

66. Lamkanfi, M. & Dixit, V. M. Mechanisms and Functions of Inflammasomes. *Cell* **157,** 1013–1022 (2014).

67. Man, S. M. & Kanneganti, T.-D. Regulation of inflammasome activation. *Immunol. Rev.* **265,** 6–21 (2015).

68. Wang, L. *et al.* PYPAF7, a Novel PYRIN-containing Apaf1-like Protein That Regulates Activation of NF-κB and Caspase-1-dependent Cytokine Processing. *J. Biol. Chem.* **277,** 29874–29880 (2002).

69. Martinon, F., Burns, K. & Tschopp, J. The inflammasome: a molecular platform triggering activation of inflammatory caspases and processing of proIL-beta. *Mol. Cell* **10,** 417–26 (2002).

70. Lacy, P. & Stow, J. L. Cytokine release from innate immune cells: association with diverse membrane trafficking pathways. *Blood* **118,** 9–18 (2011).

71. Dinarello, C. A. Immunological and Inflammatory Functions of the Interleukin-1 Family. *Annu. Rev. Immunol.* **27,** 519–550 (2009).

72. Fink, S. L. & Cookson, B. T. Caspase-1-dependent pore formation during pyroptosis leads to osmotic lysis of infected host macrophages. *Cell. Microbiol.* **8,** 1812–1825 (2006).

73. He, Y., Zeng, M. Y., Yang, D., Motro, B. & Núñez, G. NEK7 is an essential mediator of NLRP3 activation downstream of potassium efflux. *Nature* **530,** 354–357 (2016).

74. Martinon, F., Mayor, A. & Tschopp, J. The Inflammasomes: Guardians of the Body. *Annu. Rev. Immunol.* **27,** 229–265 (2009).

75. Wen, H. *et al.* Fatty acid-induced NLRP3-ASC inflammasome activation interferes with insulin signaling. *Nat. Immunol.* **12,** 408–15 (2011).

76. Netea, M. G. *et al.* Trained immunity: A program of innate immune memory in health and disease. *Science* **352,** aaf1098 (2016).

77. Ifrim, D. C. *et al.* Trained immunity or tolerance: Opposing functional programs induced in human monocytes after engagement of various pattern recognition receptors. *Clin. Vaccine Immunol.* **21,** 534–545 (2014).

78. World Health Organization. Obesity and overweight. *WHO* Key Facts Available at: http://www.who.int/news-room/fact-sheets/detail/obesity-and-overweight. (Accessed: 29th May 2018)

79. Obesity | WHO | Regional Office for Africa. Available at: https://www.afro.who.int/health-topics/obesity. (Accessed: 27th August 2018)

80. Hebebrand, J. *et al.* A Proposal of the European Association for the Study of Obesity to Improve the ICD-11 Diagnostic Criteria for Obesity Based on the Three Dimensions Etiology, Degree of Adiposity and Health Risk. *Obes Facts* **10,** 284–307 (2017).

81. LeBlanc, E., O'Connor, E., Whitlock, E. P., Patnode, C. & Kapka, T. *Screening for and Management of Obesity and Overweight in Adults*. *Screening for and Management of Obesity and Overweight in Adults* (Agency for Healthcare Research and Quality (US), 2011).

82. Debnath, M. & Sarkar, S. Obesity Induced Metaflammation : Pathophysiology and Mitigation. **1,** 1–5 (2016).

83. Weisberg, S. P. *et al.* Obesity is associated with macrophage accumulation in adipose tissue. *J. Clin. Invest.* **112,** 1796–808 (2003).

84. Wannamethee, G. G., Whincup, P. H., Rumley, A. & Lowe, G. D. O. Inter-relationships of interleukin-6, cardiovascular risk factors and the metabolic syndrome among older men. *J. Thromb. Haemost.* **5,** 1637–1643 (2007).

85. Patimah, I., Ellulu, M. S., Khaza 'ai, H., Rahmat, A. & Abed, Y. State of the art paper Obesity and inflammation: the linking mechanism and the complications. *Arch Med Sci* **13,** 851–863 (2017).

86. Taniguchi, K. & Karin, M. IL-6 and related cytokines as the critical lynchpins between inflammation and cancer. *Semin. Immunol.* **26,** 54–74 (2014).

87. Matura, L. A. *et al.* Interleukin-6 and Tumor Necrosis Factor-a Are Associated with Quality of Life–Related Symptoms in Pulmonary Arterial Hypertension. doi:10.1513/AnnalsATS.201410-463OC

88. Gluba, A. *et al.* Metabolic syndrome and renal disease. *Int. J. Cardiol.* **164,** 141–150 (2013).

89. Fujishima, S. *et al.* Involvement of IL-17F via the induction of IL-6 in psoriasis. *Arch. Dermatol. Res.* **302,** 499–505 (2010).

90. The Basic Principles of Fatty Acids. Available at: https://www.budwig-stiftung.de/en/service/the-basic-principles-of-fatty-acids.html. (Accessed: 27th August 2018)

91. Mensink, R. P. Effects of saturated fatty acids on serum lipids and lipoproteins: a systematic review and regression analysis. *World Heal. Organ.* 1–63 (2016).

92. Hu, F. B., Manson, J. E. & Willett, W. C. Types of dietary fat and risk of coronary heart disease: a critical review. *J. Am. Coll. Nutr.* **20,** 5–19 (2001).

93. Kris-Etherton, P. M. & Yu, S. Individual fatty acid effects on plasma lipids and lipoproteins: human studies. *Am. J. Clin. Nutr.* **65,** 1628S–1644S (1997).

94. Temme, E. H., Mensink, R. P. & Hornstra, G. Comparison of the effects of diets enriched in lauric, palmitic, or oleic acids on serum lipids and lipoproteins in healthy women and men. *Am. J. Clin. Nutr.* **63,** 897–903 (1996).

95. Calder, P. C. Long-chain n-3 fatty acids and inflammation: potential application in surgical and trauma patients. *Brazilian J. Med. Biol. Res.* **36,** 433–446 (2003).

96. Roberta Larson Duyff. *Academy of Nutrition and Dietetics Complete Food and Nutrition Guide, 5th Ed - Roberta Larson Duyff - Google Books*. (Houghton Mifflin Harcourt; Revised, Updated edition (April 18, 2017), 2017).

97. Kiefer, D. & Pantuso, T. Omega-3 fatty acids: An update emphasizing clinical use. *Agro Food Ind. Hi. Tech.* **23,** 10–13 (2012).

98. Navarini, L., Afeltra, A., Gallo Afflitto, G. & Margiotta, D. P. E. Polyunsaturated fatty acids: any role in rheumatoid arthritis? *Lipids Health Dis.* **16,** 197 (2017).

99. Simopoulos, A. P. Evolutionary aspects of diet, the omega-6/omega-3 ratio and genetic variation: nutritional implications for chronic diseases. *Biomed. Pharmacother.* **60,** 502–507 (2006).

100. Brouwer, I. A., Wanders, A. J. & Katan, M. B. Effect of animal and industrial trans fatty acids on HDL and LDL cholesterol levels in humans--a quantitative review. *PLoS One* **5,** e9434 (2010).

101. Johnson, E. J. & Mohn, E. S. in *World review of nutrition and dietetics* **111,** 38–44 (Karger Publishers, 2014).

102. Chianese, R. *et al.* Impact of Dietary Fats on Brain Functions. *Curr. Neuropharmacol.* **16,** 1059–1085 (2018).

103. Kaur, N., Chugh, V. & Gupta, A. K. Essential fatty acids as functional components of foods- a review. *J. Food Sci. Technol.* **51,** 2289–303 (2014).

104. Dernini, S. *et al.* Med Diet 4.0: the Mediterranean diet with four sustainable benefits. *Public Health Nutr.* **20,** 1322–1330 (2017).

105. Sofi, F., Macchi, C., Abbate, R., Gensini, G. F. & Casini, A. Mediterranean diet and health status: an updated meta-analysis and a proposal for a literature-based adherence score. *Public Health Nutr.* **17,** 2769–2782 (2013).

106. Schwingshackl, L. & Hoffmann, G. Adherence to Mediterranean diet and risk of cancer: A systematic review and meta-analysis of observational studies. *Int. J. Cancer* **135,** 1884–1897 (2014).

107. Psaltopoulou, T. *et al.* Mediterranean diet, stroke, cognitive impairment, and depression: A meta-analysis. *Ann. Neurol.* **74,** 580–591 (2013).

108. Sofi, F., Macchi, C., Abbate, R., Gensini, G. F. & Casini, A. Effectiveness of the Mediterranean Diet: Can It Help Delay or Prevent Alzheimer's Disease? *J. Alzheimer's Dis.* **20,** 795–801 (2010).

109. Kastorini, C.-M. *et al.* The Effect of Mediterranean Diet on Metabolic Syndrome and its Components: A Meta-Analysis of 50 Studies and 534,906 Individuals. *J. Am. Coll. Cardiol.* **57,** 1299–1313 (2011).

110. D'Alessandro, A. & De Pergola, G. Mediterranean Diet and Cardiovascular Disease: A Critical Evaluation of A Priori Dietary Indexes. *Nutrients* **7,** 7863–7888 (2015).

111. McGuire, S. U.S. Department of Agriculture and U.S. Department of Health and Human Services, Dietary Guidelines for Americans, 2010. 7th Edition, Washington, DC: U.S. Government Printing Office, January 2011. *Adv. Nutr.* **2,** 293–294 (2011).

112. Grimminger, F. *et al.* Synthesis of 4- and 5-series leukotrienes in the lung microvasculature challenged with Escherichia coli hemolysin: critical dependence on exogenous free fatty acid supply. *Am. J. Respir. Cell Mol. Biol.* **16,** 317–324 (1997).

113. Wolever, T. M., Bentum-Williams, A. & Jenkins, D. J. Physiological modulation of plasma free fatty acid concentrations by diet. Metabolic implications in nondiabetic subjects. *Diabetes Care* **18,** 962–70 (1995).

114. Murphy, M. C. *et al.* Postprandial lipid and hormone responses to meals of varying fat contents: modulatory role of lipoprotein lipase? *Eur. J. Clin. Nutr.* **49,** 578–88 (1995).

115. Reaven, G. M., Hollenbeck, C., Jeng, C. Y., Wu, M. S. & Chen, Y. D. Measurement of plasma glucose, free fatty acid, lactate, and insulin for 24 h in patients with NIDDM. *Diabetes* **37,** 1020–4 (1988).

116. Štolba, P., Kvapil, M., Wichterle, D. & Dvořák, P. Kinetics of Free Fatty Acids in Hypertriglyceridemia. *Ann. N. Y. Acad. Sci.* **683,** 373–375 (1993).

117. Staiger, H. *et al.* Palmitate-induced interleukin-6 expression in human coronary artery endothelial cells. *Diabetes* **53,** 3209–16 (2004).

118. Dietary Fats | EU Science Hub. Available at: https://ec.europa.eu/jrc/en/health-knowledge-gateway/promotion-prevention/nutrition/fats. (Accessed: 1st March 2020)

119. Ertunc, M. E. & Hotamisligil, G. S. Lipid signaling and lipotoxicity in metaflammation: indications for metabolic disease pathogenesis and treatment. *J. Lipid Res.* **57,** 2099–2114 (2016).

120. Chaurasia, B. & Summers, S. A. Ceramides – Lipotoxic Inducers of Metabolic Disorders. *Trends Endocrinol. Metab.* **29,** 66–67 (2018).

121. Salvadó, L., Palomer, X., Barroso, E. & Vázquez-Carrera, M. Targeting endoplasmic reticulum stress in insulin resistance. *Trends Endocrinol. Metab.* **26,** 438–448 (2015).

122. Velloso, L. A., Folli, F. & Saad, M. J. TLR4 at the Crossroads of Nutrients, Gut Microbiota, and Metabolic Inflammation. *Endocr. Rev.* **36,** 245–271 (2015).

123. Cani, P. D. *et al.* Metabolic Endotoxemia Initiates Obesity and Insulin Resistance. *Diabetes* **56,** 1761–1772 (2007).

124. Vessby, B. *et al.* Substituting dietary saturated for monounsaturated fat impairs insulin sensitivity in healthy men and women: The KANWU Study. *Diabetologia* **44,** 312–9 (2001).

125. Gregor, M. F. & Hotamisligil, S. Inflammatory Mechanisms in Obesity. (2011). doi:10.1146/annurev-immunol-031210-101322

126. Opie, L. H. & Walfish, P. G. Plasma Free Fatty Acid Concentrations in Obesity. *N. Engl. J. Med.* **268,** 757–760 (1963).

127. Averill, M. M. & Bornfeldt, K. E. Lipids versus glucose in inflammation and the pathogenesis of macrovascular disease in diabetes. *Curr. Diab. Rep.* **9,** 18–25 (2009).

128. Kennedy, A., Martinez, K., Chuang, C.-C., LaPoint, K. & McIntosh, M. Saturated Fatty Acid-Mediated Inflammation and Insulin Resistance in Adipose Tissue: Mechanisms of Action and Implications. *J. Nutr.* **139,** 1–4 (2009).

129. Lumeng, C. N., Bodzin, J. L. & Saltiel, A. R. Obesity induces a phenotipic switch in adipose tissue macrophage polarization. *J Clin Invest* **117,** 175–184 (2007).

130. Patel, P. S., Buras, E. D. & Balasubramanyam, A. The Role of the Immune System in Obesity and Insulin Resistance. *J. Obes.* **2013,** 1–9 (2013).

131. Posokhova, E. N., Khoshchenko, O. M., Chasovskikh, M. I., Pivovarova, E. N. & Dushkin, M. I. Lipid synthesis in macrophages during inflammation in vivo: effect of agonists of peroxisome proliferator activated receptors alpha and gamma and of retinoid X receptors. *Biochemistry. (Mosc).* **73,** 296–304 (2008).

132. Feingold, K. R. *et al.* Mechanisms of triglyceride accumulation in activated macrophages. *J. Leukoc. Biol.* **92,** 829–839 (2012).

133. O'Neill, L. A. J., Kishton, R. J. & Rathmell, J. A guide to immunometabolism for immunologists. *Nat. Rev. Immunol.* **16,** 553–565 (2016).

134. Odegaard, J. I. & Chawla, A. Alternative Macrophage Activation and Metabolism. *Annu. Rev. Pathol. Mech. Dis.* **6,** 275–297 (2011).

135. Namgaladze, D. & Brüne, B. Macrophage fatty acid oxidation and its roles in macrophage polarization and fatty acid-induced inflammation. *BBA - Mol. Cell Biol. Lipids* **1861,** 1796–1807 (2016).

136. van der Windt, G. J. W. *et al.* Mitochondrial Respiratory Capacity Is a Critical Regulator of CD8+ T Cell Memory Development. *Immunity* **36,** 68–78 (2012).

137. van der Windt, G. J. W. *et al.* Mitochondrial respiratory capacity is a critical regulator of CD8+ T cell memory development. *Immunity* **36,** 68–78 (2012).

138. He, Z., Zhu, X., Shi, Z., Wu, T. & Wu, L. Metabolic Regulation of Dendritic Cell Differentiation. *Front. Immunol.* **10,** 410 (2019).

139. Wculek, S. K., Khouili, S. C., Priego, E., Heras-Murillo, I. & Sancho, D. Metabolic Control of Dendritic Cell Functions: Digesting Information. *Front. Immunol.* **10,** 775 (2019).

140. Maxfield, F. R. & Tabas, I. Role of cholesterol and lipid organization in disease. *Nature* **438,** 612–621 (2005).

141. Duffy, D. & Rader, D. J. Update on strategies to increase HDL quantity and function. *Nat. Rev. Cardiol.* **6,** 455–463 (2009).

142. Klappacher, G. W. & Glass, C. K. Roles of peroxisome proliferator-activated receptor gamma in lipid homeostasis and inflammatory responses of macrophages. *Curr. Opin. Lipidol.* **13,** 305–12 (2002).

143. Kennedy, M. A. *et al.* ABCG1 has a critical role in mediating cholesterol efflux to HDL and preventing cellular lipid accumulation. *Cell Metab.* **1,** 121–131 (2005).

144. Wang, N., Lan, D., Chen, W., Matsuura, F. & Tall, A. R. ATP-binding cassette transporters G1 and G4 mediate cellular cholesterol efflux to high-density lipoproteins. *Proc. Natl. Acad. Sci.* **101,** 9774–9779 (2004).

145. Hara, H. & Yokoyama, S. Interaction of free apolipoproteins with macrophages. Formation of high density lipoprotein-like lipoproteins and reduction of cellular cholesterol. *J. Biol. Chem.* **266,** 3080–6 (1991).

146. Phillips, M. C. Molecular Mechanisms of Cellular Cholesterol Efflux. *J. Biol. Chem.* **289,** 24020–24029 (2014).

147. Ricote, M., Li, A. C., Willson, T. M., Kelly, C. J. & Glass, C. K. The peroxisome proliferator-activated receptor-γ is a negative regulator of macrophage activation. *Nature* **391,** 79–82 (1998).

148. Bouhlel, M. A. *et al.* PPARγ Activation Primes Human Monocytes into Alternative M2 Macrophages with Anti-inflammatory Properties. *Cell Metab.* **6,** 137–143 (2007).

149. Huang, S. C.-C. *et al.* Cell-intrinsic lysosomal lipolysis is essential for alternative activation of macrophages. *Nat. Immunol.* **15,** 846–855 (2014).

150. Mehta, M. M., Weinberg, S. E. & Chandel, N. S. Mitochondrial control of immunity: beyond ATP. *Nat. Rev. Immunol.* **17,** 608–620 (2017).

151. O'Neill, L. A. J., Kishton, R. J. & Rathmell, J. A guide to immunometabolism for immunologists. *Nat. Rev. Immunol.* **16,** 553–565 (2016).

152. Picot, J., Guerin, C. L., Le Van Kim, C. & Boulanger, C. M. Flow cytometry: Retrospective, fundamentals and recent instrumentation. *Cytotechnology* **64,** 109–130 (2012).

153. Brumatti, G., Sheridan, C. & Martin, S. J. Expression and purification of recombinant annexin V for the detection of membrane alterations on apoptotic cells. *Methods* **44,** 235–240 (2008).

154. Crowley, L. C. *et al.* Measuring cell death by propidium iodide uptake and flow cytometry. *Cold Spring Harb. Protoc.* **2016,** 647–651 (2016).

155. PrestoBlue™ HS Cell Viability Reagent. Available at: https://www.thermofisher.com/order/catalog/product/P50200#/P50200. (Accessed: 27th February 2020)

156. Thavarajah, R., Mudimbaimannar, V. K., Elizabeth, J., Rao, U. K. & Ranganathan, K. Chemical and physical basics of routine formaldehyde fixation. *Journal of Oral and Maxillofacial Pathology* **16,** 400–405 (2012).

157. Bonifacino, J. S., Dell'Angelica, E. C. & Springer, T. A. Immunoprecipitation. *Curr. Protoc. Protein Sci.* **18,** Unit 9.8 (1999).

158. Park, P. J. ChIP-seq: advantages and challenges of a maturing technology. *Nat. Rev. Genet.* **10,** 669–80 (2009).

159. Blecher-Gonen, R. *et al.* High-throughput chromatin immunoprecipitation for genome-wide mapping of in vivo protein-DNA interactions and epigenomic states. *Nat. Protoc.* **8,** 539–54 (2013).

160. Arrigoni, L. *et al.* Standardizing chromatin research: A simple and universal method for ChIP-seq. *Nucleic Acids Res.* **44,** 1–13 (2015).

161. Buenrostro, J. D., Giresi, P. G., Zaba, L. C., Chang, H. Y. & Greenleaf, W. J. Transposition of native chromatin for fast and sensitive epigenomic profiling of open chromatin, DNA-binding proteins and nucleosome position. *Nat. Methods* **10,** 1213–8 (2013).

162. Buenrostro, J. D., Wu, B., Chang, H. Y. & Greenleaf, W. J. ATAC-seq: A Method for Assaying Chromatin Accessibility Genome-Wide. *Curr. Protoc. Mol. Biol.* **109,** 21.29.1-9 (2015).

163. Burnette, W. N. 'Western Blotting': Electrophoretic transfer of proteins from sodium dodecyl sulfate-polyacrylamide gels to unmodified nitrocellulose and radiographic detection with antibody and radioiodinated protein A. *Anal. Biochem.* **112,** 195–203 (1981).

164. Love, M. I., Huber, W. & Anders, S. Moderated estimation of fold change and dispersion for RNA-seq data with DESeq2. *Genome Biol.* **15,** 550 (2014).

165. Benjamini, Y. & Hochberg, Y. Controlling the False Discovery Rate: A Practical and Powerful Approach to Multiple Testing. *Journal of the Royal Statistical Society. Series B (Methodological)* **57,** 289–300 (1995).

166. Theocharidis, A., van Dongen, S., Enright, A. J. & Freeman, T. C. Network visualization and analysis of gene expression data using BioLayout Express(3D). *Nat. Protoc.* **4,** 1535–1550 (2009).

167. Yu, G., Wang, L.-G., Han, Y. & He, Q.-Y. clusterProfiler: an R package for comparing biological themes among gene clusters. *OMICS* **16,** 284–7 (2012).

168. Kanehisa, M. & Goto, S. KEGG: kyoto encyclopedia of genes and genomes. *Nucleic Acids Res.* **28,** 27–30 (2000).

169. Kanehisa, M., Furumichi, M., Tanabe, M., Sato, Y. & Morishima, K. KEGG: new perspectives on genomes, pathways, diseases and drugs. *Nucleic Acids Res.* **45,** D353–D361 (2017).

170. Mi, H., Muruganujan, A., Casagrande, J. T. & Thomas, P. D. Large-scale gene function analysis with the PANTHER classification system. *Nat. Protoc.* **8,** 1551–1566 (2013).

171. Myles, I. A. Fast food fever: Reviewing the impacts of the Western diet on immunity. *Nutrition Journal* **13,** (2014).

172. Lima, T. M., Kanunfre, C. C., Pompéia, C., Verlengia, R. & Curi, R. Ranking the toxicity of fatty acids on Jurkat and Raji cells by flow cytometric analysis. *Toxicol. Vitr.* **16,** 741–747 (2002).

173. Mu, Y.-M. *et al.* Saturated FFAs, Palmitic Acid and Stearic Acid, Induce Apoptosis in Human Granulosa Cells. *Endocrinology* **142,** 3590–3597 (2001).

174. Xue, J. *et al.* Transcriptome-Based Network Analysis Reveals a Spectrum Model of Human Macrophage Activation. *Immunity* **40,** 274–288 (2014).

175. Bhattacharya, P. *et al.* Dual Role of GM-CSF as a Pro-Inflammatory and a Regulatory Cytokine: Implications for Immune Therapy. *J. Interferon Cytokine Res.* **0,** 1–15 (2015).

176. Asakura, E. *et al.* Effects of Macrophage Colony-Stimulating Factor (M-CSF) on Lipopolysaccharide (LPS)-induced Mediator Production from Monocytes in vitro. *Immunobiology* **195,** 300–313 (1996).

177. Rosenblat, M., Volkova, N., Paland, N. & Aviram, M. Triglyceride accumulation in macrophages upregulates paraoxonase 2 (PON2) expression via ROS-mediated JNK/c-Jun signaling pathway activation. *BioFactors* **38,** 458–469 (2012).

178. Picelli, S. *et al.* Tn5 transposase and tagmentation procedures for massively scaled sequencing projects. *Genome Res.* **24,** 2033–2040 (2014).

179. EMD Millipore™ Amicon™ Ultra-15 Centrifugal Filter Units ULtra-15; w/ULtracel-10 membrane; 10,000 NMWL; Dia. x L: 29.6 x 72mm; 24/Pk. EMD Millipore™ Amicon™ Ultra-15 Centrifugal Filter Units. Available at: https://www.fishersci.co.uk/shop/products/emd-millipore-amicon-ultra-15-centrifugal-filter-units-15/10781543. (Accessed: 31st August 2018)

180. 5er Set Eppis 1,5ml Volumen klar | Flaschen | DIY - Do it yourself | Shop für e-Zigaretten und e-Liquids. Available at: https://www.e-rauchershop.de/5er-set-eppis-1-5ml-volumen-klar. (Accessed: 31st August 2018)

181. Myles, I. a. Fast food fever: reviewing the impacts of the Western diet on immunity. *Nutr. J.* **13,** 61 (2014).

182. Rocha, D. M. *et al.* The role of dietary fatty acid intake in inflammatory gene expression: a critical review. *Sao Paulo Med. J.* **135,** 157–168 (2017).

183. Kochumon, S. *et al.* Palmitate Activates CCL4 Expression in Human Monocytic Cells via TLR4/MyD88 Dependent Activation of NF-κB/MAPK/ PI3K Signaling Systems. *Cell. Physiol. Biochem.* **46,** 953–964 (2018).

184. L'homme, L. *et al.* Unsaturated fatty acids prevent activation of NLRP3 inflammasome in human monocytes/macrophages. *J. Lipid Res.* **54,** 2998–3008 (2013).

185. Méndez-Barbero, N. *et al.* A major role for RCAN 1 in atherosclerosis progression. *EMBO Mol. Med.* **5,** 1901–1917 (2013).

186. Vermes, I., Haanen, C., Steffens-Nakken, H. & Reutellingsperger, C. A novel assay for apoptosis Flow cytometric detection of phosphatidylserine expression on early apoptotic cells using fluorescein labelled Annexin V. *J. Immunol. Methods* **184,** 39–51 (1995).

187. Listenberger, L. L. *et al.* Triglyceride accumulation protects against fatty acid-induced lipotoxicity. *Proc. Natl. Acad. Sci. U. S. A.* **100,** 3077–82 (2003).

188. PANTHER - Gene List Analysis. Available at: http://www.pantherdb.org/. (Accessed: 6th August 2018)

189. GeneCards - Human Genes | Gene Database | Gene Search. Available at: https://www.genecards.org/. (Accessed: 15th August 2018)

190. Sigoillot, F. D., Berkowski, J. A., Sigoillot, S. M., Kotsis, D. H. & Guy, H. I. Cell cycle-dependent regulation of pyrimidine biosynthesis. *J. Biol. Chem.* **278,** 3403–3409 (2003).

191. Quéméneur, L. *et al.* Differential Control of Cell Cycle, Proliferation, and Survival of Primary T Lymphocytes by Purine and Pyrimidine Nucleotides. *J. Immunol.* **170,** 4986–4995 (2003).

192. Kelly, B. & O'Neill, L. A. J. Metabolic reprogramming in macrophages and dendritic cells in innate immunity. *Cell Research* **25,** 771–784 (2015).

193. Liu, T., Zhang, L., Joo, D. & Sun, S. C. NF-κB signaling in inflammation. *Signal Transduction and Targeted Therapy* **2,** (2017).

194. Steury, M. D., McCabe, L. R. & Parameswaran, N. in *Advances in Immunology* **136,** 227–277 (Academic Press Inc., 2017).

195. Yang, W. S. & Stockwell, B. R. Ferroptosis: Death by Lipid Peroxidation. *Trends Cell Biol.* **26,** 165–176 (2016).

196. Kanter, J. E., Tang, C., Oram, J. F., Bornfeldt, K. E. & Bornfeldt, K. E. Acyl-CoA synthetase 1 is required for oleate and linoleate mediated inhibition of cholesterol efflux through ATP-binding cassette transporter A1 in macrophages. *Biochim Biophys Acta* **1821,** 358–364 (2012).

197. Hashimoto, S. *et al.* Serial analysis of gene expression in human monocytes and macrophages. *Blood* **94,** 837–44 (1999).

198. Goudot, C. *et al.* Aryl Hydrocarbon Receptor Controls Monocyte Differentiation into Dendritic Cells versus Macrophages. *Immunity* **47,** 582–596.e6 (2017).

199. Hwang, D. H., Kim, J.-A. & Lee, J. Y. Mechanisms for the activation of Toll-like receptor 2/4 by saturated fatty acids and inhibition by docosahexaenoic acid. *Eur. J. Pharmacol.* **785,** 24–35 (2016).

200. Ulas, T. *et al.* S100-alarmin-induced innate immune programming protects newborn infants from sepsis. *Nat. Immunol.* **18,** 622–632 (2017).

201. Franchi, L., Eigenbrod, T., Muñoz-Planillo, R. & Nuñez, G. The inflammasome: a caspase-1-activation platform that regulates immune responses and disease pathogenesis. *Nat. Immunol.* **10,** 241–7 (2009).

202. Silverman, W. R. *et al.* The pannexin 1 channel activates the inflammasome in neurons and astrocytes. *J. Biol. Chem.* **284,** 18143–51 (2009).

203. Collaborators, G. 2015 R. F. Global, regional, and national comparative risk assessment of 79 behavioural, environmental and occupational, and metabolic risks or clusters of risks, 1990–2015: a systematic analysis for the Global Burden of Disease Study 2015. *Lancet (London, England)* **388,** 1659 (2016).

204. Feigin, V. L. *et al.* Global burden of stroke and risk factors in 188 countries, during 1990-2013: a systematic analysis for the Global Burden of Disease Study 2013. *Lancet. Neurol.* **15,** 913–924 (2016).

205. Estruch, R. *et al.* Primary Prevention of Cardiovascular Disease with a Mediterranean Diet. *N. Engl. J. Med.* **368,** 1279–1290 (2013).

206. Saeed, S. *et al.* Epigenetic programming of monocyte-to-macrophage differentiation and trained innate immunity. *Science* **345,** 1251086 (2014).

207. Grygiel-Górniak, B. Peroxisome proliferator-activated receptors and their ligands: nutritional and clinical implications - a review. *Nutr. J.* **13,** 17 (2014).

208. Palomer, X., Pizarro-Delgado, J., Barroso, E. & Vázquez-Carrera, M. Palmitic and Oleic Acid: The Yin and Yang of Fatty Acids in Type 2 Diabetes Mellitus. *Trends Endocrinol. Metab.* **29,** 178–190 (2018).

209. Wang, Y. *et al.* Saturated palmitic acid induces myocardial inflammatory injuries through direct binding to TLR4 accessory protein MD2. *Nat. Commun.* **8,** 13997 (2017).

210. Liao, F., Andalibi, A., deBeer, F. C., Fogelman, A. M. & Lusis, A. J. Genetic control of inflammatory gene induction and NF-kappa B-like transcription factor activation in response to an atherogenic diet in mice. *J. Clin. Invest.* **91,** 2572–2579 (1993).

211. Osborn, O. & Olefsky, J. M. The cellular and signaling networks linking the immune system and metabolism in disease. *Nat. Med.* **18,** 363–374 (2012).

212. Lancaster, G. I. *et al.* Evidence that TLR4 Is Not a Receptor for Saturated Fatty Acids but Mediates Lipid-Induced Inflammation by Reprogramming Macrophage Metabolism. *Cell Metab.* **27,** 1096–1110.e5 (2018).

213. Wen, H., Ting, J. P.-Y. & O'Neill, L. A. J. A role for the NLRP3 inflammasome in metabolic diseases—did Warburg miss inflammation? *Nat. Immunol.* **13,** 352–357 (2012).

214. Christ, A. *et al.* Western Diet Triggers NLRP3-Dependent Innate Immune Reprogramming. *Cell* **172,** 162–175.e14 (2018).

215. McGeough, M. D. *et al.* TNF regulates transcription of NLRP3 inflammasome components and inflammatory molecules in cryopyrinopathies. *J. Clin. Invest.* **127,** 4488–4497 (2017).

216. Wang, X. *et al.* Macrophage ABCA1 and ABCG1, but not SR-BI, promote macrophage reverse cholesterol transport in vivo. *J. Clin. Invest.* **117,** 2216–2224 (2007).

217. Chun, Y., Kim, R. & Lee, S. Centromere Protein (CENP)-W Interacts with Heterogeneous Nuclear Ribonucleoprotein (hnRNP) U and May Contribute to Kinetochore-Microtubule Attachment in Mitotic Cells. *PLoS One* **11,** e0149127 (2016).

218. Prendergast, L. *et al.* Premitotic assembly of human CENPs -T and -W switches centromeric chromatin to a mitotic state. *PLoS Biol.* **9,** e1001082 (2011).

219. Cosín-Roger, J. *et al.* M2 Macrophages Activate WNT Signaling Pathway in Epithelial Cells: Relevance in Ulcerative Colitis. *PLoS One* **8,** e78128 (2013).

220. Gong, D. *et al.* TGFβ signaling plays a critical role in promoting alternative macrophage activation. *BMC Immunol.* **13,** 31 (2012).

221. Martínez, P. *et al.* RAP1 Protects from Obesity through Its Extratelomeric Role Regulating Gene Expression. *Cell Rep.* **3,** 2059–2074 (2013).

222. Cai, Y. *et al.* Rap1 induces cytokine production in pro-inflammatory macrophages through NFκB signaling and is highly expressed in human atherosclerotic lesions. *Cell Cycle* **14,** 3580–92 (2015).

223. Bekkering, S. *et al.* Innate immune cell activation and epigenetic remodeling in symptomatic and asymptomatic atherosclerosis in humans in vivo. *Atherosclerosis* **254,** 228–236 (2016).

224. Unger, T. & Li, J. The role of the renin-angiotensin-aldosterone system in heart failure. *JRAAS - J. Renin-Angiotensin-Aldosterone Syst.* **5,** S7-10 (2004).

225. van der Heijden, C. D. C. C. *et al.* Aldosterone induces trained immunity: the role of fatty acid synthesis. *Cardiovasc. Res.* **116,** 317–328 (2019).

226. Hubler, M. J. & Kennedy, A. J. Role of lipids in the metabolism and activation of immune cells. *J. Nutr. Biochem.* **34,** 1–7 (2016).

227. Wu, C. Focal Adhesion: A Focal Point in Current Cell Biology and Molecular Medicine. *Cell Adh. Migr.* **1,** 13–18 (2007).

228. Tang-Huau, T. L. *et al.* Human in vivo-generated monocyte-derived dendritic cells and macrophages cross-present antigens through a vacuolar pathway. *Nat. Commun.* **9,** 1–12 (2018).

229. Westerterp, M. *et al.* Apolipoprotein C-I Is Crucially Involved in Lipopolysaccharide-Induced Atherosclerosis Development in Apolipoprotein E Knockout Mice. *Circulation* **116,** 2173–2181 (2007).

230. Berbée, J. F. P. *et al.* Apolipoprotein CI enhances the biological response to LPS via the CD14/TLR4 pathway by LPS-binding elements in both its N- and C-terminal helix. *J. Lipid Res.* **51,** 1943–52 (2010).

231. Bouloc, A., Bagot, M., Delaire, S., Bensussan, A. & Boumsell, L. Triggering CD101 molecule on human cutaneous dendritic cells inhibits T cell proliferation via IL-10 production. *Eur. J. Immunol.* **30,** 3132–3139 (2000).

232. Tran, D. Q. *et al.* GARP (LRRC32) is essential for the surface expression of latent TGF-β on platelets and activated FOXP3+ regulatory T cells. *Proc. Natl. Acad. Sci. U. S. A.* **106,** 13445–13450 (2009).

233. Verde, G. *et al.* Lysine-Specific Histone Demethylases Contribute to Cellular Differentiation and Carcinogenesis. *Epigenomes* **1,** 4 (2017).

234. Kawai, T. & Akira, S. Toll-like receptors and their crosstalk with other innate receptors in infection and immunity. *Immunity* **34,** 637–50 (2011).

Appendix

Table 8.1: DE-gene list of up- and down-regulated genes overlapping between 24 hours OA and PA stimulated cells.

Up-regulated DE-genes	Down-regulated DE-genes
ACADVL	AC006978.2
ACSL1	AC146944.2
ADGRE3	C11orf21
CD300A	CD1A
CD300LB	CD207
CD82	DMPK
CHST15	DMWD
CTSL	ENTPD1
CYTOR	GPX3
ETS2	IRF4
FCMR	LIN7A
LDLR	MMP12
LINC01943	NDRG2
MCEMP1	NEMP1
PLIN2	NPR1
S1PR3	SH3PXD2B
SCD	SOBP
SH3RF1	STEAP4
SIPA1L2	TIFAB
SLC25A20	TSPAN32

Table 8.2: DE-gene list of up- and down-regulated genes overlapping between OA and PA-primed cells after three days wash-out.

Up-regulated DE-genes	Down-regulated DE-genes
METRN	--

Table 8.3: DE-gene list of up- and down-regulated genes overlapping between 116 hours OA_ctrl_20h_LPS and PA_ctrl_20h_LPS stimulated cells.

Up-regulated DE-genes	Down-regulated DE-genes
AC022966.2	AC126474.2
ADCY3	AL135818.1
AK1	BCL2L11
FAM213B	CD1E
GLIPR1	CISH
GSTM1	CLIC2
HYAL3	CST3
MAP4K2	CST7
SIRPB1	DEGS1
SPATA18	GGT5
SYNJ2	GGTA1P
TEAD3	GPR153
UCHL3	GRB10
	HLA-DOA
	JDP2
	LDHAP4
	NBL1

NDRG1
NET1
STAB1
SVIL
TSPAN14
TUBB2A
UBD

Publications

Hardt, Anna-Lena, Verena Schildgen, Ramona-Liza Tillmann, Michael Brockmann, and Oliver Schildgen, 'Utility of the QIAGEN/ *Artus* PCR Assays and Meningofinder™ for the Detection of Human Herpes Virus Genomes in Formalin-Fixed Paraffin-Embedded Clinical Samples', *Future Virology*, 9 (2014), 241–42 <https://doi.org/10.2217/fvl.14.7>

Kaur, Jaspreet, Verena Schildgen, Ramona-Liza Tillmann, **Anna-Lena Hardt**, Jessica Lüsebrink, Wolfram Windisch, and others, 'Low Copy Number Detection of Human Bocavirus DNA in Bronchoalveolar Lavage of Asymptomatic Adult Patients', *Future Virology*, 9 (2014), 715–20 <https://doi.org/10.2217/fvl.14.59>

Schmidt, Susanne V, Wolfgang Krebs, Thomas Ulas, Jia Xue, Kevin Baßler, Patrick Günther, **Anna-Lena Hardt**, Hartmut Schultze, Jil Sander, Kathrin Klee, Heidi Theis, Michael Kraut1, Marc Beyer, Joachim L Schultze 'The Transcriptional Regulator Network of Human Inflammatory Macrophages Is Defined by Open Chromatin.', *Cell Research*, 26 (2016), 151–70 <https://doi.org/10.1038/cr.2016.1>

Sander, Jil, Susanne V Schmidt, Branko Cirovic, Naomi McGovern, Olympia Papantonopoulou, **Anna-Lena Hardt**, Anna C. Aschenbrenner, Christoph Kreer, Thomas Quast, Alexander M. Xu, Lisa M. Schmidleithner, Heidi Theis, Thi Huong Lan Do, Hermi Rizal Bin Sumatoh, Mario A. R. Lauterbach, Jonas Schulte-Schrepping, Patrick Günther, Jia Xue1, Kevin Baßler, Thomas Ulas, Kathrin Klee, Natalie Katzmarski, Stefanie Herresthal, Wolfgang Krebs, Michael Kraut, Waldemar Kolanus, Marc Beyer, Christine S. Falk, Bettina Wiegmann, Sven Burgdorf, Nicholas A. Melosh, Evan W. Newell, Florent Ginhoux, Andreas Schlitzer, Joachim L. Schultze, 'Cellular Differentiation of Human Monocytes Is Regulated by Time- Dependent IL4 Signalling and NCOR2.', *Immunity*, 47,6 (2017), 1051-1066.e12. <doi:10.1016/j.immuni.2017.11.024>